Advances in Dielectrics
Series Editor: Friedrich Kremer

George Floudas
Marian Paluch
Andrzej Grzybowski
K.L. Ngai

Molecular Dynamics of Glass-Forming Systems

Effects of Pressure

Springer

Advances in Dielectrics

Series Editor
Friedrich Kremer

Aims and Scope

Broadband Dielectric Spectroscopy (BDS) has developed tremendously in the last decade. For dielectric measurements it is now state of the art to cover typically 8–10 decades in frequency and to carry out the experiments in a wide temperature and pressure range. In this way a wealth of fundamental studies in molecular physics became possible, e.g. the scaling of relaxation processes, the interplay between rotational and translational diffusion, charge transport in disordered systems, and molecular dynamics in the geometrical confinement of different dimensionality – to name but a few. BDS has also proven to be an indispensable tool in modern material science; it plays e.g. an essential role in the characterization of Liquid Crystals or Ionic Liquids and the design of low-loss dielectric materials.

It is the aim of "Advances in Dielectrics" to reflect this rapid progress with a series of monographs devoted to specialized topics.

Target Group

Solid state physicists, molecular physicists, material scientists, ferroelectric scientists, soft matter scientists, polymer scientists, electronic and electrical engineers.

George Floudas • Marian Paluch •
Andrzej Grzybowski • K.L. Ngai

Molecular Dynamics of Glass-Forming Systems

Effects of Pressure

Springer

Dr. George Floudas
University of Ioannina
Dept. Physics
PO Box 1186
451 10 Ioannina
Greece
gfloudas@cc.uoi.gr

Dr. Andrzej Grzybowski
University of Silesia
Inst. Physics
ul. Uniwersytecka 4
40-007 Katowice
Poland
andrzej.grzybowski@us.edu.pl

Prof. Marian Paluch
University of Silesia
Inst. Physics
ul. Uniwersytecka 4
40-007 Katowice
Poland
marian.paluch@us.edu.pl

Prof. K.L. Ngai
CNR-IPCF Associate
Dipartimento di Fisica
Università di Pisa
Largo Bruno Pontecorvo 3
I-56127 Pisa
Italy
ngai@df.unipi.it

Series Editor
Friedrich Kremer
University of Leipzig
Germany

ISSN 2190-930X e-ISSN 2190-9318
ISBN 978-3-642-04901-9 e-ISBN 978-3-642-04902-6
DOI 10.1007/978-3-642-04902-6
Springer Heidelberg Dordrecht London New York

Cover design: WMXDesign GmbH, Heidelberg, Germany

Printed on acid-free paper

Springer is part of Springer Science+Business Media (www.springer.com)

To the memory of Tadeusz Pakula

Preface

In his Science article of 1995, P.W. Anderson mentioned that "*the deepest and most interesting unsolved problem in solid state theory is probably the theory of the nature of glass and the glass transition. This could be the next breakthrough in the coming decade*." Today (some 15 years later), we claim that he was right in this prediction. Especially over the last 10–15 years, there has been more progress in our understanding of glass formation than in the previous 40 years.

A unique feature of the molecular dynamics in glass-forming systems is the continuous and dramatic increase in the structural relaxation time, from values on the order of picoseconds up to hundreds of seconds in the vicinity of the glass "transition" temperature. Other transport quantities such as the diffusion constant or viscosity show a similar increase. Another important characteristic is the non-exponential character of the relaxation function. Although cooling a liquid is the method most often employed to induce the liquid-to-glass "transition," this is not the only root towards the glassy state. Among others, a liquid can be vitrified by increasing pressure under isothermal conditions. This path was first exploited in the 1960s, but due to serious experimental difficulties in performing spectroscopic measurements under elevated pressures, it soon came to a standstill (and hence pressure became the "forgotten" thermodynamic variable). Nevertheless, such experiments are necessary to provide the complete physical description of the vitrification process. In recent years, we have witnessed a major breakthrough in the study of the dynamics of supercooled liquids and of the glass "transition" under elevated pressures, mainly by using dielectric spectroscopy and other methods (photon correlation spectroscopy, rheology, and NMR).

This book provides a comprehensive survey of the recent advances in the study of the effect of pressure on the vitrification process of simple van der Waals liquids, hydrogen-bonded systems, polymers, polymer blends, and biopolymers. We first review the important knowledge attained in the 1960s by the seminal work of G. Williams, Sasabe, and Saito, and proceed to the current understanding of the effects of pressure on the dynamics of glass-forming liquids in the vicinity of the glass "transition."

Chapter 1 discusses the pressure dependence of the structural relaxation times and the effect of pressure on the glass temperature and fragility. We also address the role played by thermal energy and density in the tremendous slowing down of the structural relaxation dynamics when approaching the glass temperature.

Chapter 2, with the ambitious title "Origin of Glass formation," discusses in detail the current understanding of the liquid-to-glass transformation and, in particular, the importance of pressure. Identifying the main control parameter that dominates the slow dynamics at the glass temperature has been a point of debate. Theoretical predictions consider thermally activated processes on a constant density "energy landscape" and "free-volume" as extreme cases. However, since changing temperature affects both the thermal energy and the volume (and thus the associated "free volume"), it is impossible to separate the two effects by temperature alone. In order to disentangle the effects of temperature and volume (or better said, the corresponding intensive variable, density) on dynamics, pressure-dependent measurements have been of paramount importance, as pressure can be applied isothermally (affecting only the density) and have been employed to provide a quantitative assessment of their relative importance. We provide two recent approaches that have led to a better understanding of the liquid-to-glass dynamics. The first is based on the newly observed dynamic feature known as "thermodynamic scaling"; the second emphasizes the role of molecular volume and local packing on the glass transition dynamics.

Knowledge of the equation of state is essential in predicting the pressure behavior of fragility and of the glass transition temperature. Chapter 3 discusses the equivalent of an "equation of state" with physically interpretable parameters for the description of the structural relaxation times as a function of temperature and pressure. In this chapter, various canonical models that incorporate both the temperature and pressure dependences of the structural relaxation time are reviewed.

Chapter 4 discusses the latest findings on the dynamics of glass formers. The new results turn out to be nearly universal, present in glass formers of different physical structures and chemical natures, and have not been addressed before and thus have tremendous impact on current concepts and theories of glass "transition." The results also point out the new physics that have to be included before the problem of glass formation is solved completely.

The important role of pressure in the miscibility of polymer mixtures has been realized only recently, as it has direct applications to processing as well as to new syntheses that involve the use of environment-friendly supercritical fluids. Chapter 5 reviews the recent progress made in understanding the effects of pressure on the thermodynamics (i.e., the critical temperature for phase separation) and dynamics of polymer blends.

Chapter 6 reviews recent efforts to investigate the hierarchical self-assembly and dynamics in an important class of biomaterials: polypeptides. Polypeptides play a vital part in the molecules designed for use in drug delivery of gene therapy and thus have been the subject of intensive studies. However, their dynamic response has only recently been explored. In the first part, we discuss the origin

of the dynamic arrest at the glass "transition". In this respect, pressure again plays a decisive role, as it is used to identify structural and dynamic defects (i.e., *solitons*). Subsequently, and as a direct consequence of the first part, we discuss that contrary to expectation and common belief, helices in concentrated polypeptide solutions are objects of low persistence. In the third part, we address the effect of confinement in controlling the type, persistence, and dynamics of secondary structures.

We would like to acknowledge the many instructive comments and suggestions for improvement of Graham Williams. George Floudas further acknowledges his coworkers at the UoI (A. Gitsas, P. Papadopoulos, K. Mpoukouvalas) who participated in parts of this work. Contributions at the University of Ioannina were cofinanced by the E.U.-European Social Fund (75%) and the Greek Ministry of Development-GSRT (25%) in the framework of the programs PENED 2001 (No 529) and PENED2003 (No 856). Contributions of M. Paluch and A. Grzybowski to this book were made as a part of the research project "From Study of Molecular Dynamics in Amorphous Medicines at Ambient and Elevated Pressure to Novel Applications in Pharmacy," operated by the Foundation for Polish Science Team Program that is cofinanced by the EU Regional Development Fund within the framework of the Innovative Economy Operational Program. This support is highly appreciated. M. Paluch and A. Grzybowski would like to further thank their coworker K. Grzybowska at the University of Silesia for her help in preparing this book. The work at NRL was supported by the Office of Naval Research.

Ioannina, Greece — George Floudas
Katowice, Poland — Marian Paluch
Katowice, Poland — Andrzej Grzybowski
Pisa, Italy — K.L. Ngai

Contents

Chapter 1
The Glass "Transition"

1.1 Introduction

Normal liquids can be transformed during the cooling process into two different solid forms: glass and crystal [1]. These "transitions" can be identified by measuring, for instance, the temperature dependence of volume on cooling or heating a specimen. Since crystallization is a first-order transition, it is manifested as a discontinuous change in volume at the crystallization temperature, T_{cryst}. In the majority of cases, volume decreases abruptly at T_{cryst}. However, there exist some examples with the opposite dependence. The most well-known example being the freezing of water where the increase of volume on cooling reflects the open structure of ice.

Since the crystallization process takes some time (critical nuclei have to be formed and subsequently they have to grow), it is also possible to supercool a liquid to below its melting temperature where it retains its liquid character. As shown in Fig. 1.1, further cooling of the supercooled liquid leads to the liquid-to-glass "transition" manifested by a characteristic change in the slope of $V(T)$ dependence in the vicinity of the glass temperature, T_{g}. Below T_{g}, supercooled liquids become amorphous solids. It is important to emphasize that any liquid is able to form a glass if cooled rapidly enough. Most of them require fast cooling to avoid crystallization, but there are also many liquids that can be easily supercooled and kept in this metastable state for a long time. The latter are particularly useful in investigating the properties of the supercooled state.

At first sight, the liquid-to-glass "transition" resembles a second-order thermodynamic transition. For this reason, some efforts have been made to describe the glass transition in terms of the Ehrenfest equations [3–6]:

$$\left(\frac{\mathrm{d}T_{\mathrm{g}}}{\mathrm{d}P}\right) = \frac{\Delta\kappa_T}{\Delta\alpha_P}, \tag{1.1}$$

$$\left(\frac{\mathrm{d}T_{\mathrm{g}}}{\mathrm{d}P}\right) = \frac{V_{\mathrm{g}}T_{\mathrm{g}}\Delta\alpha_P}{\Delta C_P}, \tag{1.2}$$

G. Floudas et al., *Molecular Dynamics of Glass-Forming Systems*,
Advances in Dielectrics 1, DOI 10.1007/978-3-642-04902-6_1,

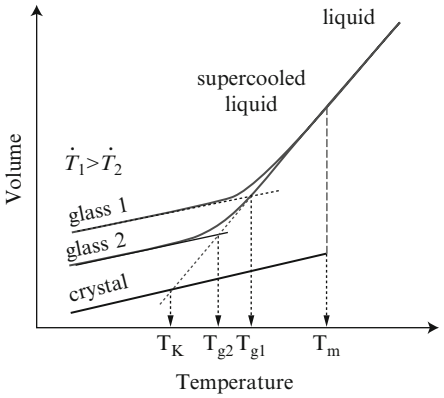

Fig. 1.1 Schematic representation of the temperature dependence of system volume for a liquid that can both crystallize and form a glass. The thermodynamic and dynamic properties of a glass depend upon the cooling rate; glass 2 was formed with a slower cooling rate than glass 1. Values T_{g1} and T_{g2} indicate the glass transition temperatures for two cooling rates $\dot{T}_1 > \dot{T}_2$. Symbol T_m denotes the melting temperature, whereas T_K, the Kauzmann temperature. This figure is taken from [2]

where $\Delta\kappa_T$, $\Delta\alpha_P$, and ΔC_P are the changes of isothermal compressibility, isobaric expansion coefficient, and isobaric specific heat, respectively, between the liquid and glassy states.

Combining (1.1) and (1.2), we obtain the Prigogine–Defay ratio:

$$\frac{\Delta\kappa_T \Delta C_P}{T_g V_g (\Delta\alpha_P)^2} = 1. \tag{1.3}$$

Evidently, important terms in these equations are pressure dependent for real materials; hence it is difficult to verify these equations in practice. Nevertheless, it was experimentally verified that (1.3) does not hold for certain glasses [7, 8]. Instead, the ratio takes values above one for several systems with typical values in the range 2–5 [7, 8]. In fact, the failure of Prigogine–Defay ratio means, as argued by Goldstein [9], that a single-order parameter description of the liquid-to-glass "transition" phenomenon may be not sufficient.

In general, the attempt to classify a liquid–glass "transition" as a thermodynamic phase transition is at odds with the well-established experimental fact that the glass temperature depends on the experimental cooling/heating rates. Slower cooling rates, $\dot{T} = \mathrm{d}T/\mathrm{d}t$, will cause a change of T_g (marked in Fig. 1.1) toward lower temperatures. This behavior is a consequence of a kinetic nature of the vitrification process. As the temperature of the supercooled liquid is changed, molecules rearrange to achieve a new equilibrium state and this process requires some time. Naturally, a new equilibrium state will be achieved if the time required for the rearrangement is shorter than the time scale related to temperature change. Otherwise, molecules will have no chance to rearrange entirely, and consequently,

experimentally observed macroscopic quantities, such as volume, will deviate from their equilibrium values. The onset of such behavior will take place as T_g is approached, where a change of the slope in $V(T)$ takes place. Thus, for slower cooling rates, the ensemble of molecules will have a chance to continue toward their equilibrium state at lower temperatures. This is the origin of the above-mentioned dependence of T_g on the cooling rate. Therefore, it is commonly believed that glass formation is a kinetic phenomenon and not a true thermodynamic phase transition [10]. Nevertheless, the term "transition" has been used in the literature in a broader sense to describe the formation of the nonequilibrium phase (glass) from the equilibrium melt state. We employ the same term here knowing that this is not a true phase transition.

Glass formation appears not only in the first and second derivatives of the state functions (i.e., volume, entropy, enthalpy and thermal expansion coefficient, and specific heat, respectively), but also in the behavior of the molecular dynamics with respect to temperature and pressure. The unique feature of molecular dynamics of glass-forming liquids is the continuous and dramatic increase of the structural relaxation time from values of the order of picoseconds (typical time scale for molecular rearrangements in the normal liquid state) up to hundreds of seconds in the vicinity of the glass transition temperature [2, 11] (Fig. 1.2). A similar behavior can be observed in other transport quantities such as diffusion constant or viscosity.

It is also well known that many supercooled liquids subjected to sudden constant mechanical, electrical, or thermal perturbation will slowly relax towards the equilibrium in a non-exponential fashion [12–14]. This nonexponential character of the relaxation function has been recognized as another important characteristic of the

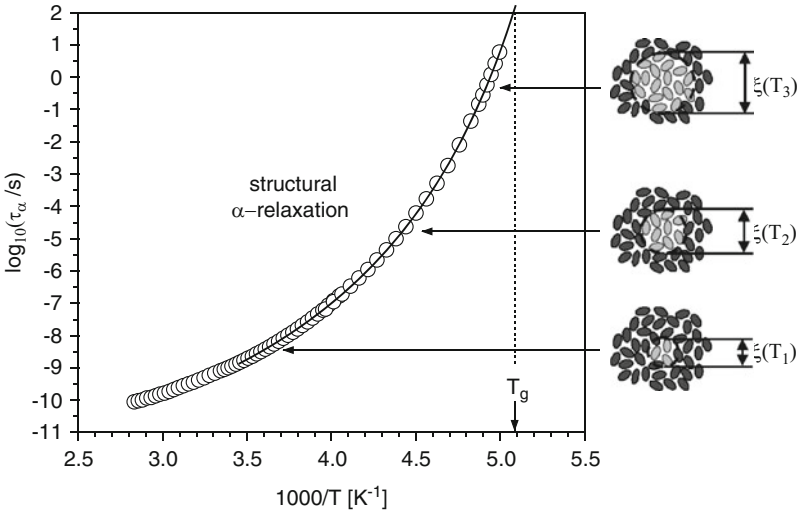

Fig. 1.2 Non-Arrhenius temperature dependence of α-relaxation times for polypropylene glycol of molecular weight 400 g/mol together with schematic illustration of increasing of cooperatively rearranging regions during cooling (ξ is so-called cooperativity length)

dynamics of glass-forming liquids. The Kohlrausch–Williams–Watts (KWW) function is commonly used to describe relaxation functions in the time domain [15, 16]

$$\varphi_{\mathrm{KWW}}(t) = \exp\left[-\left(\frac{t}{\tau_{\mathrm{KWW}}}\right)^{\beta_{\mathrm{KWW}}}\right], \tag{1.4}$$

where τ_{KWW} is a characteristic relaxation time and β_{KWW} denotes the stretching parameter, with values varying from 0 to 1 (when $\beta_{\mathrm{KWW}} = 1$, a single exponential process is recovered). A nonexponential relaxation in the time-domain corresponds to a non-Debye relaxation in the frequency domain. Transformation of the KWW function from the time- and frequency-domains is described in [16, 17] and has led to its many applications to frequency-domain dielectric data for glass-forming liquids and polymers. However, the structural relaxation process is broader than a single relaxation time process (see Fig. 1.3). To describe this broadening, the Havriliak– Negami function is most often used [18–20]:

$$\phi_{\mathrm{HN}}(\omega) = \frac{1}{\left[1 + (\mathrm{i}\omega\tau_{\mathrm{HN}})^{\alpha}\right]^{\gamma}}, \tag{1.5}$$

where α and γ are shape parameters ranging between 0 and 1, and τ_{HN} is a parameter connected to a characteristic relaxation time. The broadening of the structural relaxation function is generally believed to be due to complex cooperative character of molecular rearrangements (see for example [21, 22])

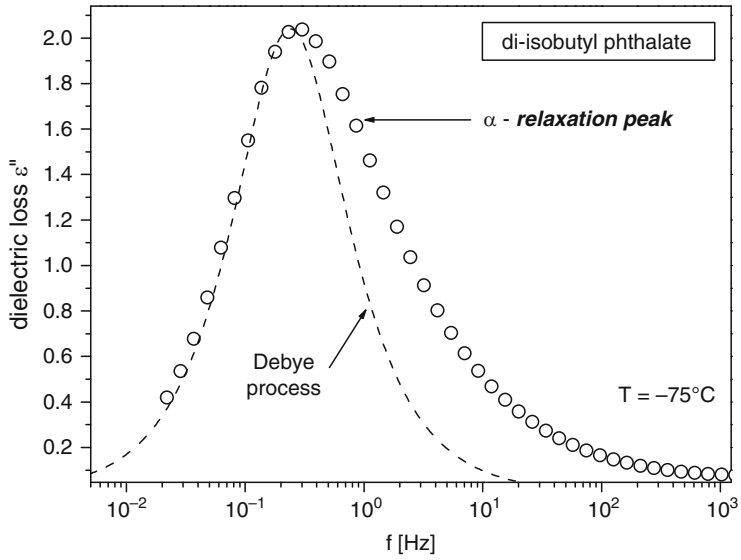

Fig. 1.3 Frequency-dependent dielectric loss ε'' of di-isobutyl phthalate near the glass transition. Experimental data (*open circles*) for structural relaxation process cannot be described by the simple Debye function (*dashed lines*)

Although cooling of a supercooled liquid is the method most often applied to induce the liquid-to-glass transition, it does not mean that this is the only route leading to the glassy state. Among other ways, there exists a possibility to pass from the liquid and glassy state by increasing pressure under isothermal conditions. However, this path has been much less exploited mainly due to serious experimental difficulties of performing both spectroscopic and thermodynamic measurements under conditions of elevated pressure. They often involved the application of a special high-pressure technique with relatively low temperatures. Nevertheless, such experiments are necessary to provide the complete physical description of the vitrification phenomenon [23, 24]. In addition, the dynamical aspects of glass formation that arise in rate-dependent thermodynamic measurements form a large, complicated, but well-understood subject [25–29].

Hydrostatic pressure is a key thermodynamic variable controlling molecular spacing. Thus, one expects that compression should have important effects on the molecular dynamics of a supercooled liquid and consequently on glass formation. By using pressure and temperature as independent, but complementary, variables, the glass transition can be approached on different trajectories in the phase space (for example, see Fig. 4.15). Therefore, it is also legitimate to ask whether there are any differences in the dynamics if T_g is approached by isobaric temperature changes or by isothermal pressure changes. This important question also relates to the lively discussion in the literature (see for example [30]) with respect to the universality of glass formation.

In recent years, we have witnessed a major breakthrough in the study of the properties of supercooled liquids and of the glass transition under elevated pressures, mainly by dielectric spectroscopy [31–34]. It should also be mentioned that at the same time other methods (photon correlation spectroscopy [35–37], viscosity measurements [38, 39], and NMR [40]) were developed that can probe the dynamics at elevated pressures.

This book provides a comprehensive survey of the recent advances in the study of the effect of pressure on the vitrification process of simple van der Waals liquids, hydrogen-bonded systems, polymers, polymer blends, and biopolymers. This overview begins with this Chapter by discussing the pressure dependence of the structural relaxation times and the effect of pressure on the glass transition temperature and fragility. We also address the role played by thermal energy and density in the tremendous slowing down of the structural relaxation dynamics by approaching T_g.

1.2 Pressure Dependence of the Structural (α-) Relaxation Time

As mentioned above, the time scale related to the structural reorganization of a liquid increases dramatically as the supercooled liquid is cooled toward T_g. Numerous experimental results show that the structural (α) relaxation time, as well as the viscosity, fails to obey the simple Arrhenius behavior

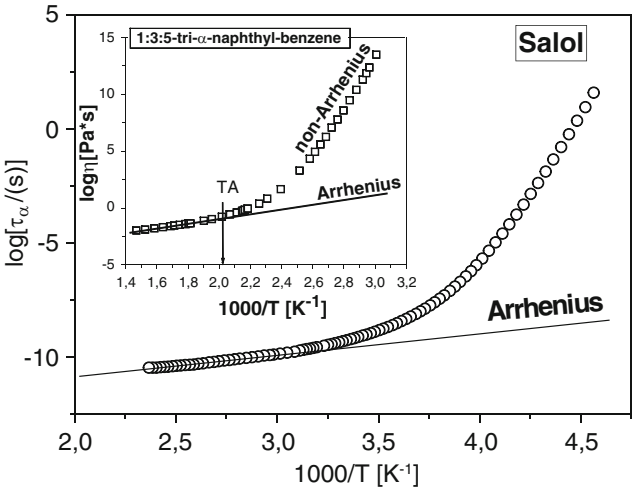

Fig. 1.4 Illustration of changes in α-relaxation times (for salol) and viscosity (in the *inset* for 1:3:5-tri-a-naphthyl-benzene) during materials cooling at ambient pressure; At high temperatures, the dependences $\log\tau_\alpha(T)$ and $\log\eta(T)$ can be described by using the Arrhenius equation, whereas at lower T, the characteristics exhibit a strong deviation from the Arrhenius law (temperature T_A denotes beginning of non-Arrhenius behavior)

$$\tau = \tau_A \exp\left(\frac{E_A}{\kappa T}\right), \tag{1.6}$$

where τ_A is a pre-exponential factor, E_A is the activation energy, and k_B is the Boltzmann constant. As depicted in Fig. 1.4, both properties display stronger temperature dependence than a simple Arrhenius law. This suggests that the activation energy is not a material constant with respect to temperature but it increases with decreasing temperature. On the contrary, the Arrhenius dependence of (1.6) is known to be valid only for some glass-forming liquids at temperatures much above the glass temperature.

A wide variety of models have been proposed for describing the non-Arrhenius temperature dependence of τ_α and η of supercooled liquids. Unfortunately, all of them fit the experimental data only within a certain temperature range. The extensive discussion of applicability of these formulas is presented in references [41, 42]. Beyond any doubt, the most frequently used equation is the empirical Vogel–Fulcher–Tammann (VFT) law [43–45]

$$\tau = \tau_{VFT}\exp\left(\frac{B}{T - T_0}\right), \tag{1.7}$$

where τ_{VFT} is a pre-exponential factor, B is a material constant, and T_0 is the temperature (known as the "ideal" glass temperature) corresponding to an infinitely slow structural relaxation time. Interestingly, both free volume theory [46] and the Adam–Gibbs model [47] can be used to rationalize the form of the VFT equation.

A tremendous increase in the structural relaxation time and in the viscosity is also observed when the liquid is compressed at constant temperature. In this respect, one can ask what type of equation is more suitable for describing the pressure dependence of the structural relaxation times. An approximate relation can be obtained in the following lines of thought. In pure thermodynamic terms, T and P cannot be considered as equivalent thermodynamic variables; for example, the thermal energy of the system decreases with decreasing T at constant P, whereas this is not the case by increasing P at constant T. However, from a dynamic point of view, decreasing temperature and increasing pressure both produce a similar effect, i.e., the slowing down of the dynamics for molecular rearrangements (for a counter-example see Chap. 5, Section 5.3.1.). Thus, from a dynamics view, pressure and temperature might be thought as "equivalent" thermodynamic variables and this would be expressed as follows:

$$T^{-1} \leftrightarrow P. \tag{1.8}$$

Taking into account the above transformation together with the temperature VFT law, we can easily derive the pressure counterpart of the temperature VFT equation [48–50]:

$$\tau = \tau_0 \exp\left(\frac{CP}{P_0 - P}\right). \tag{1.9}$$

An alternative approach leading to the pressure VFT law is based on the free volume model. In the latter, of key importance is the Doolittle equation [51] relating free volume to the structural relaxation time as

$$\tau = \tau_0 \exp\left(\frac{\upsilon}{\upsilon_f}\right). \tag{1.10}$$

To recover (1.9) it has to be assumed that $\upsilon_f = \kappa(\upsilon - \upsilon_0)$ is proportional to $(P_0 - P)/P$.

Similar to the temperature VFT law (1.7), its pressure counterpart (1.9) includes three parameters: τ_0, C, and P_0. However, only two of them: C and P_0, have to be extracted from the numerical fitting analysis. The pre-exponential coefficient, τ_0, is the relaxation time at ambient pressure and, therefore, its value can be determined directly from the measurements. As an example illustrating the pressure dependence of structural relaxation times we depict in Fig. 1.5 four different isothermal pressure dependences of dielectric α-relaxation times for di-isobutyl phthalate (DIBP) [52], Xylitol [53], polymethylphenylsiloxane (PMPS) [54] and 1-butyl-1-methylpyrrolidinium bis[oxalato]borate (BMP-BOB) [55]. The selection of these glass formers is not accidental. They represent different categories of materials: van der Waals liquids (DIBP), H-bonded liquids (Xylitol), polymers (PMPS), and ionic liquids (BMP-BOB). The common characteristic feature for all four dependencies is their

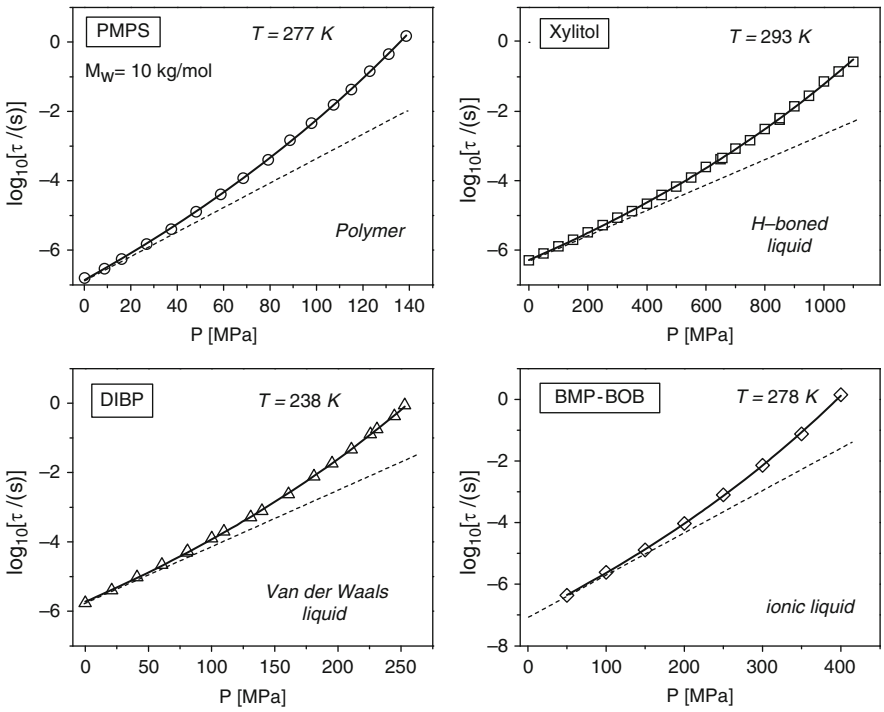

Fig. 1.5 Pressure dependences of isothermal α-relaxation times for four kinds of material: polymethylphenylsiloxane (PMPS) of molecular weight of 10,000 g/mol, di-isobutyl phthalate (DIBP), xylitol, and 1-butyl-1-methylpyrrolidinium bis[oxalato]borate (BMP-BOB), representing polymers, van der Waals liquids, H-bonded systems, and ionic liquids, respectively. *Solid lines* are fits of the experimental data to pressure-dependent VFT formula. *Dashed lines* demonstrate how the pressure dependences would look in the case of simply volume-activated processes which should obey the Arrhenius law with $\Delta V^{\#} = \text{const}$

nonlinearity. This behavior is just very well portrayed by (1.9). The effectiveness of the pressure VFT law has been demonstrated not only for dielectric relaxation data [56–60] but also for viscosity [61] measurements and photon correlation times [62].

A different approach is based on transition state theory. Eyring [63] derived a relation for the rate at which species relax from nonactivated states A_1 and A_2 toward an activated state A* as $A_1 \leftrightarrows A^* \leftrightarrows A_2$. Details of the activated complex and the derivation of the rate are given in [64, 65]. The transition state equation for τ for dielectric relaxation [64–66] is

$$\tau = (h/kT)\exp[\Delta G^{\#}/RT], \tag{1.11}$$

where $\Delta G^{\#} = \Delta H^{\#} + \Delta V^{\#}$, with $\Delta H^{\#}$ ($\Delta V^{\#}$) being the enthalpy (volume) changes with respect to the activated state (see [66–68] for a consideration of the standard states involved in the definition of $\Delta G^{\#}$ and its components).

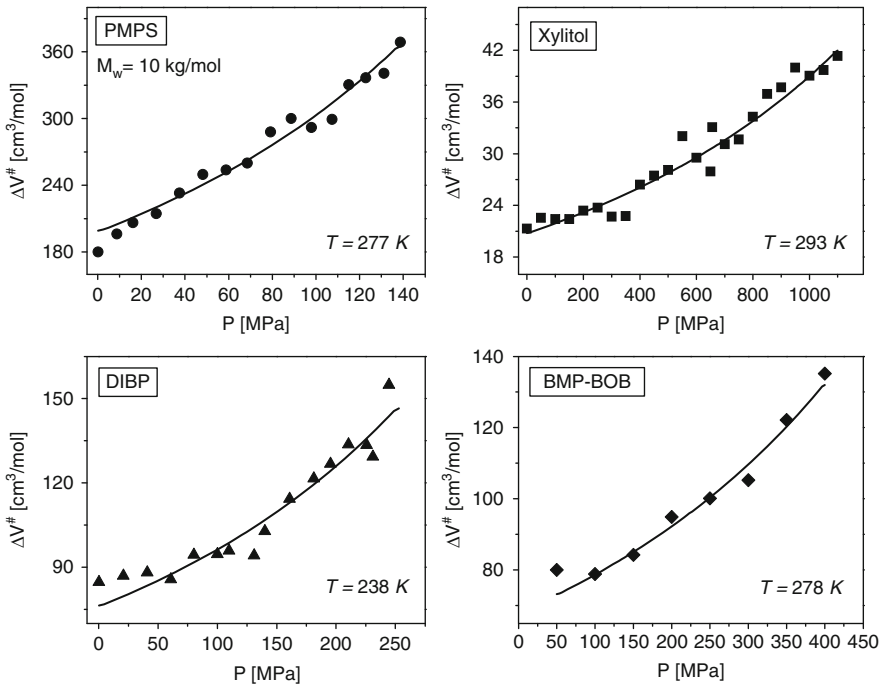

Fig. 1.6 Pressure dependences of the activation volume calculated from (1.12) for PMPS, DIBP, xylitol, and BMP-BOB

The nonlinear character of the $\tau_\alpha(P)$ dependence indicates that the apparent activation volume, $\Delta V_\alpha^\#$, is not constant – similar to that in the case of the activation energy [69]. According to the definition of $\Delta V_\alpha^\#$, the nonlinear increase of isothermal $\log_{10}\tau_\alpha$ with pressure causes the apparent activation volume to increase with P [64, 66]:

$$\Delta V_\alpha^\# = RT\left(\frac{\mathrm{d}\,\ln\tau_\alpha}{\mathrm{d}P}\right)_T \tag{1.12}$$

As can be seen in Fig. 1.6, the values of $\Delta V_\alpha^\#$ also seems to increase in some nonlinear fashion. The solid lines running through the data in Fig. 1.6 have been determined using (1.9) and (1.12). The fair agreement with the experimental points again confirm the efficiency of the pressure VFT equation.

The activation volume is a very useful parameter to characterize the relaxation processes in glass-forming liquids. Its value provides valuable information on the pressure sensitivity of the relaxation times. In the framework of the transition state theory [65, 66], the apparent activation volume $\Delta V_\alpha^\#$ is defined as the difference between the volumes occupied by a molecule in activated (transition) and nonactivated (minimum) states. Thus, the value of $\Delta V_\alpha^\#$ may reflect on the volume requirements for local molecular motion. The natural consequence of this circumstance is that the size of a relaxing molecular unit will have an influence on the

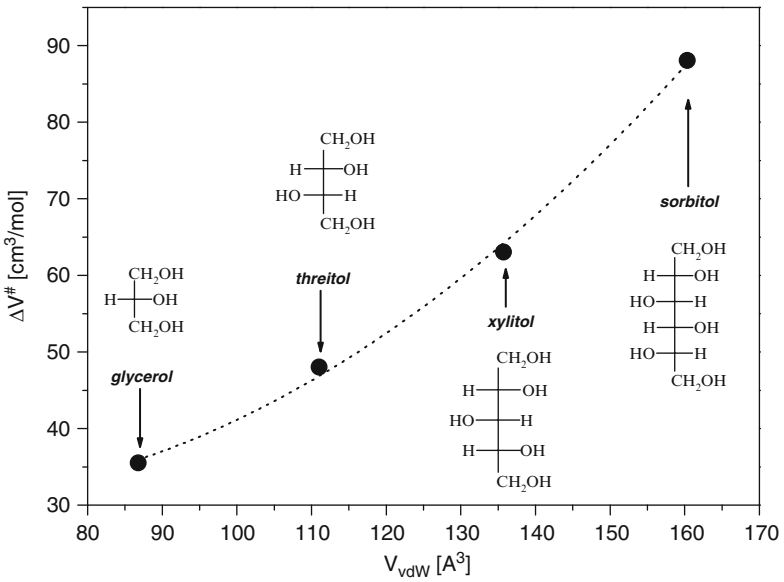

Fig. 1.7 Plot of the activation volume $\Delta V^{\#}$ for a polyalcohol series vs. their molecular volume V_{vdW} calculated on the basis of the van der Waals radius

value of $\Delta V_{\alpha}^{\#}$. The validity of the above rule is illustrated by plotting the activation volume as a function of molecular volume for polyalcohol series: glycerol, threitol, xylitol, and sorbitol [70] (see Fig. 1.7).

It has been already pointed out that the activation volume usually increases with pressure. At this point, it is interesting to analyze the dependence of $\Delta V_{\alpha}^{\#}$ as a function of temperature at constant α-relaxation time. Such a dependence is shown in Fig. 1.8 for two polymers (PMPS and PTMPS) [71, 72] and two van der Waals liquids (BMMPC and BMPC) [73]. In this case, we plotted $\Delta V_{\alpha}^{\#}$ calculated at a constant τ_{α}, versus the normalized glass transition temperature, $T_{\mathrm{g}}(P)/T_{\mathrm{g}}$ (1 bar). The observed decrease in the activation volume with increasing pressure is recognized as a distinctive behavior for glass-forming liquids. Since at higher T_{g} the sample is usually more dense, this result implies that the role of volume effects on the relaxation phenomena is weakened at high pressure. Extrapolating the data in Fig. 1.8 to the glass transition temperature at ambient pressure, one finds that $\Delta V_{\alpha}^{\#} \sim 275$ [cm^3/mol] and $\Delta V_{\alpha}^{\#} \sim 510$ [cm^3/mol] for BMPC and PMPS, respectively. These values should be compared with the molar volumes of BMPC ($V_{\mathrm{m}} =$ 178 cm^3/mol) and PMPS ($V_{\mathrm{m}} = 103$ cm^3/mol). The straightforward conclusion from the comparison above is that at least one (whole) molecular unit (or a few segments in case of a polymer) is involved in the observed structural relaxation process. By analyzing differences in values of activation volume for pairs: PMPS–PTMPS and BMPC–BMMPC, one can again find the correlation between the molecular size of relaxing unit and $\Delta V_{\alpha}^{\#}$. PTMPS in comparison to PMPS has an additional methyl group attached to the phenyl ring. Thus, the molecular volume

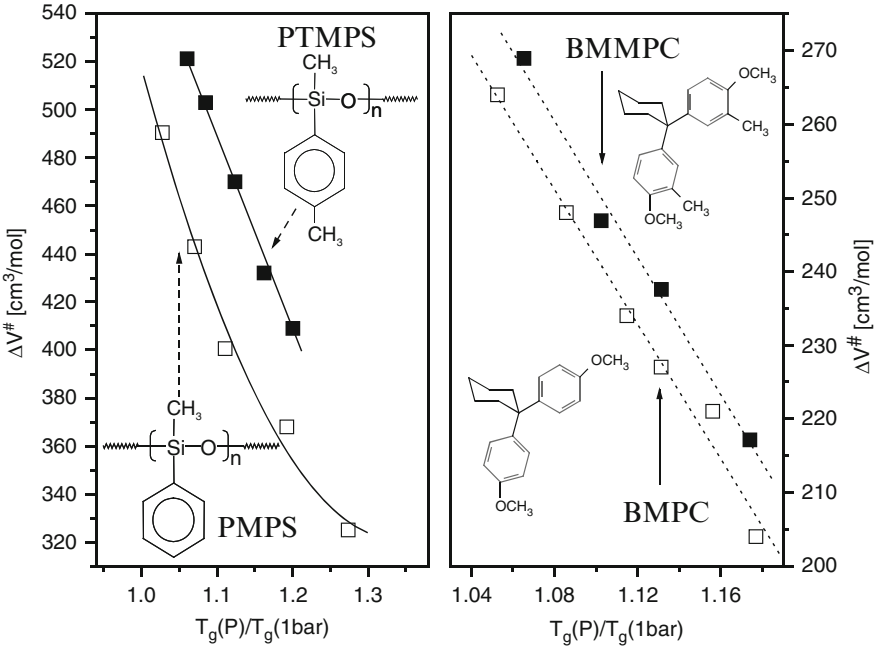

Fig. 1.8 *Left panel* presents temperature dependences of the activation volume for different isobars at constant α-relaxation time for the polymers PTMPS and PMPS. Analogous dependences are shown in the *right panel* for the van der Waals liquids BMMPC and BMPC

of the repeating unit of PTMPS is larger than that for PMPS, and this difference in molecular volumes corresponds to the difference found in values of $\Delta V_\alpha^\#$. A similar pattern of behavior can also be observed for BMMPC and BMPC. The former has two additional methyl groups, and therefore, it needs more space to reorient than the slightly smaller molecule of BMPC.

The relation between the apparent activation volume and the molecular volume has been discussed extensively in recent literature [74–80]. There, it has been shown that $\Delta V^\#$ (1) scales with the temperature difference from T_g for homopolymers of different molecular weights [73, 77], (2) shows a strong T-dependence, especially in the vicinity of T_g, and (3) approaches the monomer volume for temperatures in the range 70–90 K above T_g [76, 80]. Figure 1.9 depicts this situation for the α-process in polyisoprenes of different molecular weights. Clearly, the apparent activation volume depends only on T and not on the polymer molecular weight. The distinctly different pressure sensitivity of the segmental relaxation times of different polymers possessing different monomer units will be employed in Chap. 5 as a fingerprint of the heterogeneous dynamics in miscible or weakly phase-separated polymer blends (in Chap. 5).

Up to now we mainly considered the behavior of activation volume in relation to the pressure dependence of the α-relaxation process for glass-forming liquids and

polymers. As we will discuss in detail in Chap. 4, apart from the slow cooperative (α-) relaxation process, faster relaxation phenomena (known as secondary processes) can also be observed both above and below the glass transition temperature. It is instructive, at this point, to analyze in terms of the apparent activation volume, the pressure dependence of the relaxation times observed in the glassy state of a disaccharide, i.e., maltose [81]. The pressure dependence of secondary relaxation time for this sugar is depicted in Fig. 1.10. Evidently, a simple volume activated law:

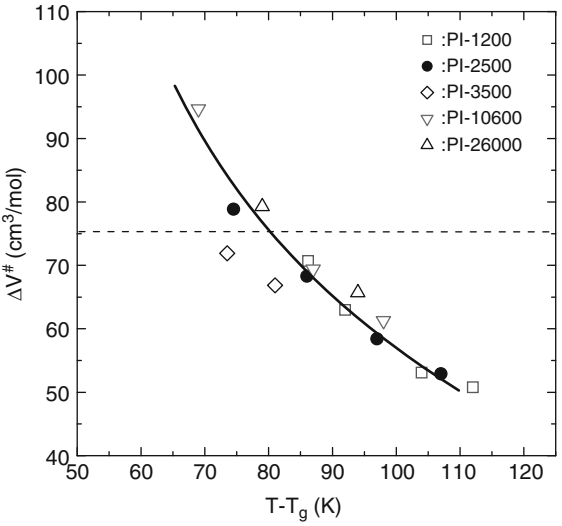

Fig. 1.9 Apparent activation volume for different polyisoprenes plotted as a function of the temperature difference from the respective T_g. The *solid line* is a guide for the eye. The *dashed line* indicates the repeat unit volume (from [77])

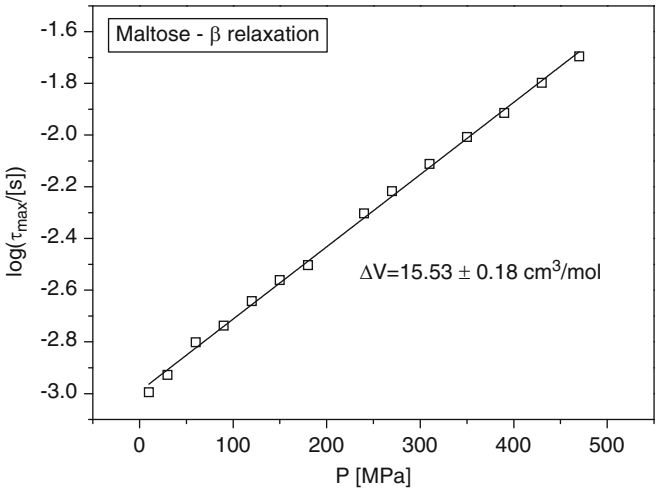

Fig. 1.10 Pressure dependence of β-relaxation times for maltose at $T = 295$ K

$$\tau = \tau_0 \exp\left(\frac{P\Delta V}{RT}\right), \tag{1.13}$$

describes fairly well the experimental data. Consequently, the activation volume for this secondary relaxation is independent of pressure within the glassy state. In the case of maltose it was found that $\Delta V_{\beta}^{\#} = 15\,\mathrm{cm}^3/\mathrm{mol}$. Moreover, it is also possible to determine what local intramolecular motion is responsible for this process by making conformational DFT calculations. Comparing the values of activation energy and activation volume, calculated for various conformational transitions with values of E_β and $\Delta V_\beta{}^{\#}$ determined from the analysis of temperature and pressure dependences of τ_α, it was found that the secondary relaxation of maltose arises from the restricted rotation of the two monosaccharide units around glycosidic linkage. Conformational states of maltose in both activated and nonactivated states obtained from DFT calculations are shown in Fig. 1.11.

Perhaps the best example of a strong secondary process of molecular origin in polymers is the poly(alkylmethacrylates). In contrast to polymers where dipolar groups are rigidly attached to the main chain, poly(alkylmethacrylates) have, in addition, dipole components in the ester side group that are flexibly attached to the main chain that can undergo motions not requiring extensive accompanying motions of the main chains [12]. These side group motions give rise to a β-relaxation process in addition to the primary α-relaxation associated with the glass transition of a polymer. In addition, the relative relaxation strengths of α- and β-processes $R_{\alpha,\beta} = \Delta\varepsilon_\alpha/\Delta\varepsilon_\beta$ depend on the tacticity of the poly(alkylmethacrylate): e.g., for poly(methylmethacrylate) (PMMA) the isotactic polymer has $R_{\alpha,\beta} > 1$, while the syndiotactic polymer has $R_{\alpha,\beta} < 1$ [12, 13].

As an example from this series, we refer to poly(*n*-ethylmethacryate) (PEMA) [32, 34, 82]. The PEMA dynamics comprise four dielectrically active processes; the segmental (α-) process associated with the liquid-to-glass transition, the local β-process at lower temperatures, the mixed (αβ)-process at higher temperatures, and a slower process associated with the ion mobility. Pressure aids in clarifying the origin of the dynamic processes by extracting the pressure sensitivity and the relative contribution of thermal energy and volume for each one of the processes [82].

Figure 1.12 depicts dielectric loss spectra of PEMA at 383.15 K as a function of increasing pressure [82]. Increasing pressure results in the demerging of the single (αβ)-process into two separate processes, α and β. In addition, pressure provides important information on the origins of the different processes that cannot be obtained by temperature variation alone. For example, pressure allows extracting the apparent activation volume for each of the processes. This is depicted in Fig. 1.13. As expected, the α-process has the higher values of $\Delta V^{\#}$ that are strongly T-dependent. Furthermore, studying the same quantity in the remaining processes results in interesting conclusions on their origin. In this respect, the origin of the (αβ)-process and, in particular, its relation to the α- and β-processes have been a point of debate. The apparent activation volume revealed [82] that the mixed (αβ)-process (at high temperatures/frequencies) is the structural relaxation, implying that it presents characteristics of a segmental process and not of the local β-process

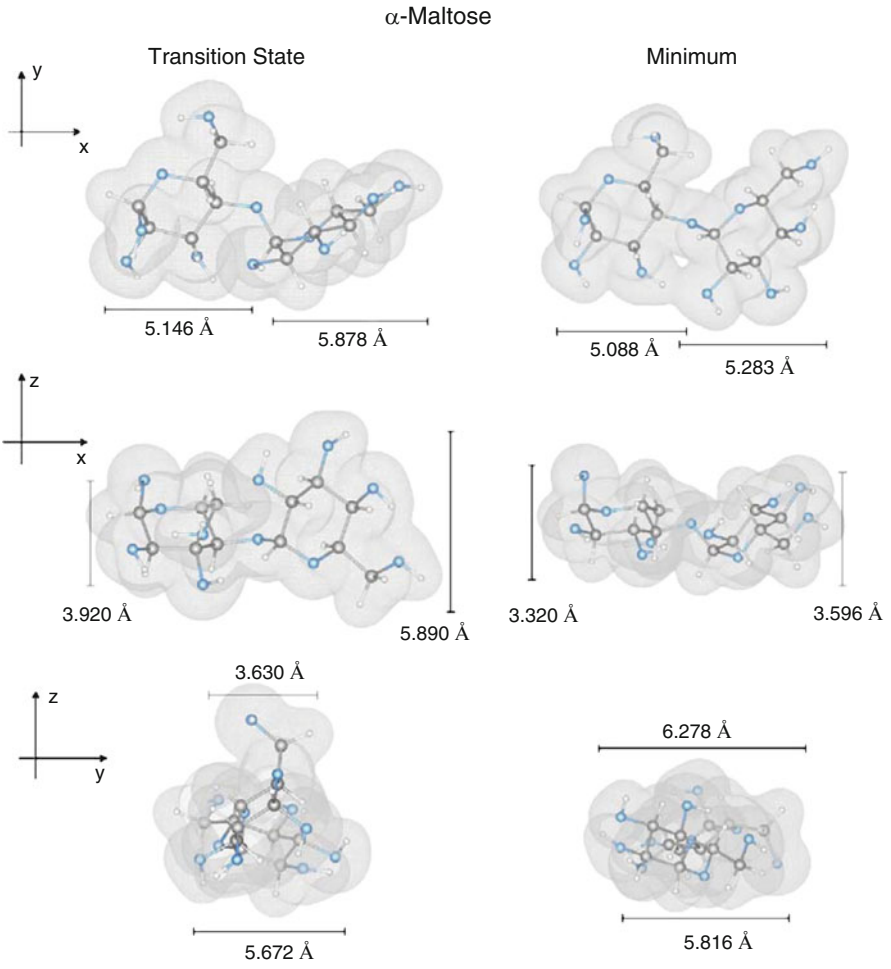

Fig. 1.11 Electron densities of α-maltose represented in *xy*, *xz*, and *yz* planes. Diameters of further constructed ellipsoids are marked

whose apparent activation volume is much smaller (~10–20 cm^3/mol). The same conclusion is reached from the values of the ratio of activation energies (to be discussed below with respect to Chap. 2), Q_V/Q_P, with approximate values of 0.60, 0.90, and 0.68, respectively, for the α-, β- and (αβ)-processes. This value for the (αβ)-process suggests that while it is controlled by both temperature and volume, the former has the greater influence. Ion mobility, despite being five orders of magnitude slower than the (αβ) process, is affected by temperature and volume in the same way as the (αβ) process [82], suggesting that ions in their motion experience a similar local friction. In an effort to rationalize the origin and interrelation among the dielectric α-, β-, and αβ-processes in amorphous polymers

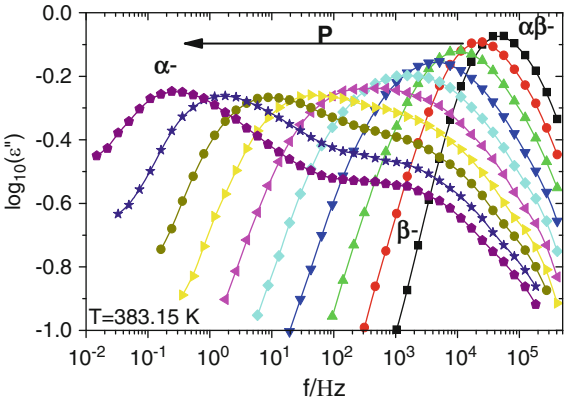

Fig. 1.12 Dielectric loss curves for PEMA ($M_w = 2.0 \times 10^3$ g/mol) under "isothermal" conditions ($T = 383.15$ K). The "isothermal" curves are at (*squares*): 0.1, (*circles*): 30, (*up triangles*): 60, (*down triangles*): 90, (*rhombus*): 120, (*left triangles*): 150, (*right triangles*): 180, (*circles*): 210, (*stars*): 240, and (*pentagons*): 270 MPa (from [82])

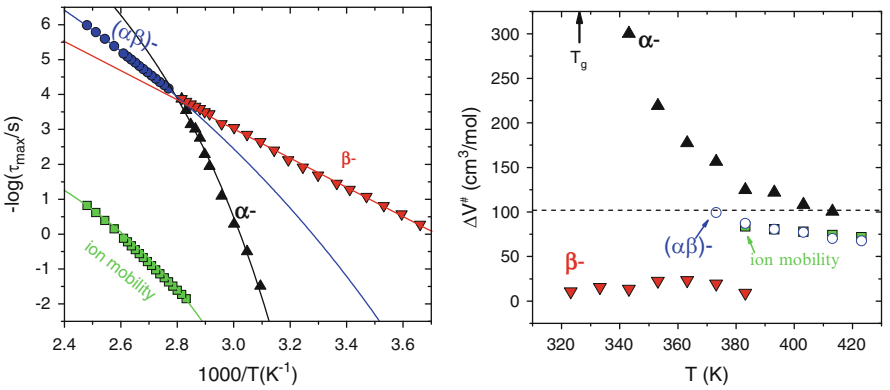

Fig. 1.13 (*Left*): Temperature dependence of the relaxation times (obtained from dielectric spectroscopy) for the different processes in PEMA ($M_w = 2.0 \times 10^3$ g/mol). At higher temperatures, the process due to the ion motion (*squares*) and the (αβ)- (*circles*) relaxation are shown, while at lower temperatures, the α- (*up triangles*) and β- (*down triangles*) processes are shown. The lines are fits to the VFT equation for the slow, (αβ)-, and α-processes, and to the Arrhenius equation for the β-process. (*Right*): Apparent activation volume, $\Delta V^{\#}$, as a function of temperature for the α- (*filled squares*), the (αβ)- (*open up triangles*), the β- (*filled circles*), and the ion mobility (*filled down triangles*) processes of PEMA. The horizontal line gives the repeat unit volume ($V_m = 102$ cm^3/mol) (from [82])

including poly(*n* alkyl methacrylates), Williams [83] introduced the concept of partial and total relaxations of dipolar groups. Details can be found in [82].

Returning to the discussion about the evolution of the structural relaxation times, it should be stressed that the satisfactory fit to experimental data by means of a single temperature VFT law can be often achieved only within a limited temperature range. In a series of papers by Stickel et al. [12, 41, 42, 84], it was pointed out that the temperature dependence of τ_α of many small molecular glass-forming liquids undergoes a change at some intermediate temperature $T_b \sim 1.2T_g$. Therefore, two VFT equations with two different sets of fitting parameters (six in total)

are required to describe the α-relaxation times both above and below this characteristic temperature. To determine the range of validity of the VFT law, as well as the value of T_b, Stickel et al. proposed an analysis of the $\tau_\alpha(T)$ dependence using the following derivative function [41, 84];

$$\phi_T(T) = \left(\frac{\partial \log \tau}{\partial(\mathrm{T}^{-1})}\right)_P^{-0.5}. \tag{1.14}$$

When this operator is applied to the VFT equation, it leads to a linear dependence with respect to T^{-1}:

$$\phi_{\mathrm{VFT}}(T) = (1 - T_0 T^{-1}) B^{-1/2}. \tag{1.15}$$

Thus, the range of validity of the VFT equation can be identified by the presence of a linear $\phi_T(T)$ dependence, as shown in Fig. 1.14 for diethyl phthalate [85].

An analogous behavior can be found in the pressure dependence of τ_α. A change in dynamics above the glass transition at elevated pressures was experimentally observed for a number of glass-forming liquids: KDE [86], PDE [86], Aroclor [87], PC [88], OTP [89], and Salol [89]. Figure 1.15 displays this "crossover" phenomenon identified for PC. Two different pressure VFT equations, valid respectively in two different pressure regimes, separated by P_b, are needed to fit experimental data and this is confirmed by the derivative analysis [87, 89]. In this case, we need to define a new derivative operator

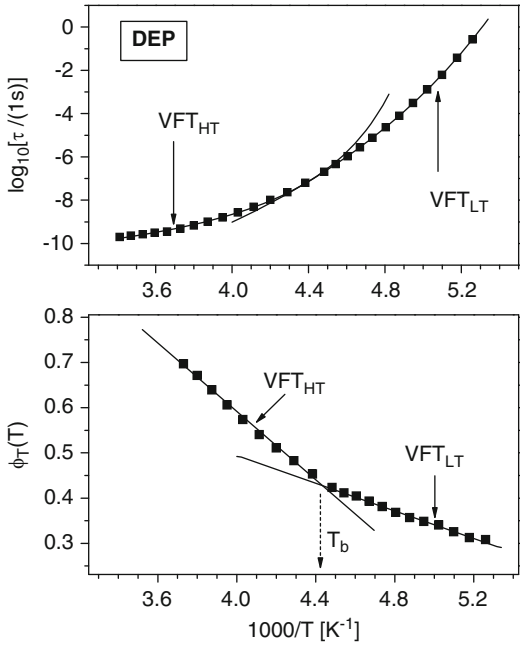

Fig. 1.14 *Upper panel* presents the temperature dependence of structural relaxation times for diethyl phthalate. *Solid lines* indicate two fits to the temperature VFT equation (1.7); $\mathrm{VFT_{HT}}$ well describes the experimental data at high temperatures, whereas $\mathrm{VFT_{LT}}$ at low temperatures. *Lower panel* shows the Stickel analysis. *Solid squares* are obtained from the calculation of differential operator (1.14) by using the temperature dependence of τ shown in the *upper panel*. *Solid lines* are evaluated on the basis of (1.15)

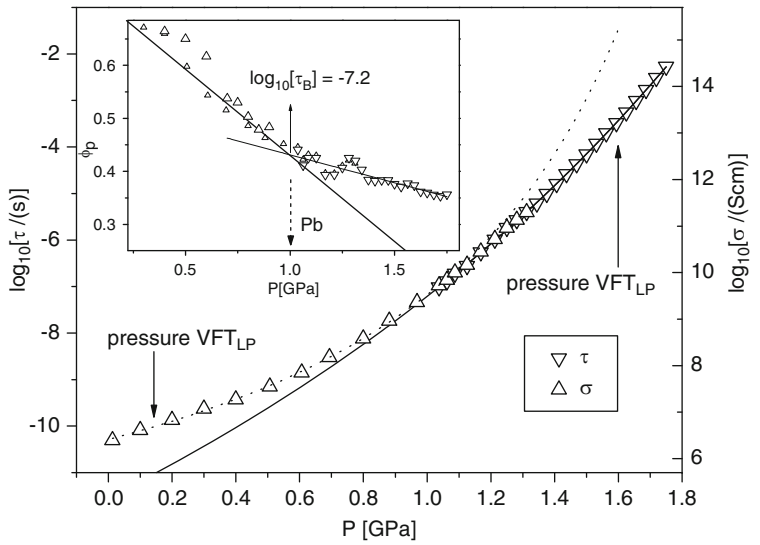

Fig. 1.15 Pressure dependence of structural relaxation times τ (*down triangles*) and dc conductivity relaxation times σ (*up triangles*) for propylene carbonate at $T = 273.2$ K. *Solid* and *dashed lines* indicate two fits to the pressure VFT equation (1.9); VFT_{HP} well describes the experimental data at high pressures, whereas VFT_{LP} at low pressures. The *inset* shows the derivative analysis. Symbols (*down triangles* and *up triangles*) are obtained from the calculation of the differential operators (1.16) by using the pressure dependence of τ and σ shown in the *main panel*. *Solid lines* are evaluated on the basis of (1.17)

$$\phi_P(P) = \left(\frac{\partial \log \tau}{\partial P}\right)_T^{-0.5} \tag{1.16}$$

that transform the pressure VFT equation to a linear form:

$$\phi_{P\,\mathrm{VFT}}(P) = (P_0 - P)(CP_0)^{-1/2}. \tag{1.17}$$

It is worth noticing that for a given liquid, the "crossover" phenomenon occurs at a constant value of τ_α – independent of the temperature and pressure conditions. Thus, the time scale of the structural relaxation is the most important parameter governing the change in dynamics [90].

1.3 The Glass Transition Temperature

Although glass "transition" bears no analogy to a true thermodynamic transition, the corresponding glass temperature is a very useful quantity [91]. There are a number of experimental methods that have been used to define the glass transition

temperature. Among the so-called thermodynamic methods, the most popular are dilatometric and heat capacity measurements. In dilatometry, the temperature dependence of volume of a glass-forming liquid is measured. Determining T_g involves a linear regression on the data as temperatures above and below the glass transition, and the temperature of intersection of these lines is taken as T_g. In an analogous way, one can obtain the value of T_g from calorimetric measurements because the temperature dependence of enthalpy, $Q_P(T)$, reveals the same pattern as the $V(T)$ curve. Alternatively, the glass transition temperature can be determined from the derivatives of $V(T)$ and $Q_P(T)$ as $(\partial \ln V/\partial T)_P$ and $(\partial Q/\partial T)_P$ that correspond to the thermal expansion coefficient and the heat capacity, respectively. These quantities are the largest in the supercooled state and drop to lower values on approaching T_g. On the other hand, taking into account the kinetic/relaxational aspect of vitrification phenomenon, it seems more natural to define T_g in terms of the structural relaxation time. Indeed, the view that a liquid at T_g is a state with an iso-relaxation time became a foundation for the dynamic definition of the glass transition temperature. According to the above view, T_g is usually defined as the temperature where $\tau_\alpha = 100$ s.

The glass transition temperature of glass-forming liquids can be altered by the application of hydrostatic pressure [92–95]. Numerous experimental results show that the value of T_g rises with increasing pressure. Within the free-volume picture, this behavior is attributed to an increase in molecular packing induced by compression. It is remarkable that the $T_g(P)$ dependence displays usually a nonlinear character. In addition, there is a decline of the gradient of the $T_g(P)$ curve on P–T plane, dT_g/dP, that indicates a weaker effect of pressure on increasing T_g at elevated pressure. Both features can be easily recognized in Fig. 1.16 in the case of PDE. They are well reconstructed by means of the following empirical equation [96]:

$$T_g(P) = T_g^0\left(1 + \frac{P}{\Pi}\right)^{1/b}. \tag{1.18}$$

Satisfactory description of $T_g(P)$ data can also be achieved using a second-order polynomial:

$$T_g(P) = T_g^0 + AP + BP^2, \tag{1.19}$$

where $A > 0$ and $B < 0$ are fitting parameters. Although the choice of the formula for the description of the experimental data seems somewhat arbitrary, the former equation (1.18) has some theoretical foundation [97]. It turns out that an analogous equation can be derived from the Avramov model presented in Chap. 3.

The sensitivity of T_g on pressure depends strongly on the material; it is thus useful to define the pressure coefficient of T_g, dT_g/dP. It is known that the values of dT_g/dP for polymers and van der Waals liquids are generally large. At the opposite extreme, there are hydrogen-bonded network glasses and metallic

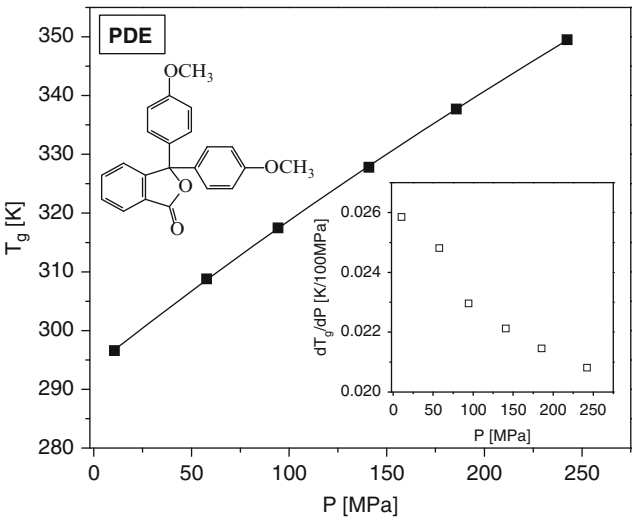

Fig. 1.16 Pressure dependence of the glass transition temperatures T_g for PDE. *Solid line* indicates an experimental data fit to the Andersson–Andersson model (1.18). The *inset* presents pressure dependence of the derivative of T_g with respect P, dT_g/dP

glasses characterized by lower values of this coefficient. The weak pressure effect on T_g, found in this class of materials, is related to their strong and orientationally restricted intermolecular bonds. The values of the pressure coefficient of T_g, dT_g/dP, for various glass-forming liquids are presented in Table 1.1 (see Appendix 1).

Discussing the $T_g(P)$ dependence, we note that dT_g/dP decreases continuously with increasing pressure (see the inset to Fig. 1.16). However, it has been suggested that at very high pressures, the increase of T_g is limited by the appearance of a high temperature asymptote, i.e., $(dT_g/dP) \to 0$ [98–101]. Consequently, a new equation for the $T_g(P)$ dependence has been proposed, namely,

$$T_g = \frac{c}{P - \Pi} + \Theta, \tag{1.20}$$

where Θ and Π denote the high temperature and the negative pressure asymptotes, respectively. On the other hand, Rzoska and coworkers [102] argued that the high temperature asymptote is apparent because dT_g/dP may change sign from positive to negative. Their arguments result from the analysis of experimental $T_g(P)$ data for a few atypical glass formers by using a modified Simon–Glatzel relation [102]:

$$T_g(P) = T_g^0 \left(1 + \frac{\Delta P}{\Pi}\right)^{1/b} \exp\left(-\frac{\Delta P}{c}\right), \tag{1.21}$$

where $\Delta P = P - P_g^0$, and T_g^0 and P_g^0 are, respectively, the correlated reference pressure and temperature, whereas c is the damping coefficient.

1.4 The Concept of Fragility

The temperature dependence of the structural relaxation times or of the viscosity can be analyzed in terms of a property known as fragility. Liquid fragility is a concept commonly used to characterize and classify the dynamic behavior of various glass-forming liquids. The idea of fragility is based on the observation that the degree of deviation of τ_α from the Arrhenius behavior is a material-specific property. A comparison of the different degrees of deviation from the Arrhenius dependence of various glass formers can be made by plotting the structural relaxation time or viscosity as a function of T_g/T (see Fig. 1.17). Oldeskop [103] was the first to use T_g as a corresponding state parameter for the liquid viscosity η in comparing different inorganic liquids. Later on, Laughlin and Uhlmann [104] found differences in the log η vs. T_g/T dependences for three different classes of materials. Finally, Angell [105] recognized the importance of the Uhlmann plot as a method of classifying the transport properties of glass-forming liquids and introduced the terms "fragile," "intermediate," and "strong" to designate these three

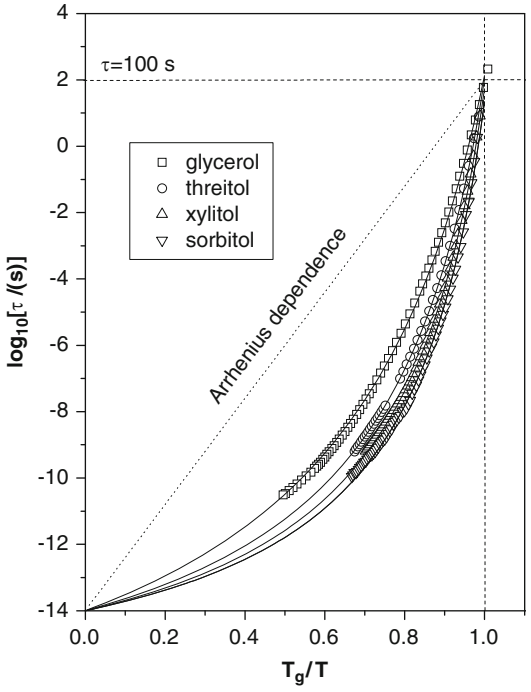

Fig. 1.17 Structural relaxation times as a function of reduced inverse temperature for a polyalcohol series. A nearly Arrhenius temperature dependence for relaxation times is characteristic of *strong* liquids, while *fragile* liquids show a pronounced VFT dependence

classes of glass formers. According to this terminology, "strong" liquids exhibit nearly an Arrhenius dependence of η (or τ_α) on temperature as T_g is approached, whereas "fragile" liquids are characterized by a non-Arrhenius behavior. There is a number of different definitions of fragility [106] used to determine the degree of deviation from the T_g-scaled Arrhenius dependence, but among them the most popular is the isobaric steepness (fragility) index, m_P, defined by

$$m_P = \left(\frac{\partial \log \tau_\alpha}{\partial (T_g/T)}\right)_P \Bigg|_{T=T_g}. \tag{1.22}$$

Introducing pressure as an additional thermodynamic parameter allows extracting the dependence of the structural relaxation times or viscosity and thus of the fragility as a function of pressure. A straightforward method that allows finding the pressure dependence of fragility requires isobaric measurements of the structural relaxation times, $\tau(T)$, at various pressures. Since the experimental dependences of $\tau(T)$ are usually fitted to the VFT equation, the steepness index can be directly calculated using the fitting parameters of the VFT equation:

$$m_P = \frac{BT_g \log_{10} e}{(T_g - T_0)^2}, \tag{1.23}$$

where $T_0 = T_0(P)$ and $T_g = T_0(P)$. An alternative way of extracting the pressure dependence of fragility is the analysis of the isothermal dependences of relaxation times, $\tau(P)$. In this method, the following relationship between the steepness index m_P, the apparent activation volume $\Delta V^{\#}$, and $dT_g/dP (= (\partial T/\partial P)_\tau|_{T=T_g})$ coefficient can be used [107]:

$$m_P = \frac{\Delta V^{\#}}{2.303R\, dT_g/dP}. \tag{1.24}$$

The above equation can be derived from the equation of state for the relaxation time, which can be expressed in following form:

$$f(x, y, z) = 0, \tag{1.25}$$

where $x = P$, $y = T^{-1}$, and $z = \log\tau$.

If variables x, y, and z satisfy the above function then the following identity is valid:

$$\left.\frac{\partial z}{\partial y}\right|_x \left.\frac{\partial y}{\partial x}\right|_z \left.\frac{\partial x}{\partial z}\right|_y = -1. \tag{1.26}$$

Equation (1.24) results from the above identity and (1.12) and (1.22). The numerous experimental results available in the literature suggest a unique behavior

for the pressure dependence of fragility. In the case of simple van der Waals liquids, a drop in fragility at elevated pressures is usually observed. So far, we know only one exception from this rather general rule. The van der Waals material is DHIQ [108] whose isobaric fragility seems to increase with compression. Polymers reveal behavior similar to that of van der Waals liquids. Thus, it can be stated that for both classes of materials, compression reduces the degree of deviation of the structural relaxation times from the Arrhenius behavior (i.e., compression reduces the fragility).

On the other hand, a complex behavior of fragility with pressure is found for associated liquids. As shown in the right panel of Fig. 1.18, the steepness index of hydrogen-bonded glycerol [111] initially increases with pressure, before becoming constant for P greater than ca. 1.5 GPa. An even more puzzling behavior of m_P can be observed for two other H-bonded liquids: di- and tripropylene glycol [109, 112] (their pressure dependences are displayed in the left panel of Fig. 1.18). It can be seen that these dependences exhibit a nonmonotonic character. Such behavior reflects the fact that temperature and pressure can influence the degree of H-bonding in a different manner. The nonmonotonic behavior of m_P, shown in Fig. 1.18, is likely to reflect the competitive contributions of temperature and pressure.

Fragility is commonly perceived as an important parameter characterizing the glass transition because it can be connected to many other liquid properties [113–119]. Among other things, it has been suggested [113] that m_P correlates with the nonexponential relaxation. According to this correlation, an increase in fragility should be manifested by adequate changes in the shape of response function for the α-relaxation process (the width of the α-dielectric loss peak should increase). In this context, it is interesting to consider whether or not a correlation between the shape of the relaxation function and the degree to which the normalized temperature dependence of relaxation times deviates from the Arrhenius dependence is still preserved under condition of high compression. A recently discovered experimental fact is that for a number of glass formers at fixed τ_α, the shape of the

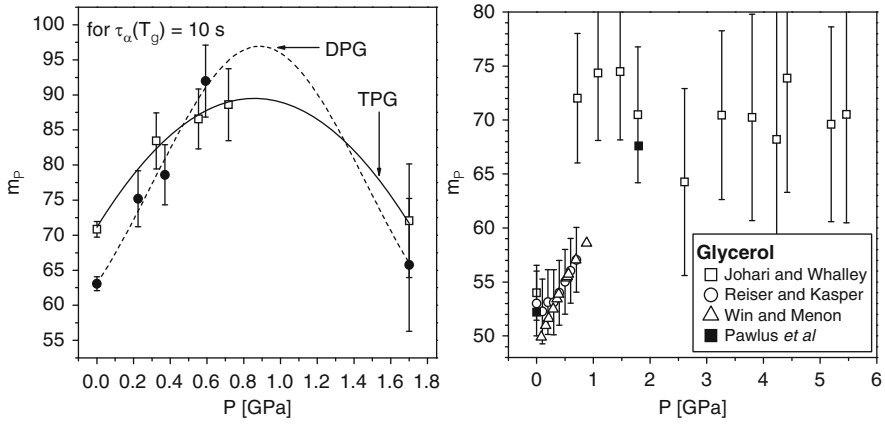

Fig. 1.18 Pressure dependences of the isobaric fragility m_P determined for DPG (*filled circle*), TPG (*open square*) at $\tau_\alpha = 10$ s (*left panel*) [109], and for glycerol (*right panel*) [110]

α-dielectric dispersion appears identical, i.e., is independent of the thermodynamic conditions (T and P) [120]. This suggests that the nonexponentiality parameter characterizing the α-relaxation process is pressure independent at the glass transition point. Taking into account this finding, we reach the conclusion that the quoted correlation between m_P and the nonexponentiality parameter is generally not valid for van der Waals liquids and polymers at elevated pressures.

In analogy with the isobaric fragility concept, Cook and coworkers [121] introduced the fragility parameter at constant temperature as the isothermal steepness index:

$$m_T = \left(\frac{\partial \log \tau_\alpha}{\partial (V_g/V)}\right)_T \Bigg|_{V=V_g}, \tag{1.27}$$

which can be used to characterize the dependence of structural relaxation dynamics on molecular packing. As emphasized by Cook et al. [121], a convenient way to compare the volume dependence of τ_α of various glass formers is by plotting $\log \tau_\alpha$ as a function of V_g/V. Such a representation could be interpreted in a manner analogous to Angell representation of $\log \tau_\alpha$ vs. T_g/T. The essential feature of isothermal fragility is its invariance with respect to temperature for van der Waals liquids and polymers (only some associated liquids are exempted from this rule). Both cases are presented in Fig. 1.19.

Finally, it should be noted that the two fragilities are correlated through

$$\frac{m_P}{m_T} = \frac{1}{\gamma} + T_g \alpha_P(T_g), \tag{1.28}$$

where α_P denotes the isobaric thermal expansion coefficient and γ is a material constant. An interesting conclusion can be drawn from the above relationship. According to the experimentally established rule for van der Waals liquids and polymers, m_P decreases with pressure and m_T is constant along the $T_g(P)$ line. Thus, this empirical fact implies decrease in the product of $\alpha_P T_g$ with pressure.

1.5 Relative Importance of Thermal Energy and Density

Lowering the temperature of a liquid at constant pressure causes both a decrease in kinetic energy (thermal energy) and an increase in the molecular packing due to the increase in density. The dynamic properties of supercooled liquids near T_g are related to these two effects. A fundamental question is whether the dramatic slowing down of the structural relaxation times is governed primarily by the decreasing volume, the decreasing temperature, or both. Early dielectric studies of the α-relaxation in poly(methyl acrylate) [32], poly(ethyl acrylate) [33], and high molecular weight poly(propylene oxide) [122] showed that values of the ratio of the

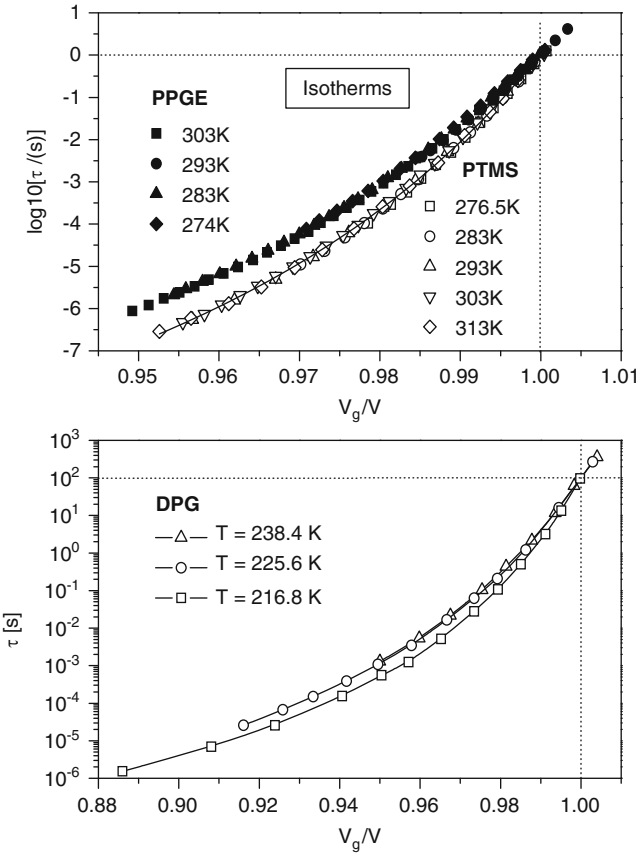

Fig. 1.19 Scaling plots of isothermal α-relaxation times versus V_g/V for polymers: PPGE and PTMS (*upper panel*) as well as for H-bonded liquid: dipropylene glycol (DPG)

apparent activation energy at constant volume, $Q_V(T, V)$, to that at constant pressure, $Q_P(T, P)$, lay in the range 0.7–0.8 [32–34, 83, 123]. As was made clear by Hoffman et al. [124], simple free-volume theories predicted that $Q_V(T, V)$ would be zero and that "a strongly negative coefficient, $(\partial v_0/\partial T)_V$, for the bound volume v_0 would have to be invoked to retain the free-volume approach" – which is an unphysical result. Later Ferrer et al. [125] and others continued to address the question of whether the dramatic slowing down of the structural relaxation times is governed primarily by the decreasing volume, the decreasing temperature, or both. Obviously, a resolution of this problem is essential in formulating a complete theory of the glass transition. Further studies explored the "fine structure" of the dynamic ratio in relation to the nature of the glass formers and the monomeric volume (Chap. 2).

Let us consider now, as extreme cases, the possibility that the molecular dynamics is controlled solely by (1) thermal energy fluctuations or (2) local density fluctuations

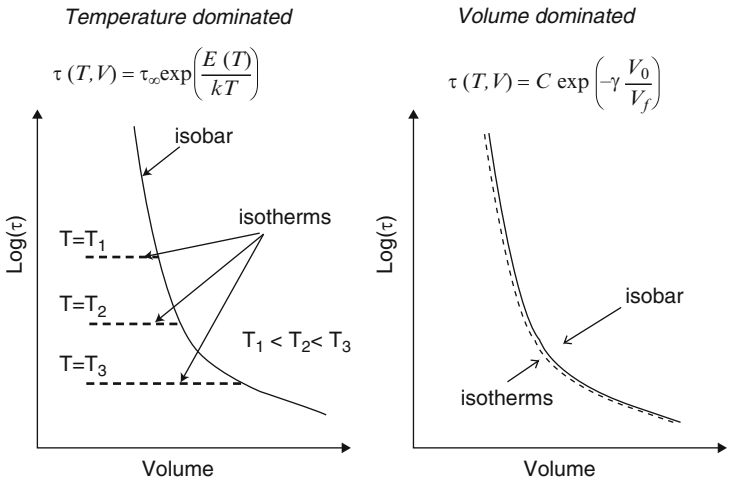

Fig. 1.20 Schematic diagram of isobaric and isothermal dependences of the structural relaxation times vs. volume illustrates two extreme cases when the molecular dynamics is controlled solely by thermal energy fluctuations (*left panel*) and local density fluctuations (*right panel*)

(free volume). Both cases are illustrated schematically in Fig. 1.20 by plotting the isobaric and isothermal dependences of the structural relaxation times on volume. The characteristic feature of the isothermal dependence is the absence of any volume dependence of τ_α, indicating that the structural relaxation process is purely thermally activated. In the second case, the isobaric and isothermal curves superimpose into a master curve and such a behavior is consistent with free-volume approaches.

By constructing analogous plots, as presented in Fig. 1.20, one can qualitatively assess the importance of thermal energy and free-volume contributions to the molecular dynamics near T_g. This procedure usually requires performing two different experiments: measurements of the equation of state (i.e., *PVT* data) and of the α-relaxation times as a function T and P. In practice, the experimentally measured relaxation times are usually not at the same T and P conditions as measured in a *PVT* experiment. Therefore, the experimental *PVT* data are interpolated by means of the Tait equation [see for example 126]:

$$V(T,P) = V(T,0)[1 - 0.0894 \ln(1 + P/B(T))]. \tag{1.29}$$

In this equation, the temperature dependence of volume at fixed pressure is described by a quadratic function

$$V(T,0) = V_0 + V_1 T + V_2 T^2, \tag{1.30}$$

while

$$B(T) = b_0 \exp(-b_1 T). \tag{1.31}$$

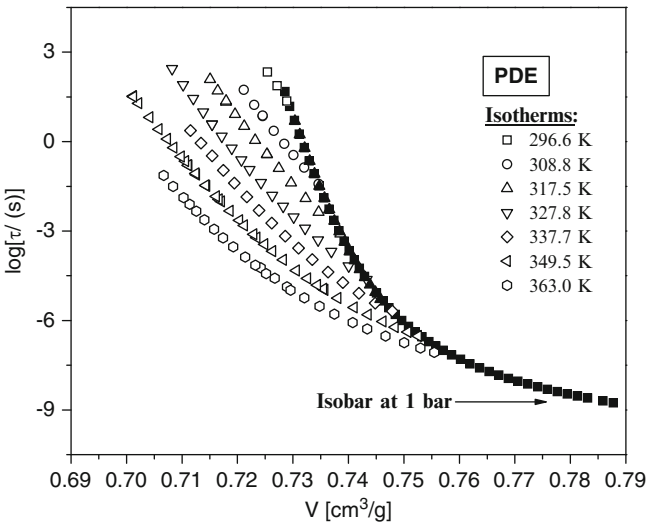

Fig. 1.21 Isothermal (*open symbols*) and isobaric (*filled squares*) dependences of the structural relaxation time on specific volume for PDE

An example of the variation of the dielectric α-relaxation times with volume for the van der Waals liquid PDE [127] is shown in Fig. 1.21. It is evident that the isobaric and isothermal data fall on different curves. In addition, the isothermal data exhibit distinct volume dependences. This shows that for PDE, both thermal energy and free volume govern the relaxation dynamics.

A critical test of the origin of the different processes and of the relative influence of volume and temperature in each case is provided by the value of the ratio $\Re$ of the apparent activation energy at constant volume, $Q_V(T,V)$, to that at constant pressure, $Q_P(T,P)$ [3, 32–34, 66, 123, 128–131]:

$$\Re = Q_V(T,V)/Q_P(T,P) = (\partial \ln \tau_\alpha/\partial(1/T)_V)/(\partial \ln \tau_\alpha/\partial(1/T)_P). \qquad (1.32)$$

The dependence of the relaxation time τ on (T,P,V) has been considered recently [82] in terms of the canonical set of equations for $(\partial \log\tau/\partial X)_Y$, where X and Y are permutations of (T,P,V). These are given in Appendix 2 and show how $\Re$ is related to these derivatives and to the isobaric expansion coefficient α_P, isothermal compressibility β_T, and thermal pressure coefficient $(\partial P/\partial T)_V = (\alpha_P/\beta_T)$.

The dynamic ratio $\Re$ (Fig. 1.22 represents one of the methods used to extract the dynamic ratio) takes values in the range 0–1 and provides a quantitative measure of the role of temperature and density on the dynamics. Values near unity suggest that the dynamics are governed mainly by the thermal energy whereas values near zero suggest that free-volume ideas prevail, since in that case, $Q_V = 0$. However, no polymer or glass-forming liquid has the extreme values of 0 or 1, suggesting that the picture is more complicated than the two extreme cases considered above.

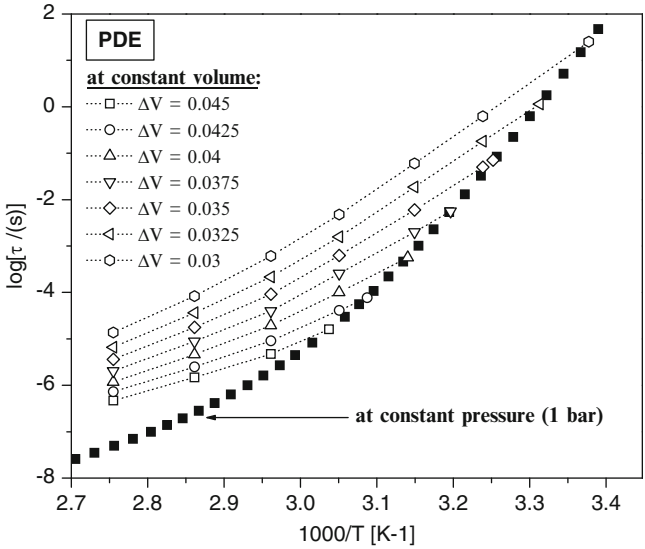

Fig. 1.22 Temperature dependences of the specific volume at constant pressure (*filled squares*) and at constant relaxation time (*open symbols*)

From the analysis of the dynamic ratio for various materials (the data are presented in Table 1.1 of Appendix 1), one can note that there is some characteristic pattern of behavior. For simple van der Waals liquids the ratio takes values around 0.5. Polymers have different values in the range of 0.4–0.8. Finally, associated liquids have values that are close to unity. The significance of the molecular volume in relation to the value of the dynamic ratio will be discussed in Chap. 2, Section 2.2.

In Sect. 1.4, the relationship between isothermal and isobaric fragilities has been reported (1.28). This equation can take the following form:

$$\frac{m_T}{m_P} = \gamma \frac{Q_V}{Q_P}. \tag{1.33}$$

Having already argued that isobaric fragility decreases with pressure and isothermal fragility is temperature independent in the case of van der Waals liquids and polymers, we now claim, based on (1.33), that the dynamic ratio, Q_V/Q_P, should generally increase with compression for these two classes of glasses. Indeed, such a trend has been already reported for PDE and PPGE. Thus, thermal effects may actually become more important at elevated pressure.

Another means of quantifying the relative contributions of thermal energy and volume in the temperature dependence of τ_α is by comparing the coefficient of isobaric expansivity $\alpha_P = (\partial \ln V/\partial T)_P$ to the coefficient of isochronal expansivity $\alpha_\tau = (\partial \ln \tau/\partial T)_P$ (which is a negative quantity since experiments show that the liquid volume always decreases on heating while following an isochrone). There is a direct relationship between α_P/α_τ and $\Re$

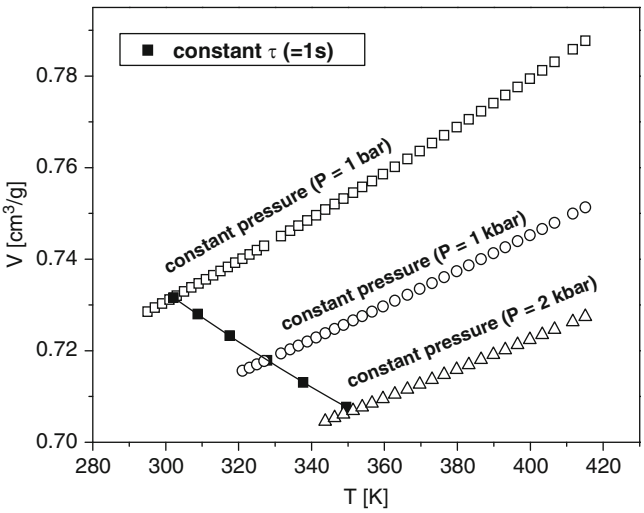

Fig. 1.23 Temperature dependences of the structural relaxation time for PDE at constant pressure (*filled squares*) and at constant volume (*open symbols*)

$$\Re = (1 - \alpha_P/\alpha_\tau)^{-1}. \tag{1.34}$$

As discussed by Ferrer et al. [125], $\lfloor\alpha_\tau\rfloor/\alpha_P \gg 1$ indicates that temperature is the dominant control variable. On the other hand, a near-zero value of the ratio $\lfloor\alpha_\tau\rfloor/\alpha_P$ suggests that the dynamics is mainly governed by volume. $\lfloor\alpha_\tau\rfloor/\alpha_P$ can be calculated from the $V(T)$ behavior evaluated at constant P and at constant τ_α (see Fig. 1.23). A further relation is given by Casalini and Roland [132]:

$$\alpha_P/\alpha_\tau = (1 - (\partial T/\partial P)_V(\partial P/\partial T)_\tau)^{-1}. \tag{1.35}$$

One should take into account that calculating the expansivities α_P and α_τ in (1.34) requires the determination of (1) α_P at the same T_g at which the ratio $\Re$ is established, and (2) α_τ at the relaxation time τ where T_g is found.

In 1964, Williams derived [66] an extension of the Eyring transition state theory for chemical reactions for application to structural relaxation in polymers that gave the following equations:

$$\begin{aligned} -RT^2(\partial \ln\tau/\partial T)_P &= \Delta H^\#(T,P) + RT/2, \\ -RT^2(\partial \ln\tau/\partial T)_V &= \Delta E^\#(T,V) + RT/2, \\ (\partial \ln\tau/\partial P)_T &= \Delta V^\#(T,P)/RT. \end{aligned} \tag{1.36}$$

Here $\Delta H^\#$, $\Delta E^\#$, and $\Delta V^\#$ are, respectively, the "activation enthalpy," "activation internal energy," and "activation volume," defined with respect to unactivated and

activated standard states of a relaxor. It is apparent that the ratio $\Re$ corresponds to $\Delta E^{\#}/\Delta H^{\#}$, ignoring the small term RT/2. This analysis has been further discussed in several papers, with a special consideration of the standard states being given by Albuquerque and Reis [67, 68] in their comprehensive thermodynamic formalism for the constant volume principle as applied to chemical reactions and molecular relaxation processes.

Appendix 1

Appendix 2

Derivation of the ratio of activation energies $\Re$ (from [82]).

The ratio $\Re$ of the apparent activation energy at constant volume, $Q_V(T,V)$, to that at constant pressure, $Q_P(T,P)$

$$\Re = \frac{(\partial \ln \tau/\partial(1/T)_V)}{(\partial \ln \tau/\partial(1/T)_P)} = \frac{Q_V(T,V)}{Q_P(T,P)}, \tag{1.37}$$

assumes values in the range $0 \leq \Re < 1$ and provides a quantitative measure of the role of temperature and density on the dynamics. Herein we review the effects of [*T*,*P*,*V*] on a relaxation time τ in *one theoretical framework*. We form the ratios $(\partial \ln \tau/\partial W)_X/(\partial \ln \tau/\partial Y)_Z$ where (*W*,*X*,*Y*,*Z*) are permutations of (*V*,*T*,*P*). For brevity and convenience we employ a compact notation $(\partial \ln \tau/\partial W)_X = WX$ that uses only the subscripts *WX*, so the required ratios are given by

$$\frac{(\partial \ln \tau/\partial W)_X}{(\partial \ln \tau/\partial Y)_Z} = \frac{WX}{YZ}. \tag{1.38}$$

Writing $\tau = \tau(T,P)$ and $V = V(T,P)$, there are thirty six possible ratios *WX*/*YZ*. We seek those ratios that allow (*WX*/*YZ*) to be related to $\Re$ and certain thermodynamic properties for a material. The six special cases *WX*/*WX*, e.g., *PT*/*PT*, are all unity so are discarded. Twelve ratios of the form *YZ*/*WX* where $X \neq Z$ are reciprocals of *WX*/*YZ*, so are eliminated, while three ratios of the form *WX*/*YX* are reciprocals of *YX*/*WX* and are also eliminated. This leaves fifteen ratios to be determined. Each ratio can be expressed as functions of $\Re$ and the isobaric expansion coefficient $\alpha_P = (\partial \ln V/\partial T)_P$, the isothermal compressibility $\beta_T = -(\partial \ln V/\partial P)_T$, and the

Table 1.1 Parameters characterizing molecular dynamics near the glass transition, which have been obtained by means of different experimental methods for different classes of materials

Class of material	Material and its acronym	T_g [K] (at $P = 0.1$ MPa)	$\left.\frac{dT_g}{dP}\right\|_{P\to 0}$ [K/GPa]	$\frac{Q_V}{Q_P}$ (at $P = 0.1$ MPa and $\tau_\alpha = 1$s)	γ	m_P (at $P = 0.1$ MPa)	$\left.\frac{dm_P}{dP}\right\|_{P\to 0}$ [GPa^{-1}] (at $\tau_\alpha = 1$s)
van der Waals liquids	Phenylphthalein-dimethylether (PDE)	249 (diel)	260 (diel) [86]	0.53	4.5	71	≈0
							−30
					4.4		−24
	o-terphenyl (OTP)	244 (diel)	260 (DTA)	0.55	4	82	
		246 (DTA)			4.25		
	Cresolphthalein-dimethylether (KDE)	313 (diel)	307 (diel)	0.49	4.5	64	−17
					4.8		
	Propylene carbonate (PC)	159 (diel)		0.64	3.7	81	−18
	Diglycidylether of bisphenol A	335 (diel)		0.6	2.8	95	≈0
					3.6		
	1,1'-di(4-methoxy-5-methylphenyl) - cyclohexane (BMMPC)	261 (diel)	270 (diel)	0.41	8.5	58	−23
		263 (LS)	227 (LS)		7.5		
	1,1'-bis(*p*-methoxyphenyl) cyclohexane (BMPC)	241 (diel)	240 (diel)	0.39	7	70	−25
		247 (LS)	182 (LS)		6.4		
Hydrogen bonded systems	Salol	221 (diel)	204 (diel)	0.43	5.2	68	−11
	Propylene glycol (PG)	185 (diel)	37 (diel)	0.67	2.5	49	>0
	Propylene glycol dimer (DPG)	210 (diel)	80 (diel)			70	>0
	Propylene glycol trimer (TPG)	206 (diel)	109 (diel)			80	>0
	1-propanol	95 (PVT)	70 (PVT)				
	D-sorbitol	267 (DTA)	43 (DTA)	0.87	0.13	128	
		273 (diel)	40 ± 5 (diel)				
	Glycerol	183 (PVT)	40 (PVT)	0.94	1.8	40	+35
		188 (diel)	27 (diel)				

			35 ± 3 (diel)				
							+40
	m-fluoroaniline (m-FA)	171 (diel)	81 (diel)		2.7 [46]		
Polymers	Polystyrene (PS)	373 (PVT) 373 (DTA)	360 (PVT) 303 (DTA)	0.64		77	−160
	Polyvinylacetate (PVAc)	302 (diel) 298 (PVT)	250 (diel) 220 (PVT)	0.6	2.6 1.4	61	≈0
	Poly(2-vinylpyridine) (P2VP)	337 (diel)	340 (diel)	0.72			
	Polymethyltolylsiloxane (PMTS)	261 (diel) 250 (diel)	340 (diel) 380 (diel)	0.55 0.59	5.0		−27
	Poly(phenol glycidyl ether)-co-formaldehyde (PPGE)	258 (diel)	154 (diel)	0.63	3.5	95	≈0
	1,2-polybutadiene (1,2-PB)	253 (diel)	240 (diel)	0.70	1.9	88	−35
	Polyvinylmethylether (PVME)	247 (diel)	177 (diel)	0.69	2.5 2.7	75	−4
	Polyvinylethylether (PVEE)	241 (diel)	215 (diel)	0.81			
	Polymethylmethacrylate (PMMA)	378 (PVT)	240 (PVT)		1.25	122	
	1,4-polyisoprene (1,4-PI)	201 (diel) 250	178 (diel)	0.96 0.76	3.0		

diel dielectric study, *PVT* volumetric measurements, *LS* light scattering, *DTA* differential thermal analysis

The detailed references to works reporting collected herein values of the glass transition temperature (T_g), the isobaric fragility (m_P), the pressure coefficients of T_g and m_P in the zero pressure limit ($dT_g/dP|_{P\to 0}$ and $dm_P/dP|_{P\to 0}$), the ratio of the isochoric activation energy and the enthalpy (Q_V/Q_P), and the scaling exponent γ can be almost entirely found in [133]

thermal pressure coefficient $(\partial P/\partial T)_V = \alpha_P/\beta_T$. There are different routes to obtain these ratios so, for convenience to a reader, details of the derivations are given below.

Ratios with $W = Y, X \neq Z$:

$$\frac{VP}{VT} = \frac{(\partial \ln \tau/\partial V)_P}{(\partial \ln \tau/\partial V)_T} = (1-\Re)^{-1} = 1 - \frac{(\partial V/\partial T)_\tau}{(\partial V/\partial T)_P}, \tag{1.39}$$

$$\frac{TV}{TP} = \frac{(\partial \ln \tau/\partial T)_V}{(\partial \ln \tau/\partial T)_P} = \Re = 1 - \frac{(\partial T/\partial P)_\tau}{(\partial T/\partial P)_V} = \frac{(\partial V/\partial P)_\tau}{(\partial V/\partial P)_T}, \tag{1.40}$$

$$\frac{PV}{PT} = \frac{(\partial \ln \tau/\partial P)_V}{(\partial \ln \tau/\partial P)_T} = -\Re(1-\Re)^{-1} = 1 - \frac{(\partial P/\partial T)_\tau}{(\partial P/\partial T)_V}. \tag{1.41}$$

Ratios with $W = Z, X = Y$:

$$\frac{TV}{VT} = \Re(1-\Re)^{-1}(\partial V/\partial T)_P = -\left(\frac{\partial V}{\partial T}\right)_\tau, \tag{1.42}$$

$$\frac{PV}{VP} = -\Re(\partial V/\partial P)_T = -\left(\frac{\partial V}{\partial P}\right)_\tau, \tag{1.43}$$

$$\frac{PT}{TP} = -\frac{(1-\Re)}{(\partial P/\partial T)_V} = -\left(\frac{\partial T}{\partial P}\right)_\tau. \tag{1.44}$$

Ratios with $W = Z, X \neq Y$:

$$\frac{TP}{VT} = (1-\Re)^{-1}\left(\frac{\partial V}{\partial T}\right)_P, \tag{1.45}$$

$$\frac{TV}{PT} = -\Re(1-\Re)^{-1}\left(\frac{\partial P}{\partial T}\right)_V, \tag{1.46}$$

$$\frac{PT}{VP} = (1-\Re)\left(\frac{\partial V}{\partial P}\right)_T, \tag{1.47}$$

$$\frac{PV}{TP} = \frac{\Re}{(\partial P/\partial T)_V}, \tag{1.48}$$

$$\frac{VP}{TV} = \frac{\Re^{-1}}{(\partial V/\partial T)_P}, \tag{1.49}$$

$$\frac{VT}{PV} = -\Re^{-1}\frac{(1-\Re)}{(\partial V/\partial P)_T}. \tag{1.50}$$

Ratios with $W \neq Z, X \neq Y$:

$$\frac{TV}{PV} = \left(\frac{\partial P}{\partial T}\right)_V, \tag{1.51}$$

$$\frac{VP}{TP} = \frac{1}{(\partial V/\partial T)_P}, \tag{1.52}$$

$$\frac{PT}{VT} = \left(\frac{\partial V}{\partial P}\right)_T. \tag{1.53}$$

Case 1. $W = Y, X \neq Z$:
For example, *VP*/*VT*, (1.39) of the text, is obtained as follows:
We start by writing $\tau = \tau(T,V)$, $\tau = \tau(T,P)$ with $V = V(T,P)$ giving,

$$\left(\frac{\partial \ln\tau}{\partial V}\right)_P = \left(\frac{\partial \ln\tau}{\partial T}\right)_V\left(\frac{\partial T}{\partial V}\right)_P + \left(\frac{\partial \ln\tau}{\partial V}\right)_T, \tag{1.54a}$$

$$\left(\frac{\partial \ln\tau}{\partial T}\right)_P = \left(\frac{\partial \ln\tau}{\partial T}\right)_V + \left(\frac{\partial \ln\tau}{\partial V}\right)_T\left(\frac{\partial V}{\partial T}\right)_P, \tag{1.54b}$$

hence,

$$\begin{aligned}\left(\frac{VP}{VT}\right) &= \frac{(\partial \ln\tau/\partial V)_P}{(\partial \ln\tau/\partial V)_T} = 1 + \left(\frac{(\partial \ln\tau/\partial T)_V(\partial T/\partial V)_P}{(\partial \log\tau/\partial V)_T}\right)\\ &= 1 - \frac{(\partial V/\partial T)_\tau}{(\partial V/\partial T)_P}.\end{aligned} \tag{1.54c}$$

Using (1.54b) to replace $(\partial \ln\tau/\partial V)_T$ on the right hand side of (1.54c) gives

$$\frac{VP}{VT} = (1-\Re)^{-1}. \tag{1.54d}$$

Equations (1.54c) and (1.54d) correspond to (1.39) of the text. Equation (1.40) follows from the definition of $\Re$ while (1.41) is obtained by a procedure similar to that used to derive (1.39).

Case 2. $W = Z, X = Y$:
For example, *PT*/*TP*, (1.44) of the text, is obtained by writing $\tau = \tau(T,P)$

$$\left(\frac{\partial \ln\tau}{\partial T}\right)_V = \left(\frac{\partial \ln\tau}{\partial T}\right)_P + \left(\frac{\partial \ln\tau}{\partial P}\right)_T\left(\frac{\partial P}{\partial T}\right)_V, \tag{1.54e}$$

$$\frac{PT}{TP} = \left(\frac{(\partial \ln \tau/\partial T)_V - (\partial \ln \tau/\partial T)_P}{(\partial \ln \tau/\partial T)_P (\partial P/\partial T)_V}\right) = -\left(\frac{(1-\Re)}{(\partial P/\partial T)_V}\right) = -\left(\frac{\partial T}{\partial P}\right)_\tau. \quad (1.54f)$$

Equations (1.42) and (1.43) of the text are obtained by a similar procedure, writing $\tau = \tau(T, V)$and $\tau = \tau(P, V)$, respectively.

Case 3. $W = Z, X \neq Y$:

For example, *TP*/*VT*, (1.45) of the text, is obtained from (1.40) and (1.42) as

$$\frac{(TV/VT)}{(TV/TP)} = \left(\frac{\partial V}{\partial T}\right)_P (1-\Re)^{-1}. \quad (1.54g)$$

In a similar manner, (1.40) and (1.44) give *TV*/*PT*, (1.46); (1.41) and (1.43) give *PT*/*VP*, (1.47); (1.41) and (1.44) give *PV*/*TP*, (1.48); (1.39) and (1.42) give *VP*/*TV*, (1.48); while (1.41) and (1.43) give *VT*/*PV*, (1.50).

Case 4. $W \neq X, Y \neq Z$:

For example, (1.51)–(1.53) may be confirmed as follows; e.g., for (1.53) using (1.44) and (1.50)

$$\frac{PT}{VT} = \left(\frac{PT}{PV}\right)\left(\frac{PV}{VT}\right) = \left(\frac{\partial V}{\partial P}\right)_T. \quad (1.54h)$$

References

1. Zallen R (1983) The physics of amorphous materials. Wiley-Interscience, New York
2. Ediger MD, Angell CA, Nagel SR (1996) J Phys Chem 100:13200
3. Ehrenfest P (1933) Leiden Comm (Suppl 726)
4. Gee G (1947) Quart Rev 1:265
5. Hirai N, Eyring H (1959) J Polym Sci 37:51
6. Prigogine I, Defay R (1954) Chemical thermodynamics, Chapter 19. Longmans-Green, NY
7. Gupta PK, Moynihan CT (1976) J Chem Phys 65:4136
8. Moynihan CT, Lesikar AV (1981) Ann NY Acad Sci 371:151
9. Goldstein M (1975) J Appl Phys 46:4153
10. Debenedetti PG (1996) Metastable liquids – concepts and principles. Princeton Academic Press, Princeton, NJ
11. Angell CA, Ngai KL, McKenna GB, McMillan PF, Martin SW (2000) J Appl Phys 88:3113
12. Kremer F, Schönhals A (eds) (2003) Broadband dielectric spectroscopy. Springer, Berlin
13. McCrum NG, Read BE, Williams G (1991) Anelastic and dielectric effects in polymeric solids. Dover, New York
14. Ferry JD (1970) Viscoelastic properties of polymers. Wiley, New York
15. Kohlrausch R (1847) Ann Phys 12:393
16. Williams G, Watts DC (1970) Trans Faraday Soc 66:80
17. Williams G, Watts DC, Dev SB, North AM (1971) Trans Faraday Soc 67:1323

18. Havriliak S, Negami S (1966) J Polym Sci C 16:99
19. Havriliak S, Negami S (1967) Polymer 8:161
20. Havriliak S, Havriliak SJ (1997) Dielectric and mechanical relaxation in materials. Hanser, München
21. Williams G (1991) J Non-Cryst Solids 131:1
22. Ngai KL (2000) J Non Cryst Solids 275:7
23. Kivelson D, Tarjus G (1998) J Non Cryst Solids 235/237:86
24. Dyre JC (2006) Rev Mod Phys 78:953
25. Kovacs AJ, Aklonis JJ, Hutchinson JM, Ramos AR (1979) J Polym Sci Polym Phys 17:1097
26. Hutchinson JM (1995) Prog Polym Sci 20:703
27. Hodge IM (1994) J Non-Cryst Solids 169:211
28. Simon LS, McKenna GB (1997) J Chem Phys 107:8678
29. Matsuoka S, Willimas G, Johnson GE, Anderson EW, Furukawa T (1985) Macromolecules 18:2652
30. (1991) 1st International discussion meeting on relaxation in complex systems (IDMRCS), 1990, Heraklion, Crete. J Non-Cryst Solids 131–133
31. O'Reilly J (1962) J Polym Sci 47:429
32. Williams G (1964) Trans Faraday Soc 60:1556
33. Williams G (1966) Trans Faraday Soc 62:2091
34. Sasabe H, Saito S (1968) J Polym Sci A-2(6):1401
35. Fytas G, Dorfmüller Th, Wang CH (1983) J Phys Chem 87:5045
36. Fytas G, Patkowski A, Meier G, Dorfmüller Th (1984) J Chem Phys 80:2214
37. Patkowski A, Paluch M, Kriegs H (2002) J Chem Phys 117:2192
38. Herbst CA, Cook RL, King HE Jr (1993) Nature 361:518
39. Cook RL, Herbst CA, King HE Jr (1993) J Phys Chem 97:2355
40. Hollander AGS, Prins KO (2001) J Non Cryst Solids 286:1
41. Stickel F, Fischer EW, Richert R (1995) J Chem Phys 102:6521
42. Stickel F, Fischer EW, Richert R (1996) J Chem Phys 10:2043
43. Vogel H (1921) Phys Z 22:645
44. Fulcher GS (1923) J Am Ceram Soc 8:339
45. Tammann G, Hesse W (1926) Z Anorg Allg Chem 156:245
46. Cohen MH, Turnbull D (1959) J Chem Phys 31:1164
47. Adam G, Gibbs JH (1965) J Chem Phys 43:139
48. Paluch M, Rzoska SJ, Habdas P, Ziolo J (1996) J Phys Condens Matter 8:10885
49. Corezzi S, Rolla PA, Paluch M, Ziolo J, Fioretto D (1999) Phys Rev E 60:4444
50. Johari GP (1973) J Chem Phys 58:1766
51. Doolitle AK, Doolitle DB (1957) J Appl Phys 28:901
52. Paluch M, Ziolo J, Rzoska SJ, Habdas P (1996) Phys Rev E 54:4008
53. Paluch M, Roland CM, Pawlus S, Ziolo J, Ngai KL (2003) Phys Rev Lett 91:115701
54. Kriegs H, Gapinski J, Meier G, Paluch M, Pawlus S, Patkowski A (2006) J Chem Phys 124:104901
55. Rivera-Calzada A, Paluch M, Kaminski K, Leon C (2008) J Phys Chem B 20:244107
56. Paluch M, Rzoska SJ, Habdas P, Ziolo J (1998) J Phys Condens Matter 10:4131
57. Paluch M, Ziolo J (1998) Europhys Lett 44:315
58. Suzuki A, Masuko M, Nakayama T, Okabe H (1997) Jpn J Tribol 42:468
59. Suzuki A, Masuko M, Nikkuni T (2000) Trib Intern 33:107
60. Casalini R, Paluch M, Psurek T (2004) J Mol Liq 111:53
61. Paluch M, Dendzik Z, Rzoska SJ (1999) Phys Rev B 60:2979
62. Paluch M, Patkowski A, Fischer EW (2000) Phys Rev Lett 85:2140
63. Glasstone ST, Leidler KJ, Eyring H (1941) Theory of rate process. McGraw Hill, New York
64. Guggenheim EA (1937) Trans Faraday Soc 33:607
65. Slater NB (1959) Theory of unimolecular reactions. Comell University Press, Ithaca, New York
66. Williams G (1964) Trans Faraday Soc 60:1548

67. Albuquerque LMPC, Reis JCR (1989) J Chem Soc Faraday Trans 85:207
68. Albuquerque LMPC (1991) J Chem Soc Faraday Trans 87:1553
69. Paluch M, Ngai KL, Henel-Bielowka S (2001) J Chem Phys 114:10872
70. Paluch M, Grzybowska K, Grzybowski A (2007) J Phys Condensed Matter 19:205117
71. Paluch M, Roland CM, Pawlus S (2002) J Chem Phys 116:10932
72. Paluch M, Pawlus S, Roland M (2002) Macromolecules 35:7338
73. Casalini R, Paluch M, Roland CM (2003) Phys Rev E 67:031505
74. Floudas G (2004) Prog Polym Sci 29:1143
75. Floudas G (2002) In: Kremer F, Schönhals A (eds) Broadband dielectric spectroscopy. Berlin, Springer
76. Floudas G, Reisinger T (1999) J Chem Phys 111:5201
77. Floudas G, Gravalides C, Reisinger T, Wegner G (1999) J Chem Phys 111:9847
78. Mpoukouvalas K, Floudas G, Verdonck B, Du Prez FE (2005) Phys Rev E 72:011802
79. Mpoukouvalas K, Gomopoulos N, Floudas G, Herrmann C, Hanewald A, Best A (2006) Polymer 47:7170
80. Papadopoulos P, Peristeraki D, Floudas G, Koutalas G, Hadjichristidis N (2004) Macromolecules 37:8116
81. Wlodarczyk P, Kaminski K, Adrjanowicz K, Wojnarowska Z, Czarnota B, Paluch M, Ziolo J, Pilch J (2009) J Chem Phys 131:125103
82. Mpoukouvalas K, Floudas G, Williams G (2009) Macromolecules 42:4690
83. Williams G (1979) Adv Polym Sci 33:60
84. Stickel F (1995) Ph.D Thesis, Main University, Germany (Shaker, Aachen)
85. Pawlus S, Paluch M, Sekula M, Ngai KL, Rzoska SJ, Ziolo J (2003) Phys Rev E 68:021503
86. Casalini R, Paluch M, Roland CM (2003) J Phys Cond Matter 15:859
87. Casalini R, Paluch M, Roland CM (2003) J Chem Phys 118:5701
88. Pawlus S, Casalini R, Roland CM, Paluch M, Rzoska SJ, Ziolo J (2004) Phys Rev E 70:061501
89. Casalini R, Roland CM (2004) Phys Rev Lett 92:245702
90. Casalini R, Ngai KL, Roland CM (2003) Phys Rev B 68:014201
91. Goldstein M (1973) J Phys Chem 77:667
92. Atake T, Angell CA (1979) J Phys Chem 83:3218
93. Floudas G, Pakula T, Fischer EW (1994) Macromolecules 27:917
94. Paluch M, Hensel-Bielowka S, Ziolo J (1999) J Chem Phys 110:10978
95. Paluch M, Hensel-Bielowka S, Ziolo J (2000) Phys Rev E 61:526
96. Andersson S, Andersson O (1998) Macromolecules 31:2999
97. Paluch M, Hensel-Bielowka S, Psurek T (2001) J Chem Phys 113:4374
98. DiMarzio ED, Gibbs JH, Fleming PD, Sanchez AJ (1976) Macromolecules 9:763
99. Bengtzelius U, Goetze W (1994) Sjoelander J 17:5914
100. Skorudonov V, Godovskii YuK (1993) Polym Sci Ser A Ser B 35:562
101. Donth E (2001) The Glass transition: relaxation dynamics in liquids and disordered material, vol II, Springer Series in Materials Science. Springer, Berlin
102. Drozd-Rzoska A, Rzoska SJ, Paluch M, Imre AR, Roland CM (2007) J Chem Phys 126:164504
103. Oldeskop VW (1957) Glastech Ber 30:8
104. Laughlin WT, Uhlmann DR (1972) J Chem Phys 76:2317
105. Angell CA (1991) J Non Cryst Solids 131/133:3
106. Richert R, Angell CA (1998) J Chem Phys 108:9016
107. Paluch M, Gapinski J, Patkowski A, Fischer EW (2001) J Chem Phys 114:8048
108. Paluch M, Pawlus S, Hensel-Bielowka S, Kaminska E, Prevosto D, Cappacioli S, Rolla PA, Ngai KL (2005) J Chem Phys 122:234506
109. Grzybowska K, Pawlus S, Mierzwa M, Paluch M, Ngai KL (2006) J Chem Phys 125:144507
110. Pawlus S, Paluch M, Roland CM (2009) J Phys: Condens Matter 21:332101
111. Paluch M, Casalini R, Hensel-Bielowka S, Roland CM (2002) J Chem Phys 116:9839

112. Casalini R, Roland CM (2003) J Chem Phys 119:11951
113. Böhmer R, Ngai KL, Angell CA (1993) Plazek DJ 99:4201
114. Plazek DJ, Ngai KL (1991) Macromolecules 24:1222
115. Roland CM, Ngai KL (1993) Macromolecules 24:5315; (1992) 25:1844
116. Ngai KL, Roland CM (1993) Macromolecules 26:6824
117. Roland CM (1992) Macromolecules 25:7031
118. Angell CA, Pool PH, Shao J (1994) Nuovo Cimento A 16:883
119. Roland CM, Ngai KL (1996) J Chem Phys 104:2967
120. Ngai KL, Casalini R, Capaccioli S, Paluch M (2005) Roland CM J Phys Chem B 106:17356
121. Cook RL, King HE, Herbst CA, Herschbach DR (1994) J Chem Phys 100:5178
122. Williams G (1965) Trans Faraday Soc 61:1564
123. Williams G, Watts DC (1972) In: Karasz FE (ed) Dielectric properties of polymers. Plenum, New York
124. Hogffman JD, Williams G, Passaglia E (1966) J Polym Sci C 173
125. Ferrer ML, Lawrence C, Demirjin BG, Kivelson D, Alba-Simonesco C, Tarjus G (1998) J Chem Phys 109:8010
126. Jain RK, Simha R (1989) Macromolecules 22:464
127. Paluch M, Casalini R, Roland CM (2002) Phys Rev B 66:092202
128. Jobling A, Lawrence ASC (1951) Proc R Soc Lond A 206:257
129. MacKenzie JD (1958) J Chem Phys 28:1037
130. Williams G, Watts DC (1971) In: Diehl P, Flick E, Kosfeld E (eds) NMR basic principles and progress, vol 4. Springer, Berlin, p 271
131. Naoki M, Endou H, Matsumoto K (1987) J Phys Chem 91:4169
132. Casalini R, Roland CM (2003) J Chem Phys 119:4052
133. Roland CM, Hensel-Bielowka S, Paluch M, Casalini R (2005) Rep Prog Phys 68:1405

Chapter 2
Origin of Glass Formation

Identifying the main control parameter that dominates the slow dynamics in glass-forming liquids, giving rise to the dynamic arrest at T_g, has been a point of debate for many years. Theoretical predictions consider two extreme cases: thermally activated processes on a constant density "energy landscape" and free-volume theories [1, 2] (Chap. 1). In the former picture [3, 4], the controlling parameter is temperature (T), the landscape is considered as fixed, and the super-Arrhenius τ (T) is attributed to changes in the barriers and the minima encountered in the exploration of the landscape. In the latter picture, the controlling parameter is volume (V) or better its corresponding intensive variable, the density (ρ), and the slowing-down results from the decrease of the available or "free" volume. Clearly, these pictures should be considered as extreme cases since molecular transport, in general, is driven by thermally activated processes with potential energy barriers that depend on local density. Since changing T affects both the thermal energy (k_BT) and the density, it is impossible to separate the two effects by T alone. In order to disentangle the effects of T and ρ on the dynamics, pressure-dependent measurements have been of paramount importance since pressure (P) can be applied isothermally (affecting only ρ) and have been employed to provide a quantitative assessment of their relative importance.

In this chapter, we provide two approaches that lead to a better understanding of the dynamics in the vicinity of the glass transition. The first one is based on the newly observed feature of dynamics in this class of materials, which is known as "thermodynamic scaling." The second approach emphasizes the role of molecular volume and local packing on glass transition dynamics.

2.1 Thermodynamic Scaling of Molecular Dynamics in Viscous Systems

2.1.1 A General Idea of Thermodynamic Scaling

The first interesting results in the area of thermodynamic scaling have been obtained for a typical van der Waals (vdW) liquid. Analyzing inelastic neutron

G. Floudas et al., *Molecular Dynamics of Glass-Forming Systems*, Advances in Dielectrics 1, DOI 10.1007/978-3-642-04902-6_2,

scattering data from ortho-terphenyl (OTP), Tölle [5] observed that the use of the well-known Lennard-Jones (LJ) potential, with its repulsive and attractive parts proportional to the following powers of interspecies distance r, r^{-12}, and r^{-6}, respectively, seems to be sufficient to describe molecular dynamics of vdW liquid. This assumption enabled him to express the relaxation times in terms of $T^{-1}V^{-4}$. This has been successfully applied by Dreyfus et al. [6] to plot rotational relaxation times for different isotherms, obtained from light-scattering data of OTP, onto a single master curve. The promising result has initiated intensive investigations of its application in other glass-forming liquids. It has been quickly pointed out by a few research teams [7–10] that the thermodynamic scaling found in OTP is generally not valid for other glass formers that belong to different kinds of materials such as vdW liquids (e.g., BMMPC, BMPC, salol, PDE, and PC), polymers (e.g., 1,2-PB, 1,4-PB, PVME, PMMA, and PVAc), and hydrogen bonded systems (e.g., sorbitol). Therefore, a generalized variable Γ has been proposed, which could replace T. Consequently, a relaxation time τ (or equivalent viscosity η, excluding materials revealing the decoupling phenomenon described in [11], which suggests a different scaling exponent γ for the relaxation time and viscosity) has been expressed as some scaling function J of the variable Γ [9]:

$$\log_{10}(\tau) = J(\Gamma), \tag{2.1}$$

where $\Gamma = T^{-1}V^{-\gamma}$ or $\Gamma = \rho^{\gamma}/T$.

Such an approach has brought a noticeable success (see Fig. 2.1). These and other related efforts enabled extracting a single material-dependent scaling exponent γ for

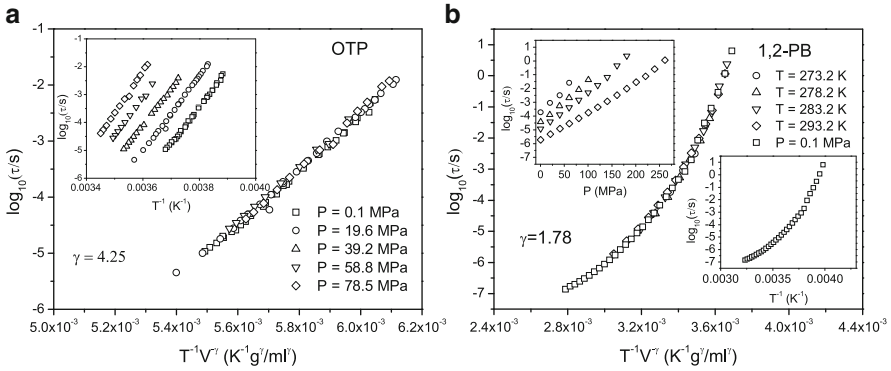

Fig. 2.1 Examples of the temperature dependences of dielectric relaxation times vs. the scaling quantity $\Gamma = T^{-1}V^{-\gamma}$ for (**a**) a typical van der Waals liquid: ortho-therphenyl (OTP), and (**b**) a polymer 1,2-polybutadiene (1,2-PB) with molecular mass equal to 3000 g/mol. The value of the scaling exponent $\gamma = 4.25$ established [8] for dielectric relaxation data obtained in various isobaric conditions for OTP differs slightly from the value $\gamma = 4.0$ found on the basis of other measurement methods [6, 8]. The obtained value $\gamma = 1.78$ for 1,2-PB is slightly smaller than the value $\gamma = 1.9$ reported in [7], where a smaller data set (excluding two isotherms at $T = 273.2$ K and 278.2 K) than that used here has been used

many glass formers, which allowed the superposition of different isothermal and isobaric relaxation times into a single master curve in accordance with (2.1). The values of the parameter γ obtained for several dozen materials are presented in Table 1.1 (see Appendix 1).

The scaling quantity Γ can be deduced from the generalized Lennard-Jones potential [12]

$$U_{\mathrm{LJ}}(r_{ij}) = 4\epsilon_{ij}\left[\left(\frac{\sigma_{ij}}{r_{ij}}\right)^{m_{\mathrm{r}}} - \left(\frac{\sigma_{ij}}{r_{ij}}\right)^{n_{\mathrm{a}}}\right], \tag{2.2}$$

where r is a distance between species i and j, and ϵ_{ij} and σ_{ij} are parameters expressed in energy and distance units, respectively, and dependent on interacting particular species. The first and second terms on the right-hand side of (2.2) correspond to the repulsive and attractive interactions between the species. If we need to keep the same proportion between the exponents m_{r} and n_{a}, as is in the original formula of the Lennard-Jones potential, then the generalization taking into account the scaling exponent γ results to $m_{\mathrm{r}} = 3\gamma$ and $n_{\mathrm{a}} = 3\gamma/2$. However, many authors [13–16] are inclined to regard only the repulsive part of the generalized Lennard-Jones potential (Fig. 2.2) as mainly responsible for the thermodynamic scaling property. Therefore, the assumption $m_{\mathrm{r}} = 3\gamma$ is usually treated as sufficient to explain the scaling property, while the exponent n_{a} is left unlimited in that sense. It is worth noting that in relation to the modified LJ potential, the scaling exponent γ can be interpreted as an indicator of "softness" of the intermolecular repulsive potential. A straightforward explanation of the form of scaling quantity, $\Gamma = T^{-1}V^{-\gamma}$, can be reduced by noting that the repulsive term (2.2) of the generalized

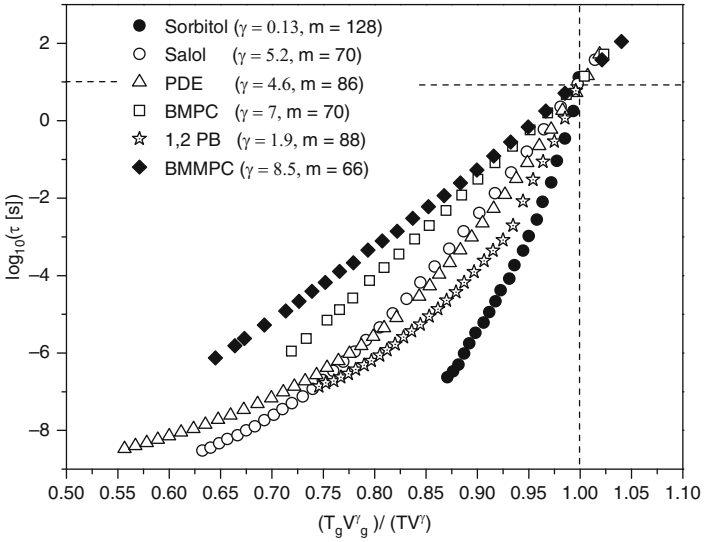

Fig. 2.2 A modified Angell plot of the rescaled fragility (similar to Fig. 4 from [7])

LJ potential can be written in the form proportional to $r^{-3\gamma}$ and substituting simply $V \sim r^3$ to the relationship $V^{-\gamma} \sim r^{-3\gamma}$. A somewhat more sophisticated account for the form of the quantity Γ will be presented at the end of this chapter by using the Euler theorem on homogeneous functions.

2.1.2 A New Measure of the Relative Temperature–Volume Influence on Molecular Dynamics

The form of the scaling quantity Γ suggests that the parameter γ reflects the relative thermal and volume effect on molecular dynamics. Thus, when γ decreases to zero, Γ tends to rely more on T, implying that the intermolecular free volume contribution will decrease and the influence of thermal activation will increase. This observation naturally encourages to search for relations of the scaling exponent γ with quantities used earlier for evaluating the relative influence of the thermal activation and free volume on relaxation phenomena near the glass transition. As shown in Chap. 1, the quantities commonly employed to achieve this aim are the dynamic ratio Q_V/Q_P, i.e., the ratio of the isochoric activation energy over the activation enthalpy [17, 18], and $\alpha_P/|\alpha_\tau|$, the ratio of the isobaric and isochronic thermal volume expansivities [19], calculated at the glass temperature T_g. To express the ratio of energies (1.32) by means of the scaling exponent γ, we first show how the fragility parameter m can be redefined by using the scaling quantity Γ [7, 20]. As can be seen in Fig. 2.2, if we replace the ratio T_g/T by the scaled ratio Γ/Γ_g, where $\Gamma_g = {T_g}^{-1}{V_g}^{-\gamma}$ is a value of the scaling quantity Γ at the glass transition temperature, we can prepare a modified Angell plot analogous to that shown in Chap. 1 (see Fig. 1.17), and consequently introduce a rescaled definition of the fragility parameter. In general, the definition can be formulated as follows:

$$m = \left(\frac{\mathrm{d}\log_{10}(\tau)}{\mathrm{d}(\Gamma/\Gamma_g)}\right)\Bigg|_{\Gamma=\Gamma_g}. \tag{2.3}$$

More precisely, considering isobaric and isochoric conditions (on which the fragility parameter is usually determined), one can propose the rescaled definitions of the isobaric and isochoric fragilities:

$$m_P = \left(\frac{\mathrm{d}\log_{10}(\tau)}{\mathrm{d}(\Gamma/\Gamma_g)}\right)_P\Bigg|_{\Gamma=\Gamma_g}, \tag{2.4}$$

$$m_V = \left(\frac{\mathrm{d}\log_{10}(\tau)}{\mathrm{d}(\Gamma/\Gamma_g)}\right)_V\Bigg|_{\Gamma=\Gamma_g}. \tag{2.5}$$

Using the standard definitions of the isobaric and isochoric fragilities (see Chap. 1), one can show [21–23] that these quantities are interrelated,

$$\begin{aligned} m_P &= \left.\frac{\partial \log_{10}(\tau)}{\partial (T_g/T)}\right|_{P=\text{const},T=T_g} \\ &= \left.\frac{\partial \log_{10}(\tau)}{\partial (T_g/T)}\right|_{V=\text{const},T=T_g} + \left.\frac{\partial \log_{10}(\tau)}{\partial V}\right|_{T=\text{const},T=T_g} \left.\frac{\partial V}{\partial (T_g/T)}\right|_{P=\text{const},T=T_g} \\ &= \left.\frac{\partial \log_{10}(\tau)}{\partial (T_g/T)}\right|_{V=\text{const},T=T_g} \\ &\quad - \left(\left.\frac{\partial \log_{10}(\tau)}{\partial (T_g/T)}\right|_{V=\text{const},T=T_g} \Big/ \left.\frac{\partial V}{\partial (T_g/T)}\right|_{\tau=\text{const},T=T_g}\right) \left.\frac{\partial V}{\partial (T_g/T)}\right|_{P=\text{const},T=T_g}. \end{aligned} \tag{2.6}$$

The last conversion in (2.6) results from the rule of the implicit partial derivative. Taking into account the standard definition of the isochoric fragility, m_V, as well as the definitions of the isobaric and isochronic thermal volume expansivities, α_P and α_τ, one can derive the following relationship between the fragilities m_P and m_V:

$$m_P = m_V\left(1 - \frac{\alpha_P}{\alpha_\tau}\right), \tag{2.7}$$

where the fragilities and the expansivities should be calculated as the limit values taken from the side of the supercooled region at the point (P_τ, V_τ, T_τ) determined by the same relaxation time τ which is usually chosen to define the glass transition. As a result, the relations given by (2.7) and (1.32) allow us to express the ratio of activation energies by the ratio of fragilities as follows:

$$\left.\frac{Q_V}{Q_P}\right|_{T=T_g} = \frac{m_V}{m_P}. \tag{2.8}$$

This last equation also follows directly from the ratio of $m_V(=\left(1/T_g\right)(\partial \log_{10}(\tau)/\partial(1/T))_V)$ with $m_P(=\left(1/T_g\right)(\partial \log_{10}(\tau)/\partial(1/T))_P)$ calculated at $T = T_g$. In this way, we gain not only a new expression for the measure of the relative effect of T and V on molecular dynamics near the glass temperature, but also an additional insight into values reached by this measure. If the quantity m_V/m_P approaches 1, i.e., if the fragility m_V, evaluated at constant volume, and the fragility m_P, obtained at constant pressure, both determined at the same glass transition temperature T_g, are equal, then one can state that thermal activation plays a decisive role in the dynamic behavior. On the contrary, the dynamics is mainly governed by an intermolecular free volume if the ratio m_V/m_P approaches 0, due to the isochoric fragility decreasing toward zero.

Analogous calculations can be made in terms of the scaling quantity Γ, by replacing T_g/T by Γ/Γ_g. As the ratio of partial derivatives of the scaling quantity Γ yields

$$\left(\frac{\partial V}{\partial(\Gamma/\Gamma_g)}\right)_P\Big|_{\Gamma=\Gamma_g}\Bigg/\left(\frac{\partial V}{\partial(\Gamma/\Gamma_g)}\right)_\tau\Big|_{\Gamma=\Gamma_g}=\left(\frac{\partial\Gamma}{\partial V}\right)_\tau\Big|_{\Gamma=\Gamma_g}\Bigg/\left(\frac{\partial\Gamma}{\partial V}\right)_P\Big|_{\Gamma=\Gamma_g}$$

$$=\frac{\left(\frac{\partial\Gamma}{\partial V}\right)_\tau\Big|_{\Gamma=\Gamma_g}}{\left(\frac{\partial\Gamma}{\partial T}\right)_V\Big|_{\Gamma=\Gamma_g}\left(\frac{\partial T}{\partial V}\right)_P\Big|_{\Gamma=\Gamma_g}}=\frac{\gamma TV^{-1}}{\left(\frac{\partial T}{\partial V}\right)_P}\Bigg|_{\Gamma=\Gamma_g}=\gamma T_g\alpha_P(T_g), \tag{2.9}$$

the relation between rescaled isobaric and isochoric fragilities can be formulated as follows [20, 24]:

$$m_P=m_V\left(1+\gamma T_g\alpha_P(T_g)\right). \tag{2.10}$$

As a consequence, the scaling exponent γ relates to the commonly used measure of the relative contribution of thermal activation and free volume to molecular dynamics of supercooled liquids through [7, 24]

$$\frac{Q_V}{Q_P}\Big|_{T=T_g}=\frac{1}{1+\gamma T_g\alpha_P(T_g)}. \tag{2.11}$$

Taking into account the empirical rule [25, 26] $\alpha_P T_g \approx$ const at ambient pressure, the scaling exponent γ can be considered as a new measure of the relative degree to which temperature and density control the dynamics [7, 27]. On the basis of (2.11), two extreme cases can be predicted. If $\gamma = 0$, then thermal energy should fully dominate molecular dynamics. If γ tends to infinity – that corresponds to the limiting case of a hard sphere potential, an intermolecular free volume should decide on the dynamics.

Moreover, the expected correlation between the exponent γ and the ratio Q_V/Q_P, has been suggested by Casalini and Roland [7, 27] (see Fig. 2.3). According to the correlation and after an analysis of values of the exponent γ for various materials (e.g., see Table 1.1 in Appendix 1), one can note some regularity. The smallest values of the scaling exponent are established for some hydrogen-bonded systems where the thermodynamic scaling is accepted to be valid. As γ increases, we first find the characteristic scaling exponents for polymers, and then evaluate the largest values of γ mainly for vdW liquids.

The use of the scaling exponent γ as the intermolecular potential-dependent measure of the relative influence of temperature/density on the molecular dynamics can be additionally substantiated by considering the approach presented by Alba-Simionesco

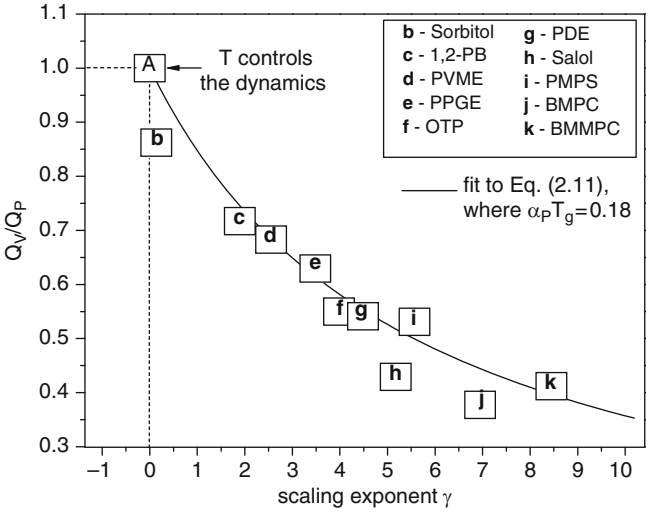

Fig. 2.3 Demonstration of the use of the scaling exponent γ for evaluating the relative effect of temperature and volume on molecular dynamics (data taken from Fig. 3 in [7])

and coworkers [23]. Normally, the thermodynamic scaling can be valid due to a closely related effect of density scaling of energy barriers for different dynamic processes in supercooled liquids. In their approach, they assume and show [23], by using results obtained from measurements on the organic glass-former OTP and the polymer polyvinyl methyl ether (PVME) as well as from computer simulations performed for a binary LJ liquid model, that the activation energy that depends on temperature and density, $E(T,\rho)$, can be scaled satisfactorily with density by means of some general equation:

$$\frac{E(T,\rho)}{e(\rho)} = J_E\left[\frac{T}{e(\rho)}\right], \tag{2.12}$$

where functions J_E and $e(\rho)$ are system dependent, and the energy barrier $E(T,\rho)$ is defined by the following expression for the relaxation time

$$\tau(T,\rho) = \tau_\infty(\rho)\exp\left[\frac{E(T,\rho)}{T}\right]. \tag{2.13}$$

The energy scaling described by (2.12) leads to the collapse of the data onto a single master curve, $E(T,\rho)/e(\rho)$ vs. $T/e(\rho)$, if the function $e(\rho)$, interpreted as the activation barrier in the high temperature limit, $E_\infty(\rho)$, is assumed to be proportional to ρ^γ, where γ is the same scaling exponent as that used in (2.1). Consequently, one can formulate a scaling equation for the relaxation time τ (or the viscosity η),

$$\log_{10}[\tau(T,\rho)] = J_\rho(X) \tag{2.14}$$

where $X = e(\rho)/T$. It can be easily seen that the scaling equations (2.1) and (2.14) are equivalent and the scaling quantities are proportional to each other, i.e., $\Gamma \propto X$.

In accordance with the idea of thermodynamic scaling, both Γ and X, independent of the thermodynamic conditions, assume a constant value at a given relaxation time τ. This important feature results in some obvious equations:

$$\left(\frac{\partial \Gamma}{\partial T}\right)\Big|_{\tau=\text{const}} = 0 \quad \text{and} \quad \left(\frac{\partial X}{\partial T}\right)\Big|_{\tau=\text{const}} = 0. \tag{2.15}$$

After simple calculations based on the above equations, namely,

$$1 + \left(\gamma T V^{-1} \frac{\partial V}{\partial T}\right)_{\tau=\text{const}} = 0 \quad \text{and} \quad 1 + \left(T \frac{\partial \ln(e(\rho))}{\partial \ln(\rho)} \frac{\partial \ln(\rho)}{\partial T}\right)_{\tau=\text{const}} = 0, \tag{2.16}$$

we can derive two closely connected relations:

$$\gamma T_\tau \alpha_\tau = -1 \quad \text{and} \quad \frac{\partial \ln(e(\rho))}{\partial \ln(\rho)} T_\tau \alpha_\tau = -1, \tag{2.17}$$

where T_τ is the temperature at which the structural relaxation time τ is equal to the value that is usually chosen to equate the glass transition temperature T_g with T_τ. Of course, the relations presented in (2.17) are identical if it is assumed that $e(\rho) = \rho^\gamma$. An interpretative advantage of the approach based on the density scaling of the energy barrier can be seen when we refer to the ratio of the isobaric and isochronal thermal volume expansivities, α_P/α_τ, that determine the relationship shown in (2.7) and its scaled representation (2.10). According to (2.17), the dependence m_P on m_V can be reformulated as follows:

$$m_P = m_V \left(1 + \alpha_P T_g \frac{\partial \ln(e(\rho))}{\partial \ln(\rho)}\right). \tag{2.18}$$

In addition, let us notice that the product $\alpha_P T_g = -(\partial \ln(\rho)/\partial \ln(T))_P\big|_{T=T_g}$. This suggests that one can extract from the ratio α_P/α_τ the contributions of both effects: the temperature dependence of a system density measured by the product $\alpha_P T_g$, and the density dependence of relaxation times quantified by the derivative $\partial \ln(e(\rho))/\partial \ln(\rho)$. This again shows that the ratio α_P/α_τ is a measure of the relative influence of temperature and density on molecular dynamics of the investigated system. Moreover, in the context of the previous considerations, the scaling exponent γ can be treated as a system-specific parameter that characterizes the density dependence of relaxation times.

It is worth noting that the condition of the constancy of Γ at a given relaxation time, $T_\tau^{-1} V_\tau^{-\gamma} = \text{const}$, which underlies (2.15), enables finding [28] a convenient method for determining the scaling exponent γ. At the glass temperature, a linear logarithmic dependence $T_g(V_g)$ is found,

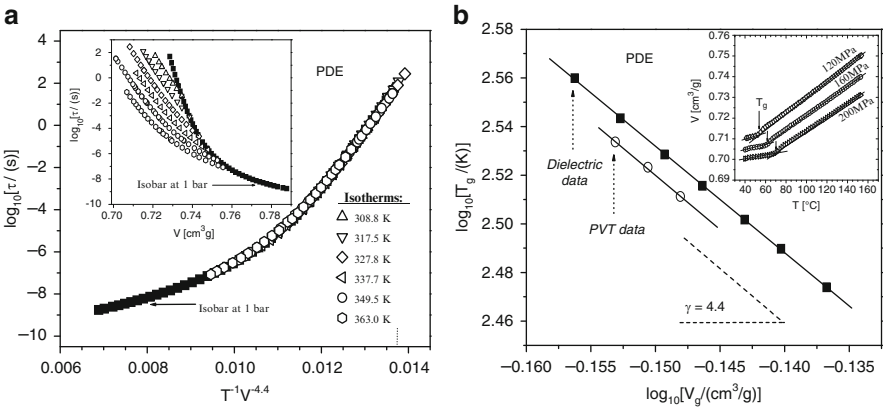

Fig. 2.4 (**a**) Thermodynamic scaling vs. the quantity $\Gamma = T^{-1}V^{-\gamma}$. The *inset* shows the isotherms and the isobar at atmospheric pressure as a function of volume; (**b**) Logarithmic plot of the glass transition temperature T_g vs. the glass transition volume V_g for PDE. *Closed squares* indicate data from dielectric measurements. *Open circles* represent data from *PVT* measurements. *Solid lines* are respective fits to the dielectric and *PVT* data according to (2.19) with the same slope γ. The *inset* shows the specific volume vs. temperature data at different isobars obtained from *PVT* measurements near the glass transition temperature, which have been used to determine T_g from PVT data

$$\log_{10} T_g = A - \gamma \log_{10} V_g \tag{2.19}$$

with parameters A and scaling exponent γ, that can be obtained by a simple linear regression.

As an example for PDE, we present how this procedure works (Fig. 2.4b) in comparison with the standard way of determining the scaling exponent γ from the plot (Fig. 2.4a) according to (2.1). From the $T_g(V_g)$ representation (2.19), we find, both from dielectric and *PVT* data, $\gamma = 4.4$, which corresponds nicely with the same parameter obtained from the standard procedure of the thermodynamic scaling. This procedure, following from (2.19), emphasizes that the scaling exponent γ can be obtained from *PVT* measurements alone [28] (although in general evaluation of the glass transition point (T_g, V_g) using the *PVT* data can be insufficiently accurate). It further suggests that the dynamic and thermodynamic properties are expected to be strongly correlated.

2.1.3 The Relaxation Time Description in Accordance with Thermodynamic Scaling

After the general considerations about thermodynamic scaling, it is worth mentioning some attempts to determine explicit expressions for the scaling functions J and J_ρ implicitly introduced into (2.1) and (2.14). Casalini and Roland have proposed

several scaled equations for the relaxation time. At first, they have indicated [7] that a simple expression,

$$\log_{10}[\tau(\Gamma)] = \log_{10}(\tau_\infty) + C\Gamma, \quad \Gamma = T^{-1}V^{-\gamma}, \tag{2.20}$$

which assumes a volume-dependent activation energy, C/V^γ, where C is a constant and γ is the scaling exponent, can rationalize the dependence of the ratio Q_V/Q_P on the exponent γ depicted in Fig. 2.3. However, as the same authors noticed, (2.20) cannot correctly describe any experimental dependence of relaxation times on the scaling quantity Γ, because each of them reveals a nonlinear behavior. Searching for some phenomenological description of the dependence $\log_{10}[\tau(\Gamma)]$, they rejected the VFT equation due to its intrinsic singularity at temperature T_0 and in the next step, they applied [20] the modified Cohen–Grest equation

$$\log_{10}[\tau(\Gamma)] = \log_{10}(\tau_\infty) + \frac{A}{\Gamma^{-1} - \Gamma_0^{-1} + \left[\left(\Gamma^{-1} - \Gamma_0^{-1}\right)^2 + B\Gamma^{-1}\right]}, \quad \Gamma = T^{-1}V^{-\gamma}, \tag{2.21}$$

where A, B, and Γ_0 are constants. However, the validity of the Cohen–Grest model at high pressures will be questioned [29] (see Chap. 3); therefore, it has not been further developed within the framework of thermodynamic scaling [30].

Some general scaling equation for the relaxation time has been proposed by Dreyfus et al. [8]. As mentioned earlier, these authors developed the concept of the temperature–density dependent activation barrier $E(T, \rho)$ and its high-temperature limit $e(\rho)$, presented herein in (2.13) and (2.14), respectively. They suggested that $\log_{10}[\tau(X)] = \log_{10}(\tau_\infty) + X\Phi(X)$, where $X = e(\rho)/T$, and assumed that the equation in the high-temperature limit should obey the Arrhenius law. Consequently, it implies that $\Phi(X)$ should tend to 1 when X approaches zero, i.e., the function Φ should be a positive monotonously increasing function of $1/T$ for $T/T_g \gg \Phi(X)$, if we recall the Angell plot construction. As for the function Φ, it has been chosen as $\exp(bX)$, which met such requirements if b is a material-dependent positive constant. Then, formulating the scaling equation in terms of the scaled quantity X/X_g, reduced with respect to the glass transition point at which the relaxation time $\tau_g = \tau\left(\rho_g, T_g\right)$, one can derive the following general expression [8]:

$$\log_{10}[\tau(X)] = \log_{10}(\tau_\infty) + \log_{10}\left(\frac{\tau_g}{\tau_\infty}\right)\frac{X}{X_g}\exp\left[bX_g\left(\frac{X}{X_g} - 1\right)\right] \tag{2.22}$$

where typically assuming that $e(\rho) \sim \rho^\gamma$ one can substitute $X/X_g = T_g\rho^\gamma(T)T^{-1}\rho_g^{-\gamma}(T)$.

Some interesting results have been achieved [13, 30] by exploiting the Avramov model (see Chap. 3) to find the scaled equation for the relaxation time:

$$\log_{10}[\tau(\Gamma_G)] = \log_{10}(\tau_\infty) + \in \log_{10}(e)\left(\frac{\Gamma_G}{\Gamma_{Gr}}\right)^D, \quad \Gamma_G = T^{-1}V^{-\gamma_G}, \quad \Gamma_{Gr} = T_r^{-1}V_r^{-\gamma_G} \tag{2.23}$$

which can be easily reduced to its form depending on the four parameters τ_∞, A, D, and γ_G,

$$\log_{10}[\tau(\Gamma_G)] = \log_{10}(\tau_\infty) + (A\Gamma_G)^D, \quad \Gamma_G = T^{-1}V^{-\gamma_G}, \quad A = [\in \log_{10}(e)]^{\frac{1}{D}}/\Gamma_{Gr} \tag{2.24}$$

where the parameter $\in = E_{max}/\sigma_r$ is expressed by the dispersion of the system at some reference state, σ_r, and the upper limit of the distribution of the energy barrier height, E_{max}. The above equation can be derived by using the basic Avramov equation [see Chap. 3, (3.23)] converted from the viscosity η into the relaxation time τ, where the system entropy, S, can be easily related to some other thermodynamic properties of the system and can be calculated from volumetric data, given at least one of the values of isobaric or isochoric heat capacity. Starting from a volume–temperature dependence of the entropy $S(T, V)$, unlike the original Avramov approach based on a pressure–temperature effect on entropy, one can show that

$$S(T,V) = S_r + C_V\left[\ln\left(\frac{T}{T_r}\right) + \frac{(C_P/C_V) - 1}{T\alpha_P}\ln\left(\frac{V}{V_r}\right)\right] \tag{2.25}$$

where S_r, T_r, and V_r denote thermodynamic variables in sequence S, T, and V at an arbitrary chosen reference state, and α_P is the isobaric thermal volume expansivity, whereas C_P and C_V are heat capacities determined at a constant pressure and a constant volume, respectively. Defining a new parameter

$$\gamma_G = \frac{(C_P/C_V) - 1}{T\alpha_P} \tag{2.26}$$

the entropy of the system can be formulated as follows:

$$S(T,V) = S_r + C_V \ln\left(\frac{TV^{\gamma_G}}{T_r V_r^{\gamma_G}}\right). \tag{2.27}$$

Introducing the above entropy formula into the basic Avramov equation (3.23), where the viscosity η is substituted by the relaxation time τ, and the parameter ϵ is usually expressed by $\ln(\tau_g/\tau_\infty)$, in which τ_g is the relaxation time at the glass transition and τ_∞ is the relaxation time in the high temperature limit, one can obtain the scaled equation for the relaxation time presented in (2.23) where its parameter D can be expressed by means of the isochoric heat capacity C_V,

$$D = \frac{2C_V}{ZR}. \tag{2.28}$$

Here, R is the gas constant and Z is the parameter representing the degree of the system degeneracy within the Avramov model. The physical meaning of the latter is the number of available pathways for local motions per molecule or polymer segment; hence it can be roughly approximated by the coordination number of the liquid lattice.

Tests performed by Casalini et al. [13, 30] for various glass formers with the scaled model given by (2.24), where the scaled quantity Γ_{Gr} at a reference state was assumed to concern the glass transition point, show that the equation successfully describes experimental relaxation data. Moreover, the advantage of the application of the Avramov model to the scaled dependences of relaxation times (2.1) is its close connection with thermodynamic properties of the investigated systems. It is worth noticing that (2.25) is a consequence of several thermodynamic relationships.

As mentioned earlier, we first exploit the entropy differential,

$$\mathrm{d}S(T,V) = \left(\frac{\partial S}{\partial T}\right)_V \mathrm{d}T + \left(\frac{\partial S}{\partial V}\right)_T \mathrm{d}V \tag{2.29}$$

where

$$\left(\frac{\partial S}{\partial T}\right)_V = \left(\frac{\partial S}{\partial U}\right)_V \left(\frac{\partial U}{\partial T}\right)_V = \frac{1}{T} C_V \tag{2.30}$$

on the basis of the definitions of the isochoric heat capacity and the internal energy U.

To find an appropriate form for the isothermal change of entropy, we consider some thermodynamic quantities and transformations. Using the Helmholtz free energy, $F = U - TS$, and its total differential, $\mathrm{d}F(T,V) = -S\mathrm{d}T - P\mathrm{d}V$, it is easily seen that

$$\left(\frac{\partial S}{\partial V}\right)_T = \left(\frac{\partial P}{\partial T}\right)_V. \tag{2.31}$$

Employing the basic thermodynamic relation for the heat capacities,

$$C_P - C_V = T\left(\frac{\partial V}{\partial T}\right)_P \left(\frac{\partial P}{\partial T}\right)_V \tag{2.32}$$

allows to develop (2.31) to the formula below:

$$\left(\frac{\partial S}{\partial V}\right)_T = \left(\frac{\partial P}{\partial T}\right)_V = \frac{C_P - C_V}{TV\alpha_P}. \tag{2.33}$$

Taking into account (2.26) and (2.33) as well as using the definition of the isothermal volume compressibility,

$$\kappa_T \equiv -\frac{1}{V}\left(\frac{\partial V}{\partial P}\right)_T = \frac{1}{V}\left(\frac{\partial V}{\partial T}\right)_P \left(\frac{\partial T}{\partial P}\right)_V = \alpha_P \left(\frac{\partial T}{\partial P}\right)_V \tag{2.34}$$

where the rule of the implicit partial derivative is exploited, one can easily find that the scaling exponent γ_{G} derived in terms of the modified Avramov model can take the following form:

$$\gamma_{\mathrm{G}} = \frac{V\alpha_P}{C_V \kappa_T} \tag{2.35}$$

which is the thermodynamic definition [31, 32] of a parameter called the Grüneisen constant. Casalini et al. [13] argued, by experimental testing of (2.35), that the volume dependence of γ_{G} is negligible and one can determine the Grüneisen constant from *PVT* data at the reference state such as the glass transition point. Thus, it can be used to represent the scaling exponent γ which is expected to be constant. It is worth noting that the Grüneisen constant [33] was originally defined as the isothermal change of frequency ν in systems of quantum oscillators with system volume V,

$$\gamma_{\mathrm{G}} \equiv -\left(\frac{\mathrm{d}\ln \nu}{\mathrm{d}\ln V}\right)_T = -\left(\frac{r\,\mathrm{d}\nu}{3\nu\,\mathrm{d}r}\right)_T. \tag{2.36}$$

Keeping in mind possible limitations of using this parameter for finding the scaling exponent γ, such as the temperature dependence of the quantity given by (2.36) and the unknown dependence of relaxation dynamics on vibrations, we note that the Grüneisen constant can lead to some interesting conclusions. Assuming that the intermolecular potential (2.2) can be reduced to its repulsive part with the exponent $m_{\mathrm{r}} = 3\gamma$, and further considering a lattice of phonons with the harmonic force constant for their vibrations given by $\partial^2 U_{\mathrm{LJ}}^{\mathrm{r}}/\partial \mathrm{r}^2 \propto \nu^2$, one can prove [34] that

$$\gamma_{\mathrm{G}} = \frac{1}{2}\gamma + \frac{1}{3} \tag{2.37}$$

i.e., a simple relation between the Grüneisen constant, which can be established from *PVT* measurements data on the basis of (2.35), and the scaling exponent γ used in (2.1), however, under the assumption that the exponent γ can be straightforwardly related to the exponent m_{r} in (2.2), i.e., if $\gamma = m_{\mathrm{r}}/3$. Nevertheless, this finding clearly shows that the thermodynamic scaling can be considered as a linkage of dynamic and thermodynamic properties. Although attempts of experimental verifications of the relation given by (2.37) are frequently unsuccessful [32] , its meaning does not depreciate, because the discrepancies with experimental

data can be caused by factors such as vibrations and secondary relaxations that do not contribute to the structural relaxation (or the segmental relaxation in the case of polymers), but may contribute to the thermodynamic parameters of (2.35) such as the isochoric heat capacity and the isobaric thermal volume expansivity [35]. Indeed, the Grüneisen constants calculated from (2.35) at temperatures near the glass transition temperature by using, instead of the total heat capacity, C_V^{liq}, found in the liquid phase, this value diminished by the corresponding heat capacity, C_V^{cryst}, for the crystalline state, results in values of γ_{G} that are in better agreement with the expectations [30].

In the above context, the scaled Avramov model leading to (2.23) not only yields a good description for experimental data, but also its scaling parameter, γ_{G}, suggests how the relaxation dynamics can be scaled by means of the thermodynamic properties. The advantage of the model can be related to its entropic nature. Additionally, Casalini et al. [30] showed that (2.23) can also be derived within the framework of Landau–Lifshitz thermodynamic fluctuation theory that generally concerns relaxation times governed by the entropy. The Adam–Gibbs model, the most popular among the entropic approaches, has been suggested by Alba-Simionesco and Tarjus [23] to apply in order to describe the relaxation times in terms of thermodynamic scaling,

$$\log_{10}[\tau(T,\rho)] = \log_{10}(\tau_\infty) + \frac{A(\rho)\log_{10}(e)}{TS_{\mathrm{c}}(\rho,T)}, \tag{2.38}$$

where the configurational entropy, $\mathrm{S_c}(\rho,T) = S_C(X)$, is a function of the same scaling quantity, $X = e(\rho)/T$, as in (2.14). However, Casalini et al. [30] draw our attention to the fact that the Adam–Gibbs model is characterized by some divergence of relaxation times analogous to the VFT equation, unlike the Avramov approach.

2.1.4 *Thermodynamic Scaling on Isothermal Conditions and Its Consequences*

An important and useful observation is the finding of the scaling behavior similar to that described by (2.1), but established for isothermal α-relaxation times plotted vs. the inverse specific volume scaled by the specific volume at the glass transition, V_{g}/V. The latter can be equivalently replaced by the corresponding ratio of densities, ρ/ρ_{g}. It has been shown [28] that the quantity V_{g}/V can scale the isothermal relaxation times obtained at different temperatures onto one master curve, specific to each system both in the case of vdW liquids and polymers (see examples in Fig. 2.5a, b, respectively), that is, analogously to the scaling quantity Γ.

Let us see why the scaling vs. V_{g}/V is valid simultaneously with scaling vs. Γ. In order to do that, we rewrite the quantity Γ in the following form:

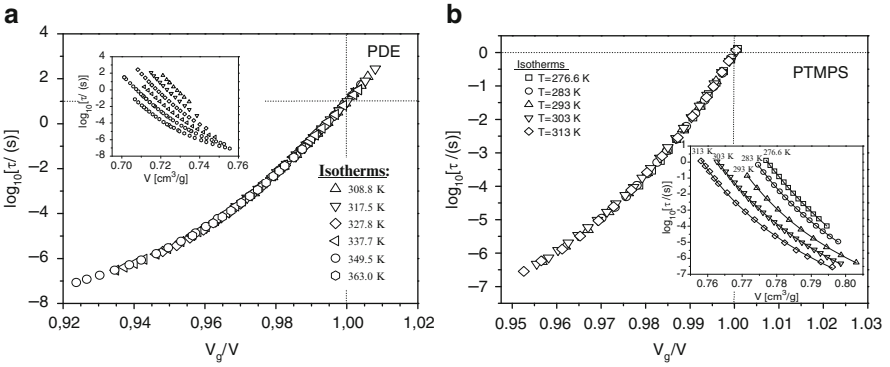

Fig. 2.5 Scaling of isothermal structural relaxation times vs. V_g/V for representatives of (**a**) van der Waals liquids (PDE) and (**b**) polymers (PTMPS). The insets show used isotherms as functions of volume

$$T^{-1}V^{-\gamma} = \left(\frac{V_g}{V}\right)^{\gamma} T^{-1}V_g^{-\gamma}. \tag{2.39}$$

If scaling vs. the quantity Γ is satisfied, then the scaling exponent γ is constant and at the glass transition temperature, T_g, one can formulate the condition

$$T_g^{-1}V_g^{-\gamma} = \text{const.} \tag{2.40}$$

From the above simple relations expressed in (2.39) and (2.40), it can be concluded that the ratio V_g/V itself leads to the scaling of isothermal relaxation times.

It is worth emphasizing that the volume scaling leads to some important consequence concerning the isothermal fragility m_T, which implies also properties of the isochoric and isobaric steepness indices, m_V and m_P. If the scaling vs. V_g/V is valid, it is obvious that the fragility parameter m_T [see its definition in Chap. 1 (1.26)], calculated at the glass transition point, is a material constant independent of pressure. Let us analyze how this feature affects the other fragilities m_V and m_P. In order to do that, we find relationships between the quantities at the point $(P, T_g(P), V(P, T_g(P)))$. From the definition of the isothermal fragility, one can derive, by exploiting the rule of the implicit partial derivative, the relationship between m_T and m_V:

$$m_T = \left(\frac{\partial \log_{10}(\tau)}{\partial (V_g/V)}\right)_T\Bigg|_{V=V_g} = -\left(\frac{V^2}{V_g}\frac{\partial \log_{10}(\tau)}{\partial V}\right)_T\Bigg|_{V=V_g}$$

$$= \left[\left(-\frac{V^2}{V_g}\right)\cdot\left(-\left(\frac{\partial \log_{10}(\tau)}{\partial (T_g/T)}\right)_V\Bigg|_{T=T_g}\Bigg/\left(\frac{\partial V}{\partial (T_g/T)}\right)_\tau\Bigg|_{T=T_g}\right)\right]\Bigg|_{V=V_g}$$

$$= -\frac{m_V}{T_g\alpha_\tau(T_g)}. \tag{2.41}$$

As shown in (2.17) the inverse negative product of the glass transition temperature T_g and the isochronic thermal volume expansivity calculated at the same temperature $T = T_g$ is equal to the scaling exponent γ. Consequently, we get a new interesting relation between the isothermal and isochoric fragilities:

$$m_T = \gamma m_V \tag{2.42}$$

which means that the isochoric fragility m_V has to be pressure independent in order for γ to remain constant in accordance with the requirements from the thermodynamic scaling. Referring to calculations from (2.6), one can obtain, even independent of the last two equations, how the parameters m_T and m_P are mutual related:

$$\begin{aligned} m_P &= -\left(\frac{\partial \log_{10}(\tau)}{\partial V}\right)_T\Bigg|_{V=V_g}\left(\frac{\partial V}{\partial (T_g/T)}\right)_\tau\Bigg|_{T=T_g} + \left(\frac{\partial \log_{10}(\tau)}{\partial V}\right)_T\Bigg|_{V=V_g}\left(\frac{\partial V}{\partial (T_g/T)}\right)_P\Bigg|_{T=T_g} \\ &= \left(-\frac{T^2}{T_g}\right)\cdot\left(-\frac{V_g}{V^2}\right) \\ &\cdot\left(-\left(\frac{\partial \log_{10}(\tau)}{\partial (V_g/V)}\right)_T\left(\frac{\partial V}{\partial T}\right)_\tau + \left(\frac{\partial \log_{10}(\tau)}{\partial (V_g/V)}\right)_T\left(\frac{\partial V}{\partial T}\right)_P\right)\Bigg|_{T=T_g,V=V_g}. \end{aligned} \tag{2.43}$$

Consequently, the ratio of isobaric and isothermal fragilities can be expressed as follows:

$$\frac{m_P}{m_T} = -T_g\alpha_\tau(T_g) + T_g\alpha_P(T_g). \tag{2.44}$$

It can be easily seen that the above equation is equivalent to (2.7) due to the relation derived in (2.41). Moreover, taking into account (2.17), the ratio from (2.44) leads to the following relation that is satisfied once the thermodynamic scaling is valid:

$$m_P = \frac{m_T}{\gamma}\left(1 + \gamma T_g\alpha_P(T_g)\right) \tag{2.45}$$

which is equivalent to (2.10) due to (2.42). The detailed analysis above shows that the experimentally known pressure dependence of the isobaric fragility results only from the pressure dependence of the product $T_g\alpha_P(T_g)$while the thermodynamic scaling is obeyed.

The above consequences of the thermodynamic scaling show that the Spencer–-Boyer rule [36, 37], $T_g\alpha_P(T_g) \approx$ const, and the following set of empirical correlations suggested by Casalini and Roland [38], namely,

1. The linear correlation between the isobaric and isochoric fragilities

$$m_P = m_0 + am_V. \tag{2.46}$$

2. The inverse linear correlation between the scaling exponent γ and the isochoric fragility

$$\gamma = \gamma_0 + bm_V^{-1}, \tag{2.47}$$

are generally limited to ambient pressure conditions. The constant parameters of linear regressions in terms of (2.46) and (2.47), that is, $m_0 = 37 \pm 3, a = 0.84 \pm 0.05$, $\gamma_0 = -1.042$, and $b = 217$, determined at atmospheric pressure [38, 39] for several glass-forming liquids could be generalized for elevated pressures only in the case of (2.47). This is obvious because the isochoric fragility m_V has been argued to be pressure independent once the thermodynamic scaling is valid. However, the pressure dependences $m_0(P)$ and $a(P)$ are expected not to be constant [40, 41], reflecting the experimentally observed changes in the isobaric fragility, m_P, with increasing pressure, that is typically a decreasing function of pressure in vdW liquids and polymers.

It is worth noting that (2.46) is not the only correlation found at ambient pressure that is broken when liquids are compressed. The next example is a rather rough correlation between the isobaric fragility m_P and the stretching exponent β_{KWW} of the Kohlrausch–Williams–Watts function [42], $m_P = 250 \pm 30 - 320\beta_{\mathrm{KWW}}$, which has been suggested by Böhmer et al. [43] at atmospheric conditions. This relation cannot give proper values of m_P at elevated pressures, since Ngai et al. [44] have recently shown, for several glass formers, which the parameter β_{KWW}, that characterizes the breadth and asymmetry of the structural relaxation peak, does not change with pressure (Chap. 1).

2.1.5 *Doubts About the Thermodynamic Scaling Universality*

Unfortunately, the above-presented appealing idea of the thermodynamic scaling cannot be treated as a universal method for the description of the structural relaxation in viscous systems.

Using high pressure measurements, it has been shown that the thermodynamic scaling vs. Γ cannot be valid for strongly hydrogen bonded systems such as DPG

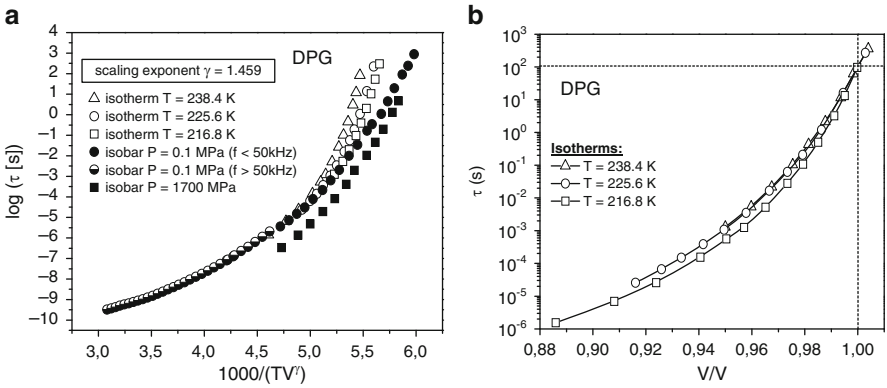

Fig. 2.6 No scaling of structural relaxation times for DPG: (**a**) Plot of α-relaxation times vs. the quantity $\Gamma = T^{-1}V^{-\gamma}$; (**b**) the scaling plot of isothermal α-relaxation times vs. V_g/V.

[40, 41] (see Fig. 2.6a) and water (from viscosity data) [45]. Similar results can be observed, although not so clearly, for glycerol for which many points shown in the master plot [46] diverge from one curve originally treated as a master curve according to (2.32). Later on, some of us have established by analyzing data for DPG [28] (see Fig. 2.6b) that the invalidity of the scaling vs. V_g/V can also be a common feature of molecular dynamics of materials forming H-bonded networks. The experiment-based analysis allows us to surmise that the expectation of the pressure independence of the scaling exponent γ can even be at variance with intrinsic properties of these materials, where the molecular structures especially vary with changing P, V, and T, because the thermodynamic conditions strongly affect the degree of H bonds (see also Chap. 5 on the pressure effects on polymer blends). This is also a credible reason for excluding H-bonded systems from the correlations given by (2.46) and (2.47). The invalidity of the thermodynamic scaling for associated liquids has been recently supported by molecular dynamics simulations performed by Dyre's group [14, 15, 47]. By using commonly known force fields for water (such as SPC/E and TIP5P), they have demonstrated that strongly H-bonded liquids do not obey a strong correlation between equilibrium fluctuations of the configurational parts of pressure and energy. This is in contrast to the LJ systems and other simple vdW liquids, such as OTP and toluene, that fulfill the correlation in the high viscous region where cooperative and local dynamic processes play a main role.

It is worth noting that the mentioned simulations yield an elegant way of determining the scaling exponent γ as a function of the exponent of the repulsive term of the LJ potential, which has also been confirmed by Coslovich and Roland [16]. However, results obtained by Bailey et al. [14] for OTP demand to rethink about relations between thermodynamics and dynamics suggested by the thermodynamic scaling. The mentioned simulations lead to a surprising value of the scaling exponent for OTP, that is $\gamma_{MD} \approx 8.0$, which is about 2 times larger than

that suggested from inelastic neutron scattering [5] and later established from the thermodynamic scaling of different relaxation and viscosity data of some glass-forming liquids (KDE, PDE, OTP, BMMPC, and BMPC) as $\gamma \approx 4.0$ [6, 8]. It is interesting that the calculations based on simulations, and some equations of state derived for the low compressibility region, which have common theoretical grounds outlined below, yield similar results.

The computational idea originates from the commonly known expression for instantaneous pressure, $p = NkT/V + W/V$, where N is the number of species of momenta $\mathbf{p}_1, \ldots, \mathbf{p}_N$ and positions $\mathbf{r}_1, \ldots, \mathbf{r}_N$ in volume V; k is the Boltzmann constant; $T = T(\mathbf{p}_1, \ldots, \mathbf{p}_N)$ is treated as "kinetic temperature" proportional to the kinetic energy per particle; and $W = W(\mathbf{r}_1, \ldots, \mathbf{r}_N)$ is the virial which yields a configurational contribution to pressure. In general, the virial can be calculated for a translationally invariant function of the potential energy $U = U(\mathbf{r}_1, \ldots, \mathbf{r}_N)$ by using the formula $W = -(1/3)\sum_i \mathbf{r}_i \cdot \nabla_i U$, as it is usually done in computer simulations [48]. Within the framework of the thermodynamic perturbation theory, a configurational contribution to pressure $P_\mathrm{r} = \langle W \rangle / V_0$ can be expressed in analogy by means of the average perturbed virial with the canonical distribution function of a reference state with a volume of V_0. However, in the case of simulations, we may take into account only the virial and potential energy values which are averages, $\langle W \rangle$ and $\langle U \rangle$, respectively, in an appropriate thermodynamic ensemble practically evaluated as some time-averages. The tested correlation has been expected to relate linearly just those averages.

If, on the contrary, one assumes that a repulsive part of the intermolecular potential is a homogeneous function with the homogeneity exponent m_r, as in (2.2), then one can find an equation of state derived from such a molecular potential, which herein is presented for a specific volume V. The Euler theorem on homogeneous functions applied to the potential U reveals a useful property of the intermolecular potential,

$$U(s\mathbf{r}_1, \ldots, s\mathbf{r}_N) = s^{-m_\mathrm{r}} U(\mathbf{r}_1, \ldots, \mathbf{r}_N). \tag{2.48}$$

If a similarity $\mathbf{r} \to s\mathbf{r}$ is additionally considered, which scale, $s = (V/V_0)^{1/3} = (\rho_0/\rho)^{1/3}$, can be determined by using a specific volume V or density ρ (where V_0 and ρ_0 are, respectively, specific volume and density at a reference state), one can explain that the volume factor of the scaling quantity Γ from (2.1) is expressed by $V^{m_\mathrm{r}/3}$ as well as one can propose a state equation for the elevated pressure region [49], $P = (RT/M\upsilon) + (V_0/V)^{m_\mathrm{r}/3} P_\mathrm{r}$, where R is the gas constant, M is the molar mass of substance, and P_r denotes herein a configurational contribution to pressure given by species of total mass equal to a unit mass of substance, which interact with each other by repulsive forces. However, the state equation is rather of low use for fitting PVT experimental data due to an undefined density–temperature dependence of the parameter P_r in the case of most real materials. Therefore, some

generalized form of the state equation has been introduced by Bardik and Shakun [50], which is presented here for a specific volume V:

$$P = \frac{RT}{MV}\left[1 + \varphi\left(\frac{1}{kT}\left(\frac{V_0}{V}\right)^{m_r/3}\right)\right]. \tag{2.49}$$

The unknown form of the φ-function can be derived by expanding in a series about a reference point with specific volume V_0, which is assumed to be characterized by a low isothermal compressibility. Then, taking into account only terms of the series up to the first order, the following expression for pressure can be obtained:

$$P = \frac{RT}{MV} \times \left[1 + \varphi\left(\frac{1}{kT}\left(\frac{V_0}{V}\right)^{m_r/3}\right)\Bigg|_{V=V_0} + \frac{1}{kT}\varphi'\left(\frac{1}{kT}\left(\frac{V_0}{V}\right)^{m_r/3}\right)\Bigg|_{V=V_0}\left(\left(\frac{V_0}{V}\right)^{m_r/3} - 1\right)\right] \tag{2.50}$$

Remembering that $m_r = 3\gamma$ in (2.2) and making additional assumptions that the configurational pressure in the reference state is given by

$$P_0 = \phi\left(\frac{1}{kT}\left(\frac{V_0}{V}\right)^{m_r/3}\right)\Bigg|_{V=V_0}\frac{RT}{MV},$$

and the first-order coefficient is only temperature dependent,

$$B(T) = \phi'\left(\frac{1}{kT}\left(\frac{V_0}{V}\right)^{m_r/3}\right)\Bigg|_{\upsilon=\upsilon_0}\frac{R}{MVk},$$

one can rewrite (2.50) as follows:

$$P = \frac{RT}{MV} + P_0 + B(T)\left[\left(\frac{V_0}{V}\right)^{\gamma} - 1\right], \tag{2.51}$$

which is the equation-of-state convenient to test the hypothesis about a single scaling parameter γ by using isothermal PVT data [52, 53]. Recently, deriving (2.51) from the definition of the configurational isothermal bulk modulus $B_T^{conf} \equiv -V\frac{\partial P^{conf}}{\partial V}\Big|_T = -\gamma\frac{\partial P^{conf}}{\partial \ln V^{\gamma}}\Big|_T$, where the configurational pressure $P^{conf} \equiv P - \frac{RT}{MV}$, a physical meaning of the temperature dependent parameter B(T) has been found [53] by expressing it as $B(T) = B_T^{conf}(P_0)/\gamma$. It is worth mentioning that earlier attempts [23, 32] to discuss an equation of state in the context of

thermodynamic scaling did not involve successfully any explicit form of the term coming from a contribution of repulsive interactions. As theoretical investigations [14–16, 23] lead to the conclusion that an inverse power law approximation of intermolecular potential is appropriate to describe dynamic properties of dense, highly viscous liquids, it is well-founded to apply the equation of state [(2.51)], derived for the low compressibility region, in studying the thermodynamic behavior of such materials.

Grzybowski et al. [52, 53] have tested fits of isothermal volumetric data to (2.51) for some representatives of vdW liquids, weakly H-bonded liquids, and polymers; phenylphthalein-dimethylether (PDE), OTP, propylene carbonate (PC), meta-fluoroaniline (m-FA), and 1,2-polybutadiene (1,2-PB). As it can be seen, for example, for OTP in Fig. 2.7, the accuracy of the fitting procedure to (2.51) is high due to prior calculation of the parameter P_0 for each isotherm at a point $(V_0,P(V_0))$ chosen separately for each isotherm and characterized by the locally lowest experimentally achieved isothermal compressibility. The scaling exponents, γ_{es}, found from the equation of state, which are presented in Table 2.1, are surprisingly at least two times larger than those determined from the standard scaling procedure based on (2.1). However, it is especially interesting to compare for OTP the scaling exponents $\gamma_{es} \approx 10.0$ and $\gamma_{MD} \approx 8.0$, with the value γ obtained from the standard scaling procedure. The result that both γ_{es} and γ_{MD} are comparable and considerably larger than $\gamma \approx 4.0$ is striking, because both the equation-of-state and calculations based on MD simulations come from the common theoretical grounds following from the virial theorem and the potential energy mainly governed by repulsive interactions in the case of highly viscous liquids. Some doubts about the thermodynamic scaling idea as a

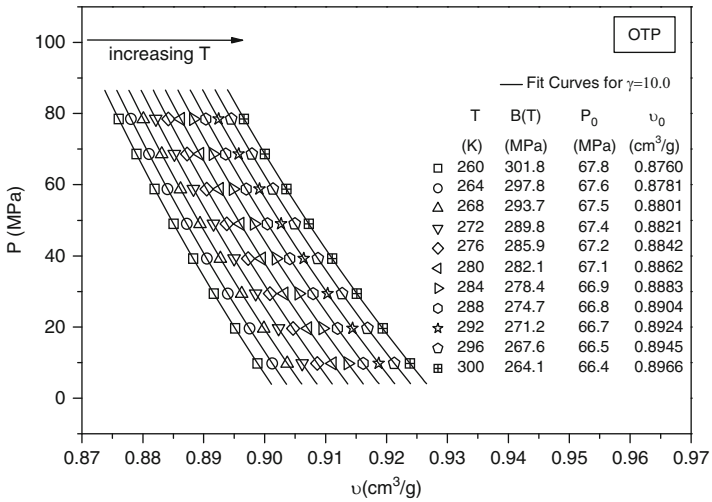

Fig. 2.7 Plot of isothermal *PVT* data for ortho-terphenyl, which is generated by using the Tait equation with its parameters proposed in [8] and retaining the original measurement range reported in [51]. *Solid lines* denote fits of the data to the equation of state given by (2.51) first presented in Fig. 2 in [52]

Table 2.1 Comparison of the values of scaling exponent γ earlier established from relaxation data by using (2.1) with those evaluated herein from volumetric data by fitting to the equation of state given by (2.51)

	γ_r [γ found from (2.1)]	γ_{es} [γ found from (2.51)]	γ_{es}/γ_r
PDE	4.5[a]	9.2 ± 0.2	2.04
OTP	4.0[b]	10.0 ± 0.1	2.50
PC	3.7[c]	9.4 ± 0.1	2.54
m-FA	2.7[d]	7.2 ± 0.1	2.67
1,2-PB	1.9[a]	9.4 ± 0.1	4.95

[a]From [7]
[b]From [6]
[c]From [10]
[d]From [46]

linkage between dynamic and thermodynamic properties of supercooled liquids arise from such a significant discrepancy between the scaling exponents γ_{es} and γ. Moreover, the finding strongly suggests that even if the thermodynamic scaling were valid at least for vdW and polymer systems in the sense considered so far, its genuine bases require to be reanalyzed. Finally, it is worth mentioning that in contrast to MD simulations, where attractive forces have to be involved, the last term describing the configurational pressure in the equation of state (2.51) is an approximation based mainly on the repulsive interactions contribution, where the attractive interactions can be considered as some nearly constant background. However, we would like to emphasize that such an approximation made for highly viscous systems cannot downgrade the conclusions drawn on that basis. It is related to some theoretical analyses first performed by Weeks et al. [54] at the beginning of the 1970s. According to them, the thermodynamic and structural properties of the LJ fluid are dominated by the repulsive part at high temperatures for all densities as well as at low temperatures for high densities.

Very recently, within the framework of the temperature-volume Avramov model described in Sect. 2.1.3, a meaningful progress in explaining the discrepancies between the found values of the exponents γ and γ_{es} has been made [55, 56]. Making a reasonable assumption that the maximal energy barrier in (2.24) can be scaled in terms of specific volume or density with some scaling exponent γ_E, i.e., $E_{max}(V) = A_E(V_r/V)^{\gamma_E}$, where A_E is some material constant that has energy units, the temperature-volume Avramov model has been adjusted to better describe dynamics of real glass-forming materials in the vicinity of the glass transition. Applying this assumption to (2.24), we find the following modified equation,

$$\log_{10}[\tau(\Gamma)] = \log_{10}(\tau_\infty) + (A\Gamma)^D,\ \Gamma = T^{-1}V^{-\gamma},$$
$$A = [\in\ \log_{10}(e)]^{1/D}/\Gamma_r,\ \Gamma_r = T_r^{-1}V_r^{-\gamma},\ \in = A_E/\sigma_r \qquad (2.52)$$

Since the value of the scaling exponent γ_E has turned out to be in very good agreement with that of γ_{es} found by fitting PVT data to the equation of state [(2.51)] for each tested representative of vdW liquids [55] and one ionic liquid

[56] near the glass transition, the scaling exponent γ in (2.52) can be related to the Grüneisen constant γ_G and the exponent γ_{es} as follows

$$\gamma = \gamma_G + \gamma_{es}/D \tag{2.53}$$

The relation is expected to have an important impact on our understanding of linkages between thermodynamic and dynamic properties of materials near the glass transition as well as intermolecular interactions responsible for the thermodynamic scaling, but it requires further investigations and tests for various materials.

2.2 The Role of Monomer Volume and Local Packing on the Glass-Transition Dynamics

The thermodynamic scaling has advantages as well as some problems as discussed above. In addition, the proposed scaling lacks a predictive power; i.e., given a molecular structure it cannot make suggestions on the thermodynamic parameter that mostly affects the dynamics. Some of us suggested on a different way [57] of analyzing the dynamic quantity Q_V/Q_P that provides a quantitative measure of the relative importance of ρ and T in the dynamics of the α-process. We demonstrate – without invoking any scaling – that the repeat unit volume and local packing play a key role in controlling this ratio and thus the dynamics of glass formers near T_g. We start by collecting literature Q_V/Q_P values from the different glass-forming systems at $P = 0.1$ MPa and at T_g (defined at $\tau = 1$ s) (obtained mainly by dielectric spectroscopy and light scattering) in Table 2.2

Apart from the dynamic ratio, Q_V/Q_P, we discuss a well-known property of amorphous systems and glass-forming liquids, namely, the presence of a degree of packing regularity reflected by the broad peaks in the wide-angle X-ray or neutron scattering curves [58–60]. For polymers in particular, the peak at higher values of the wave vector q, with an equivalent Bragg spacing of about 0.5 nm, corresponds to the vdW (VDW) contacts of atoms and is known as the vdW peak. The peak at lower q, known as the low van der Waals (LvdW) peak, reflects largely the intermolecular correlations of polymeric backbones. There are some exceptions to this; in bisphenol A polycarbonate (BPA-PC), the first (shallow) peak at $q^* \sim 6$ nm^{-1} is caused mainly by the correlation between the carbonate groups, i.e., it is of intramolecular origin. On the contrary, for glass-forming liquids, the origin of the diffraction peaks and their q^* (T) is not well understood.

In Table 2.2, the position of the LVDW peak for various glass-forming systems is reported and allows the correlation of this "static" quantity (the reported q^* values are in most cases measured in the vicinity of T_g) with the dynamic ratio Q_V/Q_P, obtained at T_g ($P = 0.1$ MPa, $\tau = 1$ s). This correlation is by no means perfect; however, in extreme cases, it allows for some conclusions. For example, in glass-formers with $q^* < 5$ nm^{-1}, the ratio Q_V/Q_P is below 0.6. Similarly, in glass formers with $q^* > 15$ nm^{-1}, the ratio Q_V/Q_P is higher than 0.6. The meaning of these correlations is that in main-chain flexible polymers (high q^*), temperature

Table 2.2 Sample code and name, glass temperature, repeat unit volume (V_m), characteristic wave vector (q^*) of the first intense peak of the static structure factor, and ratio of the constant volume activation energy (Q_V) to the enthalpy of activation (Q_P)

Code	Sample	T_g (K)	V_m (nm^3)	q^* (nm^{-1})	Q_V/Q_P [P = 1atm, T_g (τ = 1s)]
A	Poly(methyl-*p*-totyl siloxane) (PM*p*TS)	249.9	0.212	6.3	0.59
		261			0.55
B	Bisphenol A polycarbonate (BPAPC)	414	0.364	12.3	0.44
C	Poly(vinyl methyl ether) (PVME)	245.5	0.091	9.7	0.7
D	Poly(4-vinyl phenol) (PVPh)	443	–	14.1	~0.77
E	Polystyrene (PS)	373	0.169	8	0.64
F	Poly(2-vinyl pyridine) (P2VP)	367	0.185	7.8	0.7
G	1,4-Polybutadiene (PB)	263	0.093	15	0.76[a]
H	Poly(methyl acrylate) (PMA)	276	0.119	9.4	0.78[b]
I	Polyethylene (PE)	200	0.044	13.7	0.71–0.76
		225			0.81–0.85
J	1,2-Polybutadiene (PB)	253	0.094	10	0.7
K	Poly(vinyl ethyl ether) (PVEE)	240.6	0.113	8.2	0.81
L	Poly(propylene glycol) (PPG)	202.5	0.068	12.4	0.66
M	1,4-Polyisoprene (PI)	203	0.118	14	0.78
N	Polyvinylacetate (PVAc)	311	0.121	9.9	0.6
O	Poly(methyl phenyl siloxane) (PMPS)	245.7	0.171	7.2	0.46
P	Poly(*t*-butyl methacrylate) (P*t*BMA)	334	0.230	7.1	0.56
Q	Poly(*n*-ethyl methacrylate) (PnEMA)	326.7	0.170	5.6	0.55
R	*o*-terphenyl (OTP)	243.5	0.342	9.0	0.55
S	salol	220	0.282	8.0	0.43 ± 0.2
T	1,1′-bis(*p*-methoxy phenyl) cyclohexane (BMPC)	241	0.34	7.8	0.38
U	1,1′-di(4-methoxy-5-methyl phenyl) cyclohexane (BMMPC)	261	0.368	7.6	0.41
V	Phenolphthalein dimethylether (PDE)	249	0.419	–	0.52
W	Cresolphthalein dimethylether (KDE)	313	0.551	–	0.49
X	Poly[(phenyl glycidylether)-*co*-formaldehyde] (PPGE)	258	0.243	–	0.62
Y	Poly[(*o*-cresol glycidylether)-*co*-formaldehyde] (PCGE)	285	0.23	–	0.65
Z	Diglycidylether of bisphenol A (DGEBA)	335	0.4	–	0.6
1	Polyvinyl chloride (PVC)	353	0.076	–	0.8
2	Polyoxybutylene (POB)	199	0.116	–	0.75

[a]At $T = T_g + 100$ K
[b]At $T = T_g + 31$ K

through the energy barriers (k_BT) provides the main means of affecting the dynamics. Instead, in polymers with bulky side-groups (low q^*), volume effects gain importance and the dynamics are controlled by both ρ and T. Nonetheless, this correlation is not always exact. For example, BPA-PC with a low Q_V/Q_P value (~0.44) [61] has a high q^* value. This implies that parameters other than the mere interchain distance also play a role.

The broad correlation improves considerably if both the lateral distance and the distance along the backbone per repeat unit are taken into account. This is shown in

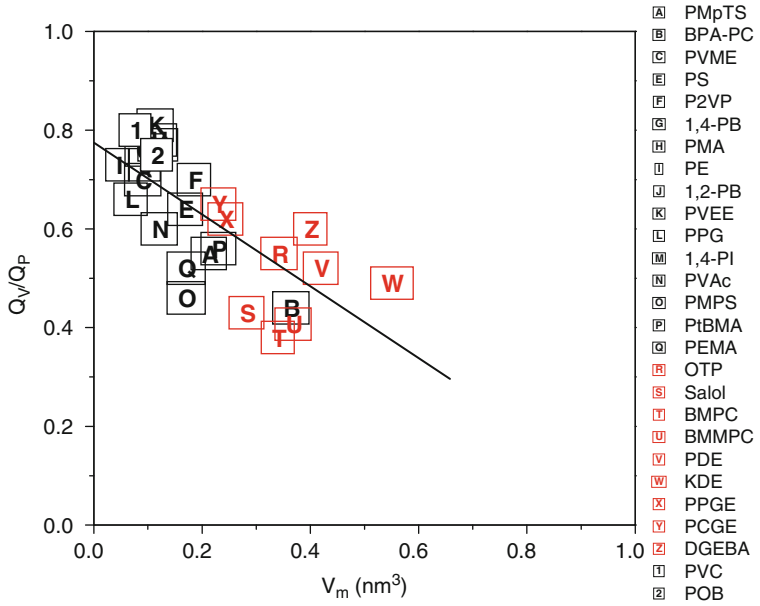

Fig. 2.8 Ratio of the constant volume activation energy (Q_V) to the enthalpy of activation (Q_P) plotted as a function of the repeat unit volume (polymers) or the molecular volume (glass-forming liquids). The results from the glass-forming liquids are presented in color. Notice the lower values of the dynamic ratio for the glass-forming liquids that result from the larger size of these molecules necessary to avoid crystallization. The line is the result of a linear fit to all data points (from [57])

Fig. 2.8 where the dynamic ratio is plotted as a function of the repeat unit volume ($V_m = M/\rho N_A$, where M is the molecular weight of the repeat unit).

This dependence suggests that the reason for the very low Q_V/Q_P values of some glass-forming liquids and some polymers (BPA-PC) is their large repeat unit volume. In the same figure, additional data from other glass-forming liquids are also included. Notice that the reason for the higher Q_V/Q_P values of poly[(phenyl glycidylether)-*co*-formaldehyde] (PPGE) and poly[(*o*-cresol glycidylether)-*co*-formaldehyde] (PCGE) compared to those of the other glass-forming liquids is the smaller volume of their repeat unit. Similarly, the low values of the activation ratio in the case of glass-forming liquids result from their larger molecular volume [57]. Large monomer volumes and irregular shapes are required as they inhibit crystallization. We mention here that the good correlation of the dynamics with the static properties such as packing and repeat unit volume can be extended to include other variables that control the dynamics, such as the Kuhn length and the packing length [62].

Thus the repeat unit volume and local packing play a key role in controlling the value of this ratio at T_g, and the dynamics associated with the glass temperature. In particular, for *flexible* main-chain polymers, temperature, through the presence of energy barriers opposing molecular motions, is the main parameter affecting the

dynamics, whereas in polymers with *bulky side-groups* or in glass-forming liquids with large molar volumes, volume effects gain importance. These ideas are by no means new. A similar conclusion was reached by a recent theory of glass formation by Dudowicz, Freed, and Douglas [63] that emphasizes the importance of repeat unit volume, and backbone and side-group rigidity. In addition, Ngai and Roland [64] showed that the degree of intermolecular cooperativity of motions and the fragility reflect these same properties, namely, backbone flexibility and the presence of bulky side-groups. What is new, however, in this approach is that it provides a quantitative account of the value of the dynamic ratio, and thus of the parameters that most affect the dynamics, in relation to the molecular volume and packing.

The monomer volume approach that emphasizes the packing properties is different from the thermodynamic scaling because it includes the attractive forces that control the packing and the thermodynamic state. It also suggests that a general theory of liquid dynamics, applicable to all ρ and T and for all glass formers should, take into account both the repulsive and attractive parts of the potential function.

The proposed correlation between the local packing and the value of the dynamic ratio also has consequences with respect to the issue of dynamic heterogeneity in polymer blends and copolymers [65]. The appropriate choice of monomers in these could result in drastically different T and P dependencies for the two components, with consequences on their dynamic and possibly their thermodynamic miscibility (see Chap. 5).

References

1. Angell CA (1995) Science 67:1924
2. Stillinger FH (1995) Science 267:1935
3. Ferry JD (1980) Viscoelastic properties of polymers, 3rd edn. Wiley, New York
4. Cohen MH, Grest GS (1979) Phys Rev B 20:1077
5. Tölle A (2001) Rep Prog Phys 64:1473
6. Dreyfus C, Aouadi A, Gapinski J, Matos-Lopes M, Steffen W, Patkowski A, Pick RM (2003) Phys Rev E 68:011204
7. Casalini R, Roland CM (2004) Phys Rev E 69:062501
8. Dreyfus C, Le Grand A, Gapinski J, Steffen W, Patkowski A (2004) Eur Phys J B 42:309
9. Alba-Simionseco C, Cailliaux A, Alegria A, Tarjus G (2004) Europhys Lett 68:58
10. Pawlus S, Casalini R, Roland CM, Paluch M, Rzoska SJ, Ziolo J (2004) Phys Rev E 70:061501
11. Roland CM, Hensel-Bielowka S, Paluch M, Casalini R (2005) Rep Prog Phys 68:1405
12. Hoover WG, Ross M (1971) Contemp Phys 12:339
13. Casalini R, Roland CM (2007) J Non-Cryst Solids 353:3936
14. Bailey NP, Pedersen UR, Gnan N, Schrøder TB, Dyre JC (2008) J Chem Phys 129:184507
15. Bailey NP, Pedersen UR, Gnan N, Schrøder TB, Dyre JC (2008) J Chem Phys 129:184508
16. Coslovich D, Roland CM (2009) J Chem Phys 130:014508
17. Williams G (1964) Trans Faraday Soc 60:1556
18. Naoki M, Endou H, Matsumoto K (1987) J Phys Chem 91:4169
19. Ferrer ML, Lawrence C, Demirjian BG, Kivelson D, Alba-Simionesco C, Tarjus G (1998) J Chem Phys 109:8010
20. Casalini R, Roland CM (2005) Phys Rev B 71:014210

21. Niss K, Alba-Simionesco C (2006) Phys Rev B 74:024205
22. Niss K, Dalle-Ferrier C, Tarjus G, Alba-Simionesco C (2007) J Phys Condens Matter 19:076102
23. Alba-Simionesco C, Tarjus G (2006) J Non-Cryst Solids 352:4888
24. Mpoukouvalas K, Floudas G, Williams G (2009) Macromolecules 42:4690
25. Boyer RF, Spencer RS (1944) J Appl Phys 15:398
26. Van Krevelen DW (1990) Properties of polymers. Elsevier, New York
27. Casalini R, Roland CM (2004) Colloid Polym Sci 283:107
28. Paluch M, Grzybowska K, Grzybowski A (2007) J Phys Condens Matter 19:205117
29. Corezzi S, Capaccioli S, Casalini R, Fioretto D, Paluch M, Rolla PA (2000) Chem Phys Lett 320:113
30. Casalini R, Mohanty U, Roland CM (2006) J Chem Phys 125:014505
31. Hartwig G (1994) Polymer properties at room and cryogenic temperatures, Chap. 4. Plenum, New York
32. Roland CM, Feldman JL, Casalini R (2006) J Non-Cryst Solids 352:4895
33. Grüneisen E (1912) Ann Phys (Leipzig) 39:257
34. Moelwyn-Hughes EA (1951) J Phys Coll Chem 55:1246
35. Roland CM (2008) In: Bhowmick AK (ed) Current topics in elastomers research, Chap. 24. CRC Press in Taylor & Francis Group, Boca Raton
36. Boyer RF, Spencer RS (1944) J Appl Phys 15:398
37. Van Krevelen DW (1990) Properties of polymers. Elsevier, New York
38. Casalini R, Roland CM (2005) Phys Rev E 72:031503
39. Casalini R, Capaccioli S, Roland CM (2006) J Phys Chem B 110:11491
40. Grzybowski A, Grzybowska K, Zioło J, Paluch M (2006) Phys Rev E 74:041503
41. Grzybowski A, Grzybowska K, Zioło J, Paluch M (2007) Phys Rev E 76:013502
42. Williams G, Watts DC (1970) Trans Faraday Soc 66:80
43. Böhmer R, Ngai KL, Angell CA, Plazek DJ (1993) J Chem Phys 99:4201
44. Ngai KL, Casalini R, Capaccioli S, Paluch M, Roland CM (2005) J Phys Chem B 109:17356
45. Roland CM, Bair S, Casalini R (2006) J Chem Phys 125:124508
46. Reiser A, Kasper G, Hunklinger S (2005) Phys Rev B 72:094204
47. Pedersen UR, Bailey NP, Schrøder TB, Dyre JC (2008) Phys Rev Lett 100:015701
48. Allen MP, Tildesley DJ (1987) Computer simulation of liquids. Oxford University Press, Oxford
49. Bardic VY, Malomuzh NP, Sysoev VM (2005) J Mol Liq 120:27
50. Bardik VY, Shakun KS (2005) Ukr J Phys 50:404
51. Naoki M, Koeda S (1989) J Phys Chem 93:948
52. Grzybowski A, Paluch M, Grzybowska K (2009) J Phys Chem B 113:7419
53. Grzybowski A, Haracz S, Paluch M, Grzybowska K (2010) J Phys Chem B 114:11544
54. Weeks JD, Chandler D, Andersen HC (1971) J Chem Phys 54:5237
55. Grzybowski A, Paluch M, Grzybowska K, Haracz S (2010) J Chem Phys 133:161101
56. Paluch M, Haracz S, Grzybowski A, Mierzwa M, Pionteck J, Rivera-Calzada A, Leon C (2010) J Phys Chem Lett 1:987.
57. Floudas G, Mpoukouvalas K, Papadopoulos P (2006) J Chem Phys 124:074905
58. Miller RL, Boyer R, Heijboer J (1984) J Polym Sci Polym Phys Ed 22:2021
59. Floudas G, Stepanek P (1998) Macromolecules 31:6951
60. Cailliaux A, Alba-Simionesco C, Frick B, Willner L, Goncharenko I (2003) Phys Rev E 67:010802
61. Mpoukouvalas K, Gomopoulos N, Floudas G, Herrmann C, Hanewald A, Best A (2006) Polymer 47:7170
62. Everaers R, Sukumaran SK, Grest GS, Svaneborg C, Sivasubramanian A, Kremer K (2004) Science 303:823
63. Dudowicz J, Freed K, Douglas JF (2005) J Chem Phys 123:111102
64. Ngai KL, Roland CM (1993) Macromolecules 26:6824
65. Floudas G, Fytas G, Reisinger T, Wegner G (1999) J Chem Phys 111:9129

Chapter 3
Models of Temperature–Pressure Dependence of Structural Relaxation Time

Up to now, the influence of pressure and temperature on structural relaxation time was discussed separately. A more general approach, however, requires considering the combined effects of P and T. This naturally relates to a search for the equivalent of an "equation of state" with physically interpretable parameters for the description of $\tau(T, P)$ dependence for different materials. Knowledge of the equation of state is of paramount importance in predicting the pressure behavior of fragility and of the glass transition temperature [1]. In this chapter, we will discuss various canonical models, proposed in the literature, that incorporate both the T and P dependences of the structural relaxation time.

3.1 The Generalized Vogel–Fulcher–Tammann Equation

Some attempts in searching for an adequate equation of state have been motivated by the fact that the Vogel–Fulcher–Tammann (VFT) equation (1.7) provides a versatile description of the relaxation times over a wide range of temperatures and for a large number of glass-forming liquids. Fytas [2] was the first to incorporate pressure as a variable into the VFT equation using two linear approximations originally proposed by Grest and Cohen [3, 4]:

$$T_0(P) = T_0(0.1\text{MPa}) + aP, \tag{3.1}$$

$$B(P) = B(0.1\text{MPa}) + bP. \tag{3.2}$$

The above transformation leads to the generalized VFT equation:

$$\tau(T,P) = \tau_0 \exp\frac{B + bP}{T - (T_0 + aP)}. \tag{3.3}$$

A somewhat different $\tau(T,P)$ equation ($\tau = \tau_0 \exp[(\mathrm{A} + \mathrm{B}P)/(R(T - T_0))]$) was subsequently suggested by G.D. Patterson and Carroll [5]. However, Leyser and

G. Floudas et al., *Molecular Dynamics of Glass-Forming Systems*, Advances in Dielectrics 1, DOI 10.1007/978-3-642-04902-6_3,

coworkers [6] demonstrated that (3.3) fails to describe the behavior of the structural (α-) relaxation times as determined from specific heat spectroscopy measurements of orthoterphenyl in the frequency range 2 Hz–6.3 kHz. The same conclusion was reached based on the analysis of the temperature and pressure dependences of dielectric relaxation data of an epoxy resin [7]. As discussed in [7], the poor agreement of the above equation with experimental data relates to the assumed linear $T_g(P)$ dependence. However, in most cases, a nonlinear pressure dependence of the glass transition temperature is observed. Thus, assuming linear $B(P)$ and $T_0(P)$ dependences is not sufficient to reproduce the (T,P) surface of relaxation times adequately. In this context, it is worth mentioning that transformations (3.1) and (3.2) also fail [8, 9] in case of the Grest–Cohen free volume model [3, 4].

3.2 The Adam–Gibbs Model

According to the model of Adam and Gibbs (AG) [10], the rate of the structural relaxation in glass-forming liquids is determined by probabilities of cooperative rearrangements. To evaluate these transition probabilities, they defined *cooperatively rearranging regions* (CRR) as the smallest volume elements that can relax to a new configuration independent of its environment. Assuming that the potential energy barrier, $\Delta\mu$, hindering the transition of a CRR to a new configuration is independent of both T and the number of molecules in a cooperative region of size z, Adam and Gibbs arrived at the following expression for the average transition probability that is inversely proportional to the structural relaxation time:

$$\tau_\alpha \propto \overline{W}(T) = A \exp\left(-\frac{z^*\Delta\mu}{kT}\right). \tag{3.4}$$

Here, z^* is a critical lower limit to the size of cooperative regions that can yield nonzero transition probabilities. The equation above implies that mainly regions whose size differ negligibly from the smallest size z^* participate in motions that give rise to cooperative rearrangements. The size of the cooperative rearranging regions has been shown to relate to the molar configurational entropy, S_c, of the macroscopic sample as

$$z^* = \frac{N_A s_c^*}{S_c}, \tag{3.5}$$

where s_c^* is the critical configurational entropy.

Equations (3.4) and (3.5) can be combined to yield the main result of the AG theory, namely, the relationship between the structural relaxation time and configurational entropy:

$$\tau_\alpha = \tau_0 \exp\left(\frac{s_c^* \Delta\mu}{kTS_c}\right) = \tau_0 \exp\left(\frac{c}{TS_c}\right). \tag{3.6}$$

The configurational entropy, S_c, is usually estimated from the excess heat capacity, $\Delta C_p = C_p^{\text{melt}} - C_p^{\text{crystal}}$, of the equilibrium melt with respect to the crystal (or eventually to glass):

$$S_c(T) \propto S_{\text{exc}}(T) = \int_{T_K}^{T} \frac{\Delta C_p(T)}{T} \mathrm{d}T. \tag{3.7}$$

However, Goldstein [11] and later Johari [12, 13], argued that determining $S_c(T)$ in such a way results in an overestimated configurational entropy because it may include vibrational terms. Nevertheless, it has been demonstrated that the use of excess entropy, S_{exc}, in (3.6) leads to the satisfactory description of the experimental data in the temperature range close to T_g. Since many glass-forming liquids reveal an inverse dependence of the excess heat capacity on temperature, i.e., $\Delta C_p = K/T$, where $K = K(P)$ is a material property, it can be shown that

$$S_c(T) = \int_{T_K}^{T} \frac{K}{T^2} \mathrm{d}T = \frac{K}{T_K} - \frac{K}{T} = S_\infty - \frac{K}{T}. \tag{3.8}$$

Substituting (3.8) into (3.7) results in the well-known temperature VFT equation [see (1.7) in Chap. 1].

In an aim to incorporate pressure to the AG model, Casalini and coworkers [14, 15] proposed adding a term related to the molar thermal expansion in (3.7):

$$S_c(T,P) = \int_{T_K}^{T} \frac{\Delta C_P(T)}{T} \mathrm{d}T - \int_0^P \Delta\left(\frac{\partial V}{\partial T}\right)_P \mathrm{d}P, \tag{3.9}$$

where $\Delta\left(\frac{\partial V}{\partial T}\right)_P = \left(\frac{\partial V}{\partial T}\right)_P^{\text{melt}} - \left(\frac{\partial V}{\partial T}\right)_P^{\text{crystal}}$ is the difference of the molar thermal expansivity and the melt relative to the crystal. The second term in (3.9) can be obtained from PVT measurements. Using the Tait equation (1.29), Casalini and coworkers obtained the following analytical expression for the pressure dependence of $S_c(T,P)$

$$\begin{aligned} S_c(T,P) = S_\infty - \frac{K(P)}{T} \\ + \delta\left\{-(\beta+\gamma-1)P + (\gamma-1)B(T)\ln\left(1+\frac{P}{B(T)}\right) + \gamma P \ln\left(1+\frac{P}{B(T)}\right)\right\}, \end{aligned} \tag{3.10}$$

where β, γ, and δ are, respectively,

$$\beta = \frac{1}{b_2 C V^{\text{melt}}(T,0)} \Delta\left(\frac{\partial V}{\partial T}\right)_{P=0}; \quad \gamma = \frac{\alpha}{b_2}; \quad \delta = C V^{\text{melt}}(T,0) b_2, \tag{3.11}$$

and $\alpha = (1/V)(\partial V/\partial T)_P$ is the coefficient of thermal expansion of the melt.

This equation has been obtained by assuming that the pressure variation of the molar thermal expansivity for the crystal can be neglected, i.e., $(\partial V^{\text{crystal}}/\partial T)_p = (\partial V^{\text{crystal}}/\partial T)_{p=0}$.

Substituting into (3.6) gives the following expression for the *T*–*P* dependence of the structural relaxation time

$$\tau(T,P) = \tau_0 \exp\left\{\frac{c}{T\left[S_\infty - \left(\frac{K}{T}\right) + \delta\left\{-(\beta+\gamma-1)P + (\gamma-1)B(T)\ln\left(1+\frac{P}{B(T)}\right) + \gamma P \ln\left(1+\frac{P}{B(T)}\right)\right\}\right]}\right\}. \tag{3.12}$$

The above equation is usually converted into the more convenient VFT-like form:

$$\tau(T,P) = \tau_0 \exp\left(\frac{DT_0^*}{T - T_0^*}\right) \tag{3.13}$$

with

$$T_0^*(P) = \frac{T_0(p=0)}{\left[1 + (\delta/S_\infty)\left\{-(\beta+\gamma-1)P + (\gamma-1)B(T)\ln\left(1+\frac{P}{B(T)}\right) + \gamma P \ln\left(1+\frac{P}{B(T)}\right)\right\}\right]}, \tag{3.13a}$$

$$D = \frac{C\Delta\mu}{K}. \tag{3.13b}$$

It has been pointed out by G. Williams that the use of *D* in (3.13) creates problems in the limit $T_0 \to 0$, as this equation does not yield the Arrhenius equation, whereas in the form exp[*B*/(*T*–T_0)], it does.

According to this approach, the strength parameter *D* is the same as that at atmospheric pressure. It is worth noting that at high pressures, a deviation of the isobaric relaxation time from the VFT behavior can be expected due to the dependence of *B*, β, γ, and δ on temperature. However, as argued in [14–16], the dependence of these parameters on temperature is usually very weak and, therefore, the expected deviation could be observed only at very high pressures ($P \gg B$). In a number of studies, it has been demonstrated that the equation derived from the AG model gives a good description of combined *T*–*P* dependence of structural relaxation times for a number of systems that include OTP [16], triphenylchloromethane [16], poly(methyl methacrylate) [16], salol [17], phenylphthaleindimethylether (PDE) [18], and 4,4′-methylenebis(*N*,*N*-diglycidylaniline) [19].

3.3 The Avramov Model

The next entropic model that is frequently employed in describing viscosity and relaxation data of glass-forming liquids in the T–P plane was originally formulated by Avramov [20] for describing viscosity on the basis of his earlier considerations in disordered systems [21–25]. A basic hypothesis of this model is that motions of molecules are purely thermally activated with a jump frequency related to a barrier energy E_i for the process:

$$v_i(E_i) \sim \exp\left(-\frac{E_i}{RT}\right). \tag{3.14}$$

However, for amorphous materials characterized by structural disorder, one needs to consider an average jump frequency that depends on some broad distribution of energy barrier heights as

$$\langle v \rangle = \sum_{i=0}^{\infty} v_i \varphi_i(E_i), \tag{3.15}$$

where $\varphi_i(E_i)$ is a probability of appearance of the activation barrier, E_i, in the energy landscape. He further assumed a truncated Poisson probability distribution function,

$$\varphi(E) \sim \exp\left(\frac{E - E_{\max}}{\sigma}\right), \tag{3.16}$$

that seems to represent the energy distribution for real physical disordered systems [21]. In (3.16), σ is the system dispersion, and the energy range, $0 \leq E \leq E_{\max}$, has its upper limit at the energy level, $E_{\max}$, that equals a single barrier height in a corresponding ordered state. Consequently, using the continuous approximation of (3.14), one can obtain for the average jump frequency:

$$\langle v \rangle = \int_0^{E_{\max}} v(E) w(E, \sigma) \mathrm{d}E. \tag{3.17}$$

In (3.17), the probability density function is given as

$$w(E, \sigma) = \frac{\exp\left(\frac{E - E_{\max}}{\sigma}\right)}{\sigma\left(1 - \exp\left(-\frac{E_{\max}}{\sigma}\right)\right)}. \tag{3.18}$$

The integral in (3.17) with the probability density of (3.18) results in an analytical form for the average jump frequency

$$\langle v \rangle = \frac{\left[1 - \exp\left(-E_{\max}\left(\frac{1}{RT} - \frac{1}{\sigma}\right)\right)\right]}{\left(\frac{\sigma}{RT} - 1\right)\left(1 - \exp\left(-\frac{E_{\max}}{\sigma}\right)\right)} v_0' \exp\left(-\frac{E_{\max}}{\sigma}\right) \tag{3.19}$$

that can be approximated for $RT < \sigma < E_{\max}$ by a simpler expression

$$\langle v \rangle \approx v_0 \exp\left(-\frac{E_{\max}}{\sigma}\right). \tag{3.20}$$

As shown earlier [21], the dispersion σ of the system can be dependent upon the system entropy S as follows:

$$\sigma = \sigma_r \exp\left(\frac{2(S - S_r)}{ZR}\right), \tag{3.21}$$

where R is the gas constant, and Z denotes the degeneracy of the system, i.e., the number of escape channels for a moving particle, or in other words, the number of available pathways for local motions of a molecule or polymer segment [26]. The latter can be practically interpreted as a value proportional to the coordination number of the liquid lattice, although it has been noted that such a treatment of the parameter Z is rather a rough approximation [21, 25, 26]. Although a range of values $2 \leq Z \leq 12$ has been considered [21], it has been suggested that $Z \approx 10$ for typical inorganic glass formers [25]. The other parameters in (3.21), σ_r and S_r are, respectively, the dispersion and the entropy of the system at some reference state.

From the average jump frequency one can calculate the macroscopic relaxation time by using the inverse proportionality

$$\tau \sim \frac{1}{\langle v \rangle}. \tag{3.22}$$

If the decoupling phenomenon described in Sect. 9 of [27] does not occur, then on the basis of the Maxwell relation between the macroscopic relaxation time and viscosity, $\eta = G_\infty \tau$, where G_∞ is the shear modulus at the high frequency limit, one can apply (3.20) and (3.21) to derive the entropic expression for viscosity also as some inverse proportionality to the average jump frequency as

$$\eta = \eta_\infty \exp\left[\in \exp\left(-\frac{2(S - S_r)}{ZR}\right)\right]. \tag{3.23}$$

Here, the preexponential factor η_∞ is the viscosity at the high temperature limit and the parameter $\in$ is given by $\in = E_{\max}/\sigma_r$. The above equation underlies the choice of the reference state at which the parameters σ_r and S_r are established. A point within the glass transition interval is usually fixed as the reference state, which can be reduced for convenience to some state at which $\in = 30$ according to (3.23), because the glass transition usually appears at viscosity $\eta_g \approx e^{30}$ P $\approx 10^{13} P$ [20].

It is worth emphasizing that the total entropy is considered in the Avramov model (3.23) unlike the Adam–Gibbs model described earlier. This is its main advantage, as the $\eta(T)$ Avramov relation is free from singularities, i.e., it does not diverge at the Kauzmann temperature. The total entropy as a state function dependent on T and P can be calculated in terms of the reference state (T_r, P_r):

$$S(T,P) = S_r + \int_{T_r}^{T} \left(\frac{\partial S}{\partial T}\right)_P \mathrm{d}T + \int_{P_r}^{P} \left(\frac{\partial S}{\partial P}\right)_T \mathrm{d}P. \tag{3.24}$$

Using the known thermodynamic relations, $(\partial S/\partial T)_P = C_P/T$ and $(\partial S/\partial P)_T = -\alpha_P V$, where C_P is the isobaric heat capacity and α_P is the isobaric thermal volume expansivity, and by assuming further that C_P and α_P are temperature independent, and α_P can be expressed by the following pressure dependent function [20, 28]:

$$\alpha_P(P) = \frac{1}{V}\left(\frac{\partial V}{\partial T}\right)_P \approx \alpha_{P_r} \frac{\Pi + P_r}{\Pi + P}, \tag{3.25}$$

where $\alpha_{P_r} = \alpha_P(P_r)$ and Π is an adjustable parameter, one can determine from (3.24) the T–P dependence of entropy in terms of the reference state as

$$S(T,P) = S_r + C_P \ln\left(\frac{T}{T_r}\right) - \alpha_{P_r} V_m (\Pi + P_r) \ln\left(\frac{\Pi + P}{\Pi + P_r}\right). \tag{3.26}$$

Here, V_m is the molar volume. Substituting (3.26) to (3.23), one can obtain the generalized expression for viscosity:

$$\eta = \eta_\infty \exp\left[\in \left(\frac{T_r}{T}\right)^a \left(\frac{\Pi + P}{\Pi + P_r}\right)^b\right], \tag{3.27}$$

where the adjustable parameters a and b have the following physical meaning:

$$a = \frac{2C_P}{ZR}, \tag{3.27a}$$

$$b = \frac{2\alpha_{P_r} V_m}{ZR}(\Pi + P_r) = a\frac{\alpha_{P_r} V_m}{C_P}(\Pi + P_r). \tag{3.27b}$$

According to (3.22), an equation analogous to (3.27) can be derived for the relaxation time as

$$\tau = \tau_\infty \exp\left[\in \left(\frac{T_r}{T}\right)^a \left(\frac{\Pi + P}{\Pi + P_r}\right)^b\right], \tag{3.28}$$

where τ_∞ is the relaxation time in the high temperature limit, and the other parameters $\in$, a, b, T_r, and P_r have the same meaning as those for the viscosity. The pressure reference state is usually chosen at ambient pressure, i.e., $P_r = P_0 \approx 0$. As mentioned previously, the reference state corresponds to the glass transition; therefore, $T_r = T_g(P_0) = T_{g0}$. Moreover, the parameter ε in (3.28) can be more generally expressed as $\in = \ln(\tau_g/\tau_\infty)$, where $\tau_g = \tau(T_g)$. Consequently, one can reduce (3.28) to the following form:

$$\tau = \tau_\infty \exp\left[\ln\left(\frac{\tau_g}{\tau_\infty}\right)\left(\frac{T_g(P)}{T}\right)^a\right], \tag{3.29}$$

where

$$T_g(P) = T_g(P_0)\left(1 + \frac{P}{\Pi}\right)^{b/a} \tag{3.30}$$

that is similar to (1.18) and

$$a = \frac{2C_P}{ZR} \tag{3.30a}$$

$$b = \frac{2\alpha_0 V_m}{ZR}\Pi = a\frac{\alpha_0 V_m}{C_P}\Pi. \tag{3.30b}$$

The pressure function of T_g derived in this way (3.30) from the Avramov model is widely used in analyzing glass transition temperatures determined from pressure experimental data. The next interesting result following from this model, besides the T–P dependent equations for η and τ, successfully applied to fit experimental data, is an observation that according to the definition

$$m_P = \left(\frac{\partial \log_{10}(\tau)}{\partial(T_g/T)}\right)_P\Bigg|_{T=T_g}$$

the parameter a is proportional to the isobaric fragility m_P

$$m_P = a(\log_{10}\tau_g - \log_{10}\tau_\infty). \tag{3.31}$$

However, the parameter a is pressure independent, due to a conveniently assumed pressure independence of Z and C_P which is practically taken as C_{P_0} (3.30a), i.e., the isobaric heat capacity at atmospheric or no pressure conditions. Thus, this prediction is not in accordance with the experimentally found pressure dependences of m_P; the latter usually decreases with increasing P for van der Waals liquids and polymers (Chap. 2), whereas it increases with P in the case of strongly

hydrogen-bonded systems. To improve the relation given by (3.31), Paluch and Roland [29] have proposed a simple linear pressure dependence of this parameter as

$$a(P) = a_0 + a_1 P. \tag{3.32}$$

Very recently, the original Avramov model was developed [28] to take into account the pressure dependence of the isobaric heat capacity, $C_P(P) \approx C_{P_0} + f(P)$, and the temperature dependence of the product $(\alpha_{P_0} V)(T) \approx \alpha_0 V_0 + \phi(T)$ where the reference state was chosen at no pressure or at atmospheric conditions (P_0, $T_g(P_0)$, $V(T_g(P_0),P_0)$). One of the results of the modified Avramov model is a new formula for the "fragility" parameter a, which better reflects the nonlinear experimental dependence $m_P(P)$

$$a(P) = a_0 \left(1 - \frac{C}{C_{P_0}} \ln\left(\frac{\Pi + P}{\Pi + P_0} \right) \right), \tag{3.33}$$

where $a_0 = \frac{2C_{P_0}}{ZR}$ and C is an additional adjustable parameter.

Finally, it has to be noted that in spite of the mentioned achievements of the Avramov model, that satisfactorily describes both the dependences $\eta(T, P)$ and $\tau(T, P)$ of the glass former PDE, this model has been recently found as potentially inapplicable to the description of some dielectric permittivity spectra. Puzenko et al. [30] have tested the shape of the dielectric spectra of some glass formers (including PDE and poly(dimethylsiloxane)) following the Avramov model. To do so, they exploited the most popular, so-called heterogeneous, paradigm in the theory of dielectrics, i.e., by assuming that the non-Debye response for the structural relaxation in glass-forming liquids can be represented by a linear superposition of Debye relaxation processes with a relaxation time probability density distribution $g(\tau)$. They have assumed that each individual relaxation time can be expressed by the inverse jump frequency given by (3.14), and replaced the average on the relaxation time τ with the distribution $g(\tau)$ by the average on the activation energy with the Poisson probability density function, $w(E, \sigma)$, as proposed by the Avramov model (3.18) [30]. Subsequently, they have shown that the asymmetrical broadening of the loss spectrum is directly related to the dispersion σ of the energy barrier distribution, and that the half-width of the loss spectrum should decrease with decreasing temperature. This last result following the predictions of the Avramov model is at odds with the experimental facts [30].

3.4 Cluster Kinetics Model

The Cluster Kinetics Model proposed by McCoy and Brenskelle [31–33], describing the temperature and pressure effects on viscosity or dielectric relaxation, is based on the concept that molecules cluster together as they approach the glass

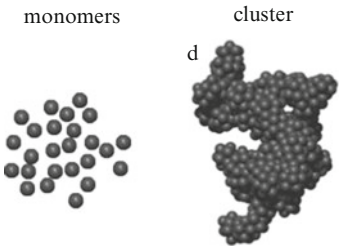

Fig. 3.1 Illustration of monomers and icosahedral cluster of 716 atoms simulated by Dzugutov et al. [34]

transition, and that this is the underlying physical phenomenon that explains glass formation. Within this model, clusters are groups of bonded molecules moving cooperatively, whereas monomers in the fluid state are separately in random thermal motion (Fig. 3.1).

The interactions "monomer–cluster" and "cluster–cluster" are modeled as reversible reaction-like mechanisms that can be regarded as representing fluctuating heterogeneous structures within the supercooled liquids:

1. Clusters may be formed by reversible addition of monomer $M(x_m)$ of molecular mass x_m to cluster $C(x)$ of mass x:

$$C(x) + M(x_m) \underset{k_g}{\overset{k_d}{\leftrightarrow}} C(x + x_m), \tag{3.34}$$

   where k_g and k_d are rate coefficients for growth and dissolution, respectively.
2. The clusters may themselves aggregate with rate coefficient k_a or fragment with breakage coefficient k_b

$$C(x) + C(x') \underset{k_b}{\overset{k_a}{\leftrightarrow}} C(x + x'). \tag{3.35}$$

It is assumed that four rate coefficients (k_g, k_d, k_a, and k_b) are independent of cluster size. According to the transition state theory, temperature–pressure dependences of the rate coefficients are proportional to $\exp(-(E + PV)/k_B T)$, where the activation energy E is the difference in energies of reactant and transition states, whereas V in this equation is the activation volume, i.e., the difference in volumes of reactant and transition states.

Molar concentrations of monomers, $m^{(0)}(t)$, and clusters, $c^{(0)}(t)$, are found, respectively, on the basis of population dynamics equations for monomers and clusters [31] as time-dependent zero moments of size distributions. According to the system of population equations, one can obtain the following set of rate expressions:

$$\frac{dm^{(0)}}{dt} = (k_d - k_g m^{(0)}) c^{(0)}, \tag{3.36}$$

$$\frac{\mathrm{d}c^{(0)}}{\mathrm{d}t} = (k_\mathrm{b} - k_\mathrm{a}c^{(0)})c^{(0)}. \tag{3.37}$$

Assuming local thermodynamic equilibrium, that is, setting the time derivatives in (3.36) and (3.37) to zero, one can obtain equilibrium monomer and cluster concentrations as the following ratios of the rate coefficients dependent on temperature, pressure, activation energy, and volume:

$$m_\mathrm{eq}^{(0)} = \frac{k_\mathrm{d}}{k_\mathrm{g}} = \kappa_\mathrm{m} \exp\left(-\frac{(h_\mathrm{m} + Pv_\mathrm{m})}{k_\mathrm{B}T}\right), \tag{3.38}$$

$$c_\mathrm{eq}^{(0)} = \frac{k_\mathrm{b}}{k_\mathrm{a}} = \kappa_\mathrm{c} \exp\left(-\frac{(h_\mathrm{c} + Pv_\mathrm{c})}{k_\mathrm{B}T}\right), \tag{3.39}$$

where the volume parameters $v_\mathrm{m} = V_\mathrm{d} - V_\mathrm{g}$ and $v_\mathrm{c} = V_\mathrm{b} - V_\mathrm{a}$ are differences in the activation volumes for (3.34) and (3.35) (see Fig. 3.2) and represent volumes of transformation for reversible growth and aggregation, whereas the energy parameters $h_\mathrm{m} = E_\mathrm{d} - E_\mathrm{g}$ and $h_\mathrm{c} = E_\mathrm{b} - E_\mathrm{a}$ are differences in activation energies for (3.34) and (3.35) (see Fig. 3.2) representing heats of transformation. The coefficients κ_m and κ_c are proportionality constants.

As presented in Fig. 3.2, the activation energies for the forward (association or aggregation) processes for (3.34) and (3.35) are always less than those for the reverse (dissociation or breakage) processes. The reaction progress of a dynamic system undergoing cooling and compression represents fluctuations among a large number of monomers and clusters as they proceed over local maxima and local minima to lower energies. Consequently, the process can be interpreted as occurring over an energy landscape defined by the energy transformation parameters h_m and h_c, and the volume transformation parameters v_m and v_c.

Exploiting the free-volume approach [35–37], the relative effect of clusters and monomers on the viscosity η, or alternatively on dielectric relaxation time τ (under the condition that the decoupling phenomenon described in Sect. 9 of [27] does not occur and thus $\tau \sim \eta$), can be expressed by the following equation:

$$\begin{aligned} \eta &= a \exp\left(b' \frac{V_\mathrm{c}}{V_\mathrm{m}}\right) = a \exp\left(b' \frac{m_\mathrm{eq}^0}{c_\mathrm{eq}^0}\right) \text{ and} \\ \tau &= \alpha \exp\left(b' \frac{V_\mathrm{c}}{V_\mathrm{m}}\right) = \alpha \exp\left(b' \frac{m_\mathrm{eq}^0}{c_\mathrm{eq}^0}\right), \end{aligned} \tag{3.40}$$

where V_c and V_m are cluster and monomer volumes, whereas a, α, and b' are constants. It should be noted that the relation between the volume and concentration ratios is valid if $m_\mathrm{eq}^{(0)}$ is taken as the number of moles of monomers per volume of

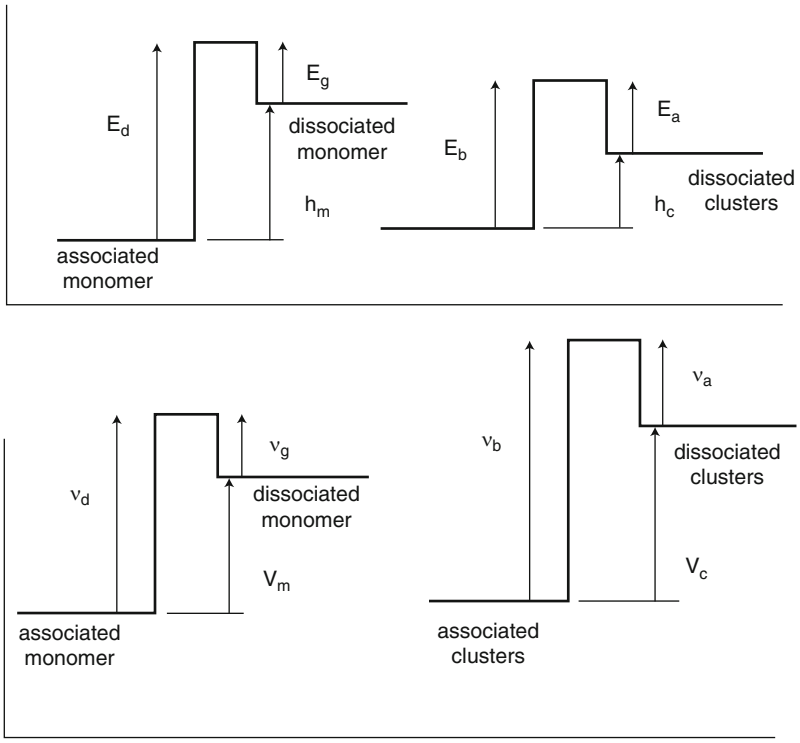

Fig. 3.2 Elements of the energy landscape. Energy and volume barriers are based on transition state theory for reversible monomer–cluster growth and dissociation and cluster–cluster association and breakage [(3.34) and (3.35)]. Energies and volumes of transformation are differences in activation energies $h_{\mathrm{m}} = E_{\mathrm{d}} - E_{\mathrm{g}}$ and $h_{\mathrm{c}} = E_{\mathrm{b}} - E_{\mathrm{a}}$, and volumes $v_{\mathrm{m}} = V_{\mathrm{d}} - V_g$ and $v_{\mathrm{c}} = V_{\mathrm{b}} - V_a$, respectively. The figure is taken from [32]

monomers, and $c_{\mathrm{eq}}^{(0)}$ as the number of moles of clusters per volume of clusters. Substituting (3.38) and (3.39) to (3.40), one can obtain, for instance, for the dielectric relaxation time,

$$\tau(T,P) = \alpha \exp[b\,\Phi(T,P)], \tag{3.41}$$

where Φ is an exponential function of T and P:

$$\Phi(T,P) = \exp\left(\frac{h + Pv}{k_{\mathrm{B}}T}\right). \tag{3.42}$$

The parameters $h = h_c - h_m$ and $v = v_c - v_m$ are invariant to T and P, and are material dependent.

On the basis of (3.41) with (3.42), one can formulate a scaled equation for the temperature and pressure dependence of dielectric relaxation time by choosing two

dielectric relaxation times, $\tau_f(T_f, P_f)$ and $\tau_g(T_g, P_g)$, in the fluid and glassy states, respectively,

$$\frac{\ln(\tau/\tau_g)}{\ln(\tau_f/\tau_g)} = \frac{\Phi - \Phi_g}{\Phi_f - \Phi_g}, \tag{3.43}$$

where $\Phi_g = \Phi(T_g, P_g)$ and $\Phi_f = \Phi(T_f, P_f)$. The superscript f represents a fluid condition, generally at maximum temperature in a constant pressure data set, or at minimum pressure in a constant temperature data set, whereas the index g indicates an arbitrary established glass transition point.

Using the general equation (3.43), the authors derived two expressions for the logarithm of the scaled relaxation time at isothermal and isobaric conditions; one for constant temperature data and another for constant pressure data [32]:

1. As a function of T_g/T for $P = \text{const}$

$$\log_{10}\left(\frac{\tau}{\tau_g}\right) = \frac{\Phi_g^{T_g/T} - \Phi_g}{\Phi_g^{T_g/T_f} - \Phi_g}\log_{10}\left(\frac{\tau_f}{\tau_g}\right), \quad \text{where } \Phi_g = \exp\left(\frac{h + Pv}{k_B T_g}\right). \tag{3.44}$$

2. As a function of P/P_g for $T = \text{const}$

$$\log_{10}\left(\frac{\tau}{\tau_g}\right) = \frac{\psi_g^{P/P_g} - \psi_g}{\psi_g^{P_f/P_g} - \psi_g}\log_{10}\left(\frac{\tau_f}{\tau_g}\right), \quad \text{where } \psi_g = \exp\left(\frac{P_g v}{k_B T}\right). \tag{3.45}$$

It is worth noting that a fitting procedure to (3.44) and (3.45) can be reduced to find two adjustable parameters Φ_g and ψ_g, respectively, given the values of $\tau_f(T_f, P_f)$ and $\tau_g(T_g, P_g)$. Several glass-forming systems have been tested including polymers and small molecules.

3.5 Defect Diffusion Model

A defect diffusion model (DDM) [38–40] has been extended by Bendler, Fontanella, and Shlesinger [41] to describe the influence of both temperature and pressure on the molecular dynamics in the vicinity of the glass transition on the basis of its first formulation in terms of only one thermodynamic variable, T. These authors originally proposed the generalized Vogel law for glass-forming liquids [42, 43]:

$$\tau_{DD} = A_{DD}\exp\left(\frac{B_{DD}}{(T - T_c)^{0.5df}}\right). \tag{3.46}$$

The above equation was derived [43] based on the following considerations:

1. A frozen-in dipole relaxes instantaneously in a lattice upon its encounter with a mobile defect and the dipole orientation correlation function can expressed by

$$\phi(t) = \exp[-c_{\mathrm{m}}N(t)], \tag{3.47}$$

where c_{m} is a concentration of mobile defects, and $N(t)$ is the number of distinct lattice sites a defect visits in a time t.

2. A defect jumps randomly on the lattice. The probability density that a defect remains at a lattice site for a time t, for the defect to jump over an activation barrier E_i, is given by $\psi_i(t) = v_i \exp[-v_i t]$, where according to the Arrhenius law, the jump frequency is given by$v_i = v_{i0}\exp[-E_i/kT]$. Consequently, considering a distribution of the activation barrier heights $\varphi(E)$, one can express the probability density of the residence of defects in lattice sites as follows:

$$\psi(t) = \int_0^\infty v\exp(-vt)w(v)\mathrm{d}v, \tag{3.48}$$

where $w(v) = \phi(E)|\mathrm{d}E/\mathrm{d}v|$ with $v = v_0\exp[-E/kT]$ and $\phi(E) = (kT_0)^{-1}$ $\exp(-E/kT_0)$. Using (3.48), the relaxation function (3.47) follows as [40]:

$$\phi(t) = \exp[-\lambda c_{\mathrm{m}}t^{\beta}], \quad \text{where } \beta = T/T_0 \text{ and } \lambda \text{ is a constant.} \tag{3.49}$$

The above equation has been determined as physically valid for $0 < \beta < 1$. Then, it can be easily reduced to the Kohlrausch–Williams–Watts expression as follows:

$$\phi(t) = \exp[-(t/\tau_{\mathrm{DD}})^{\beta}] \quad \text{where } \tau_{\mathrm{DD}} = (\lambda c_m)^{-1/\beta} = \tau_0 c_{\mathrm{m}}^{-1/\beta}. \tag{3.50}$$

3. The temperature dependence of the relaxation time, τ_{DD}, given by (3.46), has been deduced from two assumptions: the activation barrier E in (3.48) is actually treated as the free activation energy, E-TS, that take into account random distributions of the energy and entropy barriers, and the concentration, c_{m}, of defects can vary with temperature. Bendler et al. [43–45] analyzed the correlation length ξ between defects. They showed that the temperature dependence of the correlation length can be approximated by $\xi(T) \approx \tilde{L}[T_{\mathrm{C}}/(T - T_{\mathrm{C}})]^{0.5f}$, where f is a critical exponent, $\tilde{L}$ is a length constant, and T_{C} denotes a temperature at which single defects disappear and below which only defected clusters exist. Consequently, the temperature effect on the correlation volume can be described in the following form:

$$V_{\mathrm{corr}}(T) \approx \xi^3(T) \approx \tilde{V}\left(\frac{T_C}{T - T_C}\right)^{0.5df}, \tag{3.51}$$

where $\tilde{V}$ is a volume constantand d is the dimensionality of the correlation volume. It should be noted that only defects are mobile in the model, and as the temperature is lowered, the defects cluster to lower the system entropy, S.

However, one can assume that single isolated defects of concentration c_1 are more mobile than any cluster of defects; therefore, one can replace the total concentration of mobile defects c_m in (3.50) by c_1. In order to visit a site by a single defect, one must first have a defect there with probability c, and also all the neighboring sites, z, within its correlation volume should be unoccupied with probability $(1-c)^z$; consequently

$$c_1 \sim c(1-c)^z, \quad \text{where } z = V_{\text{corr}}/V_1. \tag{3.52}$$

The volume V_1 is the single defect volume and can be calculated from the nearest-neighbor lattice spacing l. From (3.51) and (3.52) and the relation for τ_{DD} given in (3.50) one can calculate the generalized temperature VFT equation (3.46) where the adjustable parameters have the following representation: $A_{DD} \sim (\lambda c)^{-1/\beta}$ and $B_{DD} = -\frac{\tilde{V}T_C^{0.5df}}{V_1\beta}\ln(1-c)$. It is worth noting that (3.46) is usually considered for correlation volume dimensionality of $d = 3$ and the exponent $f = 1$ in the mean-field limit, and thus the time diverges at $T = T_C$. The temperature T_C is also considered in the model analogously to the Kauzmann temperature, i.e., T_C is a thermodynamic "defect" transition temperature at which the extra entropy of the melt is lost, but it never occurs in real systems because the glass transition is reached due to percolating rigidity [41, 46].

To take into account the effect of pressure within DDM, it is sufficient to realize that the dipole–dipole pair correlation length $\xi(T)$ varies with T, and the temperature T_C at which single defects disappear has to depend on pressure. Assuming a decreasing nearest-neighbor spacing l with increasing pressure,

$$l^3 = l_0^3[1-\delta(T,P)], \tag{3.53}$$

where $1-\delta(T,P) = V(T,P)/V(T,0)$ is a fractional volume expressed in terms of the system volume at zero pressure and l_0 is a lattice spacing at zero pressure. This simple observation leads (3.46) to its temperature–pressure generalization, namely,

$$\tau_{DD}(T,P) = c^{-1/\beta}\tau_0 \exp\left(\frac{B^*_{DD}T_C^{0.5df}}{(T-T_C)^{0.5df}[1-\delta(T,P)]}\right), \tag{3.54}$$

where $B^*_{DD} = -\frac{\tilde{V}}{l_0^3\beta}\ln(1-c)$. Using the above equation, Bendler et al. [47] calculated the fragility parameter

$$\left.\frac{\partial \log_{10}\tau_{DD}(T,P)}{\partial\left(\frac{T_g}{T}\right)}\right|_{T=T_g} = \frac{0.22\mathrm{d}B^*_{DD}\left(\frac{T_C}{T_g}\right)^{0.5df}}{\left(1-\frac{T_C}{T_g}\right)^{1+0.5df}}, \tag{3.55}$$

and suggested that this formula can be useful to analyze the relation between T_C and T_g.

Furthermore, on the basis of (3.54) and the Nernst–Einstein equation, $\sigma = \frac{q^2 nD}{kT}$, where q and n denote the charge and the ion concentration, respectively, and by assuming that the ion diffusion constant can be expressed by $D = \langle(\mathbf{r}(t) - \mathbf{r}_0(t))^2\rangle/6\tau_{\mathrm{DD}}$, where $\langle(\mathbf{r}(t) - \mathbf{r}_0(t))^2\rangle$ is the average displacement from the position $\mathbf{r}_0(t)$, the expression for the ionic conductivity was derived as

$$\sigma(T,P) = \frac{q^2 n\left\langle(\mathbf{r}(t) - \mathbf{r}_0(t))^2\right\rangle c^{1/\beta}}{6kT\tau_0} \exp\left(-\frac{B^*_{\mathrm{DD}} T_C^{0.5df}}{(T - T_C)^{0.5df}[1 - \delta(T,P)]}\right). \quad (3.56)$$

Similarly, it is possible to derive the corresponding formula for viscosity. If the Stokes–Einstein equation, $\eta = \frac{kT}{6\pi D r_{\mathrm{eff}}}$, where r_{eff} is an effective molecular radius is valid, then one obtains

$$\eta(T,P) = \frac{kTc^{-1/\beta}\tau_0}{\pi\langle(\mathbf{r}(t) - \mathbf{r}_0(t))^2\rangle r_{\mathrm{eff}}} \exp\left(\frac{B^*_{\mathrm{DD}} T_C^{0.5df}}{(T - T_C)^{0.5df}[1 - \delta(T,P)]}\right). \quad (3.57)$$

However, in order to use (3.54),(3.56), and (3.57) successfully in describing experimental data the fractional volume $1 - \delta(T,P)$ has been expanded in a pressure-dependent series [44, 45]:

$$1 - \delta(T,P) = a_0(T) + a_1(T)P + a_2(T)P^2 + a_3(T)P^3, \quad (3.58)$$

which is argued [41, 46] by the pressure dependence of T_{C}, assumed by a Taylor series about $T_{\mathrm{C}}(0)$ at zero pressure,

$$T_{\mathrm{C}}(P) = T_{\mathrm{C}}(0) + \left(\frac{\partial T_{\mathrm{C}}(P)}{\partial P}\right)_{P=0} P + \frac{1}{2}\left(\frac{\partial T_{\mathrm{C}}(P)}{\partial P}\right)^2_{P=0} P^2 + \frac{1}{6}\left(\frac{\partial T_{\mathrm{C}}(P)}{\partial P}\right)^3_{P=0} P^3. \quad (3.59)$$

Additional fittting parameters are introduced by the functions $a_i(T)$ in (3.58) that have been used as quadratic functions of T.

Finally, within the framework of the DDM, the total volume of the mobile single defects (MSDs) can be determined as follows:

$$V_{\mathrm{single}}(T) = N_{\mathrm{total\ sites}} V_{\mathrm{MSD}} c_1, \quad (3.60)$$

while the total volume of the isolated clustered single defects (ICSDs) can be expressed by

$$V_{\mathrm{clus}}(T) = N_{\mathrm{total\ sites}} V_{\mathrm{ICSD}}(c - c_1), \quad (3.61)$$

where $N_{\mathrm{total\ sites}}$ is the total number of lattice sites, c is the total concentration of single defects, i.e., the probability that a single defect exists, and c_1 is the

concentration of MSDs characterized from (3.52) and (3.51) by the following formula under zero pressure conditions:

$$c_1(T) = \begin{cases} c \exp\left(-\frac{\beta B^*_{\mathrm{DD}} T_C^{0.5df}}{(T-T_C)^{0.5df}}\right) & \text{for} \quad T > T_{\mathrm{C}} \\ 0 & \text{for} \quad T < T_{\mathrm{C}} \end{cases}, \tag{3.62}$$

It is expected that the total volume of all defects, i.e., the total free volume in the material, is simply given by the sum

$$V_{\text{total defects}} = V_{\text{single}} + V_{\text{clus}}. \tag{3.63}$$

The above relation underlies one of the most interesting results of the DDM, that is, the expression for the free volume measured by the positronium annihilation lifetime spectroscopy (PALS):

$$V^{\mathrm{HT}}_{\mathrm{PALS}} = \frac{V_{\text{total defects}}}{N_{\text{total defects}}}, \tag{3.64}$$

where $N_{\text{total defects}}$ is the total number of all defects. Then, using the above equation with (3.60), (3.61), and (3.62), it has been shown [48] that $V^{\mathrm{HT}}_{\mathrm{PALS}}$ can be described in the following way:

$$V^{\mathrm{HT}}_{\mathrm{PALS}} = \frac{V_{\mathrm{MSD}} \exp\left(-\frac{\beta B^*_{\mathrm{DD}} T_C^{0.5df}}{(T-T_C)^{0.5df}}\right) + V_{\mathrm{ICSD}}\left[1 - \exp\left(-\frac{\beta B^*_{\mathrm{DD}} T_C^{0.5df}}{(T-T_C)^{0.5df}}\right)\right]}{\exp\left(-\frac{\beta B^*_{\mathrm{DD}} T_C^{0.5df}}{(T-T_C)^{0.5df}}\right) + \frac{1}{\bar{N}}\left[1 - \exp\left(-\frac{\beta B^*_{\mathrm{DD}} T_C^{0.5df}}{(T-T_C)^{0.5df}}\right)\right]} \quad \text{for } T > T_{\mathrm{C}} \tag{3.65}$$

because

$$V^{\mathrm{HT}}_{\mathrm{PALS}} = \frac{c_1 V_{\mathrm{MSD}} + (c - c_1) V_{\mathrm{ICSD}}}{(c - c_1)/\bar{N} + c_1}, \tag{3.65a}$$

where the total number of defects has been expressed by the average number $\bar{N}$ of single defects associated with a cluster, that is,

$$N_{\text{total defects}} = \frac{N_{\text{total sites}}(c - c_1)}{\bar{N} c_1} + N_{\text{total sites}} c_1. \tag{3.65b}$$

The DDM theoretical predictions have been tested for poly(propylene oxide) [49, 50] polyvinyl acetate [49], as well as for the ionic conductivity in polymer electrolytres [49]. More recent advances of DDM include the ability to predict the

dynamic ratio [46, 50] Q_V/Q_P as well as its relation to the monomer volume [51] discussed in Chap. 2 with respect to [52].

3.6 Dynamic Lattice Liquid Model

According to the dynamic lattice liquid (DLL) model proposed by Pakula and Teichmann [53, 54], the cooperative molecular rearrangements in glass-forming liquids are controlled by the distribution of both free volume and thermal activation but with potential barriers that depend on the local density.

The DLL model is based on a lattice structure, i.e., atoms or molecules of supercooled liquids (or segments in the case of polymer) occupy lattice sites and oscillate around them with a frequency $\nu = 1/\tau_\nu$ that is considered as the frequency of attempts to move to the neighboring lattice sites. However, such attempts can be successful only when the sum of vectors representing simultaneously attempted displacements of a group of elements (more than two) vanishes (Fig. 3.3). In other words, the collective motion paths are possible only if a form of closed loops consists of $n \geq 3$ neighboring lattice sites.

Thus, the dynamics of the system is determined by the probability of a cooperative loop formation with a given length $p(n)$ on a lattice. This probability can be used to formulate the expression for the structural relaxation time:

$$\tau = \left[\sum_{n=3}^{\infty} np(n)\right]^{-1} = \left[B\sum_{n=3}^{\infty} n^{-h+1}(\mu_0 p_s)^n\right]^{-1}, \tag{3.66}$$

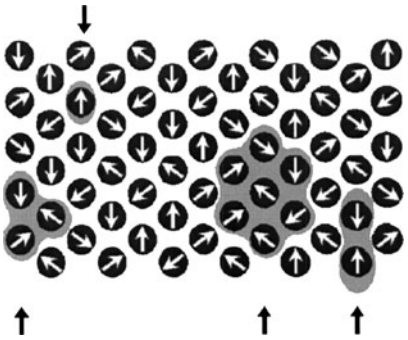

Fig. 3.3 Illustration of rearrangements considered in the DLL model. The vector field represents attempts of molecular displacements toward neighboring lattice sites. The *marked areas* represent various local situations (1) elements try to move in the opposite direction (unsuccessful attempt), (2) an attempt of motion starts from an element which would not be replaced by any of its neighbors (unsuccessful attempt), and (3) each element replaces one of its neighbors (successful attempts). The figure is taken from [55]

where B is a lattice dependent constant, h is a positive exponent that weakly depends on the dimensionality of the lattice, and μ_0 is the connectivity of the lattice in the athermal case. The dependence of the relaxation time on the thermodynamic state parameters (P, V, T) can be introduced into (3.66) via p_s that modifies the connectivity of the lattice ($p_s = 1$ for the athermal case). In order to obtain an explicit expression for the relaxation times as a function of temperature and local volume, the following assumptions have been made:

1. A local volume v is assigned to each molecule. This volume can fluctuate, assuming values not smaller than a minimum volume v_0, which correspond to a hard core picture of the system. The excess volume, $v - v_0$, can take part in a redistribution of volume in the system, which can be represented, in the simplest way, by the following exponential distribution:

$$\phi(v) = \frac{1}{\bar{v} - v_0} \exp\left(-\frac{v - v_0}{\bar{v} - v_0}\right), \tag{3.67}$$

   where $\bar{v}$ is the mean volume per molecule in the system.
2. The system is considered to expand thermally with an expansion coefficient α in a linear fashion,

$$\bar{v} = v_0[1 + \alpha(T - T_0)], \tag{3.68}$$

   where T_0 denotes the temperature corresponding to the closest packing of molecules.
3. Molecular transport is driven by a thermally activated process with potential energy barriers $E(v)$ that depend on the local density of the system. A probability for a molecule to take part in a local rearrangement is given by the Boltzmann factor,

$$p(v, T) = \exp\left(-\frac{E(v)}{kT}\right). \tag{3.69}$$

Since the higher terms in (3.66) can usually be neglected [56, 57], within the assumptions above, the formula for the relaxation time can be expressed as follows:

$$\tau \propto \langle \phi(v) p(v, T) \rangle^{-1} = \left\{ \int_{v_0}^{\infty} \phi(v) p(v, T) \mathrm{d}v \right\}^{-1}. \tag{3.70}$$

To determine an expression for the volume–temperature dependence of the relaxation time, some function of $E(v)$ has to be assumed. For an adequate description of dynamic behaviors of diverse glass-forming liquids, Pasterny et al. [57] considered four simple characteristics $E(v)$ (Fig. 3.4), suggested by the authors of DLL model as extreme cases [53, 54]:

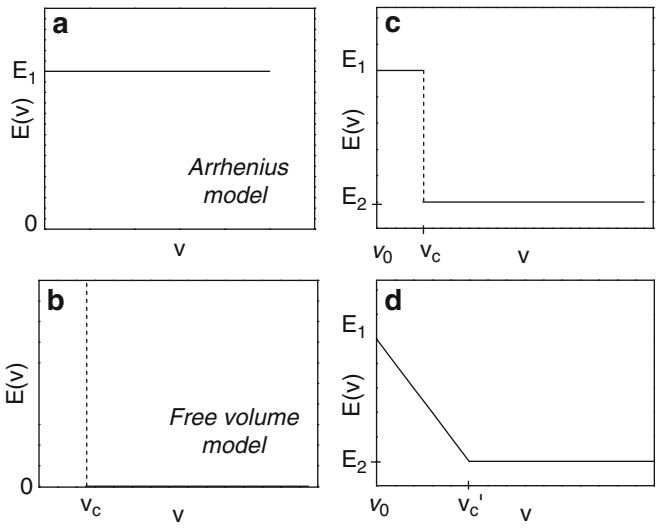

Fig. 3.4 Dependences of the activation energy E for local molecular rearrangements vs. local volume v: (**a**) $E(v) = \text{const}$ corresponding to the Arrhenius model, (**b**) a jump of the activation energy from 0 to ∞ at certain v_c corresponding to the free volume model, (**c**) a jump of the activation energy at certain v_c, from some finite value E_1 below v_c to another finite value E_2 above v_c, (**d**) a linear drop in the activation energy between v_0 and v_c' from some value E_1 to the fixed value E_2 above v_c'

1. The first assumption is that the activation energy is independent of local volume, $E(v) = \text{const}$ (Fig. 3.4a), leading to an Arrhenius temperature dependence of the relaxation times:

$$\tau = \tau_0 \exp\left(\frac{E}{kT}\right). \tag{3.71}$$

2. A discontinuous change of the activation energy at certain v_c, from infinity below v_c to 0 above v_c (Fig. 3.4b), gives the following formula:

$$\tau = \tau_0 \exp\left(\frac{v_c - v_0}{\bar{v} - v_0}\right), \tag{3.72}$$

which is the well-known Doolittle equation [58] within the framework of the free volume model.

3. The case analogous to the free volume model (2), with the only difference being in the assumption that the activation energy has values below and above v_c which are finite and nonzero, i.e., $E(v) = E_1$ for $v_0 < v < v_c$ and $E(v) = E_2$ for $v > v_c$ (Fig. 3.4c), leading to the following expression for the relaxation time:

$$\tau = \tau_0 \left\{ e^{-\frac{E_1}{kT}} \left[1 - \exp\left(\frac{v_0 - v_c}{\bar{v} - v_0}\right) \right] + e^{-\frac{E_2}{kT}} \exp\left(\frac{v_0 - v_c}{\bar{v} - v_0}\right) \right\}^{-1}. \tag{3.73}$$

Taking the limit as $E_1 \to \infty$, the (3.73) tends to the Macedo and Litovitz formula [59], whereas if simultaneously $E_2 \to 0$, then (3.73) gives the Doolitle model (3.72).

4. The last assumption of a linear drop in the activation energy from E_1 to E_2 in the range between v_0 and v'_c, and its invariability $E(v) = E_2$ above v'_c (Fig. 3.4d), gives the following formula for the relaxation time:

$$\tau = \tau_0 \left\{ \frac{1}{1 + \frac{(E_1 - E_2)}{kTw}} \left[e^{-\frac{E_1}{kT}} - e^{-\frac{E_2}{kT}} \exp(w) \right] + e^{-\frac{E_2}{kT}} \exp(w) \right\}^{-1}, \tag{3.74}$$

in which $w = (v_0 - v'_c)/(\bar{v} - v_0)$ and v'_c is a constant having the units of volume.

Equations (3.73) and (3.74), which are novel results of the model, have been tested, for example, for triphenylomethane triglycidyl ether [57, 60]. It has turned out that among them, (3.74), based on the assumption of the linear decrease in activation energy with volume, provides a better description for the isothermal and isobaric dependences of structural relaxation times for glass-forming liquids, although one should not forget that this equation requires to find all five adjustable parameters (E_1, E_2, v_0, v'_c, and τ_0). Moreover, the dependence of $E(v)$ presented in Fig. 3.4d is only a first approximation. One can expect that the characteristic of the activation energy for molecular rearrangements vs. local volume possesses a more complicated nature. However, in this case, calculations of relaxation times from (3.70) by using a more adequate function $E(v)$ are feasible only in the numerical way.

References

1. Paluch M, Hensel-Bielowka S, Psurek T (2000) J Chem Phys 113:4374
2. Fytas G, Dorfmüller T, Wang CH (1983) J Chem Phys 87:5041
3. Grest GS, Cohen MH (1979) Phys Rev B 20:1077
4. Grest GS, Cohen MH (1981) Adv Chem Phys 48:455
5. Patterson GD, Carroll PJ (1983) J Polym Sci Polym Phys 21:1897
6. Leyser H, Schulte A, Doster W, Petry W (1995) Phys Rev E 51:5899
7. Paluch M, Ziolo J, Rzoska SJ (1997) Phys Rev E 56:5764
8. Corezzi S, Capaccioli S, Casalini R, Fioretto D, Paluch M, Rolla PA (2000) Chem Phys Lett 320:113
9. Paluch M, Casalini R, Roland CM (2003) Phys Rev E 67:021508
10. Adams G, Gibbs JH (1965) J Chem Phys 43:139
11. Goldstein M (1975) J Chem Phys 64:4767
12. Johari GP (2000) J Chem Phys 112:7518
13. Johari GP (2000) J Non-Cryst Solids 307/310:387
14. Casalini R, Cappacioli S, Lucchesi M, Rolla PA (2001) Phys Rev E 63:031207
15. Casalini R, Cappacioli S, Lucchesi M, Rolla PA, Paluch M, Corezzi S, Fioretto D (2001) Phys Rev E 64:041504
16. Prevosto D, Lucchesi M, Capaccioli S, Casalini R, Rolla PA (2003) Phys Rev B 67:174202
17. Comez L, Corezzi S, Fioretto D, Kriegs D, Best A, Steffen W (2004) Phys Rev E 70:011504

18. Paluch M, Casalini R, Best A, Patkowski A (2002) J Chem Phys 117:7624
19. Casalini R, Paluch M, Psurek T (2004) J Mol Liq 111:53
20. Avramov I (2000) J Non-Cryst Solids 262:258
21. Avramov I, Milchev A (1988) J Non-Cryst Solids 104:253
22. Avramov I (1991) J Chem Phys 95:4439
23. Avramov I (1996) Therm Acta 280/281:363
24. Avramov I (1997) J Mater Sci Lett 13:1367
25. Avramov I (1998) J Non-Cryst Solids 238:6
26. Casalini R, Mohanty U, Roland CM (2006) J Chem Phys 125:014505
27. Roland CM, Hensel-Bielowka S, Paluch M, Casalini R (2005) Rep Prog Phys 68:1405
28. Avramov I, Grzybowski A, Paluch M (2009) J Non-Cryst Solids 355:733
29. Paluch M, Roland CM (2003) J Non-Cryst Solids 316:413
30. Puzenko A, Ishai PB, Paluch M (2007) J Chem Phys 127:094503
31. McCoy BJ (2002) J Phys Chem Solids 63:1967
32. Brenskelle LA, McCoy BJ (2006) J Chem Phys 124:084502
33. Brenskelle LA (2008) Cluster kinetics modeling of glassforming materials, PhD thesis
34. Dzugutov M, Simdyankin SI, Zetterling FHM (2002) Phys Rev Lett 89:195701
35. Doolittle AK (1951) J Appl Phys 22:1471
36. Debenedetti PG, Liquids M (1996) Concepts and principles. Princeton University Press, Princeton
37. Turnbull D, Cohen MH (1961) J Chem Phys 34:120
38. Bottcher CJF, Bordewijk P (1978) Theory of electric polarization, vol II. Elsevier, Amsterdam
39. Glarum SH (1960) J Chem Phys 33:639
40. Shlesinger MF, Montroll EW (1984) Proc Natl Acad Sci USA 81:1289
41. Bendler JT, Fontanella JJ, Shlesinger M (2001) Phys Rev Lett 87:195503
42. Bendler JT, Shlesinger MF (1987) J Mol Liq 36:37
43. Bendler JT, Shlesinger MF (1988) J Stat Phys 53:531
44. Bendler JT, Fontanella JJ, Shlesinger MF, Wintersgill MC (2003) Electrochim Acta 48:2267
45. Bendler JT, Fontanella JJ, Shlesinger MF, Wintersgill MC (2004) Electrochim Acta 49:5249
46. Bendler JT, Fontanella JJ, Shlesinger MF (2008) AIP conference proceedings. In: Tokuyama M, Oppenheim I, Nishiyama H (eds) 5th International workshop on complex systems, Vol 982. American Institute of Physics, New York, pp 215–218
47. Bendler JT, Fontanella JJ, Shlesinger MF (2006) J Non-Cryst Solids 352:4835
48. Bendler JT, Fontanella JJ, Shlesinger MF, Bartoš J, Šauša O, Krištiak J (2005) Phys Rev E 71:031508
49. Bendler JT, Fontanella JJ, Shlesinger MF (2001) Phys Rev Lett 19:195503
50. Bendler JT, Fontanella JJ, Shlesinger MF, Wintersgill MC (2010) J Non-Cyst Solids 356:547
51. Bendler JT, Fontanella JJ, Shlesinger MF, Wintersgill MC (2010) J Non-Cyst Solids in press, available online doi:10.1016/j.jnoncrysol.2010.07.031
52. Floudas G, Mpoukouvalas K, Papadopoulos P (2006) J Chem Phys 124:074905
53. Pakula T, Teichmann J (1997) Mat Res Soc Symp Proc 455:211
54. Pakula T (2000) J Mol Liq 86:109
55. Polanowski P, Pakula T (2003) J Chem Phys 118:11139
56. Teichmann J (1996) PhD Thesis, Universität Mainz
57. Pasterny K, Paluch M, Grzybowska K, Grzybowski A (2004) J Mol Liq 109:137
58. Doolitle AK, Doolitle DB (1957) J Appl Phys 28:901
59. Macedo PB, Litovitz TA (1965) J Chem Phys 42:245
60. Paluch M, Grzybowska K, Grzybowski A, Roland CM (2004) Slow dynamics in complex systems: 3 rd international symposium. American Institute of Physics Conference Proceedings, vol 708. pp 587–590

Chapter 4
New Physics Gained by the Application of Pressure in the Study of Dynamics of Glass Formers

4.1 Dynamics Under Pressure

Experimental studies of relaxation of glass forming liquids form the key to understanding the changes of molecular dynamics with temperature T and pressure P which lead to their vitrification. Experimental activities in the past were mostly concerned with measurements using temperature as a variable under ambient pressure. Consequently, theoretical developments aiming to solve the problem of glass transition are based principally on experimental facts acquired at ambient pressure. Much could be gained if experimental investigations and theoretical considerations were made more commonly on dynamics at elevated pressures. Early investigations of properties of glass formers under pressure referenced in Chaps. 1–3 demonstrated the benefit of adding pressure as a thermodynamic variable in the study of glass transition. However, the majority of these earlier studies are on the effect of pressure on transport coefficients (e.g., viscosity) and on dynamics only over limited spectral ranges [1–24]. The emphasis was mainly on the structural (α-)relaxation, but some studies were made of secondary relaxations. The latter includes study of the effects of pressure on the dielectric secondary process in PET [6] finding very small activation volume, little change in relaxation strength, in PVC [7] finding large effect on relaxation strength and small activation volume, and in other polymers [11]. Since the turn of the century, we have witnessed significant increase of experimental investigations of the relaxation dynamics of glass formers under elevated pressure. Mostly carried out by broadband dielectric relaxation spectroscopy, these more recent studies reveal the change in dynamics over wider ranges of frequency, temperature T, and pressure P than used earlier. The broad time/frequency range enables us to see not only the changes of the primary α-relaxation with applied pressure but also those of the fast relaxations including the secondary relaxations. In the case of some polymers, the slower normal modes of chain motion can be studied together with the α-relaxation under pressure. The results of these studies are general and fundamental properties, which should have a tremendous impact on our understanding of the dynamics and thermodynamics of glass formers. Decrease in temperature and increase in pressure both have the same effect of slowing down relaxation processes. However, the two thermodynamic

G. Floudas et al., *Molecular Dynamics of Glass-Forming Systems*,
Advances in Dielectrics 1, DOI 10.1007/978-3-642-04902-6_4,

variables cause different changes in density and entropy and cannot be considered as either equivalent or complementary. As we have seen in previous chapters, utilizing both T and P as thermodynamic variables, combinations of them enable the dynamics to be studied at constant specific volume, at constant structural relaxation time, and other chosen conditions. This chapter is devoted to show the new results in dynamics of glass formers generated by recent surge in research of applying high pressure in spectroscopy, particularly broadband dielectric spectroscopy. The new results turn out to be almost universal, present in glass formers of different physical and chemical structure, and have not been addressed before by any theory or model, and thus they have tremendous impact on current concepts and theories of glass transition. The results also point out the new physics that have to be included before the centuries old problem of glass transition can be solved [25]. Notwithstanding, mention has be made of some of the physical phenomena associated with the rate- and time-dependence of the glass transition process which have been rationalized quantitatively through phenomenological theory involving broad asymmetric relaxation functions [26–28].

4.2 General Dynamic Properties of Glass Formers Discovered by Applying Pressure

Examples of properties found at elevated pressure are given below, item by item. These properties are general and hence important. However, due to space limitation, only few sample experimental data are given for each of the general properties.

4.2.1 Coinvariance of τ_α and Width of Dispersion to Changes in P *and* T

Broadband dielectric relaxation measurements of glass formers can be made at elevated pressures of up to about 2 GPa, which is four orders of magnitude higher than the ambient pressure of 0.1 MPa. Usually, all relaxation mechanisms of glass formers slow down with increase in pressure. The slowing down at elevated pressure can be compensated by raising the temperature. Thus different combinations of P and T can be found such that the most probable α-relaxation time, τ_α, has the same value. In practice, this condition is achieved when the maxima of the dielectric loss peaks are located at the same frequency, ν_α. Concomitant with the large variations of P and T are large differences in the thermodynamic states (specific volume V and entropy S) of the glass formers although they all have the same τ_α. The remarkable finding from the experimental data of many different molecular and polymeric glass formers [29] is that the frequency dispersion (i.e., the shape) of the α-relaxation remains the same for various combinations of P and T

having the same τ_α. Hydrogen-bonded glass formers are excluded because high temperature in combination with high pressure tend to break hydrogen bonds, and these glass formers no longer have the same structure [16–18]. Numerous examples of the covariance of τ_α can be found in [29, 30]. In many glass formers, the breadth of the α-loss peak increases with τ_α, i.e., with decreasing T or increasing P but the loss peaks obtained at different P and T combinations superpose well for any choice of τ_α [29, 30].

The frequency dispersion of the α-relaxation is uniquely and well described by the one-sided Fourier transform of the Kohlrausch functions, given earlier in (3.50), and presented here as

$$\phi(t) = \exp[-(t/\tau_\alpha)^{1-n}], \tag{4.1}$$

with the exponent β_{KWW} in (3.50) rewritten here as $(1 - n)$ in order to link with the Coupling Model [31–38] later on. Fourier transform of the Kohlrausch function to frequency domain was first done analytically for $\beta_{\mathrm{KWW}} = 0.5$ by Williams and Watts [39] for α-dielectric relaxations, and numerically over a wide range of frequencies and of β_{KWW} by Williams et al. [40]. These papers opened up the use of (3.50) or (4.1) in data in the frequency domain and were the start of the remarkable growth in applications of the function [41].

When fitting the frequency dependence of the α-loss peaks, obtained by dielectric relaxation by the one-sided Fourier transform of the Kohlrausch function, emphasis of good agreement with the loss data is placed on the main peak, especially on the low frequency side, if the conductivity contribution is not present or the contribution has been removed if present. This fit takes into account nearly all the dielectric or mechanical strength of the α-relaxation and the viscosity if the glass former is not polymeric. This becomes clear if the loss data and the Kohlrausch fit are plotted linearly against log(frequency), which shows that the deviations of the Kohlrausch fit from the data, at frequencies high above the loss maximum, are small. The deviations are considered natural in the Coupling Model (CM) interpretation of the evolution of dynamics with time [31–38]. They come from relaxation processes of smaller length scales that transpire at shorter times before the dynamics evolve to the one with maximum length scale and correlation function given by the Kohlrausch function.

Lack of superposition may occur at frequencies sufficiently high compared with ν_α, attributable in some cases to the contribution from resolved or unresolved secondary relaxations at higher frequencies, whose relaxation strength may not have the same P- and T-dependences as the α-relaxation (in Ref. 12 of Chapter 1).

This general experimental fact of glass formers is supported by experimental data of many different materials, and, for a particular material, by experimental data for several different values of the relaxation time. In many cases, the dispersion broadens with increasing τ_α on decreasing temperature or increasing pressure, and thus the observed superpositioning cannot be explained trivially by constant dispersion. The glass formers include molecular liquids and amorphous polymers of

diverse chemical structures [29, 30], room-temperature ionic liquids where the structural and conductivity relaxation are coupled together [42, 43], and a component in binary mixtures of two van der Waals liquids [44, 45] or two amorphous polymers [46, 47]. All these show the property of temperature–pressure superpositioning of the frequency dispersion of the structural α-relaxation at constant τ_α. Here we show several recent examples. Figure 4.1 shows an example from electric modulus spectra [48, 49] of the room-temperature ionic liquid 1-butyl-1-methylpyrrolidinium bis[oxalato]borate (BMP-BOB), measured over wide temperature (123–300 K) and pressure (0.1–500 MPa) ranges [42, 43]. Figure 4.2 shows another example from triphenyl phosphate (TPP), a glass former with some unusual properties [50].

The general and remarkable experimental fact of constant frequency dispersion (or time dependence of the relaxation function) of the α-relaxation at constant τ_α for different combinations of T and P has an immense impact on glass transition. Although the data were mostly obtained by dielectric relaxation, the same effect was found in some glass formers by photon correlation spectroscopy [30]. The primary concern of most theories, including those mentioned in [25], is to explain the temperature and pressure dependences of the structural relaxation time τ_α. In these theories, the dispersion of the structural relaxation is either not addressed, or considered separately with additional input not involved in arriving at τ_α. Consequently, in these theories, the frequency dispersion is unrelated to the relaxation time of the structural α-relaxation, and they are unlikely to be consistent with the T,P-superpositioning property.

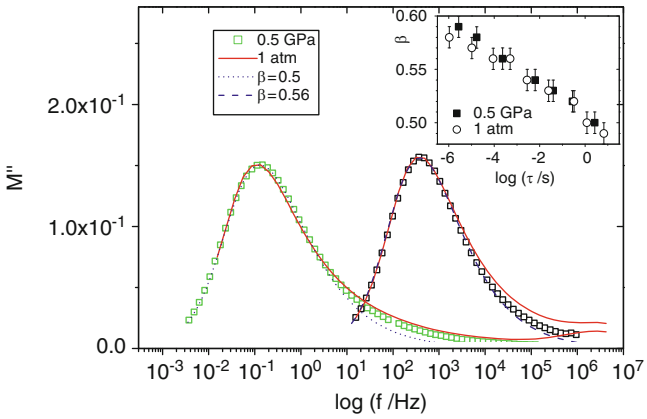

Fig. 4.1 Electric modulus relaxation spectra (M'') of the ionic liquid BMP-BOB at ambient pressure and 231 and 245 K are plotted as *solid lines*. High pressure M'' data (0.5 GPa) at the temperatures that yield relaxation times similar to those of the ambient pressure data, 283 and 308 K, are included in the figure as *squares*. Data at 0.5 GPa data are slightly shifted in frequency to match the atmospheric peak frequencies perfectly. *Long* and *short dashed lines* are fits to a Kohlrausch relaxation function with $\beta \equiv (1 - n) = 0.56$ and 0.50, respectively. The *inset* shows the good correspondence between the stretching parameter β_{KWW} and the relaxation time at different temperatures and at atmospheric pressure, and at 0.5 GPa [43]

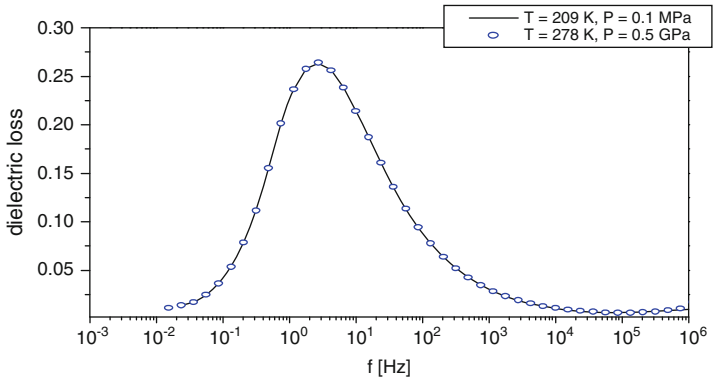

Fig. 4.2 *T*,*P*-superposition of dielectric loss data of liquid triphenyl phosphate at ambient and elevated pressure of 500 MPa [50]

The experimental fact of constant dispersion at constant τ_α for different T and P can be restated as the invariance of the Kohlrausch exponent β_{KWW}. In other words, τ_α and β_{KWW} (or n) are coinvariants of changing thermodynamic conditions (T and P). This is consistent with the CM [31–41], whose defining equation,

$$\tau_\alpha = \left[t_c^{-n}\tau_0\right]^{1/(1-n)}, \tag{4.2}$$

links together τ_α and the dispersion parameter $n = 1 - \beta_{\mathrm{KWW}}$. The crossover time, t_c, of the CM determined by the interaction potential is independent of T and P. Hence constant dispersion parameter n is a prerequisite to maintain a constant τ_α.

4.2.2 *Crossover of* T *or* P *Dependence of* τ_α *(or* η *) at the Same* τ_α *(or* η *) Independent on* T, P, *and* V *at the Crossover*

4.2.2.1 Experimental Facts

Marked changes in the temperature dependence of τ_α and viscosity η were found at temperatures above T_g in many glass formers. This general phenomenon was first observed by Plazek and Magill [51–53] in η of 1,3-bis(1-naphthyl)-5-(2-naphthyl) benzene (TNB). At temperatures high above T_g, the viscosity of TNB is Arrhenius. On cooling TNB, the Arrhenius temperature dependence changes to Vogel–Fulcher–Tammann–Hesse (VFTH) dependence [see (1.7)] at some temperature T_A, but this dependence does not persist all the way down to T_g. At some temperature T_B, in between T_A and T_g, there is a marked change to another VFTH temperature dependence. The observation of this interesting phenomenon in many other glass formers was made easy by using the model-independent derivative function

$\phi_T \equiv [\mathrm{d}\log x/\mathrm{d}(1/T)]^{-1/2}$, introduced by Stickel et al. [54, 55], where x is either τ_α or η. Any VFTH temperature dependence of τ or η, $A\exp[D/(T-T_0)]$, has a corresponding $\phi_T = (D/2.303)^{-1/2}[1-(T_0/T)]$. Hence, the crossover at fixed pressure, P_{fix}, can be easily seen in a plot of ϕ_T against reciprocal temperature. The temperature T_{B} at which the crossover occurs and the corresponding crossover α-relaxation time or viscosity, $\tau_\alpha(T_{\mathrm{B}})$ or $\eta(T_{\mathrm{B}})$, were determined. Isobaric data with pressure P_{fix} which is the same as ambient pressure P_{amb} are more common [54–60]. Data with P_{fix} at elevated levels also show the crossover [61, 62], but T_{B} depends on P_{fix} and increases significantly with P_{fix}. Thus, it is more exact to rewrite $\tau_\alpha(T_{\mathrm{B}})$ as $\tau_\alpha(T_{\mathrm{B}}(P_{\mathrm{fix}}))$. In spite of the large variations of T_{B} and P_{fix}, $\tau_\alpha(T_{\mathrm{B}}(P_{\mathrm{fix}}))$ was found to be the same for all P_{fix}.

The dynamic crossover is also evident in measurements taken as a function of pressure at fixed temperature, T_{fix} [63–66]. The pressure dependence of τ_α and η can be well described by the VFTH-like pressure dependence, $x(P) = x_0\exp[D_P P/(P_0-P)]$ [see (1.9)]. In this case, the derivative function is $\phi_P = [\mathrm{d}\log(x)/\mathrm{d}P]^{-1/2}$, which transforms the VFTH-like pressure dependence of $x(P)$ to $\phi_P = a - bP$. The crossover from one VFTH-like pressure dependence to another at P_{B} can be clearly seen in a plot of ϕ_P against P, and the α-relaxation time at the crossover, $\tau_\alpha(P_{\mathrm{B}})$ or $\eta(P_{\mathrm{B}})$, is determined. The crossover occurs for different choices of T_{fix}. P_{B} depends on T_{fix}, increasing significantly with T_{fix}. Thus, we may write $\tau_\alpha(P_{\mathrm{B}})$ or $\eta(P_{\mathrm{B}})$ as $\tau_\alpha(P_{\mathrm{B}}(T_{\mathrm{fix}}))$ or $\eta(P_{\mathrm{B}}(T_{\mathrm{fix}}))$.

An example from phenolphthalein-dimethylether (PDE) is shown in Fig. 4.3, where $\phi_T = (\mathrm{d}\log\tau/\mathrm{d}T^{-1})^{-0.50}$ and $\phi_P = (\mathrm{d}\log\tau/\mathrm{d}P)^{-0.50}$ used to linearize the

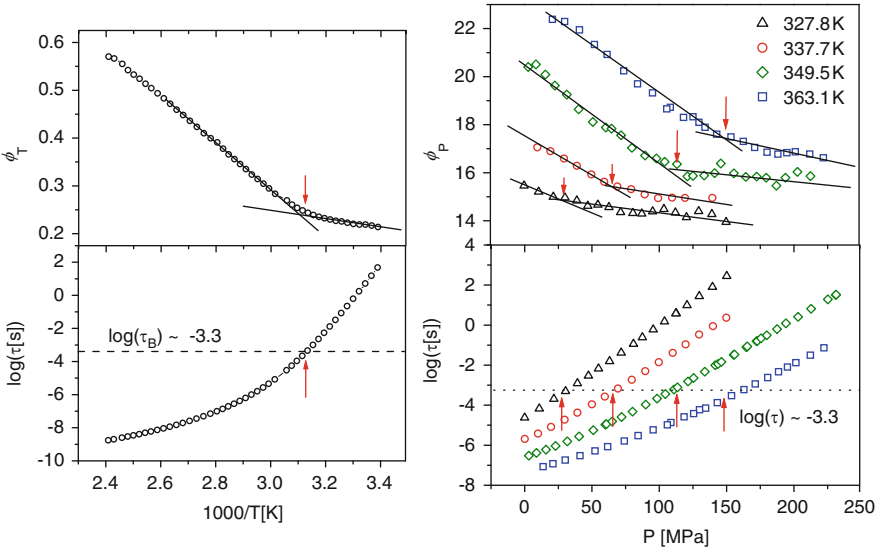

Fig. 4.3 Phenolphthalein-dimethyl-ether (PDE) data. *Left panel*, τ_α and derivative function ϕ_T at ambient pressure. *Right panel*, τ_α and derivative function ϕ_P vs pressure, obtained for isotherms at $T = 327.8$, 337.7, 349.5, and 363.1 K

VFTH T-dependence and the analog P-dependence show the crossover clearly by two straight lines with different slopes. The crossovers all occur at $\log(\tau_\alpha/s) = -3.3$. As already discussed in (4.2.1), we have the same dispersion at constant τ_α, independent of T and P. Hence, the dispersion (or n) as well as τ_α is invariant at the crossover from $(\text{VFTH})_1$ to $(\text{VFTH})_2$, or from one P-dependence to another.

The remarkable finding by experiments on several different glass formers is that $\tau_\alpha(P_B(T_{fix}))$ or $\eta(P_B(T_{fix}))$ does not depend on P_B and T_{fix}. Moreover, the constant value of $\tau_\alpha(P_B(T_{fix}))$ or $\eta(P_B(T_{fix}))$ obtained from crossover at P_B at fixed T_{fix} is the same as that for $\tau_\alpha(T_B(P_{fix}))$ or $\eta(T_B(P_{fix}))$ from crossover at T_B at fixed pressure P_{fix}. The crossover is seen under widely different thermodynamic conditions (pressure, temperature, and volume), but τ_α and η at the crossovers are constant for a given glass former.

The crossover from one VFTH dependence to another was also found generally under constant volume (isochoric) condition for PDE, 62% chlorinated biphenyl (PCB62), cresolphthalein-dimethylether (KDE), propylene carbonate (PC), 1,1′-di (4-methoxy-5-methylphenyl)-cyclohexane (BMMPC), and salol. The isochoric curve $[\mathrm{d}\log\tau_\alpha/\mathrm{d}(1/T)]^{-1/2}$ was calculated at some constant specific volume V_{fix} [61, 66]. From the crossover, the crossover temperatures $T_B(V_{fix})$ and relaxation times $\tau_\alpha(T_B(V_{fix}))$ at constant V were obtained. Remarkably, $\tau_\alpha(T_B(V_{fix}))$ under isochoric condition is the same as $\tau_\alpha(T_B(P_{fix}))$ under isobaric condition for all five glass formers studied.

Although $\tau_\alpha(T_B(P_{fix})) \approx \tau_\alpha(P_B(T_{fix})) \approx \tau_\alpha(T_B(V_{fix}))$ holds for many glass formers, their common value differs greatly when all the glass formers studied are considered. The values are not confined within the narrow range of $10^{-6.5}$–$10^{-7.5}$ s, as surmised by Novikov and Sokolov [60]. For examples, PDE has the longest relaxation times with $\tau_\alpha(T_B) = 10^{-3.3}$ s; PCB62 has $\tau_\alpha(T_B) = 10^{-5.9}$ s; BMMPC has $\tau_\alpha(T_B) = 10^{-6.1}$ s; KDE and salol has $\tau_\alpha(T_B) = 10^{-6.3}$ s; and PC has $\tau_\alpha(T_B) = 10^{-7.0}$ s [61–66]. The epoxy diglycidyl ether of bisphenol-A (DGEBA) has $T_B = 275$ K and $\tau_\alpha(T_B) = 10^{-4.3}$ s [67]. From these results alone, it is sufficient to conclude that $\tau_\alpha(T_B)$ varies over a wide range (nearly four orders of magnitude from $10^{-3.6}$ to $10^{-7.5}$ s) when the above-mentioned glass formers are considered. Hence, the results invalidate the claim by Novikov and Sokolov that $\tau_\alpha(T_B)$ has the "magic" values lying within the narrow range of $10^{-7.0\pm0.5}$ s [60]. Connection of the crossover temperature T_B to the critical temperature T_c of mode coupling theory was also made by them. This proposal is questionable because of the fact that PDE has $\tau_\alpha(T_B) = 10^{-3.3}$ s. It is inconceivable that such a long or macroscopic relaxation time can be consistent with the much shorter relaxation time at T_c of mode coupling theory [68].

4.2.2.2 Coupling Model Explanation

As reviewed by Roland et al. [66], various theoretical models either anticipate or interpret this dynamic crossover seen in many glass formers at T_B, but the explanations offered are widely different. Most of the explanations either cannot explain or

have not explained the general and remarkable property of the crossover, namely, $\tau_\alpha(T_B(P_{fix})) \approx \tau_\alpha(P_B(T_{fix})) \approx \tau_\alpha(T_B(V_{fix}))$, not to mention the other properties in subsection (4.2.1) and others in [30]. We now show that this property is a natural consequence of the CM description of glass transition. First, we give an explanation for the origin of the dynamic crossover. Next, we show that at the dynamic crossover, τ_α is independent of thermodynamic condition of the glass former.

In his thesis on dielectric relaxation of glass formers at ambient pressure P_{amb}, Stickel [54] plotted the full width at half maximum of the dielectric loss peak normalized to that of an ideal Debye loss peak, $w(T)$, as a function of temperature. From these results, the corresponding Kohlrausch nonexponentiality parameters $n(T, P_{amb})$ were readily calculated by the relation of Dixon [69], $[1 - n(T, P_{amb})] \equiv \beta_{KWW}(T, P_{amb}) = 1 - 1.047\,[1 - w(T, P_{amb})^{-1}]$, for the glass formers Stickel studied. For other glass formers, not reported in Stickel's thesis, $n(T,P_{amb})$ were obtained by fitting the dielectric loss spectra by the one-sided Fourier transform of the Kohlrausch function. Examples of the temperature dependences of $n(T,P_{amb})$ so obtained can be found in [70–74], which exhibit the following general property. For molecular glass formers, when $T > T_B(P_{amb})$, the values of $n(T,P_{amb})$ are smaller and slowly varying with decreasing temperature. But, when past $T \sim T_B(P_{amb})$, more rapid increase of $n(T,P_{amb})$ toward significantly larger value at $T_g(P_{amb})$ is evident in the regime of $T < T_B(P_{amb})$. In addition, the absolute value of $dn(T,P_{amb})/dT$ suffers a change when crossing a temperature near T_B. The increase in $n(T,P_{amb})$ from $T_B(P_{amb})$ to $T_g(P_{amb})$, measured by $[n(T_g,P_{amb}) - n(T_B,P_{amb})]$, was found to correlate with the extent of the difference between the high and low temperature VFTH functions when both are evaluated at $T_g(P_{amb})$. This can be seen in Fig. 2 in [75] when comparing OTP ($n(T_g,P_{amb}) \approx 0.5$, $T_g(P_{amb}) = 244$ K, $T_B(P_{amb}) = 290$ K) with propylene glycol ($n(T_g,P_{amb}) \approx 0.25$, $T_g(P_{amb}) = 167$ K, $T_B(P_{amb}) = 280$ K). OTP having larger $[n(T_g,P_{amb}) - n(T_B, P_{amb})]$ exhibits a larger difference between the two VFTH temperatures at $T_g(P_{amb})$ than propylene glycol.

The change of the temperature dependence of the dynamics causing the crossover of the T-dependence of τ_α at T_B is expected to have an effect on the relaxation strength. This is because both the relaxation strength and the relaxation time τ_α are characteristics of the dynamics, and has led Schönhals [76] to look for correlated changes in behaviors of τ_α and the dielectric relaxation strength $\Delta\varepsilon$ at T_B by broadband dielectric measurements. The correlated changes indeed exist when $\Delta\varepsilon$ is plotted against $\log f_p$ for dibutyl phthalate, salol, propylene carbonate, propylene glycol, dipropylene glycol, and poly(propylene glycol) [76, 77]. Here, f_p is the dielectric α-loss peak frequency and is approximately equal to $1/(2\pi\tau_\alpha)$. These plots indicate two different frequency regions of dynamics separated by f_B. The two relations when extrapolated intersect at a crossover frequency f_B. It turns out that for all glass formers, f_B is nearly the same as $1/[2\pi\tau_\alpha(T_B)]$. Similar results were also found for the polymer, poly(vinyl acetate) [73, 78]. Therefore, the change of the dependence of $\Delta\varepsilon$ on $\log f_p$ also occurs at the temperature T_B. This phenomenon can also be explained by the more rapid increase of n with decreasing temperature (frequency) after crossing T_B (f_B) because n reflects the extent or length scale of the

many body relaxation and in turn the magnitude of $\Delta\varepsilon$. The temperature dependence of $\Delta\varepsilon$ is roughly proportional $1/T$ at temperature much higher than T_B, consistent with the Kirkwood–Fröhlich theory based on the assumption of noninteracting isolated dipoles as well as the smaller coupling parameter. However, this dependence does not continue when the temperature is lowered to approach T_B and below T_B. Thus, the observed change of T-dependence of $\Delta\varepsilon$ is another indication of the increase in coupling and cooperativity (or n) of the α-relaxation with the fall in temperature after crossing T_B.

In the framework of CM, $n(T,P_{amb})$ is a measure of the strength of the intermolecular coupling or cooperativity. Thus the behavior of $n(T,P_{amb})$ can be reinterpreted as a change from a slow increase of intermolecular coupling from a small starting value with decreasing temperature above $T_B(P_{amb})$, to a more rapid increase toward larger values after crossing $T_B(P_{amb})$. This opened up the possibility of explaining the crossover of temperature dependence of $\tau_\alpha(T,P_{amb})$ at $T_B(P_{amb})$ by the CM because in this model, the $\tau_\alpha(T,P_{amb})$ and its T-dependence are controlled by $n(T,P_{amb})$ via (4.2). If this change in dynamics is a consequence of the more rapid development of stronger intermolecular coupling after crossing T_B from above, then removal of the effects of intermolecular coupling should likewise remove the crossover. The primitive relaxation is devoid of intermolecular coupling. Hence its relaxation time, $\tau_0(T,P_{amb})$, should not show any change in temperature dependence across $T_B(P_{amb})$. This prediction was assessed by using (4.2) to calculate $\tau_0(T,P_{amb})$ from the experimentally determined values of $\tau_\alpha(T, P_{amb})$ and $n(T, P_{amb})$. The temperature dependence of $\tau_0(T,P_{amb})$ is expected to vary smoothly across $T_B(P_{amb})$, in accord with a single VFTH dependence due only to changes in configurational entropy and/or specific volume with temperature [79]. This procedure was carried out for PDE, salol, PC, OTP, and 54% chlorinated biphenyl (PCB54) using their ambient pressure dielectric data. While the derivative function $\phi_T \equiv [\mathrm{d}\log\tau_\alpha/\mathrm{d}(1/T)]^{-1/2}$ exhibits a break at $T_B(P_{amb})$, indicating the change in dynamics of $\tau_\alpha(T,P_{amb})$, it is absent in the plot of the corresponding ϕ_T for $\tau_0(T,P_{amb})$. A single VFT equation describes well $\tau_0(T,P_{amb})$ over the entire temperature range [79]. The range of log τ_0 values determined is about eight decades for PDE, OTP, salol, PC, and PCB54 [79].

The next task is to explain why the same crossover is observed as a function of temperature not only at ambient pressure P_{amb} but also at any fixed elevated pressures P_{fix} or at any constant volume V_{fix}, and also as a function of pressure at any fixed temperatures T_{fix}. Moreover, the same crossover time for all conditions, i.e., $\tau_\alpha(T_B(P_{fix})) \approx \tau_\alpha(P_B(T_{fix})) \approx \tau_\alpha(T_B(V_{fix}))$, also has to be explained. These general properties either have not been explained or are not explainable by conventional theories and models. In the framework of the CM, the explanation goes as follows. First, let us recall the coinvariance of $\tau_\alpha(P,V,T)$ and $n(P,V,T)$ to all thermodynamic conditions discussed in the previous subsection, a property consistent with the CM predictions. It follows from the coinvariance, irrespective of the choice of the elevated pressure P_{fix}, that if $\tau_\alpha(T',P_{fix})$ is the same as $\tau_\alpha(T,P_{amb})$, then necessarily we have $n(T',P_{fix})$ the same as $n(T,P_{amb})$, and the following as special cases. First, for some $T'_B(P_{fix})$ such that $\tau_\alpha(T'_B,P_{fix}) = \tau_\alpha(T_B,P_{amb})$, $n(T'_B,P_{fix})$ is also

equal to $n(T_B,P_{amb})$. Second, exactly like in the case of ambient pressure, $n(T',P_{fix})$ is small if $T'>T'_B(P_{fix})$, but as T' falls below $T'_B(P_{fix})$, it increases toward the significantly larger value of $n(T'_g,P_{fix})$ at $T'_g(P_{fix})$. Hence, the explanation of crossover of $\tau_\alpha(T,P_{amb})$ at T_B, as a consequence of the development of stronger coupling or cooperativity when T falls below $T_B(P_{amb})$, applies to the crossover of $\tau_\alpha(T',P_{fix})$ at T'_B. Similar reasoning as that given above leads to the same conclusion for the crossover of $\tau_\alpha(P,T_{fix})$ at P_B and the crossover of $\tau_\alpha(T'',V_{fix})$ at T''_B. The primitive relaxation times $\tau_0(P,T_{fix})$ calculated by (4.2) from $\tau_\alpha(P,T_{fix})$ and $n(P,T_{fix})$ no longer exhibit a crossover. The same conclusion is obtained when a similar argument is applied to $\tau_0(T'',V_{fix})$ calculated from $\tau_\alpha(T'',V_{fix})$ and $n(T'',V_{fix})$.

4.2.3 An Important Class of Secondary Relaxations Bearing Strong Connection to the α-Relaxation

The loss spectra of glass formers all show the structural α-relaxation, but the features can vary greatly at higher frequencies. Some have one or more than one well-resolved secondary relaxation. Some have an "excess wing" on the high-frequency flank of the α-loss peak with either an additional or no other secondary relaxation. At ambient pressure, all these features shift to lower frequencies with decreasing temperature, and temperature alone cannot distinguish them in properties. However, this is made possible by the application of pressure. Some secondary relaxations do not shift appreciably to lower frequencies on increasing pressure, and can be considered as local motion arising from intramolecular degree of freedom and having no significance for glass transition [30]. On the other hand, the secondary relaxations that shift with pressure are sensitive to change in specific volume and entropy similar to the α-relaxation, and may have fundamental importance in considering glass transition. It turns out that these secondary relaxations belonging to this special class exhibit, besides pressure sensitivity, other properties indicating that they bear strong connection to the α-relaxation [30–34, 70, 74, 80–114]. Even before pressure was used as a criterion for distinguishing secondary relaxations related to the primary α-relaxation, in 1998 the relaxation times τ_β at T_g of secondary relaxations belonging to a special class have been shown to be strongly correlated with n in the Kohlrausch correlation function, $\exp[-(t/\tau_\alpha)^{1-n}]$, of the α-relaxation [80]. The correlation was established from the data of many glass formers of different classes. Moreover, τ_β is in approximate agreement with the primitive relaxation time τ_0 of the CM. Since then, many more experimental investigations have confirmed this and extended it to temperatures above T_g [30]. Secondary relaxation of this special class is universal and found in all kinds of glass formers, organic molecular, polymeric, metallic, inorganic, ionic, and plastic crystalline [30]. The most remarkable findings are that of the secondary relaxation in metallic glasses which are atomic particles devoid of rotational degree of freedom, and in plastic crystals which have no translational degree of freedom. These strong

connections imply that secondary relaxation in this special class plays a fundamental role in the dynamics, leading to glass transition, and theories. Unfortunately, most theories including those cited in [25] have focused their attention on the primary α-relaxation and do not consider any secondary relaxation to be important for glass transition.

The properties of these secondary relaxations mimic the primary α-relaxation, and are connected to the α-relaxation in various qualitative and quantitative ways [30–34, 70, 74, 80–114]. For lack of a better name, we have called these secondary relaxations the Johari–Goldstein (JG) β-relaxations, and the relaxation time is represented by τ_{JG}. The intention of this choice is to honor these authors for the important discovery of secondary relaxation in totally rigid molecules [115–117], which belongs to the special class. It may also be called the primitive relaxation of the CM since τ_{JG} is approximately the same as the primitive relaxation time τ_0 of the CM, and it has all the properties of secondary relaxations belonging to the special class [30–34, 80]. Here we give a few examples from recent experimental findings to show that the JG β-relaxation is inseparable from the α-relaxation and both have to be taken into account in solving the glass transition problem.

4.2.3.1 Spin–Lattice Relaxation Weighted Stimulated-Echo Spectroscopy

Böhmer and coworkers [87, 88] used spin–lattice relaxation weighted stimulated-echo spectroscopy to find evidence for a correlation of the α- and the JG β-relaxation times above the calorimetric glass transition temperature of ortho-terphenyl, D-sorbitol, and cresolphthaleindimethylether (CDE or KDE). They found that the α-relaxation can be modified by suppressing the contributions of some subensembles of the JG β-relaxation in these glass formers. An earlier deuteron NMR experiment also gave indication of a possible correlation of the α- and JG β-relaxations of polystyrene [118].

4.2.3.2 Invariance of the Ratio τ_{JG}/τ_α for Different T and P When τ_α Is Kept Constant

By applying elevated pressure and compensated by raising temperature, a spectacular experimental finding by dielectric relaxation is the invariance of the ratio τ_{JG}/τ_α for different combinations of T and P while keeping τ_α constant. This was found in the neat glass former, dipropyleneglycol dibenzoate (DPGDB), benzoin-isobutylether (BIBE), polyphenylglycidylether (PPGE), polyvinylacetate (PVAc), and diglycidyl ether of bisphenol A (DGEBA) [48, 89, 91, 92, 109]. As an example, this effect is shown in Fig. 4.4 by the isothermal dielectric loss spectra of BIBE at ambient pressure and at elevated pressures obtained by Capaccioli and coworkers [89].

For DGEBA, the data of Prevosto et al. [91], the effect is shown in Fig. 4.5 in a different way by the same τ_β at the isobaric glass transition temperatures T_g

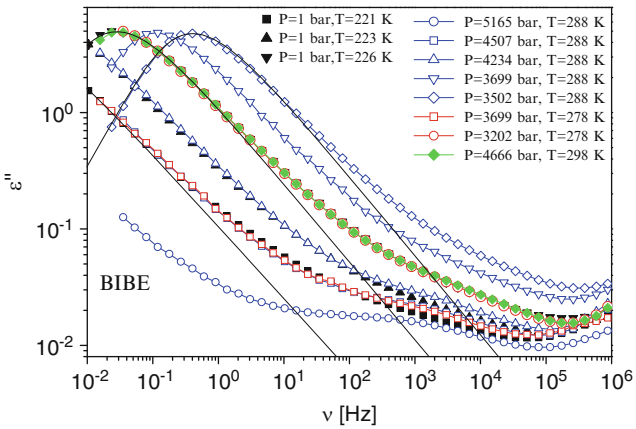

Fig. 4.4 *T–P* superposition of both α- and JG *β*-relaxation of benzoin-isobutylether (BIBE). Note that when the 1 bar data are nearly coincident with the data at elevated pressures, the former cannot be seen. Data of Capaccioli et al. [89]

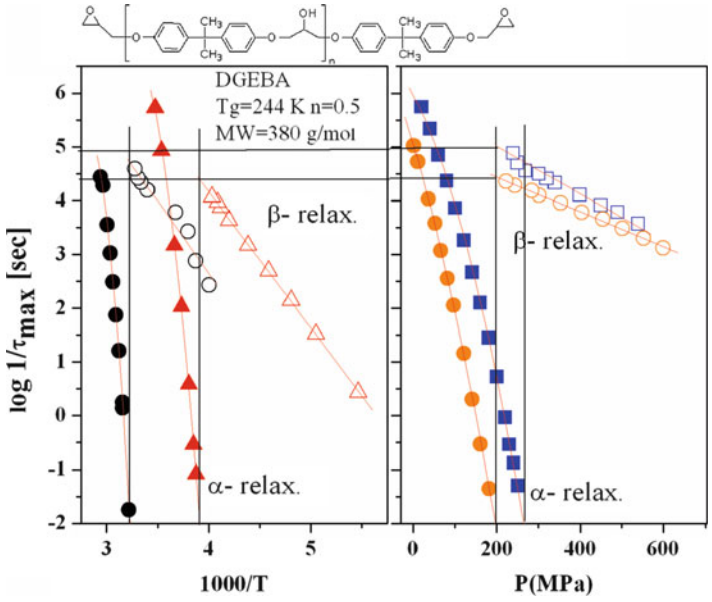

Fig. 4.5 α- and JG *β*-relaxation times of DGEBA as a function of temperature at two different pressures, 0.1 and 400 MPa (*left*), and as a function of pressure at two different temperatures, 293 and 283 K (*right*). We observed the same τ_β at the isobaric glass transition temperature T_g or the isothermal glass transition pressure P_g defined here by $\tau_\alpha(T_g) = \tau_\alpha(P_g) = 10$ s. Data of Prevosto et al. [91]

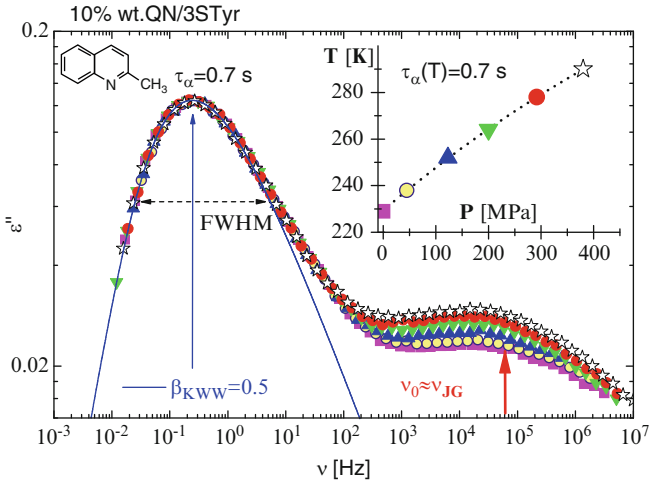

Fig. 4.6 *T–P* superposition of loss spectra for 10% QN in tristyrene measured for different T and P combinations but the same $\tau_\alpha = 0.67$ s. The line is a Fourier transform of the Kohlrausch function with $\beta_{KWW} \equiv (1-n) = 0.5$. The results demonstrate the co-invariance of three quantities, τ_α, n, and τ_{JG}, to widely different combinations of T and P. Data of Kessaire et al. [44]

(for different constant pressures) defined by $\tau_\alpha(T_g) = 10$ s, or at the isothermal glass transition pressures P_g (for different constant temperatures) defined by $\tau_\alpha(P_g) = 10$ s.

The same effect is found in the dynamics of a component in binary mixtures including *tert*-butylpyridine (TBP) [89], quinaldine (QN) [44], or picoline [48] in mixtures with oligomers of styrene. Shown here in Figs. 4.6 and 4.7 are data of 10 wt% of QN in tristyrene from Kessaire et al. [44] and Prevosto et al. [91], and in Figs. 4.8 and 4.9 the data of 25 wt% of 2-picoline in tristyrene from Mierzwa et al. [48]. Note in Fig. 4.6 that the loss peak height for the β-process changes substantially with T, P condition. As suggested by G. Williams to us, the T-changes (thermal energy) "win" over P-changes (compression), allowing a greater spatial extent of the motion at the higher T, P conditions relative to that at the lower T and ambient P.

It had been shown for many glass formers that the frequency dispersion of the α-relaxation (or n) is invariant to changes of T and P if τ_α is kept constant [29, 30]. On combining this with the currently discussed feature of the JG β-relaxation, we have coinvariance of three quantities, τ_α, τ_{JG}, and the dispersion parameter n, to widely different T and P combinations involving large variations of specific volume and entropy in the same glass former. This remarkable relation between τ_α and τ_{JG} is another strong evidence that the JG β-relaxation has fundamental significance, and its relation to the α-relaxation must be taken into account. The CM equation (4.2) clearly demonstrates coinvariance of τ_α, τ_0, and n. Thus the experimentally observed coinvariance of τ_α, τ_{JG}, and n to widely different T and P combinations is a natural consequence of the Coupling Model and the experimental fact that $\tau_0 \approx \tau_{JG}$. On the other hand, none of the theories cited in [25] has yet paid any attention to it.

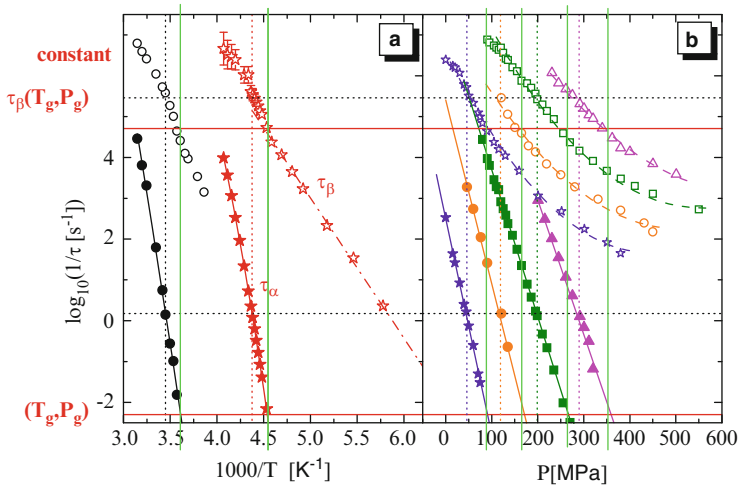

Fig. 4.7 α- and JG β-relaxation of 10 wt% of QN in a mixture with tristyrene. Same τ_β at the isobaric glass transition temperature T_g for two different pressures, or the isothermal glass transition pressure P_g at four different temperatures. Here, T_g and P_g are all defined by $\tau_\alpha(T_g) = \tau_\alpha(P_g) = 2 \times 10^2$ s. Note that there is a change of T- and P-dependence of τ_β when crossing T_g and P_g, respectively. Data of Kessaire et al. [44] and Prevosto et al. [90, 91]

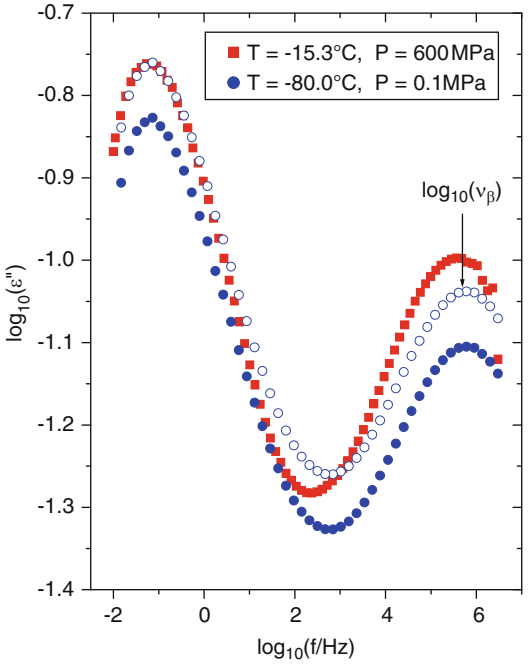

Fig. 4.8 Comparison of two spectra of 2-picoline in a mixture with tristyrene with the same relaxation frequency but measured at different thermodynamic conditions (see labels in figure). The *open circles* are obtained by shifting the data at 0.1 MPa vertically by a constant. The *arrow* indicates that JG β-relaxation frequency remains practically unchanged. Data of Mierzwa et al. [48]

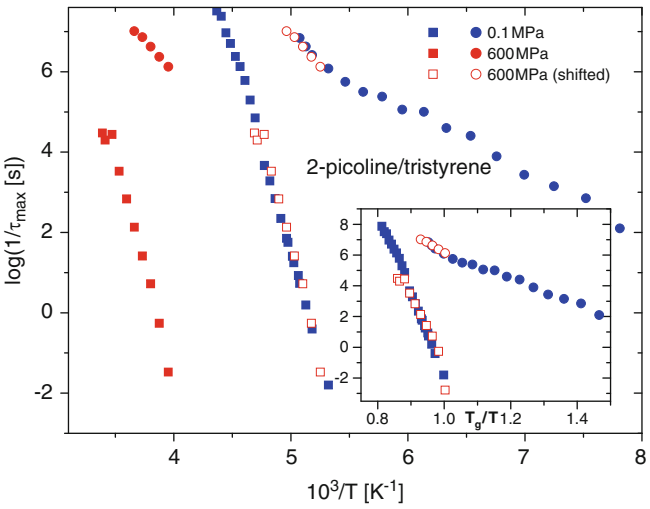

Fig. 4.9 Relaxation map of τ_α and τ_β of 25 wt% 2-picoline in a mixture with tristyrene. *Circles* are for 600 MPa and *squares* are for 0.1 MPa. *Open circles* are the data of 600 MPa after a horizontal shift of 1.3 to the right has been made. In the *inset*, the same data in the logτ vs T_g/T representation are shown. Data of Mierzwa et al. [48]

4.2.3.3 TV^γ-Dependence of τ_{JG}

By combining measurements of structural α-relaxation with both T and P as variables and using the equation of state, we have shown in Chap. 1 that the α-relaxation times can be expressed as a unique function of ρ^γ/T, or alternatively $T^{-1}V^{-\gamma}$, with the exponent varying in the range $0.13 \leq \gamma \leq 8.5$ for many glass formers investigated to date [67]. The invariance of the ratio τ_{JG}/τ_α or τ_0/τ_α for different T and P when τ_α is kept constant, shown above in (4.2.3.2), immediately leads to the conclusion that τ_{JG} is also a function of the same product variable, $T^{-1}V^{-\gamma}$, albeit weaker than that of τ_α. Thus the $T^{-1}V^{-\gamma}$ -dependence of the relaxation time is inherent to the JG β-relaxation, which has transpired long before the α-relaxation commences. From this, the origin of the $T^{-1}V^{-\gamma}$ -dependence of molecular mobility may be attributed to the JG β-relaxation. The stronger $T^{-1}V^{-\gamma}$ -dependence of τ_α than τ_{JG} is due to the many body nature of the α-relaxation, which magnifies the dependence [30, 35].

Evidence Indicating $T^{-1}V^{-\gamma}$: Dependence Originating from the Primitive Relaxation

If intermolecular potential $V(r)$ for liquids is a repulsive inverse power law, $V(r) = \varepsilon(\sigma/r)^q$, where r is the intermolecular distance, q is a constant, and ε and σ have respective dimensions of energy and length, it was shown by Hoover et al. [119, 120]. that the canonical partition function and hence, also all thermodynamic properties depend on a single density–temperature variable, $\rho(\varepsilon/kT)^{1/\gamma}$ with $\gamma = q/3$,

rather than on T and density ρ (or volume V) separately. It was later found that all reduced dynamical quantities can be cast in the form that depends on the single combined variable ρ^{γ}/T or alternatively $T^{-1}V^{-\gamma}$ with $\gamma = q/3$ [121]. Also the static structure factor and the local structure in nonassociated liquids are sensitive to the repulsive part of the potential at short distance [122, 123] but not the nature of the attractive potential extending to longer distance. Recently, Coslovich and Roland [124] simulated binary Lennard-Jones liquids with intermolecular potential $V(r)$ given before by $u_{\alpha\beta}(r) = 4\varepsilon_{\alpha\beta}[(\sigma_{\alpha\beta}/r)^q - (\sigma_{\alpha\beta}/r)^p]$, with the attractive exponent p fixed at the value of 6, and the repulsive exponent q varied over the values of 8, 12, 24, and 36. In agreement with experimental results, the diffusion coefficients for simulated Lennard-Jones liquids in normal and moderately supercooled states are a unique function of the variable ρ^{γ}/T. The magnitude of the exponent γ is always larger than $q/3$ due to the contributions of the attractive term, but not far from it. Instead γ is determined by the steepness of the repulsive part of $V(r)$, evaluated around the distance r_c of *closest* approach between particles in the supercooled regime. The distance r_c is significantly smaller than the average position of the first peak of the pair distribution function $g_{11}(r)$ of the larger particles. At such small distance, one would think that the primitive or the local JG β-relaxation is more directly related to the repulsive part of $V(r)$ than the cooperative α-relaxation which involves more particles and longer length scale. From this observation, we conclude that the dependence of dynamic quantities on ρ^{γ}/T originates in the primitive or the local JG β-relaxation. This original dependence of τ_{JG} (or τ_0) on $T^{-1}V^{-\gamma}$ is passed on to and magnified in τ_α of the structural α-relaxation at a later time after the many body dynamics have been accounted for [32]. The stronger dependence of τ_α on $T^{-1}V^{-\gamma}$ than τ_{JG} (or τ_0) follows directly from the CM equation (4.2).

4.2.3.4 Dependences of the Global and Segmental Dynamics in Polymers on TV^{γ}: Same γ but Different Functional Forms

Dielectric relaxation data were obtained for various temperatures T and pressures P on the polymers, polypropylene glycol, 1,4-polyisoprene, and poly(oxybutylene) [125, 126]. The spectra show not only the α-relaxation but also the longer-time chain-normal modes. Both the α-relaxation time τ_α and the normal mode relaxation time τ_n were shown to be functions of $T^{-1}V^{-\gamma}$ with the same γ, but $f_n(T^{-1}V^{-\gamma})$ of τ_n is weaker than $f_\alpha(T^{-1}V^{-\gamma})$. The results offer quantitative tests of the prediction that τ_α and τ_0 are different functions of the same product variable $T^{-1}V^{-\gamma}$, and they are related by an equation of the CM applied to polymer dynamics and viscoelasticity [127–131]. The normal modes and the local segmental mode have the same primitive monomeric friction coefficient $\zeta_0(T)$. Based on this, the break down of thermorheological simplicity of the viscoelastic spectrum of amorphous polymers was explained by the difference between the coupling parameter n_α and n_n of the local segmental mode and the normal modes, respectively [127–131]. By the same method, the relation between the weaker $f_n(T^{-1}V^{-\gamma})$ of τ_n and $f_\alpha(T^{-1}V^{-\gamma})$ of τ_α was explained in a quantitative manner [132].

4.2.3.5 Change of T-Dependence of JG β-Relaxation Time and Relaxation Strength on Crossing T_g

A rigorous experimental proof of change of T-dependence of τ_{JG} from a weaker and Arrhenius dependence below T_g to a stronger T-dependence above T_g was first obtained for sorbitol and xylitol by applying pressure [93]. At elevated pressures up to 1.8 GPa, the separation between the α- and JG β-relaxation peaks in the isobaric dielectric spectra is larger than at ambient pressure. Consequently, the JG β relaxation is clearly resolved, enabling τ_{JG} to be unambiguously determined above and below T_g. The data of sorbitol presented in Fig. 4.9 clearly show that the Arrhenius temperature dependence of τ_{JG} does not persist for temperatures above T_g. This result, consistent with inferences drawn from dielectric relaxation measurements at ambient pressure, is obtained directly, without the uncertainty introduced by deconvolution of the α and JG β relaxations. There are other cases where the JG β-relaxation is either clearly resolved or isolated by a procedure above and below T_g, and its relaxation time determined either directly or unambiguously. Likewise, the T-dependence of τ_{JG} was reported to change from Arrhenius dependence below T_g to a stronger T-dependence above T_g [94, 96, 100, 101, 105, 133]. The same was observed for the pressure dependence when crossing the glass transition pressure P_g isothermally [44, 45, 90–92] (see examples in Figs. 4.7 and 4.10). In all cases, the observed τ_{JG} is in agreement with the calculated primitive relaxation time τ_0, which from (4.2) obviously changes its T-dependence at T_g following the well-known behavior of τ_α. These general experimental facts are indications that the JG β-relaxation is not independent of the α-relaxation, and actually the two are well connected.

An example of this behavior of the JG β-relaxation is taken from the study by Brás et al. [113]. on the pharmaceutical, ibuprofen. The relaxation map presented in Fig. 4.11 shows the change of T-dependence of τ_{JG} at T_g, and good agreement between τ_{JG} and τ_0.

An example of a component in binary mixtures is taken from 35 wt% of water in mixtures with various ethylene glycol oligomers [101]. All mixtures show the presence of the α-relaxation of the solute hydrogen bonded with water, and a secondary relaxation originating from the water component but also influenced by hydrogen bonding with the solute. The T-dependence of the secondary relaxation time, τ_β, is Arrhenius below T_g and has activation enthalpy in the range of 40–50 kJ/mol, but it changes to a stronger dependence above T_g (see Fig. 4.12a).

The dielectric relaxation strength of the JG β-relaxation, $\Delta\varepsilon_{JG}(T)$, also changes its T-dependence on crossing T_g. It has stronger temperature dependence above T_g than below it. This is found for neat glass formers as well as for a component in binary mixtures [102, 105, 134, 135]. The dielectric strength, $\Delta\varepsilon_\beta$, of water in 35 wt% mixtures with various ethylene glycol oligomers also exhibits a change to a stronger increase with increasing T after crossing T_g (see Fig. 4.12b). This behavior of the JG β-relaxation of water is found in other aqueous mixtures, nanoconfined water [102], and hydration water of proteins and biomolecules [105]. Another example is TBP in tristyrene as shown in Fig. 4.13.

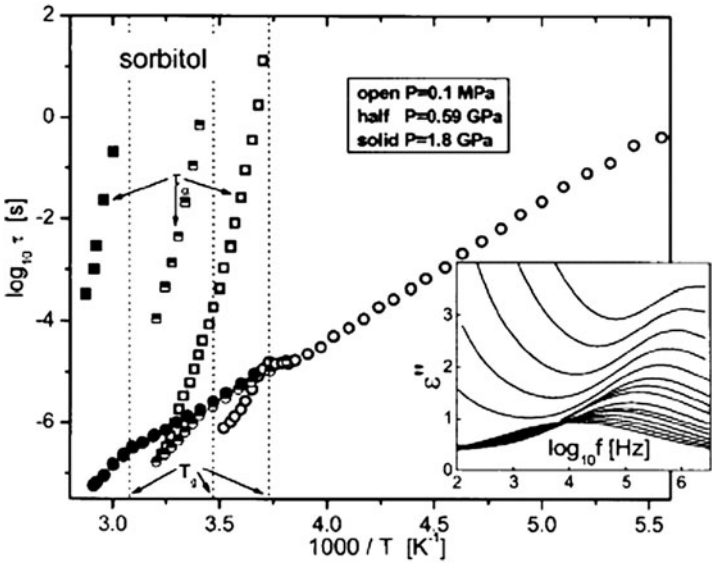

Fig. 4.10 Isobaric α-relaxation times at 0.1 MPa (*open square*), 0.59 MPa (*half-filled square*), and 1.8 GPa pressure (*filled square*), along with the corresponding JG β relaxation times at 0.1 MPa (*open circle*), 0.59 MPa (*half-filled circle*), and 1.8 GPa (*filled circle*) for sorbitol. The slope of τ_{JG} is independent of pressure, although it differs markedly for low versus high temperatures. The *inset* shows the JG peak in the dielectric loss at $P = 1.8$ GPa for temperatures from 273 to 343 K, in 5 increments (*bottom* to *top*). The α-peak is too low in frequency to appear within the measured frequency range

4.2.3.6 Relation Between the Activation Energies of τ_{JG} and τ_α in the Glassy State

In the glassy state at temperatures below T_g, and under the condition that the structure is frozen and no change is observed, the T-dependence of τ_α is Arrhenius with activation energy E_α. Data of τ_α below T_g are not easy to access because it becomes too long. However, for some glass formers, they are either available or can be extracted by analysis [89] based on fictive temperature model. Below T_g, the value of E_α is larger than the activation energy E_{JG} of τ_{JG}. Interestingly, the two activation energies are related through n by the equation $E_{JG} = (1 - n)E_\alpha$, as shown in Fig. 4.14.

4.2.3.7 Pressure–Temperature History Dependence of τ_{JG} in the Glassy State

It is well known that the structure of the glassy as well as the structural relaxation time depends on thermal history. A rapidly quenched glass at a temperature below T_g undergoes physical aging, resulting in increased density and reduced entropy to

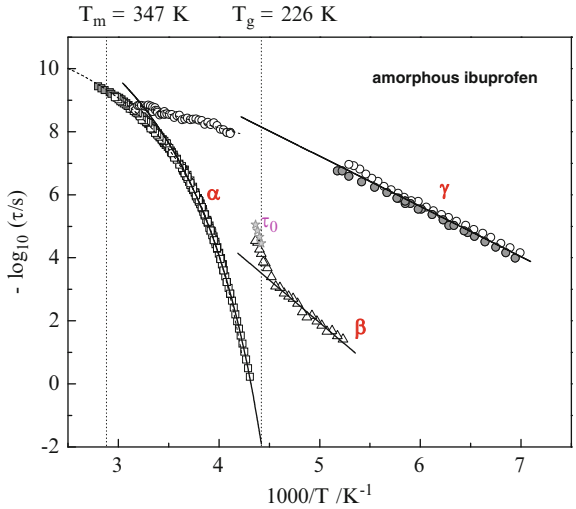

Fig. 4.11 Logarithm of the relaxation time, $\log_{10}\tau$, versus $1/T$ for all relaxation processes in ibuprofen: *open symbols*, τ from obtained isothermal loss data collected during cooling; *gray filled symbols*, τ from the isochronal plots. *Lines* are fits of the Arrhenius dependence of β- and γ-relaxation times below T_g, which is indicated by the *dotted line*. The α-relaxation times require two VFTH formulas to fit: the *solid line* is the VFTH1 fit and the dashed line is the VFTH2 fit to the data. *Light gray stars* indicate the JG relaxation time, τ_{JG}, estimated by the primitive relaxation time calculated from the Coupling Model [113]. The β-relaxation time (*open triangles*) change to a stronger T-dependence when temperature is increased above T_g, where there is good agreement with the estimated τ_{JG}. The relaxation of the hydrogen-bonded network slower than the α-relaxation is not shown. Data from Brás et al. [113]

attain the equilibrium liquid structure. The fact that the JG relaxation plays a role in physical aging can be traced back to the historic example of the observation of the effect of aging of silicate glass thermometers at room temperature over a period of 38.5 years, from April 1844 to December 1882, by James Prescott Joule [136], which was revisited by Nemilov and Johari [137]. Aging of the silicate glass caused change of the thermometer scale, which in turn was measured by the shift in the "zero-point temperature." The T_g of silicate glasses, typically in the range of 680–900 K, is much higher than room temperature, and the α-relaxation time τ_α would be much longer than a century. However, structural change of the silicate glass was found by Joule from the change of zero-point temperature of about 8°F over 38.5 years. Nemilov [138] fitted the time dependence of the zero-point temperature data of Joules by the expression 13.58–9.56 [exp(−t/13.50)], where the unit of time is year. Since τ_α is much longer, the observed change by Joule cannot be effected by the structural α-relaxation. However, τ_{JG} is much shorter and some local changes of the glass structure can occur through the JG β-relaxation. The mechanism for this observed spontaneous relaxation of glass at room temperature is attributed to the JG β-relaxation which causes local regions in the network,

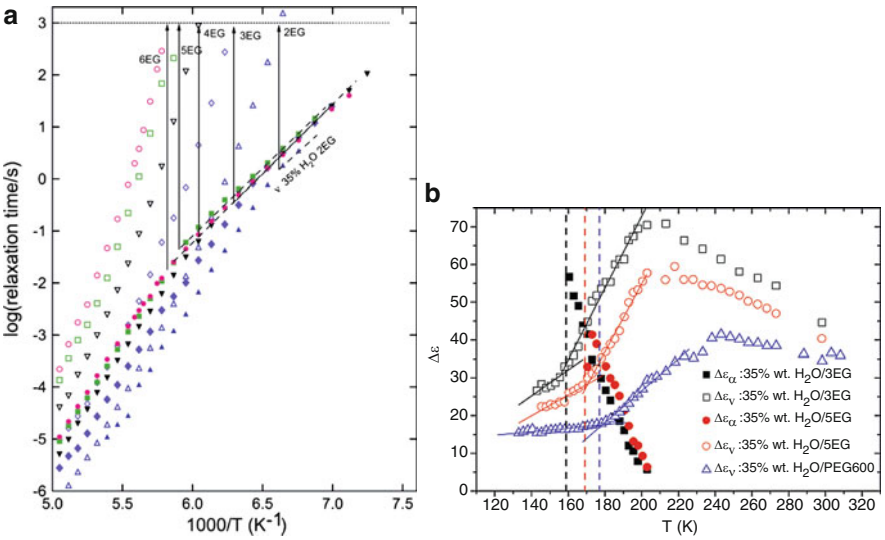

Fig. 4.12 (**a**) Temperature dependence of the dielectric relaxation time τ_α (*open symbols*) and τ_{JG} (corresponding *closed symbols*) of mixtures of 35 wt% of water with various ethylene glycol oligomers as indicated. *Circles* for 6EG. Squares for 5EG. *Downward-pointing triangles* for 4EG. *Diamond* for 3EG. *Upward-pointing triangles* for 2EG. Some of the data of τ_{JG} (*closed symbols*) overlap and cannot be easily resolved. For this reason, we use the *dashed lines* to indicate the Arrhenius temperature dependences assumed by τ_{JG} of the mixtures starting approximately at temperatures below T_g of the mixtures defined by $\tau_\alpha(T_g) = 10^3$ s located by the *vertical arrows*. There is a change in the temperature dependence of τ_{JG} at T_g. From Capaccioli et al. [101]. (**b**) Dielectric strengths $\Delta\varepsilon_\alpha$ and $\Delta\varepsilon_\beta$ of the mixture of 65 wt% of 3EG, 5EG, and PEG600 with water. *Full symbols* are for $\Delta\varepsilon_\alpha$ of the α-relaxation and *open symbols* for $\Delta\varepsilon_\beta$ of the JG β-relaxation. *Full lines* are linear fits of $\Delta\varepsilon_\beta$ below and above T_g. Each *dashed vertical line* indicates the temperature T_g near which the elbow-shaped crossover of temperature dependence of $\Delta\varepsilon_\beta$ occurs. Here T_g is defined as the temperature at which $\log_{10}[\tau_\alpha(T_g)/s]\sim 3$] [101]

and in turn the Si–O–Si bond angles in the immediate surroundings, to change [137]. There are some studies of aging in the recent past that touch upon the JG β-relaxation. The classical monograph of Struik [139] has already mentioned that secondary relaxation is responsible for aging at low temperatures. Others have seen change in dielectric relaxation strength and/or relaxation time of the resolved JG β-relaxation or the unresolved JG β-relaxation via the excess wing [96, 140–150]. These results indicate that the JG β-relaxation is sensitive to change in volume and entropy. In two of these studies [96, 150], a connection between JG β-relaxation time and the α-relaxation time in the glassy state was found in accord with the CM. Also, in the glassy state, JG β-relaxation was found to govern the rate of crystal nucleation, the initial process of crystallization [151, 152].

Elevated pressure has also been employed to observe the dependence of the relaxation time of JG β-relaxation [153, 154] as well as non-JG γ-relaxation [153–155] on the T and P path used to take the liquid initially at ambient pressure P_i and temperature T_i ($>T_g$) to the glassy state at an elevated pressure P_f, and T_f

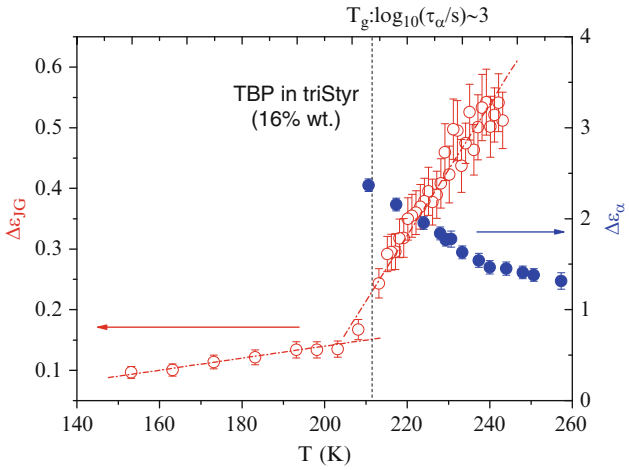

Fig. 4.13 Dielectric strengths $\Delta\varepsilon_\alpha$ and $\Delta\varepsilon_\beta$ of the mixture of 16 wt% *tert*-butyl-pyridine (TBP) in tristyrene. *Full symbols* are for $\Delta\varepsilon_\alpha$ of the α-relaxation (*right axis*) and *open symbols* for $\Delta\varepsilon_\beta$ of the JG β-relaxation (*left axis*). *Dotted lines* are linear fits of $\Delta\varepsilon_\beta$ below and above T_g. *Dashed vertical line* indicates $T = 211.5$ K [where $\log_{10}(\tau_\alpha/\text{s})\sim3$] and is near the temperature at which the elbow-shaped crossover of temperature dependence of $\Delta\varepsilon_\beta$ occurs. From Capaccioli et al. [102]

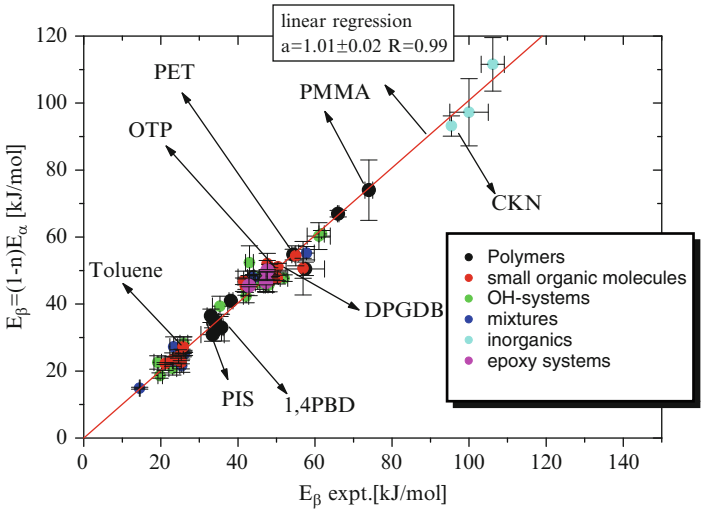

Fig. 4.14 Linear correlation between the experimental activation energy in the glassy state for the JG β-relaxation process (abscissa) and the activation energy predicted by the Coupling Model for the primitive relaxation (ordinate). Symbols for simple van der Waals molecules, H-bonded systems, polymers, chlorobenzene/toluene mixture, inorganics, and epoxy oligomers are shown in the figure. The *solid line* is a linear regression of data (linear coefficient 0.99 ± 0.01). Data after Capaccioli et al. [89]

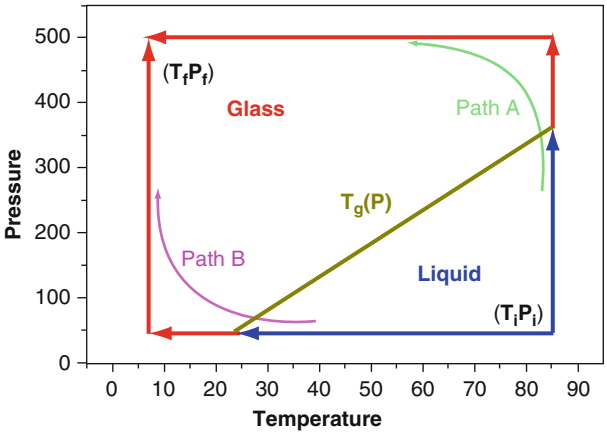

Fig. 4.15 Schematic representation of the thermodynamic paths used in the experiment to vitrify the systems. In experiments, the starting point (T_i,P_i) is in the liquid state and the final point (T_f,P_f) in the glassy state

($>T_g$). One choice of thermodynamic path is to elevate pressure from P_i to P_f in the liquid state, and finally decrease temperature from T_i to T_f in the glassy state formed by compression. This is path A as illustrated in Fig. 4.15. The other choice is to cool the liquid from T_i to T_f to form a glass, and then elevate pressure from P_i to P_f (path B). Although at the same $T = T_f$ and $P = P_f$, the two glasses obtained via paths A and B have different density and entropy. The spectra of the secondary relaxation of the two glasses taken at $T = T_f$ and $P = P_f$ are then compared. Observation of difference in the observed loss peaks either in frequency or in intensity is an indication that the JG β-relaxation is sensitive to the structure of the liquid or glass. This is observed in the case of JG β-relaxation in two epoxy resins [110, 156], PPGE and DGEBA as shown in the top and bottom panels of Fig. 4.16. The fact that the secondary relaxations of the two epoxies are genuine JG β-relaxation was borne out by the pressure sensitivity of the relaxation time [91], which is demonstrated explicitly in Fig. 4.5 here for DGEBA. On the other hand, the JG β-relaxation of 1,1′-bis(*p*-methoxyphenyl)cyclohexane (BMPC) is not resolved. The resolved secondary relaxation of BMPC shown in Fig. 4.16 is the non-JG γ-relaxation because it is insensitive to pressure [157]. No difference was found for the non-JG γ-relaxation of the two glasses arrived at by path A or path B, as shown in the middle panel of Fig. 4.16. This is evidence that the non-JG γ-relaxation is a local and intramolecular process and hence insensitive to volume and entropy. Examples can be taken from the works of J. Heijboer on secondary relaxations for polymers with alicyclic side groups; one example can be found in McCrum, Read, and Williams [9]. Differences in the resolved non-JG γ-relaxation of three glasses from different T and P paths were found in diisobutyl and diisoctyl phthalates [155]. However, these two are hydrogen-bonded glass formers, and the different paths may change the hydrogen-bonding scheme and, in turn, the local relaxation.

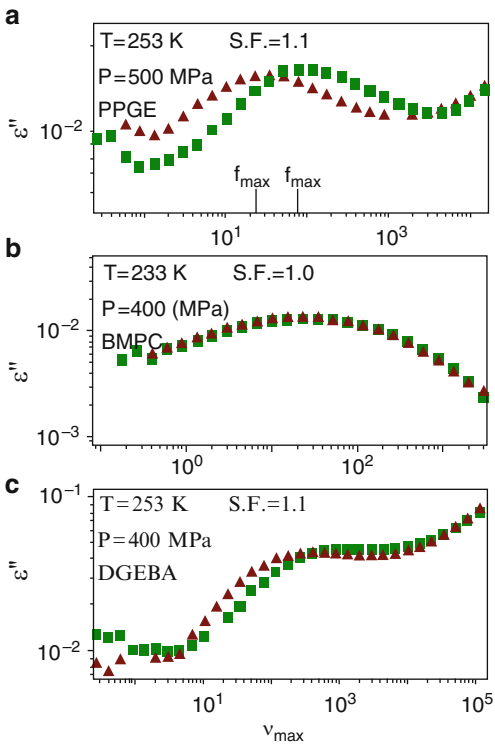

Fig. 4.16 Loss spectra of the secondary relaxation measured after vitrification along paths A (*triangles*) and B (*squares*) for (**a**) PPGE, (**b**) BMPC, and (**c**) DGBEA. The spectra measured after vitrification along path A are vertically shifted by shift factor to obtain the same value of maxima loss as those measured after vitrification along path B [153, 154]

4.2.3.8 JG β-Relaxation Causes Cage Decay and Terminates the Nearly Constant Loss

At times earlier than the onset of JG β-relaxation, all molecules are mutually caged and the caged dynamics are manifested as the nearly constant loss (NCL), which is motion confined within the anharmonic intermolecular potential. This loss has no characteristic times, and therefore, it is a power law, $\varepsilon''(\omega) = A\omega^{-\mu}$, typically $0 < \mu < 0.2$. This caged dynamics persist to longer times until the cages start to decay by rotational or translational relaxation of the entire molecule, i.e., the JG β-relaxation. As discussed in [102, 158, 159], the NCL is a more general feature than the so-called β-process of the Mode Coupling Theory [68]. Experimental data have shown that $\omega_{JG} = (\tau_{JG})^{-1}$ is located near the lower bound of $\varepsilon''(\omega)$=$A\omega^{-\mu}$. This fact shown to hold in many glass formers supports that cage decay and termination of the NCL are caused by the JG β-relaxation. The intensity of the NCL when plotted as a function of temperature also changes the slope at T_g [30, 158, 159].

4.2.3.9 JG β-Relaxation Is Responsible for the Anomalous T-Dependence of γ-Relaxation Time

In several glass formers, secondary relaxation has been reported to exhibit anomalous behavior at temperatures in the vicinity of T_g [141, 149, 160–163]. It turns out that all these secondary relaxations are non-JG γ-relaxation [164], although the distinction was not made in earlier works [141, 160] understandably so because the paper that gives the criteria to classify secondary relaxations was not published until 2004 [34]. The anomaly is that the *relaxation time* τ_γ *decreases* on *cooling* from the equilibrium liquid state down to the glassy state [141, 149]. This unexpected T-dependence of τ_γ on cooling continues sometimes until a minimum is reached and thereafter τ_γ reverts to its normal behavior of monotonic increase with decreasing temperature in the glassy state. Such anomaly was reported in hydrogen-bonded glass formers including di- and tri-propylene glycol (2PG and 3PG) and polypropylene glycol of molecular weight $M_w = 400$ g/mol (PPG400) [160–163], and van der Waals liquid di-*n*-octyl phthalate (DOP) [149]. To explain this peculiar behavior, Dyre and Olsen [160] utilized an asymmetric double-well potential to model the γ-relaxation and with special assumptions, they constructed the so-called "minimal model" that can successfully explain the behavior. Similar success was found in applying the "minimal model" to the γ-relaxation in other glass formers, PPG400 and DOP. These works have generated interest in the glass transition research community and two alternative explanations have been proposed [164, 165]. A change in temperature dependence of τ_γ on cooling at a temperature far above T_g in epoxy resins DGEBA and PPGE was found, although no minimum of τ_γ was observed [110, 156]. This change of T-dependence of the epoxy resins has been explained in a similar way as τ_γ in other glass-formers [164].

Ngai et al. [164] pointed out that the anomaly of τ_γ in all cases occurs at temperatures where τ_{JG} becomes close to τ_γ. This is due to the fact that, without exception, the slower JG relaxation has a stronger Arrhenius T-dependence than the γ-relaxation below T_g, and hence the JG relaxation encroaches toward the γ-relaxation when temperature is raised toward T_g and tends to exceed it above T_g. If τ_{JG} gets close to τ_γ, then the supposedly observed γ-relaxation spectrum is rendered more complex, and cannot be considered as entirely due to the γ-relaxation. The JG relaxation involves essentially the motion of the entire molecule, or the entire repeat unit in the case of a polymer [34]. On the other hand, the γ-relaxation is the motion of a part of the molecule. This part of the molecule eventually also participates in the slower JG relaxation. Deep in the glassy state, where τ_γ is much shorter than τ_{JG}, the γ-relaxation is decoupled from and not influenced by the JG relaxation and τ_γ has the usual Arrhenius temperature dependence. However, near T_g and especially above T_g, τ_{JG} becomes comparable to τ_γ, and the γ-relaxation and the JG relaxation are no longer independent of each other because that part of the molecule responsible for the γ-relaxation has to relax in concert with the rest of the molecule to execute the JG relaxation. This means that the γ-relaxation is *hybridized* by the JG relaxation, and consequently, τ_γ is shifted toward τ_{JG} and

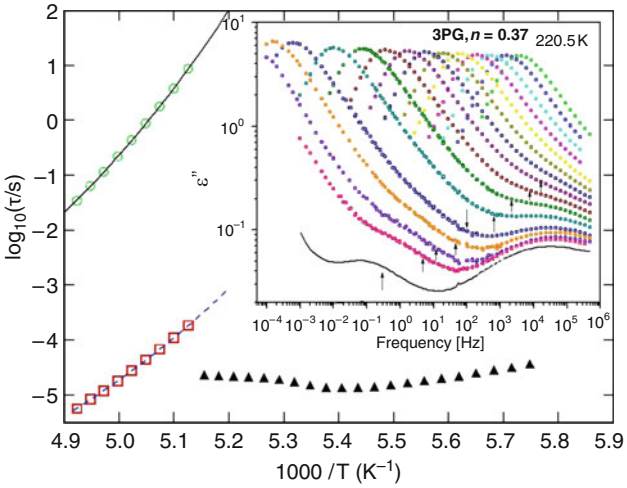

Fig. 4.17 Encroachment of τ_{JG} toward τ_γ of 3PG. The *open squares* are τ_{JG} calculated. The *filled triangles* are τ_γ determined from isothermal experimental spectra. The *inset* shows dielectric loss data of 3PG [166] measured at 220.5 K and various pressures (from *right* to *left*: 33.4, 61.9, 93.0, 120.7, 150.0, 180.2, 209.3, 237.5, 268.6, 297.2, 331.3, 373.4, 415.3, 447.2, 463.7, 510.2, and 591.3 MPa). Figure taken from [164]

becomes longer than the Arrhenius T-dependence (established deep in the glassy state) would predict. On increasing temperature, τ_{JG} and τ_γ get closer to each other; the shift of τ_γ toward τ_{JG} is larger, and hence, the minimum.

An example from 3PG of the anomalous T-dependence of τ_γ is given in Fig. 4.17. The relaxation map shows τ_α, τ_{JG}, and τ_γ as functions of reciprocal temperature. While τ_α and τ_γ are from experimental data at ambient pressure [162], τ_{JG} is estimated from τ_0 calculated by (4.2) with $n = 0.37$ (main figure) obtained by fitting the α-loss peak by one-sided Fourier transform of the Kohlrausch function. The inset shows dielectric loss data of 3PG [166] measured at 220.5 K and various pressures. The JG relaxation is resolved at higher pressures. The vertical arrows indicate the location of $\nu_0 \equiv 1(2\pi\tau_{JG})$ calculated by (4.2) with $n = 0.37$. In both the main figure and the inset, it is clear that τ_{JG} gets closer to the supposedly τ_γ on increasing T (main part) or decreasing P (inset). This together with the fact that dispersion of the γ-relaxation is very broad, hybridization of the γ-relaxation with the JG relaxation in causing the anomalous T-dependence of τ_γ is highly probable.

The data of 2PG and PPG400, PPG1025, PPG4000, and DOP are similar and exhibit the encroachment of τ_{JG} toward τ_γ in the temperature range where the anomalous T-dependence of τ_γ is observed. The same explanation of hybridization by the JG β-relaxation applies to these cases.

The JG relaxation exists in DGEBA and PPGE, but can only be resolved near and below T_g [48, 156]. Above T_g, τ_{JG} can be estimated by the primitive relaxation time, τ_0, calculated by (4.2) with $n = 0.47$ deduced by the fits to the α-relaxation by the Fourier transform of the Kohlrausch function (4.1) shown in Fig. 4.18 for

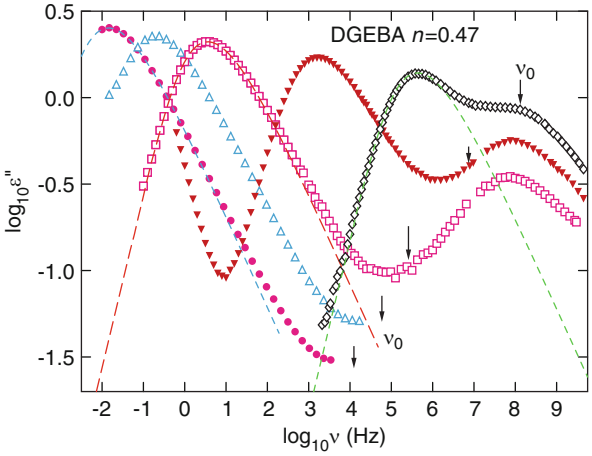

Fig. 4.18 Dielectric loss spectra at ambient pressure of DGEBA. The *vertical arrows* indicate the location of the calculated $\nu_0 \equiv 1(2\pi\tau_0) \approx 1(2\pi\tau_{JG})$ by (4.2) with $n = 0.47$. The *dashed lines* are fit to the α-relaxation by the Fourier transform of the Kohlrausch function with $n = 0.47$ [164]

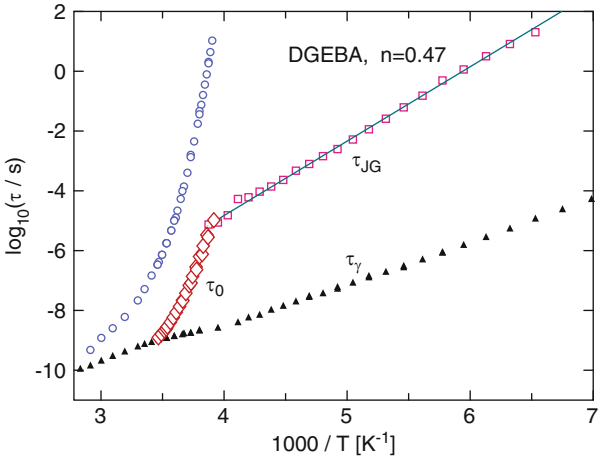

Fig. 4.19 Relaxation map of DGEBA. The *open diamonds* are τ_{JG} calculated by (4.2) with $n = 0.47$ from the Kohlrausch function fit to the α-relaxation as shown in Fig. 4.18 [164]

DGEBA. The anomaly of temperature dependence of τ_γ found in DGEBA and PPGE [110, 156] differs from the others discussed earlier. It occurs in the liquid state high above T_g as shown in Fig. 4.19 for DGEBA. The encroachment of $\tau_{JG} \approx \tau_0$ toward τ_γ can be seen either in Fig. 4.18 or 4.19 in the temperature region where the anomaly of τ_γ occurs. Similar results have been obtained for PPGE. The relaxation strength of the JG relaxation increases with temperature, and this behavior makes the JG relaxation very competitive when compared with the γ-relaxation. The hybridization of the γ- and JG relaxation again explains the anomaly.

4.3 Conclusions

The results from the recent flourish of studies of dynamics of glass formers under elevated pressures have had a great impact on the frontiers of glass transition research. Striking and yet general and fundamental properties were found showing that the width of the dispersion of the structural α-relaxation, or equivalently the nonexponential parameter β_{KWW} of its Kohlrausch relaxation function, governs these newly found properties. The implication of these properties is that intermolecular coupling and many molecule relaxation dynamics are other important factors that control dynamic properties in addition to volume, entropy, pressure, and temperature. This conclusion is evident from the prominent role played by β_{KWW} in the Ngai CM. The latter is a measure of the extent of the many molecules cooperative α-relaxation due to intermolecular coupling. Studies at elevated pressure also bring out the fundamental importance of a special class of secondary relaxations called the JG β-relaxation, the counterpart of the primitive relaxation of the CM. Experimental data discussed here, especially those at elevated pressure, confirm that it is strongly connected to the α-relaxation via the nonexponentiality parameter β_{KWW}. The two relaxations are inseparable when considering the glass transition problem. Elevated pressure studies have found that not only τ_α but also the τ_{JG} (or τ_0) has $T^{-1}V^{-\gamma}$-dependence. Since the JG or primitive relaxation is the precursor of the α-relaxation, it is suggested that the dependence on ρ^γ/T originates in the former. This original dependence of τ_{JG} (or τ_0) on $T^{-1}V^{-\gamma}$ is passed on to and magnified in τ_α by the many body dynamics constituting the structural α-relaxation. The stronger dependence of τ_α on $T^{-1}V^{-\gamma}$ than τ_{JG} (or τ_0) also follows directly from the CM equation. Additional support of this comes from theoretical consideration as well as molecular dynamics simulations that demonstrate that the $T^{-1}V^{-\gamma}$-dependence is determined by the steepness of the repulsive part of $V(r)$, evaluated around the distance r_{c} of *closest* approach between particles in the supercooled regime, which is significantly smaller than the average position of the first peak of the pair distribution function $g_{11}(r)$ of the larger particles. Moreover, the JG β-(or primitive) relaxation is instrumental in terminating the caged molecules dynamics manifested as NCL in general for all glass formers, and also causing the anomalous temperature dependence of the non-JG γ-relaxation in some glass formers. Thus, the JG β-(or primitive) relaxation plays indispensable roles to bridge the shorter time dynamics to the terminal structural relaxation.

All the above experimental facts must be taken additionally into consideration in any serious attempts to solve the long-standing problem of glass transition. Theoretical models must include both thermodynamics and many body dynamics in order to describe accurately the general properties of the glass transition discovered by applying pressure, and those even at ambient pressure not described here. At the present time, among theories and models, only the CM has predictions that are consistent with these experimental facts. This is because the CM takes into account the effect of intermolecular coupling via n and the important relationship between the JG β-relaxation (via the primitive relaxation of the model) and the

structural α-relaxation. However, the CM in the present form is not yet a complete theory of glass transition. A complete theory would have to provide a first-principle account of the JG β-relaxation together with a rigorous treatment of intermolecular coupling, leading to the heterogeneous many molecule dynamics of the α-relaxation, together with the effects of volume, entropy, pressure, and temperature. Construction of such a complete satisfactory theory is understandably difficult and it may not be available in the near future.

References

1. Bridgman PW (1926) Proc Am Arts Sci 61:57
2. Schug KU, King HE Jr, Böhmer R (1998) J Chem Phys 109:1472
3. Gilchrist A, Earley JE, Cole RH (1957) J Chem Phys 26:196
4. Williams G (1964) Trans Faraday Soc 60:1548
5. Williams G (1964) Trans Faraday Soc 60:1556
6. Williams G (1966) Trans Faraday Soc 62:2091
7. Williams G, Watts DC (1971) Trans Faraday Soc 67:1971
8. Williams G (1979) Adv Polym Sci 33:60
9. McCrum NG, Read BE, Williams G (1991) Anelastic and dielectric effects in polymeric solids. Dover, New York
10. Sasabe H, Saito S (1968) J Polym Sci Polym Phys Ed 6:1401
11. Saito S, Sasabe H, Nakajima T, Yada K (1968) J Polym Sci Part 6:1297
12. Sasabe H, Saito S, Asahina M, Kakutani H (1969) J Polym Sci Polym Phys Ed 7:1405
13. Johari GP, Whalley E (1972) Faraday Symp Chem Soc 6:23
14. Naoki M, Matsumoto K, Matsushita M (1986) J Phys Chem 90:4423
15. Naoki M, Endou H, Matsumoto K (1987) J Phys Chem 91:4169
16. Naoki M, Katahira S (1991) J Phys Chem 95:431
17. Naoki M, Ujita K, Kashima S (1993) J Phys Chem 97:12356
18. Okuchi T, Cody GD, Mao HK, Hemley RJ (2005) J Chem Phys 122:244509
19. Fytas G, Dorfmüller Th, Wang CH (1983) J Phys Chem 87:5041
20. Fytas G, Patkowski A, Meier G, Dorfmüller Th (1982) Macromolecules 15:21
21. Oliver WF, Herbst CA, Lindsay SM, Wolf GH (1991) Phys Rev Lett 67:2795
22. Atake T, Angell CA (1979) J Phys Chem 83:3218
23. Takahara S, Ishikawa M, Yamamuro O, Matsuo T (1999) J Phys Chem B 103:792
24. Yamamuro O, Takahara S, Suga H (1995) J Non-Cryst Solids 183:144
25. For an editorial in New York Times touting the importance of glass transition and the difficulty in solving this problem, see Chang K (2008) The nature of glass remains anything but clear. The New York Times, July 29, 2008.)
26. Kovacs AJ (1963) Fortschr Hochpolym Forsch 3:S394
27. Kovacs AJ, Aklonis JJ, Hutchinson JM, Ramos AR (1979) J Polym Sci Polym Phys Ed 17:1097
28. Hodge IM (1994) J Non-Cryst Solids 169:211
29. Ngai KL, Casalini R, Capaccioli S, Paluch M, Roland CM (2005) J Phys Chem B 109:17356
30. Ngai KL, Casalini R, Capaccioli S, Paluch M, Roland CM (2006) In: Kalmykov YP, Coffey WT, Rice SA (eds) Adv Chem Phys. Part B, Fractals, diffusion and relaxation in disordered complex systems (chapter 10), vol 133. Wiley, New York, p 497
31. Ngai KL (2003) J Phys Condens Matter 15:S1107
32. Ngai KL (2005) J Non-Cryst Solids 351:2635
33. Ngai KL, Capaccioli S (2008) J Phys Condens Matter 20:244101

34. Ngai KL, Paluch M (2004) J Chem Phys 120:857
35. Ngai KL, Tsang KY (1999) Phys Rev E 60:4511
36. Ngai KL (2001) IEEE Trans Dielectr Electr Insul 8:329
37. Ngai KL (1979) Comments Solid State Phys 9:127
38. Ngai KL (1987) Evidences for universal behavior of condensed mater at low frequencies/long times. In: Ramakrishnan TV, Raj Lakshmi M (eds) Non-Debye relaxation in condensed matter. World Scientific, Singapore, pp 23–193
39. Williams G, Watts DC (1970) Trans Faraday Soc 67:1971
40. Williams G, Watts DC, Dev M, North A (1971) Trans Faraday Soc 67:1971
41. Cardona M, Chamberlin RV, Marx W (2007) Ann Phys (Leipzig) 16(12):842
42. Rivera-Calzada A, Kaminski K, Leon C, Paluch M (2008) J Phys Chem B 112:3110
43. Ngai KL, Capaccioli S, Prevosto D, Paluch M (2010) In: Rzoska S, Drozd-Rzoska A, Mazur S. Rzoska, A. Drozd-Rzoska, Mazur V (eds) Metastable systems under pressure. NATO science for peace and security series-A: chemistry and biology. Springer, Heidelberg, pp 3–30
44. Mierzwa M, Pawlus S, Paluch M, Kaminska E, Ngai KL (2008) J Chem Phys 128:044512
45. Kessairi K, Capaccioli S, Prevosto D, Lucchesi M, Sharifi S, Rolla PA (2008) J Phys Chem B 112:4470
46. Alegria A, Gomez D, Colmenero J (2002) Macromolecules 35:2030
47. Roland CM, McGrath KJ, Casalini R (2006) Macromolecules 39:3581
48. Macedo PB, Moynihan CT, Bose RA (1972) Phys Chem Glasses 13:171
49. Howell FS, Bose RA, Macedo PB, Moynihan CT (1974) J Phys Chem 78:639
50. Mierzwa M, Paluch M, Rzoska SJ, Ziolo J (2008) J Phys Chem B 112:10383
51. Plazek DJ, Magill JH (1966) J Chem Phys 45:3038
52. Magill JH, Plazek DJ (1967) J Chem Phys 46:3757
53. Ngai KL, Magill JH, Plazek DJ (2000) J Chem Phys 112:1887
54. Stickel F (1995) Ph.D. Thesis, Mainz University, Germany (Shaker, Aachen)
55. Stickel F, Fischer EW, Richert R (1995) J Chem Phys 102:6251, (1996) J Chem Phys 104:2043
56. Schneider U, Lunkenheimer P, Brand R, Loidl A (1999) Phys Rev E 59:6924
57. Angell CA, Ngai KL, McKenna GB, McMillan PF, Martin SF (2000) J Appl Phys 88:3113
58. Rault J (2000) J Non-Cryst Solids 271:177
59. Casalini R, Roland CM (2002) Phys Rev B 66:180201
60. Novikov VN, Sokolov AP (2003) Phys Rev E 67:031507
61. Casalini R, Roland CM (2005) Phys Rev B 71:014210
62. Roland CM, Casalini R (2005) J Chem Phys 122:134505
63. Casalini R, Paluch M, Fontanella JJ, Roland CM (2002) J Chem Phys 117:4901
64. Casalini R, Paluch M, Roland CM (2003) J Chem Phys 118:5701
65. Casalini R, Paluch M, Roland CM (2003) J Phys Condens Matter 15:S859
66. Roland CM, Hensel-Bielowka S, Paluch M, Casalini R (2005) Rep Prog Phys 68:1405
67. Corezzi S, Beiner M, Huth H, Schröter K, Capaccioli S, Casalini R, Fioretto D, Donth E (2002) J Chem Phys 117:2435
68. Götze W (1999) J Phys Condens Matt 11:A1
69. Dixon PK (1990) Phys Rev B 42:8179
70. Hensel-Bielowka S, Paluch M, Ngai KL (2005) J Chem Phys 123:014502
71. León C, Ngai KL (1999) J Phys Chem B 103:4045
72. Ngai KL (1999) J Chem Phys 111:3639
73. Ngai KL, Roland CM (2002) Polymer 43:567
74. Ngai KL, Lunkenheimer P, Léon C, Schneider U, Brand R, Loidl A (2001) J Chem Phys 115:1405
75. Ngai KL (2000) J Non-Cryst Solids 275:7
76. Schönhals A (2001) Europhys Lett 56:815
77. Schönhals A, Kremer F, Hofmann A, Fischer EW, Schlosser E (1993) Phys Rev Lett 70:3459

78. Tyagi M, Alegría A, Colmenero J (2005) J Chem Phys 122:244909
79. Casalini R, Ngai KL, Roland CM (2003) Phys Rev B 68:01420
80. Ngai KL (1998) J Chem Phys 109:6982
81. Brand R, Lunkenheimer P, Loidl A (2002) J Chem Phys 116:10386
82. Ngai KL, Gopalakrishnan TR, Beiner M (2006) Polymer 47:7222–7230
83. Beiner M, Ngai KL (2005) Macromolecules 38:7033
84. Bedrov D, Smith GD (2005) Macromolecules 38:10314
85. Ngai KL, Capaccioli S, Roland CM (2006) Macromolecules 39:8543
86. Ngai KL (2007) J Non-Cryst Solids 353:4237
87. Böhmer R, Diezemann G, Geil B, Hinze G, Nowaczyk A, Winterlich M (2006) Phys Rev Lett 97:135701
88. Nowaczyk A, Geil B, Hinze G, Böhmer R (2006) Phys Rev E 74:041505
89. Capaccioli S, Prevosto D, Lucchesi M, Rolla PA, Casalini R, Ngai KL (2005) J Non-Cryst Solids 351:2643
90. Prevosto D, Capaccioli S, Sharifi S, Lucchesi M, Rolla PA (2007) J Non-Cryst Solids 353:4278
91. Prevosto D, Capaccioli S, Lucchesi M, Rolla PA, Ngai KL (2009) J Non-Cryst Solids 355:705
92. Ngai KL, Prevosto D, Capaccioli S, Roland CM (2008) J Phys Condens Matter 20:244125
93. Paluch M, Roland CM, Pawlus S, Ziolo J, Ngai KL (2003) Phys Rev Lett 91:115701
94. Nogales A, Sanz A, Ezquerra TA (2006) J Non-Cryst Solids 352:4649
95. Kramarenko VYu, Ezquerra TA, Privalko VP (2001) Phys Rev E 64:051802
96. Prevosto D, Capaccioli S, Lucchesi M, Rolla PA, Ngai KL (2004) J Chem Phys 120:4808
97. Ngai KL, Kaminska E, Sekuła M, Paluch M (2005) J Chem Phys 123:204507
98. Capaccioli S, Kessairi K, Prevosto D, Lucchesi M, Ngai KL (2006) J Non-Cryst Solids 352:4643
99. Ngai KL (2006) J Non-Cryst Solids 352:404
100. Capaccioli S, Kessairi K, Prevosto D, Lucchesi M, Rolla P (2007) J Phys Condens Matter 19:205133
101. Capaccioli S, Ngai KL, Shinyashiki N (2007) J Phys Chem B 111:8197
102. Capaccioli S, Shahin Thayyil M, Ngai KL (2008) J Phys Chem B 112(50):16035
103. Kaminski K, Kaminska E, Paluch M, Ziolo J, Ngai KL (2006) J Phys Chem B 110:25045
104. Capaccioli S, Kessairi K, Prevosto D, Lucchesi M, Rolla P (2008) J Phys Chem B 112:4470
105. Ngai KL, Capaccioli S, Shinyashiki N (2008) J Phys Chem B 112:3826
106. Kaminski K, Kaminska E, Wlodarczyk P, Paluch M, Ziolo J, Ngai KL (2008) J Phys Condens Matter 20:335104
107. Kaminski K, Kaminska E, Wlodarczyk P, Pawlus S, Kimla D, Kasprzycka A, Paluch M, Ziolo J, Szeja W, Ngai KL (2008) J Phys Chem B 112:12816
108. Kessairi K, Capaccioli S, Prevosto D, Sharifi S, Rolla PA (2007) J Non-Cryst Solids 353:4273
109. Prevosto D, Capaccioli S, Sharifi S, Kessairi K, Lucchesi M, Rolla PA (2007) J Non-Cryst Solids 353:4278
110. Capaccioli S, Kessairi K, Prevosto D, Lucchesi M, Rolla P (2007) J Non-Cryst Solids 353:3984
111. Brás AR, Noronha JP, Antunes AMM, Cardoso MM, Schönhals A, Affouard F, Dionísio M, Correia NT (2008) J Phys Chem B 112:11087
112. Nath R, Nowaczyk A, Geil B, Böhmer R (2007) J Non-Cryst Solids 353:3788
113. Carpentier L, Decressain R, Desprez S, Descamps M (2006) J Phys Chem B 110:457
114. Johari GP, Powers G, Vij JK (2002) J Chem Phys 116:5908
115. Johari GP, Goldstein M (1970) J Chem Phys 53:2372. For a recent view, see M. Goldstein, "*The past, present, and future of the Johari–Goldstein relaxation*," to be published in J. Non-Cryst. Solids (2010 or 2011), Special issue of papers presented in the 6th IDMRCS, Rome, Italy, August 30th–September 4th (2009)

116. Johari GP (1973) J Chem Phys 58:1766
117. Johari GP (1976) Ann NY Acad Sci 279:117
118. Leisen J, Schmidt-Rohr K, Spiess HW (1993) Physica A 201:79
119. Hoover WG, Ross M (1971) Contemp Phys 12:339
120. Hoover WG, Ross M, Johnson KW, Henderson D, Barker JA, Brown BC (1970) J Chem Phys 52:4931
121. Hiwatari Y, Matsuda H, Ogawa T, Ogita N, Ueda A (1974) Prog Theor Phys 52:1105
122. Chandler D, Weeks JD, Andersen HC (1983) Science 220:787
123. Hansen JP, McDonald IR (1986) Theory of simple liquids, 2nd edn. Academic, London
124. Coslovich D, Roland CM (2008) J Phys Chem B 112:1329
125. Roland CM, Casalini R, Paluch M (2004) J Polym Sci Polym Phys Ed 42:4313
126. Casalini R, Roland CM (2005) Macromolecules 38:4363
127. Ngai KL, Plazek DJ, Rendell RW (1997) Rheol Acta 36:307
128. Ngai KL, Schönhals A, Schlosser E (1992) Macromolecules 25:4915
129. Plazek DJ, Schönhals A, Schlosser E, Ngai KL (1993) J Chem Phys 98:6488
130. Ngai KL, Plazek DJ (1995) Identification of different modes of molecular motion in polymers that cause thermorheological complexity. Rubber Chem TechRubber Rev 68:376–434
131. Ngai KL, Fytas G (1986) J Polym Sci Part B Polym Phys 24:1683
132. Ngai KL, Casalini R, Roland CM (2005) Macromolecules 38:1779
133. Blochowicz T, Rössler EA (2004) Phys Rev Lett 92:225701
134. Johari GP, Power G, Vij JK (2002) J Chem Phys 116:5908, J Chem Phys 117:1714
135. Power G, Johari GP, Vij JK (2003) J Chem Phys 119:435
136. Joule JP (1867) Mem Manchr Literary Phil Soc 3(3rd series) 292; (1884) The scientific papers of J. P. Joule, Vol 1. Physical Society, London, p 558
137. Nemilov SV, Johari GP (2003) Philos Mag 83:3117
138. Nemilov SV (1995) Thermodynamics and kinetic aspects of the vitreous state. CRC Press, Boca Raton, (2000) Glass Phys Chem 26:511Y530
139. Struik LCE (1978) Physical aging in amorphous polymers and other materials. Elsevier, Amsterdam
140. Johari GP (1982) J Chem Phys 77:4619
141. Olsen NB (1998) J Non-Cryst Solids 235–237:399
142. Leheny RL, Nagel SR (1998) Phys Rev B 57:5154
143. Schneider U, Brand R, Lunkenheimer P, Loidl A (2000) Phys Rev Lett 84:5560
144. Johari GP, Power G, Vij JK (2002) J Chem Phys 117:1714
145. Power G, Vij JK, Johari GP (2006) J Chem Phys 124:074509
146. Etienne S, David L, Duval E, Mermet A, Wypych A, Simeoni G (2006) Solid State Phenomena 115:99
147. Wypych A, Duval E, Boiteux G, Ulanski J, David L, Mermet A (2005) Polymer 46:12523
148. Lunkenheimer P, Wehn R, Schneider U, Loidl A (2005) Phys Rev Lett 95:055702
149. Kaminska E, Kaminski K, Hensel-Bielowka S, Paluch M, Ngai KL (2006) J Non-Cryst Solids 352:4672
150. Casalini R, Roland CM (2009) Phys Rev Lett 102:035701
151. Hikima T, Adachi Y, Hanaya M, Oguni M (1995) Phys Rev B 52:3900
152. Hatase M, Hanaya M, Oguni M (2004) J Non-Cryst Solids 333:129
153. Sharifi S, Prevosto D, Capaccioli S, Lucchesi M, Paluch M (2007) J Non-Cryst Solids 353:4313–4317
154. Sharifi S (2008) Ph.D. Thesis, University of Pisa, Pisa, Italy
155. Paluch M, Pawlus S, Hensel-Bielowka S, Kaminski K, Psurek T, Rzoska SJ, Ziolo J, Roland CM (2005) Phys Rev B 72:224205
156. Corezzi S, Beiner M, Huth H, Schroter K, Capaccioli S, Casalini R, Fioretto D, Donth E (2002) J Chem Phys 117:2435
157. Hensel-Bielowka S, Ziolo J, Paluch M, Roland CM (2002) J Chem Phys 117:2317
158. Ngai KL, Habasaki J, León C, Rivera A (2005) Z Phys Chem 219:47

159. Ngai KL (2004) Philos Mag 84:1341
160. Dyre J, Olsen B (2003) Phys Rev Lett 91:155703
161. Pawlus S, Hensel-Bielowka S, Grzybowska K, Ziolo J, Paluch M (2005) Phys Rev B 71:174107
162. Grzybowska K, Grzybowski A, Paluch M, Cappacioli S (2006) J Chem Phys 125:044904
163. Grzybowska K, Grzybowski A, Ziolo J, Rzoska SJ, Paluch M (2007) J Phys Condens Matter 19:376105
164. Ngai KL, Grzybowska K, Grzybowski A, Kaminska E, Kaminski K, Paluch M, Capaccioli S (2008) J Non-Cryst Solids 354:5085
165. Grzybowska K, Grzybowski A, Paluch M (2008) J Chem Phys 128:134904
166. Casalini R, Roland CM (2004) Phys Rev B 69:094202

Chapter 5
Pressure Effects on Polymer Blends

5.1 Theoretical Background

The important role of pressure on the miscibility of polymer mixtures has been realized only recently [1, 2]. Pressure has direct applications to processing as well as to new syntheses that involve the use of environmental-friendly supercritical fluids. From a fundamental point of view, the thermodynamics of polymer blends are frequently discussed in the framework of the incompressible random phase approximation (RPA) [3, 4]. However, an incompressible system should be unaffected by pressure and this notion is in sharp contrast to many recent experimental findings that will be discussed in detail in the next Sect. 5.2.

Blend miscibility is governed by the free energy of mixing

$$\Delta G_{\mathrm{mix}} = \Delta H_{\mathrm{mix}} - T\Delta S_{\mathrm{mix}}, \tag{5.1}$$

where ΔG_{mix} is the change in the Gibbs free energy of mixing, and ΔH_{mix} and ΔS_{mix} are the excess enthalpy and mixing entropy, respectively. Mixing occurs spontaneously when $\Delta G_{\mathrm{mix}} < 0$. However, this is rarely the case in polymer blends. In most cases, the unfavorable interactions between unlike segments drive the system to the phase-separated state. Nevertheless, some systems that show a miscibility gap do exist; i.e., blends that phase-separate upon lowering the temperature (thus exhibiting an upper critical solution temperature, UCST) and some that phase-separate upon raising the temperature (exhibiting a lower critical solution temperature, LCST).

For reasons discussed above, it is both of academic and industrial interest to examine the effect of pressure on blend miscibility. More precisely, we need to know the effect of pressure on the critical temperature T_{c}, i.e., the temperature for phase separation at each fixed pressure. It can be shown [5] from classical thermodynamics that the latter is given by

$$\frac{\mathrm{d}T_{\mathrm{c}}}{\mathrm{d}P} \approx T_{\mathrm{c}} \frac{\Delta V^{\mathrm{c}}_{\mathrm{mix}}}{\Delta H^{\mathrm{c}}_{\mathrm{mix}}}, \tag{5.2}$$

where $\Delta V^{\mathrm{c}}_{\mathrm{mix}}$ and $\Delta H^{\mathrm{c}}_{\mathrm{mix}}$ are the volume and enthalpy changes on mixing evaluated at the critical point, where T_{c} could correspond, in general, to an UCST or LCST. An

G. Floudas et al., *Molecular Dynamics of Glass-Forming Systems*,
Advances in Dielectrics 1, DOI 10.1007/978-3-642-04902-6_5,

increase in pressure for LCST-type polymer blends always increases the miscibility, i.e., raises the LCST, since both ΔV_{mix} and ΔH_{mix} (exothermic) are negative. On the contrary, increasing pressure for UCST-type blends can have two effects. Since UCST blends have a positive enthalpy of mixing (endothermic), the pressure dependence of the critical temperature depends solely on the sign of the volume change on mixing; a positive (negative) change ΔV_{mix} raises (lowers) the UCST. This situation [6] for both LCST and UCST blends is shown schematically in Fig. 5.1.

Different theoretical approaches are available that explore the effect of pressure on the miscibility of polymer blends. A first approach by Rabeony et al. [7] considers, as the main control parameter, the interaction energy density $(\chi/u_0)RT$, where χ is the Flory interaction parameter and u_0 is a reference volume. This approach assumes negligible volume changes on mixing; hence the only effect of pressure is to modify the energetics of the pure polymers described by a corresponding-states principle. However, several experimental results [8] suggested that the shift in critical temperature as a result of applied pressure correlates with the volume changes on mixing. Since the latter affects not only the purely enthalpic term (as suggested in this theory), but also the entropy of the system, this approach is incapable of describing the role of pressure on the thermodynamics of polymer blends.

A second approach by Kumar [9] took into account the entropic contributions to the pressure dependence of χ and suggested that the pressure dependence of χ in miscible polymer blends is directly related to the volume change on mixing. This approach assumed (1) identical compressibilities for the two components, (2) identical thermal expansion coefficients for the homopolymers and the blends, and (3) χ independent of composition. Under these assumptions, the following approximate prediction for the pressure coefficient of the critical temperature was proposed:

$$\left(\frac{\partial T}{\partial P}\right)_{\mathrm{c}} \sim \kappa_T T \left[\frac{\delta_{\mathrm{ip}}}{\delta}\right]^2 \frac{1}{1-\beta T-\kappa_T P}, \tag{5.3}$$

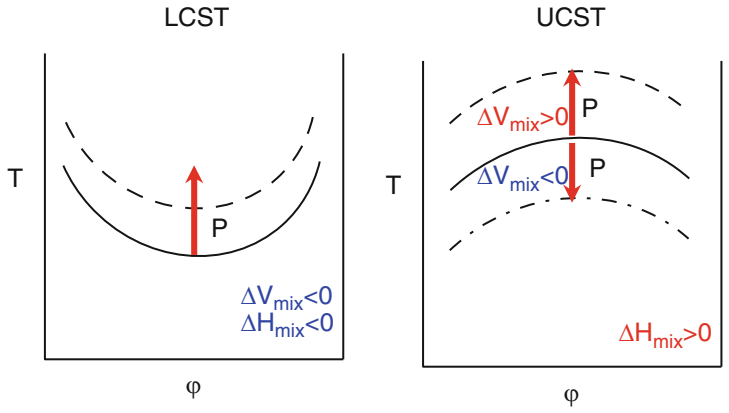

Fig. 5.1 Schematic of the effect of pressure on blend miscibility. For an LCST-type blend (*left*) increasing pressure always increases miscibility, i.e., raises the LCST. For an UCST-type blend (*right*), increasing pressure can increase ($\Delta V_{\mathrm{mix}} > 0$) or decrease ($\Delta V_{\mathrm{mix}} < 0$) miscibility

where δ_{ip} is the internal pressure, δ is the solubility parameter, κ_T is the isothermal compressibility, and β is the coefficient of thermal expansion. Employing some representative values: $\delta/\delta_{ip} \sim 0.72$ and $\kappa_T = 2 \times 10^{-4}$ MPa^{-1}, and $\beta = 4.5 \times 10^{-4}$ K^{-1}, we obtain $dT_c/dP \sim 0.15$ K/MPa at $T = 300$ K, a value that is in reasonable agreement with experimental findings.

A third approach by Lipson [6, 10, 11] is a theoretical lattice-based equation of state for polymers. In contrast to the Flory–Huggins theory, this approach accounts for the effects of both compressibility and nonrandom mixing. Briefly, the theory employs an athermal reference state along with an integral equation formalism [that is based on the Born–Green–Yvon (BGY) lattice theory] to determine the nearest neighbor probabilities, for all possible neighboring pairs, at finite temperature. These probabilities lead to the calculation of the system's internal energy and, ultimately, produce a closed-form expression for the Helmholtz free energy. The resulting equation of state is expressed in terms of a set of transferable microscopic parameters. This means that these parameters can be determined by *fitting* to a limited set of experimental data on known physical properties, and then used to *predict* other properties. The BGY equation of state, in particular, has been used in conjunction with homopolymer *PVT* data, along with a mixing rule, to make specific predictions about the effects of *T*, *P*, and component molecular weights on blend miscibility. Two specific model predictions for the effect of pressure on the critical temperature in an UCST system are shown in Fig. 5.2 [6]. In Fig. 5.2a, b, there is a positive change of volume on mixing ($\Delta V_{mix} > 0$) and this results in an increasing UCST with pressure. In Fig. 5.2c, d, the negative change in volume on mixing ($\Delta V_{mix} < 0$) gives rise to a decreasing critical temperature with pressure. Furthermore, the amount by which the UCST changes over a given pressure range is less in case (c, d) compared to that in (a, b) due to the smaller values of ΔV_{mix} in the former case. The theory further suggests that volume change on mixing for a UCST blend may be induced by altering the molecular weights of the blend components. In fact it has been suggested by these authors [6] that by a judicious choice of polymer molecular weights, the response of the UCST to pressure may be controlled to a point at which a blend can exhibit a pressure-independent UCST.

5.2 Effect of Pressure on the Dynamics of Miscible Polymer Blends: Dynamic Heterogeneity

The dynamics of miscible polymer blends is far more rich than originally anticipated. The components, despite being thermodynamically mixed, can exhibit distinct dynamic behavior, known as *dynamic heterogeneity* [12–19]. This dynamic heterogeneity, which has also been found in polymer/solvent mixtures [20, 21], manifests itself by (1) the two segmental processes with different temperature dependences, (2) the broadening of the relaxation spectra in the case of a single dielectrically active component, and (3) the breakdown of the time–temperature

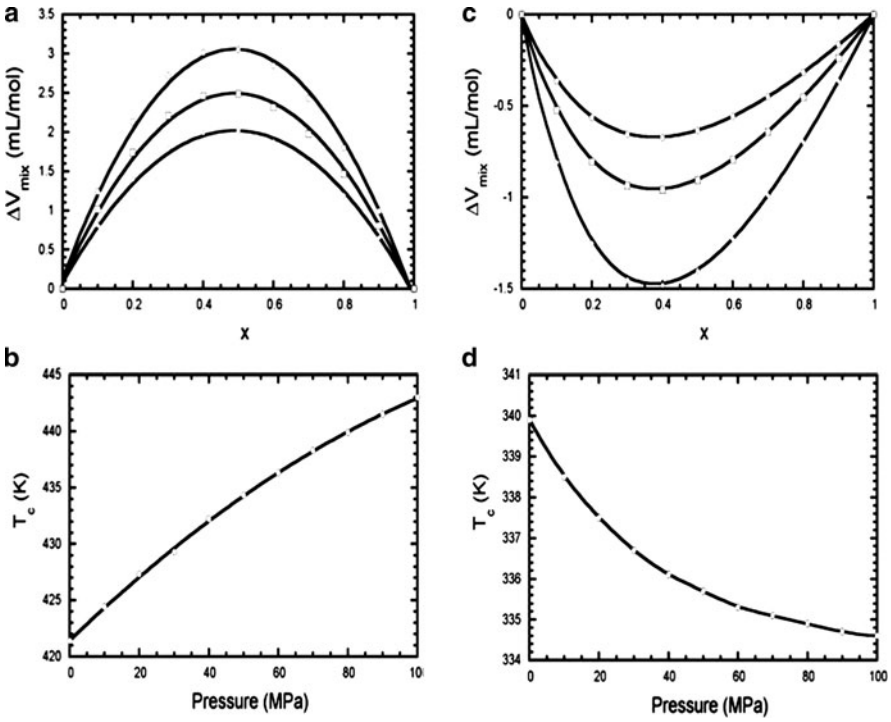

Fig. 5.2 Effect of pressure in a UCST blend having a positive change of volume on mixing (**a**, **b**) and a negative change of volume on mixing (**c**, **d**). From [6]

superposition for the single broad peak of such systems. Different models have been proposed to account for the distinct component dynamics that emphasize either *intermolecular* concentration effects through the concentration fluctuation approach [22] or *intramolecular* effects through the chain connectivity [23] or various combinations of both [24–31]. The former emphasizes the importance of the thermodynamically controlled intermolecular concentration fluctuations. According to this view [22], the slowing down of the dynamics on approaching T_g is due to the increasing cooperative volume that would diverge at the Vogel temperature. The latter intramolecular effects are emphasized in the recently proposed "self-concentration" model of Lodge and McLeish (LM) [23]. According to the model, the average composition of the local environment around any chosen segment is enriched in the same species because of chain connectivity effects (*correlation hole* effect). Because of this, each species will experience a different average local environment, and to the extent that the glass transition is sensitive to composition, each polymer will sense its own composition-dependent glass temperature. In a binary blend of homopolymers A and B, the effective local concentration is defined by

$$\varphi_{\mathrm{eff,i}} = \varphi_{\mathrm{S,i}} + (1 - \varphi_{\mathrm{S,i}})\langle\varphi\rangle, \tag{5.4}$$

where i represents component A or B, φ_S is the self-concentration, and $\langle\varphi\rangle$ is the average blend composition. According to the LM model [23], the relevant length scale in evaluating the self-concentration is the Kuhn length (l_K) of the polymer. This is a reasonable approximation since l_K is an intramolecular length scale (associated with the extent of backbone conformational transitions) that is independent of blend composition and only weakly dependent on T and P variations. Then the self-concentration is determined from the volume fraction occupied by monomers in one Kuhn length in a volume $V = l_K^3$ as

$$\varphi_S = \frac{C_\infty M_0}{k\rho N_A V_K}, \tag{5.5}$$

where C_∞ is the characteristic ratio, M_0 is the repeat unit molar mass, N_A is the Avogadro number, and k is the number of backbone bonds per repeat unit. The model associates the average local concentration of each component with a local glass temperature

$$T_{g,\text{eff}} = T_g(\varphi)|_{\varphi=\varphi_{\text{eff}}}. \tag{5.6}$$

Hence the effective glass temperature $T_{g,\text{eff}}$ is determined from the macroscopic $T_g(\varphi)$ but evaluated at φ_{eff} rather than at φ. For the macroscopic composition dependence of the glass temperature, the well-known Fox equation is usually assumed, but with the effective concentration for each component instead of the total blend composition $\langle\varphi\rangle$ as

$$\frac{1}{T_g(\varphi)} = \frac{\varphi_A}{T_{g,A}} + \frac{1-\varphi_A}{T_{g,B}}. \tag{5.7}$$

The model predictions for $T_g(\varphi)$ are then compared against experimental data. The main prediction of the model is that *miscible* polymer blends should have *two glass temperatures* [32]. The model predictions will be tested at elevated pressures with respect to the poly(methyl methacrylate)/poly(ethylene oxide) (PMMA/PEO) athermal blend (below).

5.2.1 *Athermal Polymer Blends/Copolymers (PI-PVE, PMMA/PEO)*

5.2.1.1 PI-*b*-PVE

It is well documented in the literature of polymer blends [27, 33] that the dielectric loss data of polyisoprene-*b*-poly(vinylethylene) (PI-*b*-PVE) copolymers and of PI/PVE blends display a double peak structure at several compositions. The origin of

the dual processes is a "fast" PI segmental relaxation (the PI chain relaxation, i.e., the end-to-end vector relaxation through the cumulative dipole moment along the chain contour, is too slow compared to the segmental process) and a "slower" PVE segmental relaxation (Fig. 5.3). Application of pressure makes the bimodal appearance of the $\varepsilon''(f)$ spectra less apparent [34]. In fact, as seen in Fig. 5.3, the spectra become more symmetric with increasing P. Since T and P can influence the two segmental relaxations differently, the loss spectra are compared under isokinetic conditions, i.e., at T, P conditions with the same relaxation time as that for the main ("slow") process. This representation leads to a good superposition at low frequencies; however, at high frequencies, the two sets of spectra are quantitatively different. The disparity in the high frequency part of the spectrum of the pressurized sample arises from the distinctly different P-dependence of the "fast" process associated with the PI segmental process. Thus the main process in the copolymer spectra is due to the "slow" PVE relaxation [34].

As we will see below, this remarkable result can be traced back to the different pressure sensitivities of the segmental relaxations of the respective homopolymers [34]. The apparent activation volume, extracted as usual from the pressure dependence of the relaxation times, has a strong T-dependence and increases with decreasing T in a qualitatively similar way as with the cooperative volume. This is depicted in Fig. 5.4 together with the homopolymers at temperatures equidistant from T_g. Notice that the homopolymers have significantly different activation volumes and that this is also reflected in the monomer volumes, implying local packing effects. In the representation of Fig. 5.4, the observed similarity of $\Delta V^{\#}$ in the diblock with the pure PVE corroborates the notion that the main relaxation in the former is due to the hard component (PVE) that is noticeably characterized by a lower $\Delta V^{\#}$, compared to the soft block (PI) under similar ΔT_g. For independent

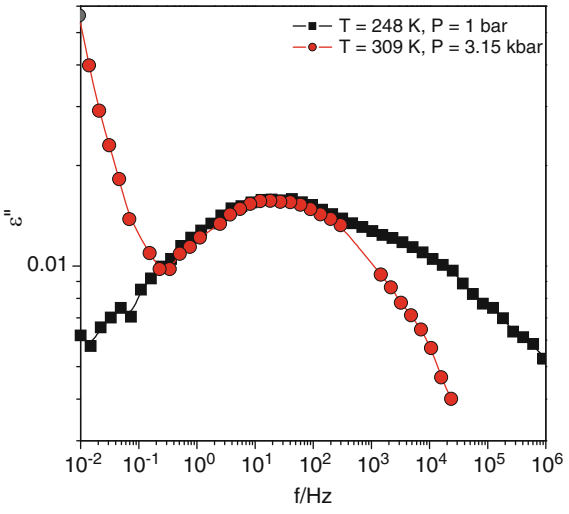

Fig. 5.3 Comparison of the measured dielectric loss spectra under isokinetic conditions for the PI-*b*-PVE copolymer with a PI volume fraction of 0.495. The main peak for both spectra correspond to about 0.2 ms. From [34]

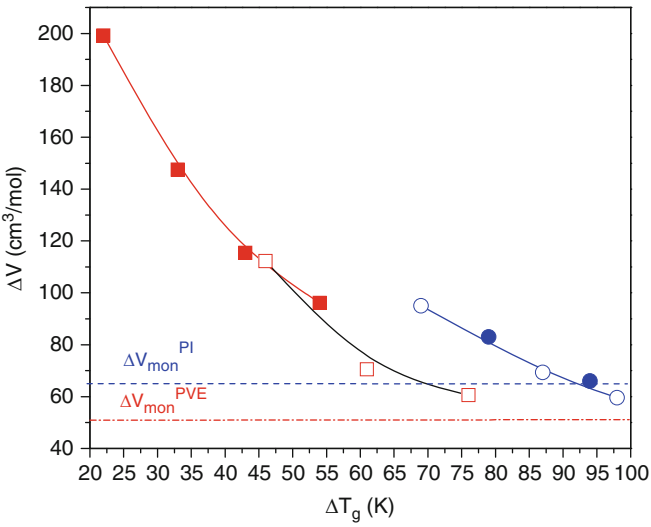

Fig. 5.4 Apparent activation volumes for the segmental relaxation of PI [(*open circle*): $M_W = 2.6 \times 10^4$ (g/mol), (*filled circle*): $M_W = 1.06 \times 10^4$ (g/mol) and PVE (*filled square*) homopolymers as well as of the PI-*b*-PVE copolymer (*open square*) are plotted at temperatures equidistant from the corresponding T_gs. For the T_g, the following values were used: 272, 208, and 233 K for PVE, PI, and PI-*b*-PVE, respectively, and correspond to the temperature where the maximum relaxation time in DS is 10 s. From [34]

component dynamics, pressurization of the copolymer would slow down the fast (PI) more efficiently rather than the slow (PVE) component simply because of the higher $\Delta V^{\#}$ requirement in the latter. Although decreasing temperature and increasing pressure produce qualitatively similar broadening at low frequencies, pressure unlike temperature has an additional function: high pressure induces dynamic homogeneity in PI-*b*-PVE in contrast to temperature. There is a need for expanding these results in other dynamically heterogeneous but apparently miscible blends. It is especially intriguing that it is the softer component (lower T_g) that is affected more by pressure, giving rise to induced homogeneity at elevated pressures.

5.2.1.2 PMMA/PEO

Poly(methyl methacrylate)/poly(ethylene oxide) (PMMA/PEO) is by far the most studied [13, 35–43] miscible blend because (1) it remains miscible over the whole composition range (provided that PEO stays in the melt state) and (2) of the very large difference between the component glass temperatures ($\Delta T_g \sim 180$ K) that effectively exemplifies the dynamic heterogeneity. Herein [44], pressure provides an additional critical test of the self-concentration (LM) model. According to the LM model, the origin of the distinctly different component dynamics in miscible blends

is the intramolecular connectivity that biases the local concentration to values away from the average blend composition. As already mentioned, LM proposed that the relevant length scale for evaluating the self-concentration is of the order of the Kuhn segment, l_K. As such the length scale is polymer specific, independent of blend composition, and only weakly dependent on the other thermodynamic variables of temperature (T) and pressure (P). Given the small variation of the Kuhn length and of the corresponding self-concentration with pressure, it is possible to investigate whether the PMMA segmental dynamics in the blends can be described equally well at atmospheric and elevated pressures. A strong pressure dependence would be against the predictions of the LM model.

To this end, we need to mention that the liquid-to-glass transition in PMMA is driven mainly by intramolecular effects ($Q_V/Q_P \sim 0.7$ at $T = T_g$ and at $P = 0.1$ MPa) [44]. Therefore, it suffices, to a good approximation, to employ only such effects in discussing the PMMA segmental dynamics in its blends with PEO. The model that has these ingredients, i.e., intramolecular effects and non-diverging length scales, is the LM model. In Fig. 5.5, we plot the measured glass temperatures from DSC and DS (defined at $\tau \sim 1$ s) for the PMMA and PEO components as a function of PMMA composition (φ_{PMMA}) [M_w(PMMA) = 21,400 g/mol, M_w(PEO) = 17,300 g/mol]. The thick solid line is the prediction of the Fox equation, whereas the corresponding model predictions using (5.6) for the PMMA and PEO glass temperatures are shown, respectively, with the thinner solid lines. In the calculation we have used, $C_\infty = 9$, $M_0 = 0.100$ kg/mol, $k = 2$, $\rho = 1.130$ kg/m^3, and $l_K = 1.38$ nm, resulting in $\varphi_S = 0.25$ for PMMA, and $C_\infty = 5.5$, $M_0 = 0.044$ kg/mol, $k = 2$, $\rho = 1.212$ kg/m^3, $l_K = 0.81$ nm, and $\varphi_S = 0.21$ for PEO. Clearly, the self-concentration model predictions for the PMMA segmental dynamics in the blends provide an adequate description of the experimental data without using any adjustable parameter. On the contrary, the model predictions fail for PEO, but this is due to the PEO crystallization in the PEO-rich blends that locally enriches the PEO component and drives the system to phase separation. Therefore, in the remaining, we discuss the PMMA segmental dynamics by focusing in the temperature range where the system is in a thermodynamically mixed state.

With respect to Fig. 5.5, the model predictions were tested for the dynamic (DS) T_g, at a single relaxation time of approximately 1 s. Subsequently, in Fig. 5.6, we test the model predictions for the PMMA segmental dynamics against the full $\tau(T)$ dependence at 0.1 MPa. In the figure only the α-process is shown that has been deconvoluted from the faster (and more intense) β-process of PMMA. The two Arrhenius relaxation maps display the same relaxation times for the PMMA and PEO homopolymers and four PMMA/PEO blends rich in PMMA against the LM model predictions using the theoretical Kuhn length ($l_K = 1.38$ nm) or the adjustable length ($l_K = 1.62$ nm). In doing so, we have used the following VFT parameters: $B = 1056$ K, $\tau_0 = 8 \times 10^{-12}$ s, and $T_0 = 358$ K for PMMA, and $B = 3570$ K, $\tau_0 = 1 \times 10^{-14}$ s, and $T_0 = 115$ K for PEO. For the PMMA segmental dynamics in the blends, we have further assumed

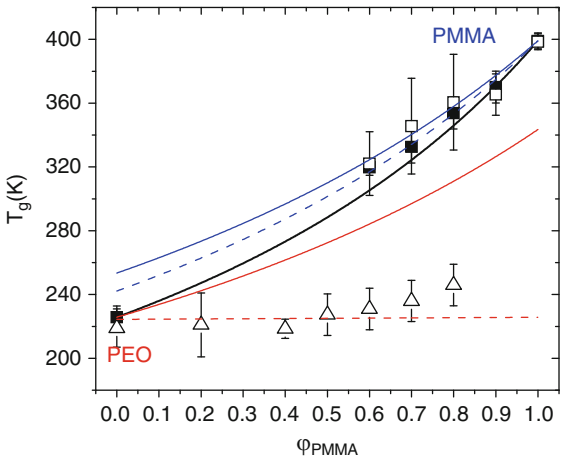

Fig. 5.5 Glass temperatures obtained from DSC (*open symbols*) and DS (*filled symbols*) plotted as a function of PMMA concentration. The PMMA and PEO glass temperatures are indicated with *squares* and *triangles*, respectively. The *black line* is the prediction of the Fox equation. The predictions of the self-concentration model for the PMMA ($l_K = 1.38$ nm) and PEO ($l_K = 0.81$ nm) segmental dynamics are given by the *solid lines*. The *dashed line* for the high T_g component (PMMA) is the result of a fit to the DS data through the self-concentration model but now using l_K as a free parameter ($l_K^* = 1.62$ nm). The *dashed line* for the low T_g component (PEO) indicated a $l_K^* = 0.48$ nm corresponding to $\varphi_s = 1$. From [44]

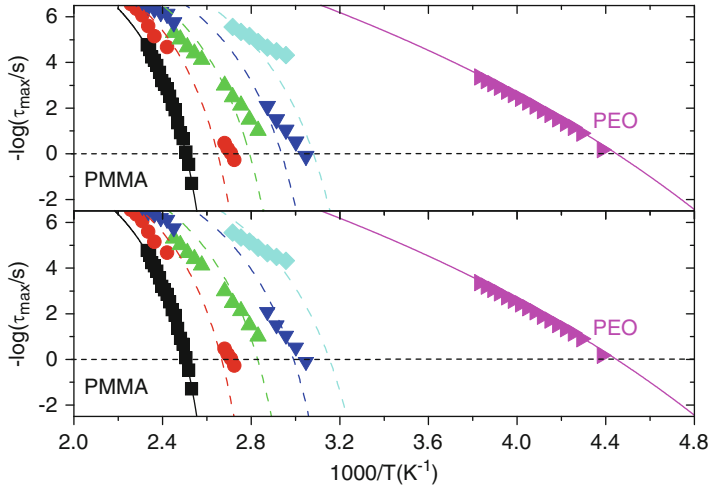

Fig. 5.6 Arrhenius relaxation map of the segmental dynamics in the homopolymers [(*squares*): PMMA, (*right triangles*): PEO] and the PMMA/PEO blends with $\varphi_{PMMA} = 0.9$ (*circles*), $\varphi_{PMMA} = 0.8$ (*up triangles*), $\varphi_{PMMA} = 0.7$ (*down triangles*) and $\varphi_{PMMA} = 0.6$ (*rhombus*). The *solid lines* represent VFT fits to the homopolymer relaxation times. The *dashed lines* are also VFT fits to the PMMA dynamics in the PMMA/PEO blends using the self-concentration model either with the theoretical l_K (=1.38 nm) (*top*) or the adjustable l_K (=1.62 nm) (*bottom*). The *horizontal dashed lines* correspond to a segmental relaxation time of $\tau \sim 1$ s. From [44]

$$\tau_{\mathrm{i}}(\varphi_{\mathrm{eff}}, T) = \tau_{0,\mathrm{i}} \exp\left(\frac{B_{\mathrm{i}}}{T - T_{0,\mathrm{i}}(\varphi_{\mathrm{eff}})}\right) \tag{5.8}$$

with identical B_i and $\tau_{0,\mathrm{i}}$ parameters as for bulk PMMA (and PEO), where only the ideal glass temperature varies with composition, and

$$T_{0,\mathrm{i}}(\varphi_{\mathrm{eff}}) = T_{0,\mathrm{i}} + \left[T_{\mathrm{g,i}}(\varphi_{\mathrm{eff}}) - T_{\mathrm{g,i}}\right] \tag{5.9}$$

where $T_{0,\mathrm{i}}$ is the ideal glass temperature for homopolymers A or B, and $T_{0,\mathrm{i}}(\varphi_{\mathrm{eff}})$ is the ideal glass temperature for each component in the blends. Clearly, the model predictions with the above approximations are in sufficient agreement with the experimental $\tau(T)$ and this agreement improves in the case of the adjustable l_{K} (=1.38 nm) (full quantitative agreement requires treating B_{i} and $\tau_{0,\mathrm{i}}$ as adjustable parameters). As expected, the agreement further improves by allowing l_{K} to adjust for each blend composition. Thus the self-concentration model adequately describes the PMMA segmental dynamics in the PMMA/PEO blends rich in PMMA.

Next, the model predictions are tested at elevated pressures as follows: from the $\tau(T)$ and $\tau(P)$ dependences, we can extract the pressure dependence of the glass temperature (defined at $\tau \sim 1$ s). This is shown in Fig. 5.7 for bulk PMMA and the blends rich in PMMA.

Both isothermal and isobaric data are included as well as the *PVT* literature data for PMMA and two PMMA/PEO blends with $\varphi_{\mathrm{PMMA}} = 0.9$ and 0.8. There is an excellent agreement of the $T_{\mathrm{g}}(P)$ dependences as obtained from the literature *PVT* [45] and DS. The $T_{\mathrm{g}}(P)$ dependence can be parameterized according to (1.17). The extracted initial slopes (at $P = 0.1$ MPa) assume the following values for PMMA and the blends with $\varphi_{\mathrm{PMMA}} = 0.9$, 0.8, and 0.7; $(\mathrm{d}T_{\mathrm{g}}/\mathrm{d}P)_{P\to 0} = 0.22$, 0.29, 0.26,

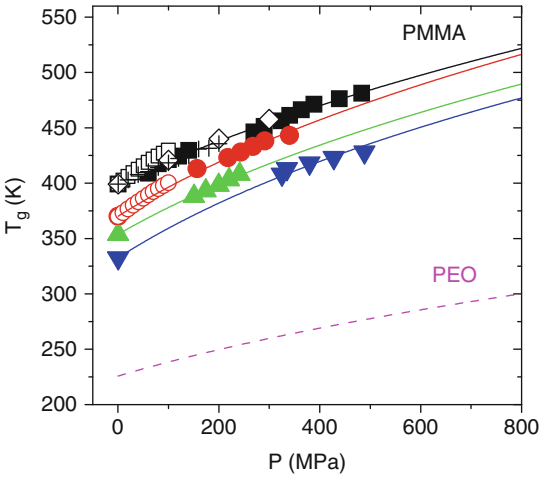

Fig. 5.7 Pressure dependence of the glass temperature T_{g} of the PMMA homopolymer (*black symbols*) and the blends with $\varphi_{\mathrm{PMMA}} = 0.9$ (*circles*), $\varphi_{\mathrm{PMMA}} = 0.8$ (*up triangles*), and $\varphi_{\mathrm{PMMA}} = 0.7$ (*down triangles*). The *filled triangles* are from DS. The *open squares*, *open circles*, and *crosses* are the results from *PVT* measurements. The *open rhombus* are DS results from [45]. The *lines* are fits to (1.17). From [44]

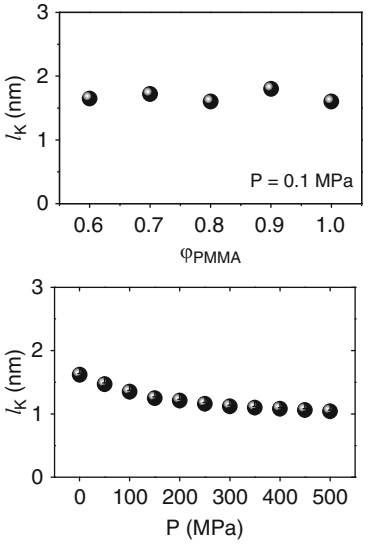

Fig. 5.8 Composition dependence of l_K at $P = 0.1$ MPa (*top*) and pressure dependence of l_K extracted from the PMMA segmental dynamics in the PMMA-rich blends, according to the predictions of the LM model (*bottom*). From [44]

and 0.29 K/MPa, respectively. Notice that the pressure coefficients of T_g are similar in blends rich in PMMA.

The dependence of the characteristic length scale on (1) the blend composition, extracted from the $\tau(T)$ dependences at 0.1 MPa (Fig. 5.6), and (2) on pressure, extracted from the $T_g(\varphi_{PMMA})$ dependence at elevated pressures (Fig. 5.7), are depicted in Fig. 5.8. The figure displays a weak dependence of the Kuhn length on blend composition, as expected by the LM model, and a weak dependence on pressure, for pressures up to 500 MPa. The latter is also anticipated; increasing pressure should result in the shrinkage of all length scales (density effect). Thus practically, the same length that was used to describe the PMMA segmental dynamics in the blends at atmospheric pressure can be used to describe the same process at elevated pressures. This constitutes a test of the validity of the self-concentration model as proposed by LM at elevated pressures.

5.2.2 *Miscible But Not Athermal Polymer Blends (PS/PMPS, PS/PVME, and PCHMA/PaMS)*

A general remark for such blends, where one of the components has nearly zero dipole moment, is that the dielectric response is dominated by the second component. As we will see below, this gives rise to the observation of the dielectrically active component in different environments.

5.2.2.1 PS/PMPS

An example of a miscible blend that exhibits a UCST behavior and has a large dynamic asymmetry ($\Delta T_g \sim 113$ K at $P = 0.1$ MPa) is the polystyrene/poly(methyl phenyl siloxane) (PS/PMPS) system. The miscibility and segmental dynamics have been investigated at atmospheric pressure and depending on the molecular weight, they were found to exhibit dynamic heterogeneity [46, 47]. This system has a complication in that the glass temperature, T_g, of the hard phase (PS) interferes with the demixing process, thus giving rise to pinning of the domain structure at a certain stage. Figure 5.9 provides with the theoretical prediction for the Gibbs free energy of mixing (ΔG_{mix}) as a function of composition [at atmospheric pressure (0.1 MPa)] for the $PS_{28}/PMPS_{17}$ blend according to the lattice-based theory of Lipson et al. [48]. The predicted curve shows two points of inflection, indicating the presence of two phases. Shown in the insets of Fig. 5.9 are ΔV_{mix} and ΔH_{mix} as a function of composition at a temperature of 260 K and atmospheric pressure. As expected for UCST-type blends, ΔH_{mix} is positive, and the lattice-based theory by Lipson et al. further predicts a positive ΔV_{mix} ($\Delta V_{mix}/V \approx 1.1 \times 10^{-4}$ at $\varphi_{PS} = 0.5$).

The complete theoretical phase diagram for the $PS_{28}/PMPS_{17}$ blend at $P = 0.1$ MPa is shown in Fig. 5.10. The phase boundary terminates at a predicted UCST of 309 K, and thus, the theory predicts two-phase behavior below 309 K. A direct visualization of the process of phase separation in a higher molecular weight but symmetric $PS_{120}/PMPS_{15}$ blend is provided by fluorescence spectroscopy in Fig. 5.11. In this blend, PS if fluorescently labeled and appears green whereas PMPS domains are dark. The effect of annealing at temperatures above the critical temperature on the phase separation process is to produce large spherical dark (PMPS) domains that are surrounded by a majority of PS-labeled chains. There is a strong effect of annealing on the size of the spherical domains. Furthermore,

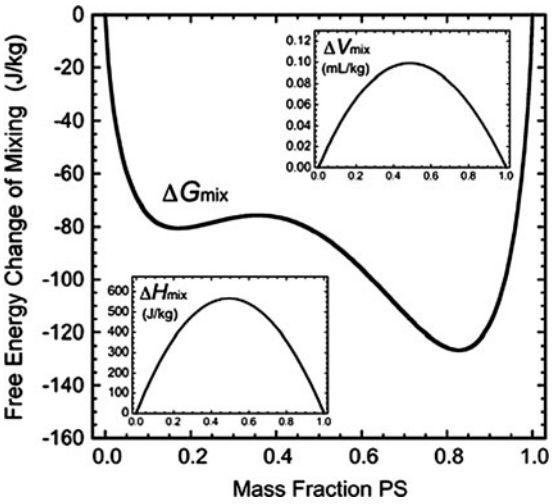

Fig. 5.9 Model predictions for the thermodynamic mixing functions at 260 K and atmospheric pressure. Given here is the Gibbs free energy of mixing (ΔG_{mix}) as a function of composition for the $PS_{28}/PMPS_{17}$ system. Included in the insets are the corresponding enthalpy and volume changes on mixing (ΔH_{mix} and ΔV_{mix}). From [48]

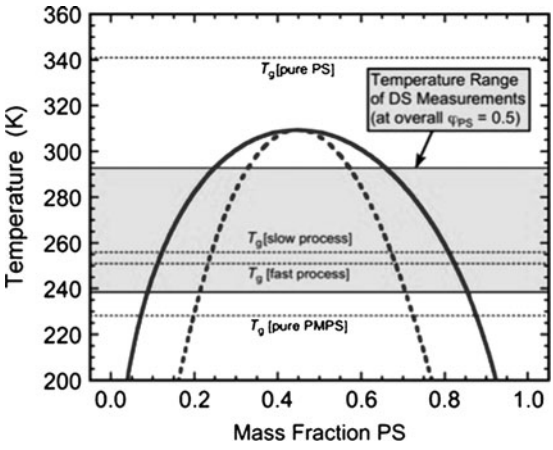

Fig. 5.10 Predicted phase diagram for $PS_{28}/PMPS_{17}$ at atmospheric pressure. Given are the binodal (*solid*) and spinodal (*dashed*) curves. The *shaded* region indicates the temperature range of the DS measurements (all performed at a single overall blend composition of $\varphi_{PS} = 0.5$). Also marked (by *dashed lines*) are the glass temperatures (defined by $\tau = 1$ s) for the fast and slow processes as well as those for pure PS and PMPS. From [48]

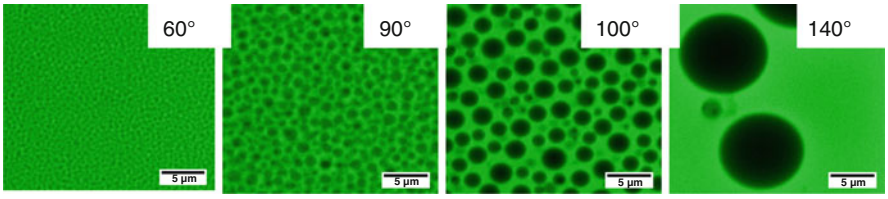

Fig. 5.11 Fluorescence correlation spectroscopy images showing the effect of annealing on the phase separation of a $PS_{120}/PMPS_{15}$ blend. In this blend, the PS is fluorescently labeled and appears *green*. Notice that annealing at higher temperatures gives rise to large dark spherical domains (PMPS) that are surrounded by the majority of PS segments. Unpublished, by courtesy of Dr. K. Koynov (MPIP, Mainz)

fluorescence correlation spectroscopy allows investigating the PS dynamics in the PS-rich phase, at the phase boundaries and even within the PMPS-rich phase.

The segmental dynamics of the $PS_{28}/PMPS_{17}$ blend that was studied theoretically at atmospheric pressure (Fig. 5.10) can now be compared with the results of the segmental dynamics from dielectric spectroscopy that are shown in Fig. 5.12. The figure depicts the "slow" and "fast" relaxation times as a function of temperature together with the homopolymer segmental dynamics. All relaxation times display the usual VFT temperature dependence.

As can be seen, the "slower" process in the blend approaches the faster one with decreasing temperature. This $\tau(T)$ for the slower process is peculiar and is uncommon for miscible polymer blends, as we will see below. In addition, below about 255 K, the dielectric strength of the faster processes is dramatically reduced and the associated dynamics become weakly dependent on temperature. The latter may reflect the confinement effects on the faster process by the slower moving species (see the discussion below with respect to the polystyrene/poly(vinyl methyl ether) [PS/PVME] blend).

We further propose at this point that the "slow" and "fast" processes in the blend reflect the PMPS segmental dynamics in PS-rich and PMPS-rich domains. There

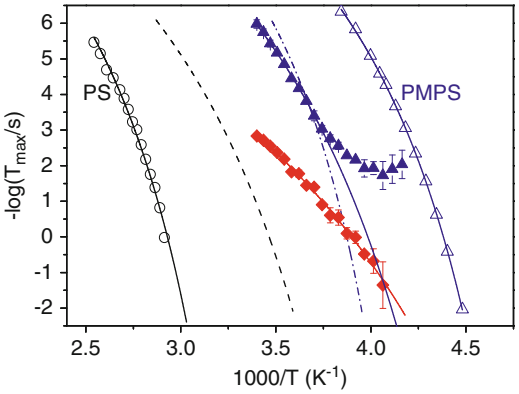

Fig. 5.12 Arrhenius relaxation map of the relaxation processes in the $PS_{28}/PMPS_{17}$ blend and the corresponding homopolymers (*open symbols*), (*circles*): PS, (*triangles*): PMPS, (*filled rhombus*): "slow" process in the blend, (*filled triangles*): "fast" process in the blend. *Solid lines* are fits to the VFT equation. *Dashed* and *dash-dotted lines* are the predictions of the LM model for the PS and PMPS segmental dynamics in the blend. From [48]

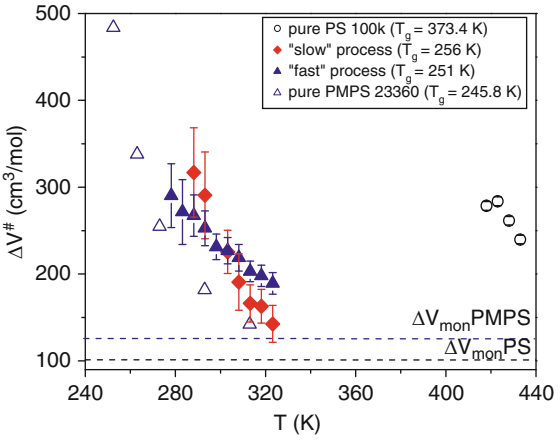

Fig. 5.13 Apparent activation volume, $\Delta V^{\#}$, for the "fast" (*filled triangles*) and "slow" (*filled rhombus*) processes in the $PS_{28}/PMPS_{17}$ blend compared to PMPS homopolymer (*open triangles*) and PS homopolymer (*open circles*). Notice the proximity of the values for the "slow" and "fast" processes to the bulk PMPS values. *Dashed horizontal lines* give the monomer volumes of PMPS (*blue*) and PS (*black*). From [48]

are experiments that can test this hypothesis. One such experiment is the application of pressure and is based on the different pressure sensitivity of the segmental relaxations of different polymers. The pressure sensitivity can be parameterized through the apparent activation volume (defined as $\Delta V^{\#} = RT(\partial \ln\tau/\partial P)_T$). Figure 5.13 gives the calculated apparent activation volumes corresponding to the "slow" and "fast" modes in the $PS_{28}/PMPS_{17}$ blend. The effect of pressure is to slow down the segmental dynamics through densification, but the extent of this effect depends largely on the temperature and the polymer involved. As can be seen in Fig. 5.13, both the "slow" and "fast" processes have $\Delta V^{\#}$ values in the vicinity of bulk PMPS (open triangles), thus confirming the assignment as reflecting PMPS segmental relaxations (in PS- and PMPS-rich domains).

A second experiment is through the pressure sensitivity of the glass temperature. In Fig. 5.14 the $T_g(P)$ dependences of the "slow" and "fast" components in the blend are compared with the respective homopolymers. In the same plot, we include the model prediction for $T_c(P)$, which will be discussed latter. The $T_g(P)$ again can be described according to the empirical equation (1.18). Notice the similar $T_g(P)$ dependence for the two modes in the blend, as with the bulk PMPS, that can be distinguished from the steeper $T_g(P)$ dependence of bulk PS (also included in the figure). This is also shown by the proximity of the pressure coefficients of the "fast" process to the PMPS homopolymer value.

These experimental results as a function of pressure have been tested in the same $PS_{28}/PMPS_{17}$ blend using modeling calculations by Lipson et al. [48]. The theoretically calculated phase diagram at elevated pressures shows phase separation in the range of the experimental conditions. The general trends in ΔV_{mix} and ΔH_{mix} are similar at the critical temperature (see Fig. 5.9) and thus (5.2) indicates that the UCST should increase with pressure. The model predictions for the UCST as a function of pressure are included in Fig. 5.14 with a solid line. As can be seen, the critical temperature increases (by ~11 K) upon increasing the pressure to 250 MPa (from 309 K to 320 K). The model calculations confirm that the $PS_{28}/PMPS_{17}$ system is phase separated over nearly the entire range of the DS measurements at elevated pressures. Based on the different pressure sensitivities of the critical and glass temperatures, we can further predict the pressure at which the system becomes thermodynamically homogeneous. From $dT_c/dP \sim 0.07$ K/MPa, the prediction is that the blend will become thermodynamically homogeneous above about

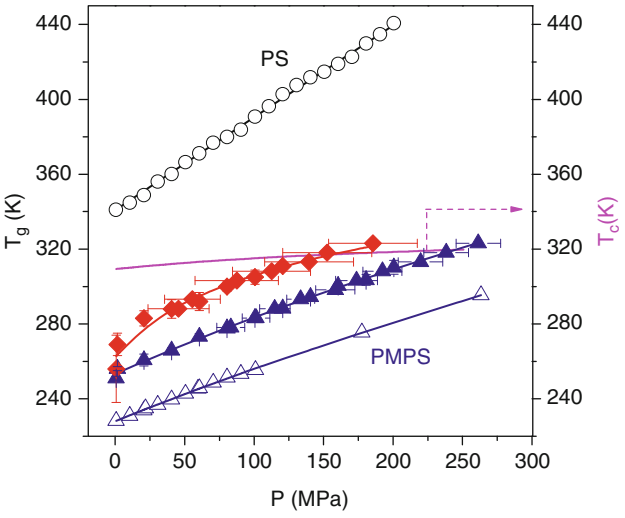

Fig. 5.14 Pressure dependence of T_g (defined at $\tau \sim 1$ s) for the "fast" (*filled triangles*) and the "slow" (*filled rhombus*) processes in the $PS_{28}/PMPS_{17}$ blend and of the PMPS (*open triangles*) and PS (*open circles*) homopolymers. Notice the proximity of the two T_g's at all pressures investigated. The *solid line* (*magenta*) is the $T_c(P)$ theoretical prediction. From [48]

250–300 MPa (i.e., within a range that is in the limit of our experimental window). Nevertheless, the model predictions confirmed the presence of phase-separated domains in the $PS_{28}/PMPS_{17}$ blend that allows understanding the peculiar dynamics (Fig. 5.12) in terms of PMPS segmental relaxation in two different environments.

5.2.2.2 PS/PVME

The issue of dynamic heterogeneity has been investigated in the polystyrene/poly(vinyl methyl ether) (PS/PVME) blend as a function of pressure by several groups [1, 49–52]. The system, as with the PS/PMPS blend, has only one dielectrically active component (PVME), and the asymmetric broadening of the dielectric loss peak at different compositions and at atmospheric pressure has been discussed in terms of the model of concentration fluctuations [22]. Furthermore, the first dielectric investigation of this blend at elevated pressures [1] identified the main loss peak as reflecting solely the PVME characteristics (i.e., the very asymmetric peak had practically the same activation volume as the PVME homopolymer). A more recent investigation [50] revealed some interesting new features for the PS/PVME blend. It was shown that the temperature–pressure superposition applies not only to the pure PVME but also to the PVME dynamics in the blends. This is depicted in Fig. 5.15, where dielectric loss spectra are plotted for different T, P conditions that lead to isochronal conditions. As with homopolymers, the position of the dielectric loss peak is solely responsible for the breadth of the peak, at least for the 25/25 and 50/50 PS/PVME blend compositions. This finding is in agreement with the earlier study [1] that suggested the same behavior of the peak in the blends with the PVME homopolymer.

In the same study [50], the confinement effects of the low T_g component, due to the rigid matrix of the high T_g component, were investigated. Such confinement results were very evident for the 75/25 PS/PVME blend composition. The respective relaxation times for different pressures for this blend composition are shown in Fig. 5.16. As can be seen, the experimental points at each pressure depart from the high-temperature VFT behavior and gradually change to an Arrhenius temperature dependence by decreasing temperature. The diagonal dotted lines in the figure indicate the temperature range where the PVME dynamics in the blend start to deviate from the VFT behavior. This effect has been discussed [50] in terms of the fact that below the T_g of the blend, the system is practically away from equilibrium and the low T_g component becomes confined by the rigid matrix formed by the high T_g component.

In the same study [50], the concept of thermodynamic scaling (see Section 2.1) was studied for the different blend compositions. It was shown that the thermodynamic scaling fails if data from a broad range of temperatures and pressures are employed, and this is especially the case for the 75/25 PS/PVME blend. One important problem emerges, however, in using the thermodynamic scaling for the dynamics of one component in the blends. The volume V as used in the scaling is

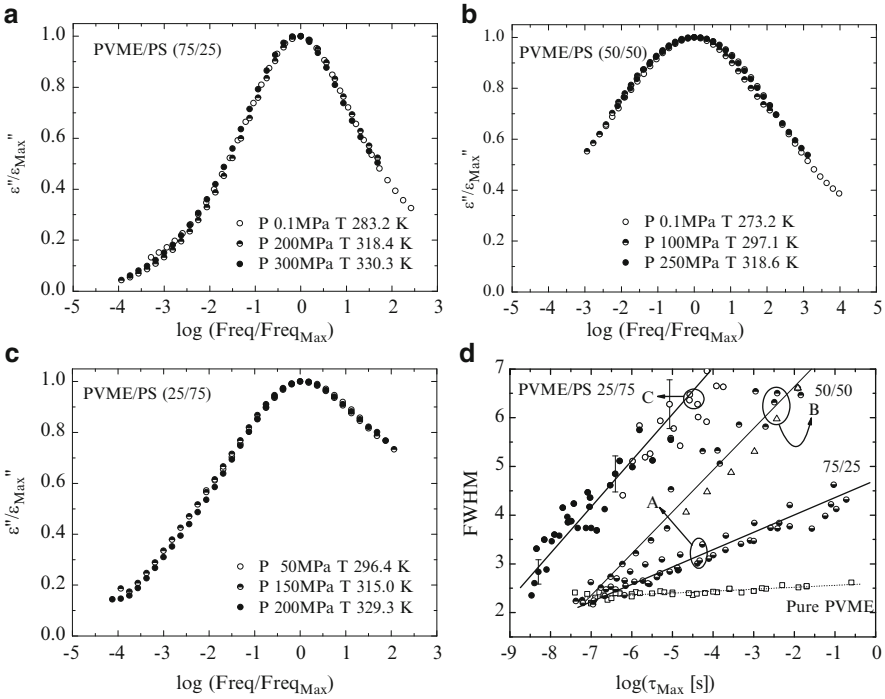

Fig. 5.15 Temperature–pressure superposition of the dielectric loss spectra in PS/PVME blends with 25/75, 50/50, and 75/25 composition. *Open squares* are data for pure PVME. There is a good overlap, at least for the 25/75 and 50/50 blends, meaning that once the peak frequency is known, the distribution of relaxation times is also fixed to its atmospheric pressure curve. From [50]

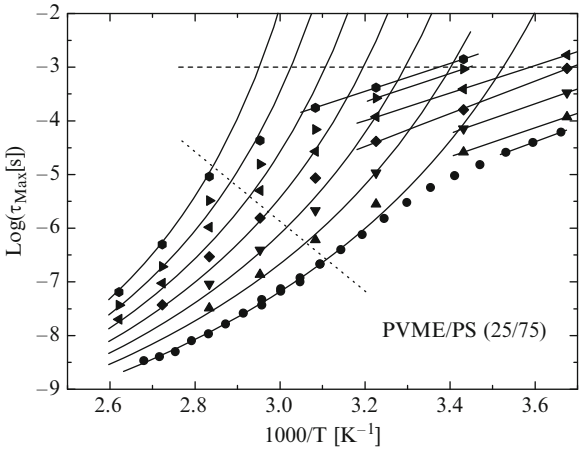

Fig. 5.16 Relaxation times plotted vs. inverse temperature plotted at different pressures for a PS/PVME (75/25) blend. The *diagonal dotted lines* refer to the temperature below which the high T_g component is out of equilibrium and hence confinement effects appear. From [50]

taken from *PVT* measurements of the blend; however, the dynamics as probed by DS reflect the segmental motion of the more polar component (PVME). Thus it is not clear which volume should be used in the thermodynamic scaling.

The same authors employed [50] the Adam–Gibbs (AG) theory together with the chain connectivity model to describe the PS/PVME dynamics at elevated pressures. The work is an extension of the AG theory to describe the component segmental dynamics in miscible blends [29] but now at elevated pressures. Starting from the AG equation (3.6), it assumes the same form for the segmental relaxation time for the A component in the blend

$$\tau^{\mathrm{A/blend}}(T,P) = \tau_0 \exp\left[\frac{C^{\mathrm{A/blend}}(T,P)}{TS_{\mathrm{ex}}^{\mathrm{A/blend}}(T,P)}\right]. \tag{5.10}$$

Here, $C^{\mathrm{A/blend}}$ is a material constant and $S_{\mathrm{ex}}^{\mathrm{A/blend}}$ is the excess entropy that refer to regions centered around a segment of polymer A, and are calculated as

$$\begin{aligned} S_{\mathrm{ex}}^{\mathrm{A/blend}}(T,P) &= \phi_{\mathrm{eff}}^{\mathrm{A}} S_{\mathrm{ex}}^{\mathrm{A}}(T,P) + (1-\phi_{\mathrm{eff}}^{\mathrm{A}}) S_{\mathrm{ex}}^{\mathrm{B}}(T,P) \\ C^{\mathrm{A/blend}}(T,P) &= \phi_{\mathrm{eff}}^{\mathrm{A}} C^{\mathrm{A}} + (1-\phi_{\mathrm{eff}}^{\mathrm{A}}) C^{\mathrm{B}}, \end{aligned} \tag{5.11}$$

where $S_{\mathrm{ex}}^{\mathrm{A}}(T, P)$ and $S_{\mathrm{ex}}^{\mathrm{B}}(T, P)$ are the excess entropy as a function of pressure and temperature for the neat homopolymers. Clearly, these expressions are only valid for athermal mixtures. In (5.11), ϕ_{eff} is the effective concentration defined by (5.4) with the self-concentration defined as

$$\phi_{\mathrm{s}}^{\mathrm{A/blend}} = \frac{3 l_{\mathrm{K}} l_{\mathrm{p}}}{2\pi[\alpha(P)]^2}\left[S_{\mathrm{ex}}^{\mathrm{A/blend}}(T,P)\right]^{2/3}, \tag{5.12}$$

where l_{K} and l_{p} are the Kuhn and packing lengths, respectively, and α is a proportionality constant between the radius r_{c} of the relevant volume centered in a given monomer and occupied by the polymer chain of such a monomer as

$$r_{\mathrm{c}} = \alpha S_{\mathrm{ex}}^{-1/3}. \tag{5.13}$$

The model predictions for the segmental relaxation times in the PS/PVME 50/50 blend are shown in Fig. 5.17 as a function of temperature. As can be seen, the model describes the blend relaxation times reasonably well for the different pressures. The model predictions for the CRR in the same blend (50/50) are plotted in Fig. 5.18. It can be seen that the size of CRR is of the order of 1 nm. There is a small but systematic increase in the temperature sensitivity of the size of CRR with increasing pressure that may reflect the differences of the monomeric volume of the two homopolymers [53].

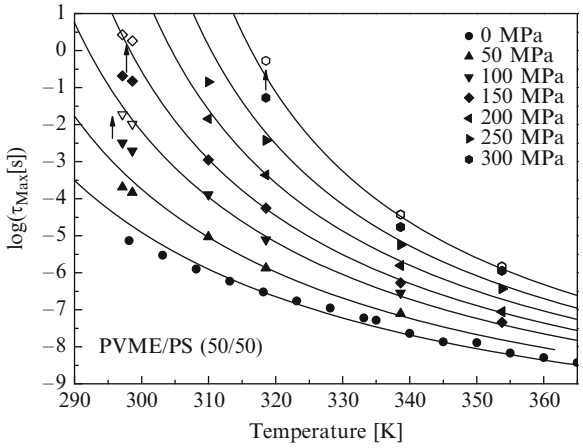

Fig. 5.17 PVME relaxation times plotted a function of temperature at different pressures for the PS/PVMS 50/50 blend. *The solid lines* are fits to the experimental data using the AG model together with the chain connectivity concept. From [50]

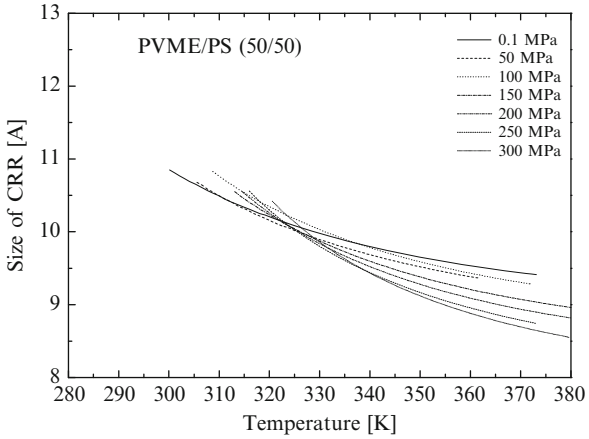

Fig. 5.18 Diameter of the relevant volume for the segmental relaxation plotted as a function of temperature at different pressures as indicated, for PVME in PS/PVMD 50/50 blend. From [50]

5.2.2.3 PCHMA/PaMS

Poly(cyclohexyl methacrylate) and poly(α-methyl styrene) (PCHMA/PaMS) form thermodynamically miscible blends, with their lower critical temperature exceeding 560 K. The dynamic asymmetry is very small ($\Delta T_g \sim 7$ K), and practically only PCHMA is dielectrically active in the copolymers. Dielectric relaxation experiments revealed [52] an anomaly in the dynamics and glass temperatures in the blend; PCHMA in the blend has a higher T_g, despite the fact that the other component (PαMS) has a lower T_g. This practically means that in the LM self-concentration

model, the Fox equation (5.7) needs to be replaced by the Brekner equation for the composition dependence of T_g [52]. Following this procedure, the LM model resulted in a PCHMA self-concentration of 0.2. In addition, the thermodynamic scaling was found to result in a higher volume exponent (γ) for PCHMA in the blend, compared to the copolymer, despite the fact that the blend dielectric activity originates practically from PCHMA. An open question here, as with the PS/PVME blend, remains the use of the copolymer volume V in the thermodynamic scaling for a blend process that reflects mainly the PCHMA dynamics.

5.2.3 *Polymer Blends with Strong Specific Interactions*

A way to compatibilize polymer blends is through specific interactions that not only bring about thermodynamic miscibility but also effectively couple the components' dynamics. Recently, the component dynamics have been investigated in hydrogen-bonded blends composed of poly(4-vinylphenol) (PVPh) [54] as one component and poly(ethylene-co-vinylacetate) (EVA) [55] or poly(vinyl ethyl ether) (PVEE) as the second component. In these systems, the ability of intermolecular hydrogen bonding between the hydroxyl groups of PVPh and the carbonyl groups of EVA or the ether oxygen atoms in PVEE resulted in the coupling of the components' segmental dynamics, and this despite the extreme dynamic asymmetry based on the difference in the glass transition temperatures (ΔT_g of 173 K and 186 K for the PVPh/EVA and PVPh/PVEE, respectively). Nevertheless, the coupling of the components' dynamics is not perfect. Two dielectrically active processes were found for some compositions, called "fast" and "slow," reflecting, respectively, the dynamics of the unassociated (or "free") PVEE segments and the intermolecular hydrogen-bonded PVPh and PVEE segments.

Herein we review the more pertinent results of pressure in the PVPH/PVEE blends [53]. In the PVEE-rich blends, increasing temperature and pressure results in the broadening of the distribution of relaxation times through the weakening of hydrogen bonds and the associated decoupling of the segmental dynamics. In Fig. 5.19, the dielectric loss curves of the PVPh/PVEE (10/90) blend recorded at different T, P combinations are compared under different isokinetic conditions (the blend data have been slightly shifted vertically to match the ε''_{max} values, but not horizontally). The data show an increasing slope in the high-frequency side at $T > 294$ K. This finding suggests increasing strength of the faster α-process corresponding to PVEE segmental relaxation at the expense of the slower α-process corresponding to hydrogen-bonded PVPh and PVEE segments. Thus the raw data suggest increasing heterogeneity above 294 K, which is proposed to arise from the presence of an LCST near 294 K [54]. At and below 294 K, the relaxation time distributions do not change at different isokinetic T, P combinations.

Overall, the effect of increasing temperature and pressure in the PVPH/PVEE blends is to broaden the distribution of relaxation times through the weakening of hydrogen bonds and the associated decoupling of the segmental dynamics. The strong

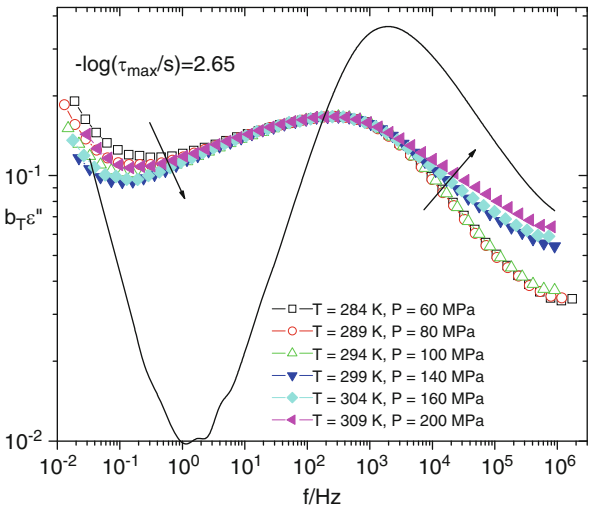

Fig. 5.19 Comparison of some isokinetic (T, P) sets of dielectric loss curves for the PVPh/PVEE (10/90) blend. The *solid lines* give the PVEE dielectric loss curves at $T = 299.15$ K, $P = 140$ MPa (for $-\log(\tau_{max}/s) = 2.65$). From [54]

effect of pressure on the dynamic heterogeneity can be discussed in terms of the specific requirements of hydrogen-bonded segments. Hydrogen bonds require a certain distance and directionality and these are perturbed by pressure, giving rise to the observed dynamic heterogeneity. Further examples of the hydrogen-bonded blends are expected to shed more light on the effect of pressure.

5.3 Effect of Pressure on Nanophase Separated Copolymers

Block copolymers with their well-controlled nanometer size nanodomains can be employed for studying the effect of confinement on the thermodynamic and dynamics properties of crystallizable and amorphous blocks [56]. The type of confinement here is "soft" in the sense that the confining medium is the same component forming the block structure. In addition, pressure can influence the dynamics of the different components within the nanodomains. Here we review two such cases: the first case is a copolymer formed by two structurally similar polymers [57]. This system has the advantage that the dynamic changes can be more easily discussed in terms of the structural differences of the two components. The second system is composed of one crystallizable and one amorphous component [58]. It is of interest here to examine how pressure affects the crystallization and glass temperatures. In this latter case, one can design cases where crystallization may take place within a "soft" or a "hard" matrix and this can be influenced by pressure.

5.3.1 *PMVE*-b-*PiBVE*

Studying structurally similar polymers have the advantage that the dynamic changes can be more easily discussed in terms of the structural differences of the two components. Copolymers and blends of the structurally similar PVME and poly (isobutyl vinyl ether) (PiBVE) have remarkable thermo-adjustable surfactant properties that originate from the LCST behavior of the PVME segments in an aqueous environment. The respective homopolymers are closely matched in their glass transition temperatures ($\Delta T_g \sim 7$ K) and can be considered as "dynamically symmetric" [57]. However, the application of pressure enhances the existing dynamic heterogeneity. As discussed below, the reason behind this is the distinctly different pressure sensitivities of the two homopolymers, as with the athermal mixture PI-*b*-PVE. In addition, we discuss the role of packing in the dynamic heterogeneity of polymer blends/copolymers.

At atmospheric pressure, all dielectric loss curves were bimodal, reflecting the PVME and PiBVE dynamics, but the intensity of the faster process (PVME) was higher in the blend at the expense of the slower (PiBVE) process. The higher intensity for the slower process in the copolymer may suggest that the mobility at the interface is controlled by the slower moving species (PiBVE).

The effect of pressure on the heterogeneous copolymer dynamics is spectracular; pressure enhances the dynamic asymmetry. This is shown in Fig. 5.20, where the dielectric loss curves for $PVME_{38}$-*b*-$PiBVE_{54}$ are examined under "isothermal" conditions by increasing pressure. The figure clearly depicts the increasing dynamic heterogeneity with increasing pressure. In some cases, it has been argued that

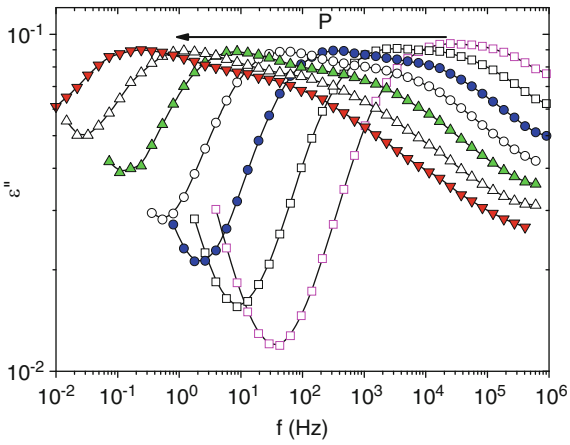

Fig. 5.20 Dielectric loss curves of the $PVME_{38}$-*b*-$PiBVE_{54}$ diblock copolymer at $T = 290$ K for different pressures: (*filled square*): $P = 0.1$ MPa, (*open square*): $P = 40$ MPa, (*filled circle*): $P = 80$ MPa, (*open circle*): $P = 120$ MPa, (*up-pointing filled triangle*): $P = 160$ MPa, (*up-pointing open triangle*): $P = 200$ MPa, (*down-pointing filled triangle*): $P = 240$ MPa. The *arrow* gives the direction of increasing pressure. Notice that pressure induces dynamic heterogeneity. From [57]

increasing pressure has the same effect as decreasing temperature. The present system provides a clear case where this notion is violated. For example, decreasing temperature could not enhance the dynamic asymmetry of the block segmental dynamics the way that increasing pressure does. The reason behind the pressure-induced dynamic asymmetry is the different packing properties of the two homopolymers. In this respect, the result from the analysis of the bimodal copolymer distribution with respect to the "isothermal" relaxation times, $\tau(P)$, revealed that the dynamic asymmetry is enhanced by increasing P, as shown by the different slopes for the "fast" and "slow" moving segments reflecting, respectively, the PVME and PiBVE segments. From the slopes of the respective "isotherms," the apparent activation volume for each component in the copolymer can be extracted and compared with the respective homopolymer.

The result of this comparison is shown in Fig. 5.21. There is a strong temperature dependence of the apparent activation volume for both homopolymers. Furthermore, at $T \sim T_g + 75$ ($T_g + 55$) this quantity is comparable to the PVME (PiBVE) monomer volumes. In addition, the "fast" and "slow" processes in the copolymer have an apparent activation volume that is very near to the respective homopolymers. Then the enhanced dynamic asymmetry in the copolymers reflects the disparity in the $\tau(P)$ dependencies of PVME and PiBVE homopolymers. PiBVE, with the longer side-chain and a low van der Waals peak at 6.3 nm^{-1} (with a corresponding inter-chain distance of ~1 nm, obtained from wide-angle X-ray scattering), is poorly packed as compared to PVME. The less efficient packing makes PiBVE more prone to pressure and explains its higher apparent activation volume.

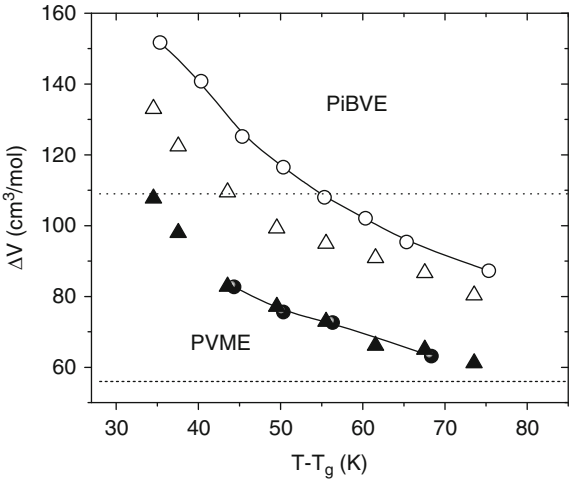

Fig. 5.21 T_g-scaled apparent activation volume for the PVME (*filled circle*) and PiBVE (*open circle*) homopolymers and for the "fast" (*filled triangle*) and "slow" (*open triangle*) processes in the $PVME_{38}$-*b*-$PiBVE_{54}$ diblock copolymer. The *dashed* and *dotted lines* give the respective monomer volumes. From [57]

Thus the homopolymer dynamic asymmetry drives the copolymer component dynamics to become more heterogeneous with the application of pressure. Again, the reason behind the enhanced dynamic asymmetry is a static property, i.e., local packing.

It is of interest now to compare these results for the more heterogeneous PVME-*b*-PiBVE copolymers with the athermal PI-*b*-PVE diblock copolymer bearing two dielectrically active components. In the latter system, the dynamic heterogeneity was reflected in the "fast" and "slow" processes reflecting the relaxation of the low T_g (PI) and high T_g (PVE) components, and pressure was found to induce dynamic homogeneity, i.e., opposite to that in PVME-*b*-PiBVE. In both cases, the reason behind this effect is the different pressure sensitivity of the two components. However, unlike the PVME-*b*-PiBVE case, where $\Delta V_{\text{fast}} < \Delta V_{\text{slow}}$, in PI-*b*-PVE, the fast-moving species (PI) possess the higher apparent activation volume, i.e., $\Delta V_{\text{fast}} > \Delta V_{\text{slow}}$; thus increasing pressure resulted in a more dynamically miscible blend.

These intriguing results require a theoretical input. Although both cases were explained in terms of the different pressure sensitivity of the respective homopolymers, it is not yet known how this pressure sensitivity relates to the magnitude of the glass temperature. In addition, it is not known how this pressure sensitivity (i.e., the apparent activation volume) is influenced by the thermodynamic state (i.e., the presence of weak phase separation as opposed to the thermodynamically mixed state).

5.3.2 *pODMA*-b-*ptBA*-b-*pODMA*

Nano-confined semi-crystalline–amorphous block copolymers provide with the advantage of allowing investigating the effect of pressure on both the crystallization and glass temperatures of the respective blocks. In this respect, a series of poly(*n*-octadecyl methacrylate)-*b*-poly(*tert*-butyl acrylate)-*b*-poly(*n*-octadecyl methacrylate) (pODMA-*b*-p*t*BA-*b*-pODMA) triblock copolymers were recently investigated [58] with dielectric spectroscopy, as a function of temperature and pressure. The main effects of confinement were found in the triblocks with the more antisymmetric compositions when the radius of gyration of the confined block was comparable to the cylinder radius (Fig. 5.22). It was found that the dynamics of the amorphous block accelerate upon confinement. On the contrary, confinement of the crystallizable block within cylindrical nanodomains results in the depression of the crystallization temperature. The investigation of the segmental dynamics in the pODMA-*b*-p*t*BA-*b*-pODMA triblock copolymers resulted in the true thermodynamic (*T*–*P*) phase diagram at each copolymer composition. It was shown that the glass temperature of the amorphous p*t*BA is consistently higher than the crystallization temperature of the crystallizable pODMA, at all temperatures and pressures investigated. Furthermore, for the initial pressure coefficients, $(dT_g/dP)_{P\to 0} > (dT_c/dP)_{P\to 0}$, and as a consequence, pODMA crystallization in the

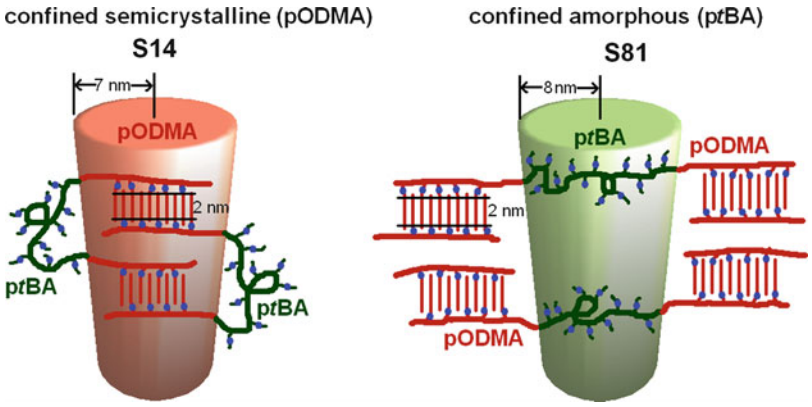

Fig. 5.22 (*Left*) Schematic representation of the two extreme cases; confinement of the crystallizable block (pODMA, *left*) within cylinders embedded within the glassy amorphous p*t*BA matrix, and (*right*) confinement of the amorphous block (p*t*BA) within cylinders embedded within the pODMA matrix. The *blue dots* represent the dipoles, situated on the side chains of both polymers. From [58]

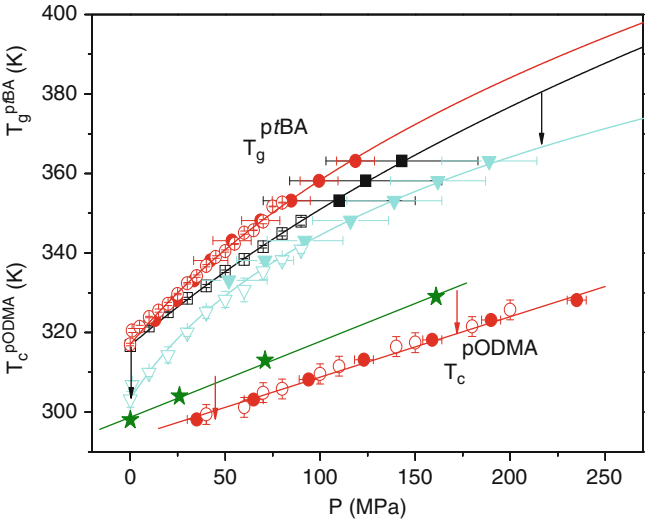

Fig. 5.23 The pressure dependence of the glass temperature of p*t*BA (T_g^{ptBA}) and of the crystallization temperature of pODMA (T_c^{pODMA}) in the different triblock copolymers: bulk p*t*BA (*squares*), S14, $f_{ODMA} = 0.14$ (*circles*), S81 (*down triangles*, $f_{ODMA} = 0.81$), pODMA (*stars*); *open* and *filled symbols* correspond to data obtained under "isobaric" and "isothermal" conditions, respectively. *The solid lines* represent the $T_g(P)$ fits and the $T_c(P)$ fits to the Clausius–Clapeyron equation, respectively. The effect of confinement, at the two extreme cases, is to decrease the T_g^{ptBA} by approximately 15 K (in S81), and to decrease the T_c^{pODMA} (in S14). From [58]

copolymers under elevated pressures takes place within a p*t*BA environment that is deeper into the glassy phase.

The two main effects of confinement in the triblocks with the more antisymmetric compositions are shown in the $T_g(P)$ and $T_c(P)$ representations in Fig. 5.23. Confinement of the pODMA block within the cylindrical domains results in the depression of the crystallization temperature. Confinement of the p*t*BA block within the cylindrical domains results in the speed up of the segmental dynamics and to a T_g depression at about 15 K. These results demonstrate that the well-controlled nanometer size nanodomains of block copolymers can be employed for studying the effect of confinement on the thermodynamic and dynamics properties of crystallizable and amorphous blocks. In addition, the different pressure sensitivity of the crystallization and glass temperatures can result in cases where crystallization takes place within a glassy or a fluid matrix. One main obstacle in the application of pressure in such nanophase separated systems is the lack of knowledge on how pressure is transmitted in the "hard" and "soft" nanophases. It was assumed above that pressure is evenly transmitted to both nanophases; however, this requires further investigations possibly by employing macroscopically oriented systems.

Acknowledgments George Floudas acknowledges the coworkers at the UoI who participated in this work (Dr. A. Gitsas and Dr. K. Mpoukouvalas) as well as Dr. K. Koynov for Fig. 5.11, Dr. G. Schwartz for sending original figures on the PS/PVME blend system and Prof. JEG Lipson and RP White for providing Figs 5.2, 5.9 and 5.10 as well as for several instructive comments on the lattice-based equation of state.

References

1. Floudas G (2002) In: Kremer F, Schönhals A (eds) Broadband dielectric spectroscopy. Springer, Berlin; Chapter 8
2. Roland CM, Hensel-Bielowka S, Paluch M, Casalini R (2005) Rep Prog Phys 68:1405
3. de Gennes P-G (1979) Scaling Concepts in Polymer Physics. Cornell University Press, Ithaca and London
4. Binder K (1994) Adv Polym Sci 112:181
5. Myers DB, Smith RA, Katz J, Scott RL (1966) J Phys Chem 70:3341
6. Lipson JEG, Tambasco M, Willets KA, Higgins JS (2003) Macromolecules 36:2977
7. Rabeony M, Lohse DJ, Garner RT, Han SJ, Graessley WW, Migler KB (1998) Macromolecules 31:6511
8. Janssen S, Schwahn D, Mortensen K, Spinger T (1993) Macromolecules 26:5587
9. Kumar SK (2000) Macromolecules 33:5285
10. Lipson JEG (1998) Macromol Theory Simul 7:263
11. Tambasco M, Lipson JEG, Higgins JS (2006) Macromolecules 39:4860
12. Wetton RE, MacKnight WJ, Fried JR, Karasz FE (1978) Macromolecules 11:158
13. Colby RH (1989) Polymer 30:1275
14. Roovers RH, Toporowski PM (1992) Macromolecules 25:1096
15. Chin YH, Zhang C, Wang P, Inglefield PT, Jones AA, Kambour RP, Bendler JT, White DM (1992) Macromolecules 25:3031
16. Roland CM, Ngai KL (1991) Macromolecules 24:2261

17. Pathak JA, Colby RH, Floudas G, Jerome R (1999) Macromolecules 32:2553
18. He Y, Lutz TR, Ediger MD (2003) J Chem Phys 119:9956
19. Krygier E, Lin G, Mendes J, Mukandela G, Azar D, Jones AA, Pathak JA, Colby RH, Kumar SK, Floudas G, Krishnamoutri R, Faust R (2005) Macromolecules 38:7721
20. Floudas G, Steffen W, Fischer EW, Brown W (1993) J Chem Phys 99:695
21. Floudas G, Fytas G, Brown WJ (1992) Chem Phys 96:2164
22. Zetsche A, Fischer EW (1994) Acta Polym 45:168
23. Lodge TP, McLeish TCB (2000) Macromolecules 33:5278
24. Chung G-C, Kornfield JA, Smith SD (1994) Macromolecules 27:964
25. Shenogin S, Kant R, Colby RH, Kumar SK (2007) Macromolecules 40:5767
26. Kant R, Kumar SK, Colby RH (2003) Macromolecules 36:10087
27. Kamath S, Colby RH, Kumar SK, Karatasos K, Floudas G, Fytas G, Roovers JEL (1999) J Chem Phys 111:6121
28. Kumar SK, Colby RH, Anastasiadis SH, Fytas G (1996) J Chem Phys 105:3777
29. Cangialosi D, Alegria A, Colmenero J (2006) Macromolecules 39:7149
30. Colby RH, Lipson JEG (2005) Macromolecules 38:4919
31. Liu W, Bedrov D, Kumar SK, Veytsman B, Colby RH (2009) Phys Rev Lett 103:037801–4
32. Lodge TP, Wood ER, Haley JC (2006) J Polym Sci B Polym Phys 44:756
33. Roland CM (1987) Macromolecules 20:2557
34. Floudas G, Fytas G, Reisinger T, Wegner G (1999) J Chem Phys 111:9129
35. Schmidt M, Maurer FH (1998) J Polym Sci B Polym Phys 36:1061
36. Zoller P, Walsh D (1995) Pressure–volume–temperature data for polymers. Technomic, Lancaster, PA
37. Fytas G, Kanetakis J, Floudas G, Wang CH (1990) Polym Commun 31:437
38. Maranas JK (2007) Curr Opin Colloid Interface Sci 12:29
39. Sakai VJ, Maranas JK, Chowdhuri Z, Peral I, Copley JRD (2005) J Polym Sci B Polym Phys 43:2914
40. Liu J, Sakai VJ, Maranas JK (2006) Macromolecules 39:2866
41. Genix A-C, Arbe A, Alvarez F, Colmenero J, Willner L, Richter D (2005) Phys Rev E 72:031808
42. Lutz TR, He Y, Ediger MD, Cao H, Lin G, Jones AA (2003) Macromolecules 36:1724
43. Haley JC, Lodge TP (2005) J Chem Phys 122:234914
44. Mpoukouvalas K, Floudas G (2008) Macromolecules 41:1552
45. Theobald S, Pechwald D, Stoll B (2001) Polymer 42:289
46. Karatasos K, Vlachos G, Vlassopoulos D, Fytas G, Meier G, Du Chesne A (1998) J Chem Phys 108:5997
47. Vlassopoulos D, Koumoutsakos A, Anastasiadis SH, Hatzikiriakos SG, Englezos PJ (1997) J Rheol 41:739
48. Gitsas A, Floudas G, White RP, Lipson JEG (2009) Macromolecules 42:5709
49. Alegria A, Gomez D, Colmenero J (2002) Macromolecules 35:2030
50. Schwartz GA, Colmenero J, Alegria A (2007) Macromolecules 40:3246
51. Schwartz GA, Alegria A, Colmenero J (2007) J Chem Phys 127:154907
52. Roland CM, Casalini R (2007) Macromolecules 40:3631
53. Floudas G, Mpoukouvalas K, Papadopoulos P (2006) J Chem Phys 124:074905
54. Mpoukouvalas K, Floudas G, Zhang SH, Runt J (2005) Macromolecules 38:552
55. Zhang SH, Casalini R, Runt J, Roland CM (2003) Macromolecules 36:9917
56. Hadjichristidis N, Pispas S, Floudas G (2002) Block copolymers: synthetic strategies, physical properties and applications. Wiley, New York
57. Mpoukouvalas K, Floudas G, Verdock B, Du Prez FE (2005) Phys Rev E 72:011802
58. Gitsas A, Floudas G, Butt H-J, Pakula T, Matyjaszewski K (2010) Macromolecules 43:2453

Chapter 6
Polypeptide Dynamics

6.1 Introduction

Proteins are complex macromolecules composed of a sequence of amino-acids (there are 20 amino acids). The sequence of amino acids controls to a large extent the dynamics and function of each protein. As a matter of definition, the lower molecular mass proteins are known as polypeptides. Polypeptides play a vital part of the molecules designed for use in drug delivery of gene therapy and thus have been the subject of intensive studies [1–9]. It is conceivable that among the different polypeptides, chains composed from a single amino acid are by far the easiest to study. However, we should keep in mind that nature employ combinations of all 20 different amino acids giving rise to extremely complex biomacromolecules and functions [1–9].

Nature provides several examples where the structure and function of biological polypeptide-based materials can be precisely controlled. As an example, the superb performance of such polypeptides as hair or spiders' silk is due to a hierarchical superstructure with several length scales where structure control is exerted at every level of hierarchy [10]. Their two most common local conformations, known as secondary structures, are the α-helix, stabilized by intramolecular hydrogen bonds, and the β-strand, stabilized by intermolecular bonds. These secondary structures can be probed directly by different techniques such as solid state NMR [11, 12], FTIR and their packing can be obtained by X-rays. In addition, the α-helical structure posts a permanent dipole moment along its backbone, and can be, therefore, classified as type-A polymer in Stockmayer's classification [13]. This dipole moment can be measured precisely using dielectric spectroscopy and can be used as a probe of the persistence length of the secondary structure, which is difficult to obtain with other methods [2, 14, 15].

Protein function depends on its internal motions. In addition in biological systems, the surrounding water molecules play an important role as is well known that proteins need this hydration layer to establish full biological activity (dry proteins are biologically inactive) [16, 17]. Thus, both internal protein motions and motions within the hydration layer are taking place and give rise to specific protein functions. With respect to the protein dynamics, there exist two different lines of thought. The first

G. Floudas et al., *Molecular Dynamics of Glass-Forming Systems*,
Advances in Dielectrics 1, DOI 10.1007/978-3-642-04902-6_6,

[16–20] emphasizes the importance of the surrounding water molecules in a hydration layer to induce the "slaving" of the large-scale protein dynamics to the fluctuations in the bulk solvent. According to this view, large-scale protein dynamics are controlled by the solvent mobility within a hydration layer and thus are absent in the bulk. The internal protein motions are controlled by hydration and are practically slaved to the beta fluctuations of the hydration shell [16]. The second approach [21], established recently in model synthetic polypeptides composed of a single type of amino acid, revealed that polypeptides possess dynamics that are reminiscent to disordered macromolecules. In this approach, the dynamics are an inherent property of the polypeptide chain and exist even in the absence of solvent. Following this line of thought recent efforts addressed (1) the origin of a dynamic arrest at a "glass transition" temperature [21, 22], i.e., at a temperature where the protein internal dynamics are practically frozen and thus unable to function; (2) the correlation length of α-helices; and (3) the effect of chain topology and confinement on the type, persistence and dynamics of secondary structures [23–31]. We need to comment here on the nature of the "glass transition" in polypeptides as this term is mainly used for amorphous materials. In the latter systems, the transition is from a liquid (i.e., completely amorphous) state to a glassy state, whereas in polypeptides the transition is from a structured (i.e., ordered) liquid to the glass. In this respect, the structured liquid has similarities to the type of order found in liquid crystalline phases.

This chapter reviews recent efforts [23–31] to investigate the hierarchical self-assembly and dynamics of polypeptides. The chapter is organized as follows: In the first part we discuss the origin of the dynamic arrest of polypeptides at the glass "transition." For this purpose, the dynamics of several model oligo- and polypeptides is studied as a function of the number of residues, the presence or absence of side-groups, the type of secondary structure, and the temperature and pressure dependencies. Subsequently, and as a direct consequence of the first part, we discuss that, contrary to expectation and common belief, helices in concentrated polypeptide solutions are objects of low correlation lengths. In the third part, we address the effect of confinement in controlling the type, the persistence and dynamics of secondary structures. In this case we refer to two very different types of confinement; the first is provided by the thermodynamic field (created by the repulsive interactions of the unlike blocks) of nanophase-separated block copolypeptides (discussed as "soft" confinement), whereas the second is the confinement within the porous of anodic aluminum oxide (AAO – discussed as "hard" confinement). The complex self-assembly and the dynamics on different length and time scales require the use of a variety of powerful characterization techniques such as X-ray scattering, NMR, and dielectric relaxation, as well as the application of hydrostatic pressure.

6.2 Polypeptide Liquid-to-Glass "Transition" and its Origin

The internal dynamics of proteins and other biopolymers at different time and length scales are essential for their function. For example, the dynamic arrest at a temperature known as the glass "transition" temperature (T_g) is an

essential feature of protein dynamics that can inhibit biological function [19–21]. Such a dynamic arrest has been observed in a number of different experiments; for example, in the temperature dependence of the atomic mean-squared displacements obtained by inelastic neutron scattering [18], Mössbauer spectroscopy [32] and infrared spectroscopies [33], as well as in molecular dynamics simulations [19, 20, 34, 35]. Although there is consensus about the presence of a dynamic arrest at T_g, its origin is not well understood. For example, the very broad distribution of relaxation times suggested the freezing of the collective protein dynamics, whereas in some cases the reduced solvent mobility [18–20] was thought to be the dominant factor in determining the atomic fluctuations.

Recent experimental work in proteins and polypeptides has shed more light on the issue of the liquid-to-glass transition [16, 17]. Dielectric spectroscopy and thermal measurements on the dynamics of myoglobin in water revealed multiple dynamic processes reflecting both the dynamics of solvent and the internal dynamics of myoglobin [17]. Despite this progress, it is not known if temperature and the associated energy landscape (from both intramolecular and intermolecular origin in this case) are the only important parameters controlling the dynamics. To obtain more insight into this problem, a series of model oligopeptides and polypeptides is needed possessing different repeat units and different secondary motifs. Despite the fact that these polypeptides are composed of a single type of amino acid, and thus are extremely simple systems as compared to proteins, they do provide with important information on the origin of the liquid-to-glass transition that cannot be easily accessed in proteins.

The systems reviewed [36, 37] here include: oligopeptides and polypeptides of γ-benzyl-L-glutamate (BLG) and PBLG, poly(ε-carbobenzyloxy-L-lysine) (PZLL), poly(γ-benzyl-L-tyrosine) (PTyr), polyglycine (PGly), poly(L-leucine) (PLeu), and poly(L-alanine) (PAla). Notice that the first three possess long side chains, whereas PGly is composed of the simplest amino-acid. As a first step, structural techniques (NMR, X-rays, and FTIR) are needed to identify the type of the peptide secondary structure. For example, it is well known that the peptide local conformation is encoded in the ^{13}C chemical shifts, hence the polymer secondary structure can be identified using ^{13}C cross-polarization magic-angle spinning (CPMAS) solid state NMR [38]. Using this as input it was found that PBLG and PZLL form solely α-helices whereas PGly forms β-strands. On the other hand, PLeu and PAla form both α-helices and β-strands.

These synthetic polypeptides, in the dry state, display some interesting thermal properties when studied by differential scanning calorimetry (DSC). The traces of PZLL (a) and PBLG (d and e) display a similar step associated with the structured liquid-to-glass transition. The PBLG extruded fiber also displays the same step but the change in heat capacity is reduced as compared to the powder sample, reflecting the effect of the external macroscopic flow field on the motions that are coupled to the enthalpy relaxation. On the other hand, the trace of the β-strand forming polypeptide (PGly), shows a less pronounced step and at a much higher temperature ($T \sim 400$ K) (Fig. 6.1).

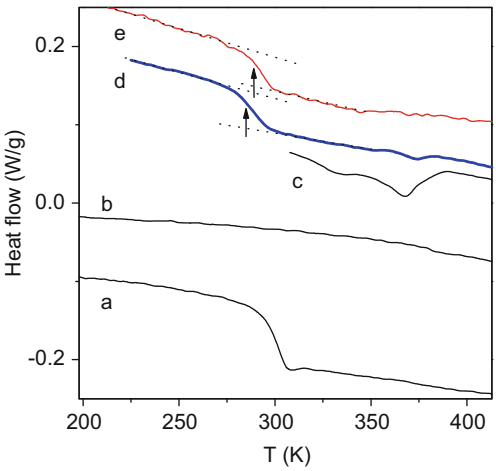

Fig. 6.1 Differential scanning calorimetry traces from different bulk polypeptides: (*a*) poly (ε-carbobenzyloxy-L-lysine) (PZLL), (*b*) polyglycine (PGly), (*c*) PBLG powder sample (first heating), (*d*) the same PBLG as in (*c*) but recorded during the second heating (rate 10 K/min), and (*e*) a PBLG extruded fiber discussed latter with respect to Fig. 6.3

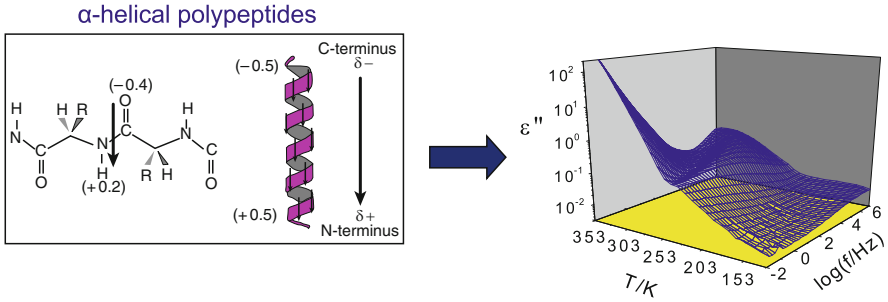

Fig. 6.2 (*Left*): The α-helical secondary structure stabilized through intramolecular hydrogen bonds. This gives rise to a dipole moment along the chain (type A polymers). The dipole moment results from the C=O bonds and N–H bonds that for helical amino acids are hydrogen bonded to form a peptide group N–H···O=C resulting in a net dipole of about 3.4 Debye (*right*). This large dipole along the chain is used as a probe of the correlation length of the helical structures with the aid of dielectric spectroscopy. (*Right*): Dielectric loss spectra of $PBLG_{45}$ plotted as a function of frequency for different temperatures, which are dominated by this "slow" mechanism

These results show unambiguously that the polypeptide structured liquid-to-glass temperature has nothing to do with the solvent. It is a property of the polypeptide chain itself.

Additional information of the polypeptide dynamics can be obtained by following the dipolar relaxation within an oscillating electric field using DS. Figure 6.2 depicts a schematic of the polypeptide backbone indicating the large dipole moment as well as representative dielectric loss spectra originating from the large dipole moment.

A detailed example the main relaxation processes in PBLG as a function of temperature is provided in Fig. 6.3.

In addition, the figure depicts a 2D wide-angle X-ray scattering (WAXS) image from an oriented fiber of the same sample [22]. The WAXS pattern displays strong

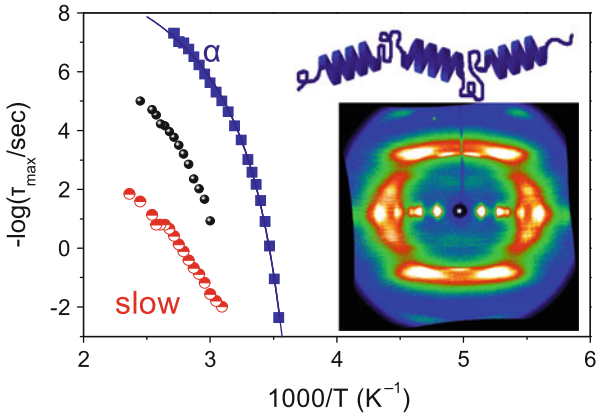

Fig. 6.3 Arrhenius relaxation map of the different processes in poly(γ-benzyl-L-glutamate). The usual segmental process associated with the freezing of the amorphous segment dynamics at the structured liquid-to-glass temperature is shown with squares (α-). The intense slower process is associated with the relaxation of the peptide secondary structure whereas the intermediate process (*filled circles*) reflects the dynamics of amorphous chains. (*Inset*): Wide-angle X-ray image of PBLG taken at 303 K (from an extruded fiber). The image shows the typical scattering from the α-helix. The schematic of the broken α-helix (*top*) is discussed in the text

equatorial reflections with relative positions reflecting hexagonal packing of α-helices and some layer lines. The positions of the lines indicates a normal α-helical conformation of 18 residues in 5 turns with a repeat unit of $c = 2.7$ nm, i.e., an 18/5 helix. This structure has been described as a nematic-like paracrystal with a periodic packing of helices in the direction lateral to the chain axis, whereas along the chain axis, the mutual levels of chains are irregular. Similarly, in FTIR, the α-helical secondary structures can be identified from the amide I and II bands at 1.655 cm^{-1} and 1.550 cm^{-1}, respectively.

As seen in Fig. 6.3, the PBLG dynamics in the bulk state are dominated by three non-Arrhenius processes at temperatures above T_g. From the three processes it is the slower that bears the highest dielectric activity, and as we will see below, it associates with the relaxation of the peptide secondary structure (α-helical in this case). The process indicated as α- in Fig. 6.3, as will be discussed below, is the usual segmental process associated with the structured liquid-to-glass "transition."

Figure 6.4 displays all processes in the different polypeptides, both above and below T_g [21, 22]. The relaxation map is very reminiscent of amorphous polymers, in that it contains Arrhenius processes at lower temperatures with an activation energy typically around 50 kJ/mol, followed by some strongly non-Arrhenius processes with relaxation times $\tau(T)$ that conform to the VFT equation $\tau = \tau_0 \exp(D_T T_0/(T–T_0))$ with exemplary values $D_T = 4.9$, 7.9, and 8 for $PBLG_{45}$, $PZLL_{135}$, and $PGly_{342}$, respectively and ideal glass temperatures $T_0 = 243$ K, 241 K, and 271 K, respectively. This process in the different polypeptides is the typical α-process found in amorphous polymers and glass-forming liquids associated with the glass-to-liquid relaxation of amorphous segments. This assignment is

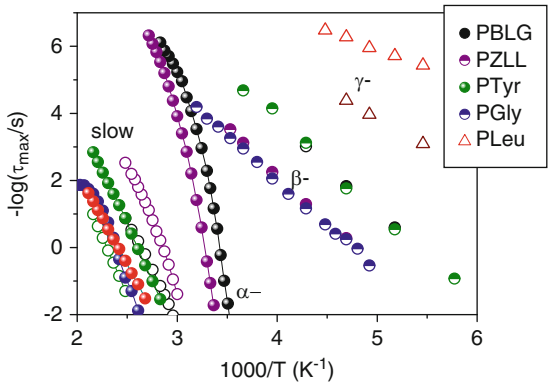

Fig. 6.4 Relaxation times at maximum loss (obtained through dielectric spectroscopy) for five different homopolypeptides: (*black*): poly(γ-benzyl-L-glutamate) (PBLG), (*purple*): poly (ε-carbobenzyloxy-L-lysine)(PZLL), (*green*): poly(γ-benzyl-L-tyrosine) (PTyr), (*blue*): polyglycine (PGly), and (*red*): poly(L-leucine) (PLeu). Four processes are shown: the γ-process (*open symbols*), the β-process (*half-filled symbols*), the α-process (*filled circles*) associated with the liquid-to-glass temperature, and the "slower" process (*open circles*) associated with the relaxation of the secondary structure

based on (1) the existence of a step in the specific heat (Fig. 6.1), Δc_P; (2) the strong $\tau(T)$ dependence; (3) the broad and T-dependent distribution of relaxation times (from a Kohlrausch–Williams–Watts stretched exponent of $\beta_{\mathrm{KWW}} \sim 0.28$ at T_g to 0.4 at $T_g + 30$ K that characterizes the changing association in the hydrogen bonding structures); (4) the molecular weight dependence of the dynamic T_g, (following the Fox-Flory equation: $T_g(x) = 285.9 - 83.7/\langle x \rangle$ for PBLG [22]); and (5) the pressure effects [21] (described briefly below). This process reflects the cooperative dynamics of defects created by the breaking/weakening of hydrogen bonds within the chain and at the chain ends. In addition, the $\tau(T)$ dependencies for the α-helical and β-sheet forming polypeptides, suggest a change from "fragile" to "strong" behavior in going from the α-helical to the more compact β-sheet polypeptides (PGly, PAla).

To determine the origin of the strong $\tau(T)$ dependence of the α-process and the associated dynamic arrest at T_g (i.e., insufficient volume vs. lack of thermal energy as discussed extensively in Chap. 2), pressure is needed as the relevant additional thermodynamic parameter. Then the $\tau(P)$ and $\tau(T)$ relaxation times can be combined with pressure–volume–temperature (PVT) data for the polypeptides that allow casting the T- and P-dependencies of the α-relaxation times in a single representation by using the density as the only variable [21]. For this purpose the measured PVT data of PBLG in the liquid state were parameterized according to the Tait equation as $V(P, T) = V(0, T)\{1 - 0.0894 \ln(1 + P/B(T))\}$, where $V(0, T) = A_0 + A_1 T + A_2 T^2$ is the specific volume at atmospheric pressure and $B(T) = B_0 \exp(-B_1 T)$ (T in °C) ($A_0 = 0.788$, 0.826, 0.604 cm^3; $A_1 = 4.92 \times 10^{-4}$, 4.96×10^{-4}, 1.5×10^{-4} cm^3/K; $A_2 = 7.57 \times 10^{-7}$, 8.01×10^{-7}, 0 cm^3/K^2 for PBLG, PZLL, and PGly, respectively; and $B_0 = 142$, 151, 1.190 MPa for PBLG,

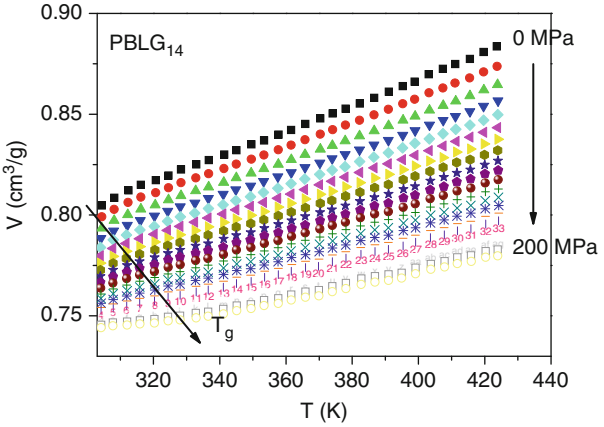

Fig. 6.5 *PVT* measurements for a $PBLG_{14}$ obtained at different pressures in the range from 0.1 to 200 MPa (steps of 10 MPa). The *arrow* gives the pressure dependence of the glass temperature

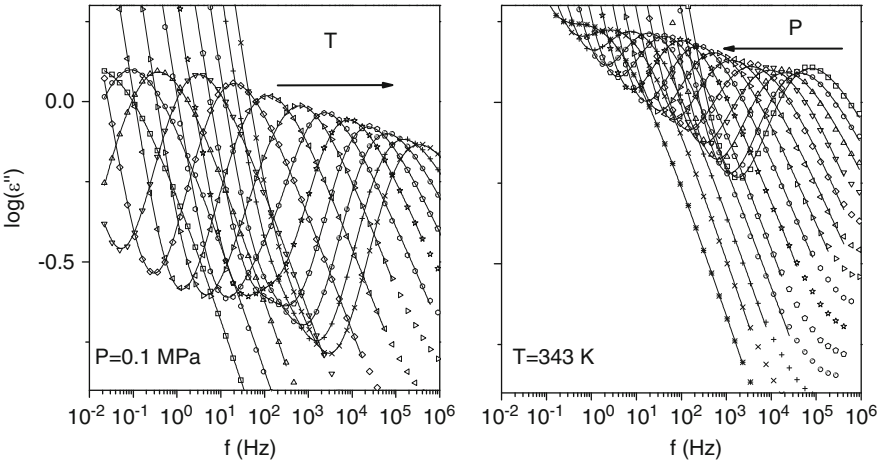

Fig. 6.6 Dielectric loss curves of $PZLL_{135}$ under (*left*) "isobaric" conditions (at $P = 0.1$ MPa) for different temperatures in the range $297 < T < 353$ K and (*right*) under "isothermal" conditions ($T = 343$ K) for pressures in the range $2 < P < 260$ MPa. From [21]

PZLL, and PGly, respectively, and $B_1 = 4.3 \times 10^{-3}$, 4.3×10^{-3}, 2.5×10^{-3} °C^{-1} for PBLG, PZLL, and PGly, respectively). The PBLG *PVT* data are depicted in Fig. 6.5. Figure 6.6 gives the α-process dynamics of $PZLL_{135}$ as a function of temperature and pressure.

Subsequently, following the procedure outlined in Sect. 2.2, the measured relaxation times are plotted as a function of density aiming at extracting the ratio of the activation energies at constant density and pressure, Q_V/Q_P. This procedure,

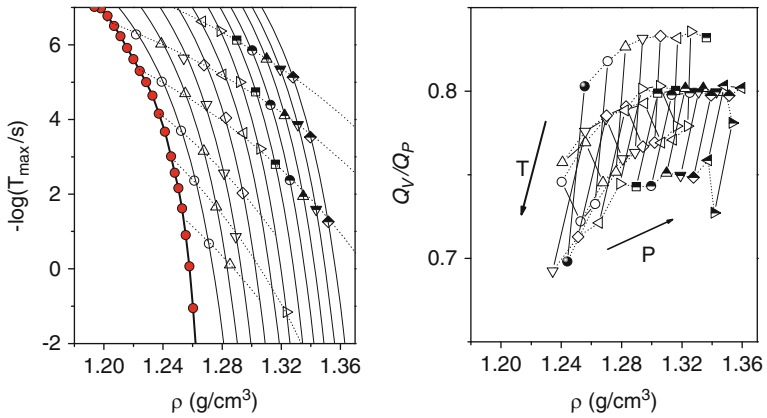

Fig. 6.7 (*Left*) Relaxation times at maximum loss for the $PBLG_{45}$ under "isothermal" and "isobaric" conditions plotted as a function of density. The filled data correspond to the relaxation times at 0.1 MPa. *Solid* and *dashed lines* are fits to the "isobaric" (P from 0.1 to 220 MPa in steps of 20 MPa) and "isothermal" ($T = 297$, 308, 333, 353, and 373 K) times, respectively. (*Right*) Ratio of activation energies Q_V/Q_P, plotted as a function of density. The high values of the ratio suggest intramolecular correlations and hydrogen-bonding as being responsible for the liquid-to-glass transition in polypeptides. For details see [21]

which was discussed in detail in Sect. 2.2, is shown in Fig. 6.7 for the relaxation times corresponding to the α-process of $PBLG_{45}$.

The dynamic ratio can be directly obtained from the slopes of the "isobaric" and "isothermal" curves shown in Fig. 6.7 at their respective crossings as follows: [39]

$$\frac{Q_V}{Q_P} = 1 - \frac{\left(\frac{\partial \ln \tau_{max}}{\partial \rho}\right)_T}{\left(\frac{\partial \ln \tau_{max}}{\partial \rho}\right)_P} \tag{6.1}$$

and it is also plotted as a function of density in Fig. 6.7. Notice that values in the range 0.7–0.85 are obtained under the different (T, P) conditions. To facilitate the comparison among the different polypeptides, this ratio was evaluated at $T \sim T_g + 30$ K and $P = 0.1$ MPa. The ratio Q_V/Q_P, amounts to 0.78, 0.83, and 0.8 for $PBLG_{45}$, $PZLL_{135}$ and $PGly_{342}$, respectively, revealing that decreasing thermal energy is far more important in peptide glass-formation (through the stronger hydrogen bonds that impede conformational changes) than the decrease in the available volume. The close proximity of the above ratio for the different polypeptides, possessing different secondary structures, suggests that the strength of the intra- (α-helices) and inter- (β-strand) molecular hydrogen bonds is similarly affected by T. This suggests that the main controlling parameter of the local "segmental" dynamics in polypeptides associated with the structured liquid-to-glass transition is the intramolecular barriers associated with hydrogen bonding and not the available or "free" volume [21]. However, it should be mentioned that the ratio is not 1, that is, intermolecular correlations and packing still play some role.

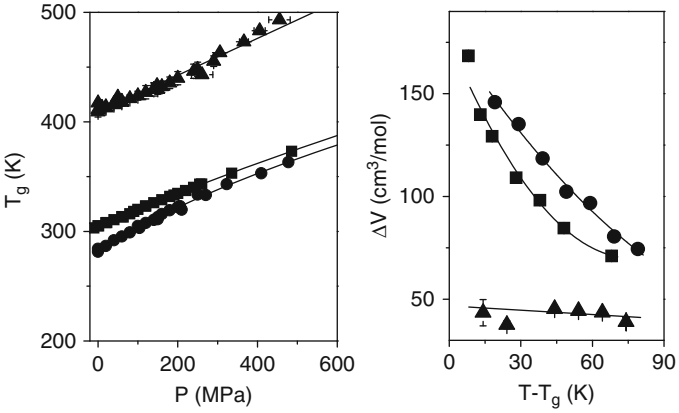

Fig. 6.8 (*Left*) Dependence of glass temperature (defined at $\tau = 1$ s) on pressure for $PBLG_{45}$ (*circles*), $PZLL_{135}$ (*squares*), and $PGly_{342}$ (*triangles*). Lines are fits to (1.17). (*Right*): Calculated apparent activation volume (ΔV) are plotted as a function of the temperature difference from the respective T_g. Lines are guides for the eye. From [21]

Knowledge of the pressure dependence of relaxation times, $\tau(P)$, allows extracting the $T_g(P)$ dependence. These (at $\tau = 1$ s) dependencies for the three polypeptides are compared in Fig. 6.8. $PBLG_{45}$ has a stronger $T_g(P)$ dependence that is in line with its lower Q_V/Q_P ratio. To better quantify the effect of pressure on the dynamics of the α-process, the corresponding apparent activation volumes obtained from the respective initial slopes of $\tau(P)$ (at $P = 0.1$ MPa) are also compared in Fig. 6.8 as a function of the T-difference from their respective T_g's. ΔV for PBLG and PZLL is much higher than that of PGly in accordance with the vastly different monomeric volumes. In addition, the α-helical polypeptides (PBLG and PZLL) exhibit a stronger ΔV (T), as opposed to the weaker T-dependence for the β-strand forming PGly [the latter has also a weak $\tau(T)$ dependence]. Therefore, it appears that the type of secondary structure influences both the fragility and the apparent activation volume.

We mention that similar dynamics have been obtained for dilute solutions of PBLG and PZLL in *m*-cresol. The solvent (*m*-cresol, in this case) does not arrest the polypeptide dynamics, but instead conducts its own local (α-) dynamics at a lower temperature than the polypeptide segmental motion. This is depicted in Fig. 6.9. The two time scales (solvent and polypeptide) differ by 2–4 orders of magnitude revealing that the process associated with the dynamic glass transition is not a property of the solvent but reflects the intrinsic peptide dynamics. Despite the very simple nature of the peptides reviewed here, these findings could have consequences on the dynamic arrest of more complex proteins.

These results have shown that DS is a very efficient method for studying the dynamics (provided that the molecules posses some dipole moment). However, to infer the geometry of motion from DS alone is a very difficult task that requires several assumptions to be made. On the other hand, NMR has the capacity of providing the geometry corresponding to the DS motional rates. The relevant molecular information on the side- and backbone dynamics in PBLG can be obtained [26]

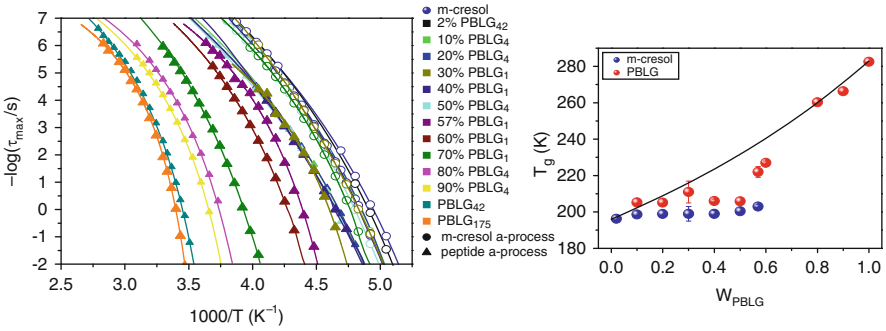

Fig. 6.9 (*Left*): Arrhenius relaxation map for the α-process associated with the liquid-to-glass "transition" in PBLG/*m*-cresol solutions, shown for different concentrations; The PBLG and solvent dynamics are shown with the *filled* and *empty symbols*, respectively. Notice that the polypeptide and solvent relaxations are well-separated. (*Right*) Extracted glass temperatures for the polypeptide (*red symbols*) and *m*-cresol (*blue symbols*) liquid-to-glass dynamics. The *solid line* is the prediction of the Fox equation

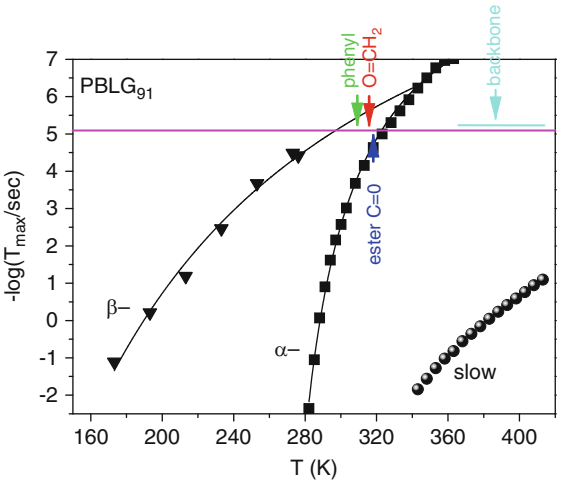

Fig. 6.10 Relaxation times for the Arrhenius β- (*triangles*) and α-processes (*squares*) and the "slower" process (*spheres*) of $PBLG_{91}$, obtained from DS plotted as a function of temperature. The *solid lines* are fits to an Arrhenius and VFT equations for the β- and α-processes, respectively. The ^{13}C NMR resonances are indicated with *arrows* at the relevant NMR frequency. For details see [28]

by following the temperature dependence of the ^{13}C NMR spectra associated with the phenyl ring, the OCH_2, and side ester groups and the backbone amide C=O resonances. On the basis of the combined information from DS and ^{13}C NMR experiments on the motional rates and the geometry of motion at the single NMR frequency, respectively, the relaxation times of PBLG are compared in Fig. 6.10. Notice that the collective dynamics of α-helical segments are orders of magnitude slower than the local segmental dynamics within the amorphous-defected regions. The dynamics from ^{13}C NMR are indicated with arrows at the "relevant" NMR frequency. Notice that the phenyl, the OCH_2, and side group ester dynamics are located in the vicinity of the merging of the α- and β-processes.

Since the motion of the phenyl group itself is dielectrically inactive, we conclude that the β-process, as probed dielectrically, reflects the ester C=O and OCH_2 dynamics. Backbone motions, as probed by NMR, start at higher temperatures than the DS segmental α-process. This is conceivable because DS is sensitive to the backbone dynamics within the "defected" amorphous regions, which do not show up in our NMR spectra since the latter are dominated by the signals of the α-helices. Therefore, NMR probes the backbone dynamics within the α-helical segments, or in general, in more ordered regions. The NMR process can be considered as a precursor for the unfreezing of the helical dynamics probed dielectrically.

Summarizing, the α-process, which is strongly non-Arrhenius and non-Debye, is associated with the dynamic arrest at T_g is an intrinsic feature of peptide dynamics irrespective of the type of amino acid and of the peptide secondary structure; it also exists in polypeptide solutions and is decoupled from the solvent dynamics. Using *T*- and *P*-dependent DS coupled with the equation of state reveals that the cause of the structured liquid-to-glass transition in polypeptides is mainly the insufficient thermal energy to overcome the energy barriers. Glass formation in these materials is associated with the breaking/weakening of hydrogen bonds at certain defects. The type of peptide secondary structure has an influence on (1) the $\tau(T)$ dependence and the associated fragility and (2) the $\tau(P)$ dependence. The selective sensitivity of NMR to the dynamics of the α-helical secondary structure is of great importance in understanding the geometry of the DS dynamical processes.

6.3 Correlation Length of α-Helices

Despite the valuable knowledge of the type of secondary structure that is provided by several "structural" techniques, these probes provide limited information on the correlation of α-helices. One can envisage that the presence of defected hydrogen bonded segments, associated with the structured liquid-to-glass transition, may have consequences on the persistence of α-helical structures. It is well known that dielectric spectroscopy is a sensitive probe of the correlation length of type-A polymers [such as 1,4-polyisoprene or poly(propylene glycol)] [13]. For α-helical forming polypeptides, in particular, the dipole moment results from the C=O bonds (dipole moment of 2.31 Debye) and N–H bonds (1.31 Debye) that for helical amino acids are hydrogen bonded to form a peptide group N–H···O=C resulting in a net dipole of about 3.4 Debye per repeat unit.

Ample literature exists on dielectric measurements of PBLG in dilute solutions of helicogenic solvents [40, 41] and in the related rod-like polymers the polyalkyl isocyanates [14, 42, 43]. These studies revealed a strong process, which was attributed to the reorientations of the α-helix as a rigid rod. The relaxation times had a $\tau \sim M^3$ molecular weight dependence, which is consistent with the rigid-rod model. A strong slow process also shows up in the bulk and in the past, it was assumed that α-helices remain rigid as in solutions with their rotation restricted within a cone rather than being completely free [43–45]. The model is also

described by Doi and Edwards [46] as the "chopstick" model. In this model, two separate vectors ($\vec{u}$ and $\vec{n}$) give the polymer and tube directions, respectively, and these vectors move together like a pair of chopsticks. The external field affects the rapidly moving polymer vector, $\vec{u}$, which drags the slowly moving tube vector $\vec{n}$ through the coupling potential. This model has similarities with the model proposed by Wang and Pecora [47] for the restricted rotational diffusion of a rod-like molecule within a cone of angle θ. Moscicki and Williams [48] applied the Wang–Pecora model to their dielectric data for poly-hexyl isocyanate/toluene solutions in the lyotropic-nematic LC state. Subsequently, the details of the Wang–Pecora and Doi models for dielectric relaxation arising from restricted rotational diffusion of rods in a tube/cone were compared [49, 50]. The Doi model and Wang–Pecora model were shown to be formally equivalent and it was shown that only a part of $\langle\mu^2\rangle$ is relaxed by this process, i.e., $\left[\langle\mu^2\rangle - \langle\mu\rangle^2\right]$, the remainder $\langle\mu\rangle^2$ awaits to be relaxed by a slower (overall) motional process. Following this line of thought, a chain of independent parts/units, each unit relaxing $\left[\langle\mu^2\rangle - \langle\mu\rangle^2\right]$ of $\langle\mu\rangle^2$ for that unit, then a sequence n of units, all pointing along the same direction along the same axis would build-up a cumulative residual relaxation strength $n\langle\mu\rangle^2$ awaiting to be relaxed.

Despite these successes in understanding the dynamics of peptide α-helices theoretical and experimental results exist, that favor flexibility of PBLG in solution [51–53] and in the bulk. Recent work on a series of PBLG homopolymers with different molecular weights [22] showed that the helices are not perfect. Both the relaxation times and dielectric strength of this process were almost independent of the chain molecular weight, implying that it is not an end-to-end relaxation, but rather a motion of smaller parts of the chain.

A freely rotating rigid (i.e., "ideal") helix would give rise to a dielectric process with strength [54]

$$\Delta\varepsilon = \frac{N\mu^2}{3\varepsilon_0 kT}, \tag{6.2}$$

where N is the number density of helices and μ is the total dipole moment of the helix that is proportional to the degree of polymerization. In this equation, it is assumed that the rotation of each helix is independent of that of the others (the local field correction factor is not taken into account due to the relatively large size of the helix). Equation (6.2) can be rewritten as

$$\Delta\varepsilon = \frac{N_A\rho}{3\varepsilon_0 kT\langle x\rangle M_m}\left(\mu_m\langle x\rangle\right)^2 = \frac{N_A\rho}{3\varepsilon_0 kTM_m}{\mu_m}^2\langle x\rangle, \tag{6.3}$$

where ρ is the density, $\langle x\rangle$ is the average degree of polymerization, M_m the molecular weight of the monomer, and μ_m the dipole moment per monomer unit (from the solution studies $\mu_m \sim 3.4$ Debye). However, (6.3) suggests that $\Delta\varepsilon$ for an ideal helix should be directly proportional to $\langle x\rangle$, which is contrary to recent experimental finding for PBLG. This implies that the helices in bulk PBLG are

not rigid and they contain "defects," i.e., broken hydrogen bonds. Hence the "slow" process reflects the relaxation of the broken helical parts.

Recently, and in order to quantitatively take into account the helical defects, a model of a "defected" helix was proposed [55]. The helix is assumed to be composed of N_P "ideal" helical parts of equal length ξ that can rotate on the surface of a cone of angle θ. The rotation of each part is independent from the others, but the axes of all cones are parallel. This is a reasonable assumption, because X-ray measurements (Fig. 6.3) have shown that helices are hexagonally packed. The dipole moment of each part is $\mu_P = 3.4$ Debye (ξ/0.15 nm), since the α-helix length is 0.15 nm/monomer. The dielectric strength is given by

$$\Delta\varepsilon = \frac{NN_P\left(\langle\vec{\mu}^2\rangle - \langle\vec{\mu}\rangle^2\right)}{3\varepsilon_0 kT} = \frac{N_A\rho}{3\varepsilon_0 kTM_m}(3.4\,\text{Debye})^2(\xi/0.15\,\text{nm})\sin^2\theta. \qquad (6.4)$$

The last equation reveals that $\Delta\varepsilon$ is independent of $\langle x\rangle$, and this is in agreement with the experimental results [22]. The only parameter needed to extract ξ is the angle θ. The X-ray scattering from oriented fibers (Fig. 6.3) can be used to obtain an upper limit, i.e., $\theta_{max} \approx 0.25$ rad. This allows a calculation of ξ, which is plotted in Fig. 6.11 for a series of PBLG homopolymers. The calculated values of the correlation length are in the order of 1–2 nm, i.e., helices are far from rigid objects.

The persistence of the α-helical secondary structures was also investigated in a series of PBLG solutions in *m*-cresol, covering the concentration range from 2% w/w to bulk PBLG. At low concentration, the measured dipole moment shows that helices are rigid, but their persistence length decreases as polymer concentration increases above ~20% w/w. PBLG with a low amount of *m*-cresol (e.g., 80 or 90% w/w PBLG) exhibits a stronger slow process than pure PBLG and has a higher persistence length.

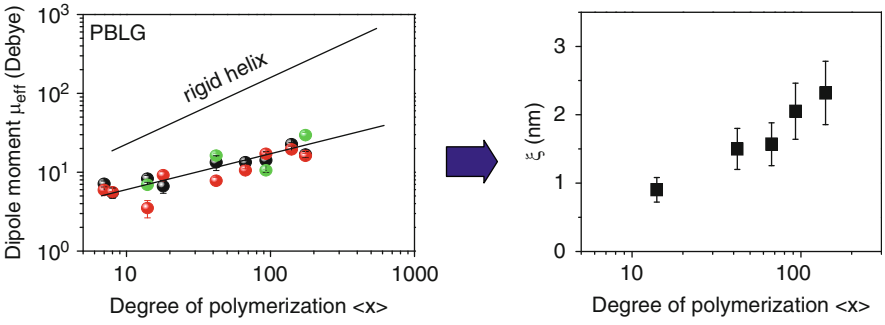

Fig. 6.11 (*Left*) Effective dipole moment for the "slower" process as a function of the degree of polymerization of PBLG. The *solid line* gives the theoretical value of the effective dipole moment per chain. Notice that broken helices appear that are independent of the degree of polymerization. (*Right*) Correlation length, ξ, calculated with the aid of (6.4) of the α-helical structure for a series of PBLG homopolyptides. Notice that $\xi \sim 2$ nm for the higher degrees of polymerization. For details see [22, 55]

These results show that the origin of the glass transition and the low correlation length of the α-helical secondary structures in polypeptides are coupled; the broken network of hydrogen bonds responsible for the dynamic arrest at the glass temperature is also responsible for the low persistence of the helical segments. It is only in dilute solutions in helicogenic solvents that the helical defects are annihilated.

6.4 Effects of Nanoconfinement on the Peptide Secondary Structure and Dynamics

6.4.1 "Soft" Confinement: Confinement Within the Nanodomains of Block Copolypeptides

Block copolypeptides can be employed as model systems that follow nature's strategies for producing supramolecular bioactive assemblies with potential applications in tissue engineering and drug delivery. Copolypeptides of particular interest are those composed of both α-helical and β-strand motifs [22, 25, 31, 36, 37]. In block copolypeptides, both secondary motifs are exposed to the same thermodynamic field created by the block copolymer nature and this allows studying their stability and persistence.

The system reviewed here is a block copolypeptide composed from PBLG and PGly blocks, i.e., an example of "soft" confinement to the polypeptide chain. The confinement is provided by the thermodynamic field of the blocks themselves because of the incompatibility that drives the system to nanophase separation. The two blocks differ substantially not only in their secondary structures, but also in their packing efficiency (Gly bears no side group as opposed to the long side group of BLG) and segmental mobility. The X-ray investigation revealed a lamellar microdomain morphology with embedded hexagonally packed PBLG helices and sheets of PGly, i.e., *cylinder-in-lamellar* morphology [25]. Interestingly, a lamellar microdomain morphology is obtained despite the very asymmetric block composition ($f_{PBLG} = 0.79$). The X-ray investigation further identified that the measured PGly domain spacing in the copolymers is a small fraction of the size of a fully extended chain. This shows that the PGly chains are multiply folded in their β-strand conformation. The thermodynamic confinement by the nanodomain and the disparity in the packing efficiency of PBLG and PGly results in multiple chain folding, so as to keep a uniform density. As a consequence of chain folding, the lamellar morphology is stabilized for very asymmetric compositions.

A combination of structural and dynamic (DS) probes allows extracting the orientation of secondary structures within the nanodomain and the correlation length of α-helices. For the former, 2D WAXS from an extruded PBLG-*b*-PGly fiber (shown in Fig. 6.12) depicts two sets of equatorial reflections suggesting that both the PBLG chains forming the α-helices and the PGly chains forming the β-strands are perpendicular to the interface.

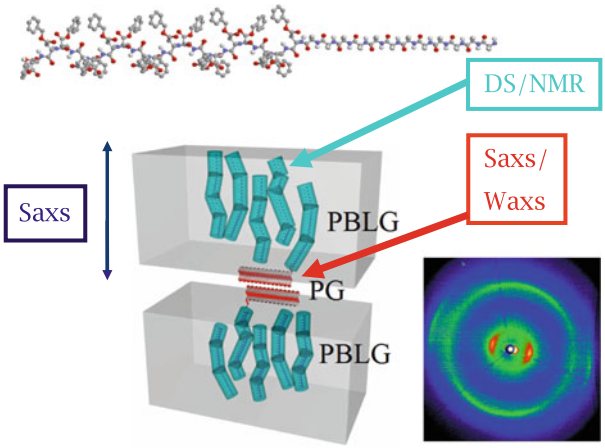

Fig. 6.12 Schematic model of PBLG-*b*-PG copolymers with $f_{PBLG} < 0.8$ (i.e., within the lamellar nanodomain morphology), which is consistent with the results of the static (NMR, SAXS, and WAXS) and dynamic (DS) methods. PBLG helices contain defects that allow for the partial interdigitation. PGly chains fold several times in accordance with ^{13}C NMR and SAXS experiments. For details see [25, 56]

On the basis of the results from the static (WAXS, SAXS) and dynamic (DS) methods mentioned above, a schematic model for the self-assembly in the PBLG-*b*-PG copolymers can be reconstructed in Fig. 6.12 depicting the copolymer nanodomain and peptide secondary structures inside the domains [25, 56]. The two blocks are well separated (strong segregation, based on DS and SAXS), the PBLG helices are defected causing them to bend at certain positions (DS), PGly chains fold several times (SAXS, WAXS) and finally PBLG α-helices and PGly β-strands are organized perpendicular to the interface (WAXS). The incomplete interdigitation of helices is easily explained in this figure; the gaps that would remain in the case of ideal helices are now filled due to the defects that allow helices to bend.

These results reveal that the nanoscale confinement of dissimilar peptidic blocks can be used as a means of controlling the correlation length of the secondary peptide motifs with the larger effect produced for β-strands. It also shows that a dynamic technique (DS) can be combined with structural probes that can provide the phase state and type of peptide secondary structure to provide a detailed picture of the organization and dynamics within the nanodomains.

6.4.2 "Hard" Confinement: Confinement Inside Nanoporous Anodic Aluminum Oxide

It is well known that the self-organization of polypeptides in the proximity of interfaces is different from that in the bulk; however, little is known as to how pore diameter and rigid pore walls influence the dynamics of the confined

biomolecules. PBLG peptide nanorods can be synthesized inside nanoporous anodic aluminum oxide (AAO) hard templates with pore diameters ranging from 25 to 400 nm [28]. The synthesis involved the silane coupling agent 3-aminopropyltriethoxysilane (APTES) bound to the pore walls as initiator for the polymerization of *N*-carboxy anhydride of benzyl-L-glutamate (BLG-NCA).

Here we review the strong dependence of the segmental dynamics of PBLG synthesized in self-ordered AAO with mean D values of 25, 35, 65, 200, and 400 nm and a pore depth of 80–95 μm on the pore diameter [28]. Although released PBLG nanorods (by etching the AAO) of all diameters and nanorods located in AAO with D values of 200 and 400 nm show bulk-like behavior, considerably different segmental dynamics was found for PBLG confined to AAO hard templates with D values equal or smaller than 65 nm.

Figure 6.13 depict TEM images of the PBLG nanorods synthesized in the pores of AAO hard templates. The images show AAO filled with PBLG and finally etched AAO (released PBLG nanorods). The usual structural probes (X-ray scattering, solid state NMR, and FTIR) have shown the formation of PBLG α-helices that were hexagonally packed.

The segmental dynamics of the amorphous-like fraction of the embedded PBLG nanorods can be studied by means of dielectric spectroscopy (DS) [28]. The result on the primary (α-) relaxation is depicted in Fig. 6.14. The figure displays an Arrhenius plot of the segmental relaxation times $\tau(T)$ of disordered PBLG segments in PBLG nanorods confined to AAO with various pore diameters as a function of inverse temperature. Bulk PBLG and the PBLG located in AAO with D values of 200 and 400 nm show typical "fragile" dynamic behavior, that is, pronounced $\tau(T)$ dependence. The VFT parameters of PBLG residing in pores with D values of 400 and 200 nm deviate only from that of bulk PBLG slightly. However, PBLG confined to pores with D values between 25 and 65 nm exhibits completely different segmental

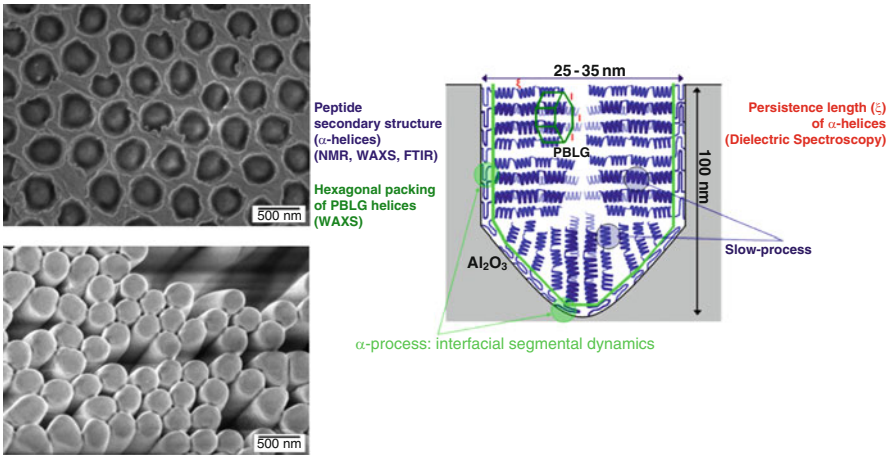

Fig. 6.13 (*Left*) Scanning electron microscopy images of (top) AAO ($D = 400$ nm) containing PBLG nanorods and (*bottom*) the same PBLG nanorods released from AAO. (*Right*) A schematic of the peptide self-assembly within AAO. From [30]

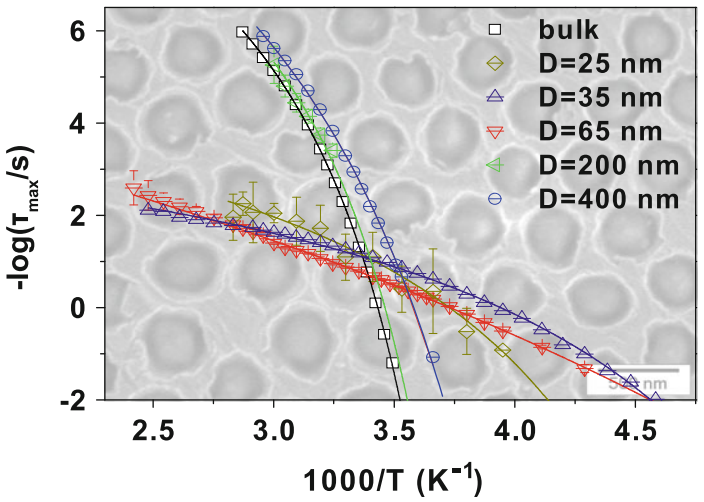

Fig. 6.14 Segmental relaxation times plotted in the Arrhenius representation; *black squares*, bulk PBLG; *blue circles* with *horizontal lines*, nanorods located in AAO with a *D* value of 400 nm; *green left triangles* with *horizontal lines*, nanorods located in AAO with a *D* value of 200 nm; *red down triangles* with *horizontal lines*, nanorods located in AAO with a *D* value of 65 nm; *dark blue up triangles* with *horizontal lines*, nanorods located in AAO with a *D* value of 35 nm; and *dark yellow rhombuses* with *horizontal lines*, nanorods located in AAO with a *D* value of 25 nm. The lines are fits to the VFT equation. From [30]

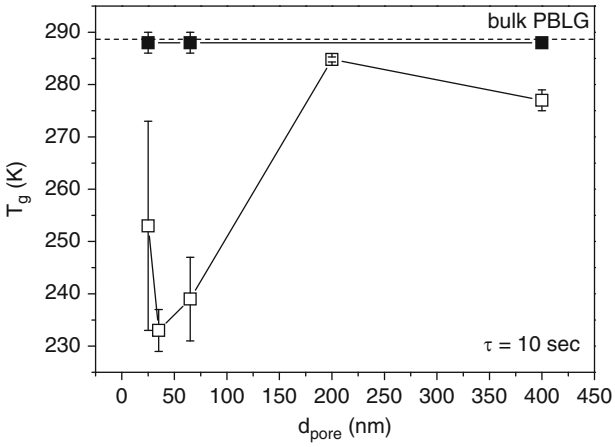

Fig. 6.15 Glass temperature (obtained from DS at $\tau \sim 10$ s) as a function of the AAO pore diameter for the embedded (*open symbols*) and released (*filled symbols*) nanorods. Notice the T_g reductions for embedded PBLG within AAO with diameter below 65 nm

dynamics characterized by "strong" dynamic behavior with a significantly weaker dependence of the segmental relaxation times on the temperature. Moreover, the glass temperatures, T_g, are reduced by as much as 50 K relative to that of bulk PBLG or PBLG located in AAO with pore diameters of 200 and 400 nm.

Figure 6.15 summarizes the results of the dynamic investigation on the glass temperature for the embedded and released nanorods. The glass temperature is operationally defined as the temperature where the segmental relaxation time is at 10 s (this definition minimizes the extrapolations). Notice the reduction of the glass temperature for the embedded nanorods with pore diameters below 65 nm and the insensitivity of the glass temperature for the released nanorods.

Apparently, the presence of the rigid pore walls in AAO with pore diameters of 65 nm and below induces the change of segmental dynamics rather than the geometric confinement itself. The weak $\tau(T)$ dependence results from the redistribution of hydrogen bonds of the polypeptide backbone with the silanol groups at the surface of the APTES layer. The additional hydrogen bonds disrupt the backbone conformations and are also responsible for the absence of the slower process associated with the migration of helical sequences along the chain [30].

6.5 Conclusion

Recent efforts on exploring the self-assembly and dynamics of a series of model polypeptides and block copolypeptides, with a variety of techniques, have shed light to the origin of glass transition, the persistence of the α-helical peptide secondary motif, and the effects of confinement on the type and persistence of secondary structures. There are several examples where protein function and applications depend on these issues. Despite the simple nature of these systems, as compared to the more complex protein structures, they do provide insight into long lasting questions. With respect to the freezing of the dynamics at the structured liquid-to-glass temperature, application of pressure together with temperature and the equation of state has shown that the origin of this effect is a network of broken hydrogen bonds. It is the diffusion of these defects along the chain that give rise to the strongly non-Arrhenius dynamics associated with T_g. Glass formation is largely independent of the presence or absence of side-groups and is decoupled from the solvent dynamics. Furthermore, for the first time, the selective probing of the α-helical motifs by NMR elucidated the geometry of the respective dynamic processes.

The presence of defected hydrogen-bonded regions has also consequences on the correlation length of α-helices. This can be documented by following the dipole moment of the backbone by means of dielectric spectroscopy. We need to emphasize here that despite the existence of several structural techniques that can probe the type of peptide secondary structure, it is only dielectric spectroscopy that can provide their persistence (for α-helical secondary structures). Using PBLG as an example, it was shown that helices are objects of rather low persistence in the bulk as well as in concentrated solutions in helicogenic solvents.

The effects of confinement on the type and persistence of secondary structures can be studied either by employing the thermodynamic field of copolypeptides ("soft" confinement) or nanoporous AAO templates ("hard" confinement). Copolypeptides with their inherent nanometer length scale of phase separation provide

means of manipulating both the type and persistence of peptide secondary structures. As an example, we refer to the induced chain folding of β-strands in block copolypeptides with incommensurate dimensions. These effects should be taken into account when such peptides are going to be employed in drug delivery. On the other hand, a striking change from "fragile" to "strong" dynamic behavior occurred when PBLG is confined to AAO hard templates with pore diameters equal or smaller than 65 nm. The temperature dependence of segmental dynamics became significantly weaker than in case of the bulk PBLG, and the effective glass temperature was reduced by as much as 50 K. This effect was discussed in terms of the newly formed hydrogen bonds between the silanol groups and the peptide backbone. Again, these results have to be considered when designing membrane configurations based on the functionality of biopolymers located in nanopores.

Acknowledgment We thank several people that contributed to the work presented in this chapter: Prof. N. Hadjichristidis, Prof. H. Iatrou, Prof. H.-A. Klok and Dr. H. Duran for the synthesis; Dr. M. Mondeshki and Prof. H.W. Spiess for the solid state NMR studies and for many fruifull discussions; and Dr. P. Papadopoulos and Dr. A. Gitsas for the dielectric studies.

References

1. Walton AG, Blackwell J (1973) Biopolymers. Academic, New York
2. Block H (1983) Poly(γ-benzyl-L-glutamate) and other glutamic acid containing polymers. Gordon and Breach Science Publishers, New York
3. Kricheldorf HR (2006) Angew Chem Int Ed 45:5752
4. Frauenfelder H, Sligar SG, Wolynes PG (1991) Science 254:1598
5. McCammon JA, Gelin BR, Karplus M (1977) Nature 267:585
6. Sali A, Shakhnovich E, Karplus M (1994) Nature 369:248
7. Deming TJ (1997) Nature 390:386
8. Klok HA, Lecommandoux S (2006) Adv Polym Sci 202:75
9. Duncan R (2003) Nat Rev Drug Discovery 2:347
10. Hakimi O, Knight DP, Knight MM, Grahn MF, Vadgama P (2006) Biomacromolecules 7:2901
11. Shoji A, Ozaki T, Saito H, Tabeta R, Ando I (1984) Macromolecules 17:1472
12. van Beek JD, Beaulieu L, Schafer H, Demura M, Asakura T, Meier BH (2000) Nature 405:1077
13. Stockmayer WH (1967) Pure Appl Chem 15:539
14. Block H (1979) Adv Polym Sci 33:93
15. Bur AJ, Roberts DE (1969) J Chem Phys 51:406
16. Frauenfleder H, Chen G, Berendzen J, Fenimore PW, Jansson H, McMahon BH, Stroe IR, Swenson J, Young RD (2009) Proc Natl Acad Sci USA 106:5129
17. Jansson H, Swenson J (2010) Biochim Biophys Acta 1804:20
18. Doster W, Cusack S, Petry W (1989) Nature (London) 337:754
19. Vitkup D, Melamud E, Moult J, Sander C (2000) Nat Struct Biol 7:34
20. Rasmussen BF, Stock AM, Ringe D, Petsko GA (1992) Nature (London) 357:423
21. Floudas G, Mpoukouvalas K, Papadopoulos P (2006) J Chem Phys 124:07490
22. Papadopoulos P, Floudas G, Klok HA, Schnell I, Pakula T (2004) Biomacromolecules 5:81
23. Floudas G, Papadopoulos P, Klok HA, Vandermeulen GWM, Rodriguez-Hernandez J (2003) Macromolecules 36:3673

24. Papadopoulos P, Floudas G, Schnell I, Klok HA, Aliferis T, Iatrou H, Hadjichristidis N (2005) J Chem Phys 122:224906
25. Papadopoulos P, Floudas G, Schnell I, Aliferis T, Iatrou H, Hadjichristidis N (2005) Biomacromolecules 6:2352
26. Mondeshki M, Mihov G, Graf R, Spiess HW, Müllen K, Papadopoulos P, Gitsas A, Floudas G (2006) Macromolecules 39:9605
27. Koynov K, Mihov G, Mondeshki M, Moon C, Spiess HW, Müllen K, Butt HJ, Floudas G (2007) Biomacromolecules 8:1745
28. Gitsas A, Floudas G, Mondeshki M, Spiess HW, Aliferis T, Iatrou H, Hadjichristidis N (2008) Macromolecules 41:8072
29. Gitsas A, Floudas G, Modenshki M, Butt HJ, Spiess HW, Iatrou H, Hadjichristidis N (2008) Biomacromolecules 9:1959
30. Duran H, Gitsas A, Floudas G, Mondeshki M, Steinhart M, Knoll W (2009) Macromolecules 42:2881
31. Gitsas A, Floudas G, Mondeshki M, Lieberwirth I, Spiess HW, Iatrou H, Hadjichristidis N (2010) Macromolecules 43:1874
32. Keller H, Debrunner PG (1980) Phys Rev Lett 45:68
33. Iben IET, Braunstein D, Doster W, Frauenfelder H, Hong MK, Johnson JB, Luck S, Ormos P, Schulte A, Steinbach PJ, Xie AH, Young RD (1989) Phys Rev Lett 62:1916
34. Smith J, Kuczera K, Kaplus M (1990) Proc Natl Acad Sci USA 87:1601
35. Norberg J, Nilsson L (1996) Proc Natl Acad Sci USA 93:10173
36. Aliferis T, Iatrou H, Hadjichristidis N (2004) Biomacromolecules 5:1653
37. Aliferis T, Iatrou H, Hadjichristidis N (2005) J Polym Sci A Polym Chem 43:4670
38. Schmidt-Rohr K, Spiess HW (1994) Multidimensional solid-state NMR and polymers. Academic, New York
39. Papadopoulos P, Peristeraki D, Floudas G, Koutalas G, Hadjichristidis N (2004) Macromolecules 37:8116
40. Wada AJ (1958) Chem Phys 29:674; 1959, 30:328; 1959, 30:329
41. Mori Y, Ookubo N, Hayakawa R, Wada Y (1982) J Polym Sci Polym Phys Ed 20:211
42. Moscicki K, Williams G (1983) J Polym Sci Polym Phys Ed 21:197
43. Watanabe J, Uematsu I (1984) Polymer 25:1711
44. Schmidt A, Lehmann S, Georgelin M, Katana G, Mathauer K, Kremer F, Schmidt-Rohr K, Boeffel C, Wegner G, Knoll W (1995) Macromolecules 28:5487
45. Hartmann L, Kratzmüller T, Braun HG, Kremer F (2000) Macromol Rapid Commun 21:814
46. Doi M, Edwards SF (1986) The theory of polymer dynamics. Oxford University Press Inc., New York
47. Wang C, Pecora R (1980) J Chem Phys 72:5333
48. Moscicki JK, Williams G (1983) J Polym Sci Polym Phys Ed 21:213
49. Williams G (1982) J Polym Sci Polym Phys Ed 20:1963
50. Williams G (1983) J Polym Sci Polym Phys Ed 21:2037
51. Zimm BH, Bragg JK (1959) J Chem Phys 31:526
52. Flory PJ (1978) Macromolecules 11:1126
53. Flory PJ, Frost RS (1978) Macromolecules 11:1134
54. Kremer F, Schönhals A (eds) (2003) Broadband dielectric spectroscopy. Springer, New York
55. Papadopoulos P, Floudas G (Sept 2005) Dielectrics Newsletters
56. Floudas G, Spiess HW (2009) Macromol Rapid Commun 30:278

Index

G. Floudas et al., *Molecular Dynamics of Glass-Forming Systems*, Advances in Dielectrics 1, DOI 10.1007/978-3-642-04902-6,

Q

R

S

T